UNIVERSITÉ DU QUÉBEC À MONTRÉAL

CATALYSEURS À BASE D'ALUMINOSILICATES MODIFIÉS POUR L'OZONATION DE POLLUANTS ORGANIQUES ET MÉDICAMENTEUX

MÉMOIRE

PRÉSENTÉ

COMME EXIGENCE PARTIELLE

DE LA MAÎTRISE EN CHIMIE

PAR

FARIDA BOUDISSA

JUILLET 2020

REMERCIEMENTS

Tout d'abord, je tiens à remercier mon directeur de recherche professeur Azzouz Abdelkrim, pour l'intérêt constant qu'il a porté à ce travail en acceptant de diriger cette étude. Je le remercie profondément de m'avoir offert ses savoirs, ses conseils judicieux, ses encouragements et sa disponibilité durant toutes ces années de recherche.

Professeur Azzouz Abdelkrim m'a ouvert des grandes portes dans la recherche scientifique; il m'a aidé à trouver des solutions dans tous les cas et m'a aussi poussé à être indépendante. Je lui dois un profond respect.

Je remercie vivement le professeur René Roy, mon co-directeur de recherche de m'avoir accepté dans son laboratoire et pour son soutien et ses encouragements tout au long de ma maitrise.

Je remercie les membres du jury qui ont m'ont honorée par leur acceptation d'évaluer le contenu de mon mémoire de maîtrise: Pr. Jacques Lesage, Pr. Livain Breau et Pr. Sylvain Canesi, qui a présidé ce jury. Leurs évaluations m'ont été d'un grand apport dans la correction finale pour améliorer la qualité du manuscrit.

Je tiens également à exprimer mes remerciements au Dr. Rami Abdelhaq pour ses conseils et son aide au cours de toutes ces années passées à l'université.

Mes remerciements vont aussi au personnel du département de chimie ainsi qu'à toute l'équipe dirigée par Pr. René. Roy et Pr. Abdelkrim. Azzouz.

Pour finir, je tiens à témoigner ici ma vive reconnaissance à mon mari pour son soutien inconditionnel et mes enfants qui ont donné à ce travail un goût spécial. J'exprime ma gratitude extrême à mes parents qui m'ont soutenue et encouragée tout au long de ce travail.

CONTENTS

LIST OF FIGURES

LIST OF SCHEMES

LIST OF TABLES

LIST OF ABREVIATIONS

AOP	Advanced Oxidative Processes
BPA	Bisphenol-A
CEC	Cation Exchange Capacity
CO_2	Carbon Dioxide
COD	Chemical Oxygen Demand
CRC	Carbon Dioxide Retention Capacity
EE2	17α-ethinylestradiol
H_2O	Water
HPLC-ToF-MS	High-Performance Liquid Chromatography-Time-of-Flight Mass Spectrometry
LAB	Lewis-Acid-Base
MB	Methylene Blue
MG	Methyl Green
MO	Methyl Orange
Mt	Montmorillonite
MTB	Methylthymol Blue
SBA	Santa Barbara Amorphous type materials
SEM	Scanning Electron Microscopy
TOC	Total Organic Carbon
TPD	Thermal Programmed Desorption

WRC	Water Retention Capacity
XRD	X-Ray Diffraction

LIST OF SYMBOLS AND UNITS

A	Absorbance
^{o}C	Degree Celsius
g	Gram
h	Hour
k	Reaction Rate Constant
L	Liter
M	Molar
min	Minutes
n	Reaction Order
nm	Nanometer
Sec	Second
V	Volt
λ	Wavelength

RÉSUMÉ

Cette étude fournit des données fondamentales utiles sur la manière dont les matériaux argileux peuvent agir en tant que catalyseurs efficaces dans l'oxydation des polluants organiques. Le concept original consiste à démontrer que les aluminosilicates naturels ont des propriétés intrinsèques à peine explorées lors de l'élimination des polluants organiques et que l'activation par un acide commode et peu coûteuse peut considérablement améliorer leur activité catalytique. L'obtention de l'élimination complète des polluants organiques en quelques minutes sans traces résiduelles de dérivés dangereux est une nouveauté en soi. À cette fin, nous avons abordé une approche judicieuse pour comprendre le comportement à la fois de la surface du catalyseur et des molécules de polluants organiques en corrélant l'activité catalytique aux propriétés acide-base et au caractère hydrophile. À notre connaissance, une telle approche n'a encore jamais été abordée. Les résultats obtenus ici fournissent des données fondamentales pour la conception d'un processus efficace visant l'élimination totale des polluants organiques, quelle que soit leur structure.

MOTS-CLÉS : Ozonation catalytique; Catalyseurs à base d'argile; Polluants organiques; Procédés d'oxydation avancée.

ABSTRACT

The present study provides useful fundamental data on how clay materials can act as effective catalysts in the oxidation of organic pollutants. The original concept resides in demonstrating that natural aluminosilicates have intrinsic properties that have barely been explored in organic pollutant removal and convenient and low cost acid-activated can markedly improve their catalytic activity. Achieving complete removal of organic pollutants in few minutes without residual traces of hazardous derivatives is a novelty by itself. For this purpose, we tackled a judicious approach to understand the behavior of both the catalyst surface and organic pollutants molecules by correlating the catalytic activity with the acid-base-properties and hydrophilic character. To the best of our knowledge, such an approach has never been tackled so far. The results obtained herein provide fundamental data for designing effective process aiming total removal of organic pollutants regardless to their structures.
We strongly believe that this work will be of high interest to a wide range of scientists, researchers in chemistry, chemical and environmental engineering and other data users.

KEYWORDS: Catalytic ozonation; Clay catalyst; Organic pollutants; Advanced Oxidation Processes.

INTRODUCTION

L'eau est le principal constituant des êtres vivants et demeure l'élément indispensable à toute forme de vie. Elle recouvre plus de 71% de la surface du globe terrestre mais seulement 2,6% de la masse d'eau est douce. De cette masse, moins de 1% est directement accessible et le reste est stocké sous forme de glace. La raréfaction des eaux douces et le problème de la pollution par les matières organiques rendent l'accès à une eau propre potable plus difficile et plus chère.

La forte croissance démographique, l'industrialisation et l'agriculture intensives ont largement contribué à la dégradation de la qualité des eaux. En effet, elle représente une préoccupation à l'échelle planétaire qui suscite un intérêt au sein de la communauté scientifique. Ces eaux sont fortement riches en colorants, en pesticides, en médicaments, en produits pharmaceutiques, en métaux lourds…etc [1, 2]. Le rejet direct de ces polluants dans le milieu aquatique sans traitement préalable présente des risques pour la santé humaine et pour la biodiversité. Certains de ces composés ont été reconnus pour leurs effets cancérigènes, mutagènes ou susceptibles d'interférer avec le système hormonal des êtres vivants [3, 4]. Du fait de leur complexité structurale et de leur stabilité élevée ils ne peuvent pas être résorbés par les processus naturels d'autoépuration. Pour résoudre cette problématique, plusieurs techniques de traitement comme l'adsorption, la coagulation-floculation, la précipitation, l'échange d'ions et la séparation membranaire ont été utilisées.

Cependant, ces méthodes semblent inefficaces pour une minéralization complète de certains contaminants organiques réfractaires [5, 6]. Ainsi que l'utilisation de certains produits chimiques commencent à susciter des inquiétudes et préoccupation. Plusieurs

études ont montré que la présence de traces des ions d'aluminium dans les eaux potables peut provoquer la maladie d'Alzheimer ainsi que de fortes concentrations en fer provoquent la maladie de Parkinson. Le tableau 1 présente les principaux bénéfices et inconvénients de quelques procédés utilisés pour le traitement d'eaux contenant des polluants organiques

Tableau 1 Principaux avantages et inconvénients des méthodes classiques de taritement des eaux.

Procédé	Avantages	Inconvénients
Coagulation-Précipitation	Coût très abordable; Mise en œuvre relativement simple;	production de boues; Adjonction de produits chimiques; Coagulant non réutilisable;
Filtration membranaire	Bonne capacité d'élimination cations métalliques; Pas d'ajout de produits chimiques;	Risque de colmatage et coût élevés; Sélectif;
Echange d'ions	Bonne capacité d'élimination d'une grande variété de pollluants;	Nécessité de régénérer la résine; Coût des solvants de régénération élevé;
Adsorption	Technologie simple Faible coût d'utilisation pour certains adsorbants;	Lent et limité en volume; Sélectif; Nécessité de régénérer l'adsorbant;

Afin de réduire le coût de traitement et d'augmenter son efficacité des nouvelles techniques nommées les procédés d'oxydation avancée (POA) ont été développées. Certaines de ces méthodes sont capables de minéraliser complétement la matière organique en dioxyde de carbone, en eau et autres composés minéraux (SOx, NOx) [7-13]. Parmi les POA, l'ozonation et plus particulièrement l'ozonation catalytique ont montré une efficacité appréciable pour une minéralisation complète et rapide de polluants organiques.

L'ozonation est une voie intéressante pour la dégradation des polluants organiques, mais l'ozonation seule ne conduit pas à une minéralisation complète des molécules organiques réfractaires [14, 15]. Cela est dû à la faible solubilité de l'ozone dans l'eau. Cette dernière conduit à une forte consommation d'énergie ceci entraîne souvent une accumulation de sous-produits organiques résiduels, souvent plus toxiques que la molécule mère. Ces derniers sont généralement des aldéhydes, des cétones et/ou des acides organiques à chaîne courte. Dans le but d'augmenter l'efficacité de l'ozonation, l'ozone a été couplé au peroxyde d'hydrogène, aux rayons ultra-violets et à des catalyseurs métalliques.

1. Système ozone / peroxyde d'hydrogène

La décomposition de l'ozone en présence de peroxyde d'hydrogène est initiée par la forme dissociée de H_2O_2. L'attaque très rapide de l'anion HO_2^- sur une molécule d'ozone conduit à la formation de radicaux hydroxyles. Même si ce système est plus efficace que l'ozonation seule, son efficacité est limitée par la vitesse de réaction entre O_3 et H_2O_2 et la faible solubilité de l'ozone, et dépend de plusieurs paramètres tels que les caractéristiques phisico-chimiques des eaux à traiter, les concentrations d'oxydants utilisés et la structure des molécules à dégrader.

2. Système ozone / UV

En phase aqueuse, l'absorption des radiations UV par l'ozone engendre du peroxyde d'hydrogène (Eq 1) qui initialise sa décomposition en radicaux hydroxyles (Eq 2). Ainsi l'irradiation UV accroît la dégradation des polluants organiques par la formation des radicaux hydroxyles. L'efficacité de ce système dépend du type et de la turbidité de l'effluent à traiter. La pénétration du rayonnement ultraviolet dans l'eau trouble est faible.

$$O_3 + H_2O + h\nu \rightleftharpoons H_2O_2 + O_2 \qquad \text{(Eq 1)}$$

$$O_3 + H_2O_2 \rightleftharpoons HO^{\cdot} + HO_2^{\cdot} + O_2 \qquad \text{(Eq 2)}$$

$$HO^{\cdot} + \text{polluant organique} \rightleftharpoons \text{produits} \qquad \text{(Eq 3)}$$

3. Système ozone / catalyseur

3.1. Catalyse en phase homogène

La catalyse est homogène lorsque le catalyseur se trouve dans la même phase que les réactifs et les produits. Le catalyseur peut être un solide dissous dans un milieu aqueux ou un gaz dans un mélange gazeux. Plusieurs ions métalliques sont utilisés dans la catalyse en phase homogène tels que Ti^{2+}, Mn^{2+}, Cu^{2+}…etc. Les ions métalliques ont montré une efficacité, mais leur pouvoir catalytique n'est digne d'intéerêt que pour certains polluants organiques, d'où le recours au couplage du peroxyde d'hydrogène aux ions ferreux (réaction Fenton), qui peut s'appliquer à toutes les substrats organiques quelles que soient leurs strutures.

Procédés Fenton

Ce procédé a été découvert en 1894 par Henry J. Fenton mais fait encore l'objet d'un grand nombre de recherches dans le domaine du traitement des eaux. La réaction de Fenton est basée sur la production des radicaux hydroxyles à partir de la décomposition du peroxyde d'hydrogène catalysée par des sels ferreux selon la réaction (4) :

$$Fe^{2+} + H_2O_2 \longrightarrow OH^{\cdot} + HO^{-} + Fe^{3+} \qquad (Eq\ 4)$$

Le procédé Fenton est un procédé efficace, facile à contrôler et relativement peu coûteux. Néanmoins, ce procédé est limité par le manque de régénération du catalyseur et nécessite un apport constant en réactif. De plus, l'obligation de traiter en milieu acide (pH≈ 3) peut limiter l'utilisation de cette technique.

3.2. Catalyse en phase hétérogène

La catalyse est hétérogène lorsque le catalyseur forme une phase distincte de celle des réactifs et/ou des produits. Le cas le plus courant est celui d'un catalyseur solide dans un milieu aqueux ou gazeux. L'utilisation d'un catalyseur solide s'est déjà révélée être une stratégie judicieuse en raison de l'implication de l'adsorption dans le processus d'ozonation catalytique [16, 17]. Il améliore l'efficacité de l'ozone en augmentant sa solubilité dans l'eau. Des études ont montré que l'ozonation en présence d'un catalyseur solide nécessite presque 4 fois moins d'ozone que sans catalyseur, et cela permet de réduire le coût du traitement. Contrairement aux catalyseurs dissous, leurs homologues solides peuvent être récupérés et réutilisés.

Plusieurs types de catalyseurs ont été testés pour améliorer l'ozonation des polluants organiques comme les oxydes mixtes, le charbon actif, les zéolites, les pseudos-zéolites, la silice et les minéraux argileux [12, 18-21]. Ces derniers ont déjà montré des performances appréciables dans l'élimination de polluants organiques par minéralisation totale. À cela, il faut ajouter d'autres avantages de ce genre de matériaux que sont leur disponibilité naturelle, le coût réduit de leur conditionnement sous formes de catalyseurs et leur recyclabilité.

Parmi les différentes familles d'argile, la montmorillonite a connu un essor considérable dans l'ozonation catalytique ces dernières années [8, 12, 14, 22]. L'intérêt croissant porté à ce matériau se justifie par sa surface spécifique élevée, sa capacité d'échange cationique, sa porosité, sa structure lamellaire, son faible coût et son abondance naturelle. De plus, il ne représente aucun risque pour l'environnement. Les cations interfoliaires sont échangeables et peuvent être facilement modifiés selon le type de polluant à traiter. La montmorillonite est une argile appartenant au groupe des smectites. Elle est de type 2/1, qui signifie qu'un feuillet de montmorillonite est constitué d'une couche octaédrique $Al_2(OH)_6$ comprise entre deux couche tétraédriques $(SiO_4)_4$. Les ions Al^{3+} des couches octaédriques peuvent être remplacés par Mg^{2+} ou Fe^{2+}. Ces substitutions entraient un déficit de charges négatives qui est compensé par les cations compensateurs.

Objectif de ce mémoire

L'ozonation des polluants organiques en présence d'un catalyseur solide de type aluminosilicate a fait l'objet de peu d'études et le mécanisme de dégradation n'est pas clairement défini. C'est dans ce contexte que s'inscrit ce travail. En effet, ce dernier consiste en la dégradation avancée des polluants organiques par l'ozonation en présence d'un catalyseur argileux en solution aqueuse. De plus, il permet de comprendre le principe de l'ozonation catalytique hétérogène. Pour cela, trois classes

de polluants ont été pris comme modèle: les colorants, le bisphénol A et l'ethinylestradiol. Chacun d'entre eux représente un secteur industriel, à savoir les colorants représentent l'industrie textile, le bisphénol A - l'industrie du plastique et l'ethinylestradiol - l'industrie pharmaceutique. Deux types de montmorillonite ont été préparés. La première montmorillonite a été modifiée par le sodium (Na^+) et/ou par le fer (Fe^{2+}). En effet, l'échange cationique permet à la fois de modifier le cation interfoliaire mais aussi d'augmenter la surface spécifique. La deuxième montmorillonite a été activée par un acide fort afin d'augmenter son caractère organophilique et modifier les propriétés acido-basiques de surface.

Ce mémoire est structuré en trois parties.

La première partie de ce travail porte sur l'étude de la dégradation de quelques colorants organiques par l'ozonation catalytique en présence de la montmorillonite (Mt). Cette dernière est un aluminosilicate capable de manifester des interactions optimales acide-base et hydrophobe avec des espèces organiques dans l'eau par simple purification et modification du matériau de départ (bentonite ou montmorillonite). Ces propriétés influencent fortement l'équilibre d'adsorption-désorption des intermédiaires d'ozonation et produits, dont la présence induit des fluctuations de pH qui déterminent la charge et la dispersion des lamelles de Mt. Les intermédiaires moins oxydés doivent se comporter différemment des acides à chaîne courte par rapport à la surface de l'argile. Une connaissance plus approfondie de la basicité de surface du catalyseur et de son caractère hydrophile peut permettre d'élucider les interactions du catalyseur avec le polluant organique, l'eau et l'ozone en corrélation avec les structures à la fois du catalyseur et de la molécule de colorant. Cet objectif a été réalisé grâce à la technique de désorption thermoprogrammée (TPD) du dioxyde de carbone (CO_2) et de l'eau (H_2O), qui fournit également la distribution de la force des sites d'adsorption. Des tests comparatifs d'ozonation de différents colorants organiques ont été effectués en présence de montmorillonites échangées ioniquement (NaMt et Fe(II)Mt), de bentonites brute et activées par un acide (HMt) à différents temps d'activation. Les

phénomèmes de surface étudiés sont discutés en termes d'interactions électrostatique, acido-basiques et hydrophobe et de contribution de l'étape d'adsorption à la cinétique du processus global. À notre connaissance, une telle approche n'a jamais été abordée.

La deuxième partie de cette recherche s'est fixée comme objectif une dégradation avancée d'un polluant conventionnel reconnu pour son impact négatif à long terme sur la santé humaine et la biodiversité. Il s'agit du Bisphénol A, qui a été soumis à l'ozonation dans l'eau en présence de divers types de catalyseurs qui diffèrent par leur rapport Silice/Alumine. La variation de ce rapport offre une gamme variée de catalyseurs allant de la silice pure (SBA-15) à diverses montmorillonites ayant différentes teneurs en silice, alumine et cations échangeables. La corrélation de l'activité catalytique avec la basicité de la surface et le caractère hydrophile (déterminés par TPD), le potentiel zêta et la taille des particules permet d'avoir des données qui peuvent expliquer le rôle des groupes silanols en termes d'interactions acide-base de Lewis entre les réactifs, l'eau et la surface du catalyseur.

La troisième partie est consacrée à l'ozonation d'un autre type de polluant impliqué dans la soi-disante ''féminisation des espèces vivant en milieux aquatiques''. Il s'agit d'un agent estrogène dit ''l'ethinylestradiol (EE2)''. La faible solubilité dans l'eau de EE2 a consitué un défi difficile à surmonter, car l'ozonation devait se réaliser en milieu aqueux sans solvant. Pour des raisons de coût et de rentabilité du procédé, la décomposition de EE2 a été réalisée en présence des mêmes catalyseurs que précédemment. Les résultats ont été mis en corrélation avec la densité de charge de surface, les propriétés acido-basiques et le caractère hydrophile du catalyseur. Ceci a été rendu possible grâce aux données obtenues par la technique de désorption thermoprogrammée (TPD) du CO_2 et de l'eau, du potentiel zêta et de la taille des particules. Cela a permis d'expliquer le processus catalytique hétérogène en termes d'interactions acide-base de Lewis entre les espèces chimiques impliquées et le caractère hydrophile de la surface du catalyseur. À cette fin, les performances de

différents types de catalyseurs, à savoir la bentonite brute et ses équivalents purifiés et échangés par des ions (NaMt et Fe(II)Mt) ont été étudiées. L'identification des intermédiaires par chromatographie liquide à haute performances couplée à la spectrométrie de masse avec temps de vols (HPLC-ToF-MS a permis d'élucider le rôle de l'adsorption du polluant par diverses interactions dans l'activité du catalyseur.

Ce mémoire se termine par une conclusion générale qui fournit les fondements expliquant l'action de catalyseurs de types aluminosilicates dans l'ozonation de trois types de substrat organiques. Le travail entrepris ouvre de grandes perspectives à l'utilisation de matériaux argileux, peu couteux et très disponibles dans des procédés économiques et écologiques de traitement d'eaux contaminées. Ce travail a ouvert de nouvelles brèches en recherche, qui méritent d'être poursuivies par des études supplémentaires visant à réduire le coût du procédé et la consommation d'énergie.

Structure de mémoire :

Ce mémoire est rédigé sous forme de trois articles soumis dont un a déjà été publié. Il comporte cinq parties : l'introduction générale, trois articles sous formes de chapitres, ainsi qu'une conclusion générale et quelques perspectives.

CHAPITRE I

ARTICLE I: ACID-TREATED CLAY CATALYSTS FOR ORGANIC DYE OZONATION – THOROUGH MINERALIZATION THROUGH OPTIMUM CATALYST BASICITY AND HYDROPHILIC CHARACTER

Farida Boudissa[a], Diana Mirilà[b], Alisa-Vasilica Arus[b], Thizizi Terkmani[a], Sirène Semaan[a], Mélanie Proulx[a], Ileana-Denisa Nistor[b], Rné Roy[a], Abdelkrim. Azzouz[a,*]

[a] *Nanoqam, Department of Chemistry, University of Quebec at Montreal, QC, Canada H3C 3P8.*

[b] *Catalysis and Microporous Materials Laboratory, Vasile-Alecsandri University of Bacau, Romania.*

**Correspondence: azzouz.a@uqam.ca; Tel: 1 514-987-3000, ext. 4119*

Publié dans le Journal of Hazardous Materials : Journal of Hazardous Materials 364 (2019) 356-366.

Contribution des co-auteurs

Ma contribution personnelle à cet article: Réalisation des expériences, obtention des résultats et traitement des données, conception des figures et des tableaux, essais d'interprétation des résultats. Rédaction préliminaire de l'article.

Mirilà Diana : Réalisation des tests expérimentaux complémentaire.

Vasilica-Alisa Arus : Synthèse et caractérisation complète des bentonites activées à l'acide.

Terkmani Thizizi : Réalisation des tests expérimentaux préliminaires.

Semaan Sirène : Réalisation des tests expérimentaux préliminaires.

Proulx Mélanie : Réalisation de mesures par thermo-désorption programmée de la basicité et du caractère hydrophile des bentonites activées à l'acide.

Ilena-Denisa Nistor : Échanges de résultats de tests expérimentaux sur l'ozonation de colorants organiques.

Roy René : Correction de l'article.

Azzouz Abdelkrim : Conception et direction de la recherche sur l'ozonation des polluants organiques, vérification et corrections des interprétations des résultats, finalisation de l'article, soumission de l'article et initiation de l'étudiante au processus de soumission.

CHAPITRE I

ARTICLE I: ACID-TREATED CLAY CATALYSTS FOR ORGANIC DYE OZONATION – THOROUGH MINERALIZATION THROUGH OPTIMUM CATALYST BASICITY AND HYDROPHILIC CHARACTER

Abstract

Catalytic ozonation of Methylene Blue, Methyl Green, Methyl Orange and Methyl-thymol Blue was investigated in the presence of ion-exchanged montmorillonite (NaMt and Fe(II)Mt), crude bentonite and acid-activated counterparts. An original approach never tackled so far consisted in correlating the basicity and hydrophilic character to the dye-catalyst interactions occurring on the catalyst surface. This was achieved through CO_2 and water thermal programmed desorption. Kinetics study revealed that ozonation starts in the bulk solution, and dye adsorption turns out to be an essential requirement for high catalytic effectiveness. On NaMt, dye molecules appear to adsorb mainly via hydrophobic interaction. On Fe(II)Mt, the contributions of hydrophobic interaction, cation-exchange and Fe^{2+} mobility to the catalytic activity prevail. Acid activated clay catalysts exhibited lowest hydrophilic character favoring adsorption through organophilic interaction and affording thorough and fast dye mineralization. This was explained in terms of increased number of silanols and -Si-O-Si- groups. For all catalysts, short ozonation of all dye molecules resulted in similar end-chain products, which were totally eliminated after prolonged reaction times. This result is of great

importance because it provides valuable theoretical findings that allow envisaging total mineralization of organic molecules by recyclable metal-free clay catalysts.

1.1 Introduction

Textile manufacturing is undoubtedly the major source of dye-rich wastewaters [1,2], which can generate a wide variety of harmful oxidized derivatives once released in nature [3–6] with negative impacts on aquatic media and biodiversity [7] even at low concentration. Primary water treatments are well recognized to be quite unsatisfactory [8,9], and should be completed by effective techniques such as Advanced Oxidation Processes (AOPs) that lead to total mineralization of organic pollutants [10–17]. Among AOPs, ozonation is an energy-consuming method but undoubtedly the most eco-friendly and convenient route, requiring low investment and operating cost with small devices that can be implemented where needed. Unlike other oxidative treatments such as Fenton process, photooxidation, ozonation and their combined variants [10,11,18–23], catalytic ozonation can rapidly decompose a wide variety of dyes in aqueous solutions into harmless oxides [24–26] and refractory short chain acids [15,27–30].

However, total mineralization of organic substrates often requires higher ozone consumption than necessary due to the low solubility in water. Catalytic ozonation may allow overcoming this drawback, and solid catalysts appear as being much more interesting because dissolved catalysts are potential sources of water contamination [31,32]. In addition, solid catalysts should enhance reactant adsorption and/or concentration in the vicinity of the surface [33,34]. Those displaying high porosity and specific surface area should show high efficiency in this regard [35].

Catalysts may convert ozone into highly reactive radical species [36], reducing the ozonation time [37]. In some cases, they also improve the mineralization process [38].

Many types of catalysts [11] such as activated carbon [39–41], zeolites and clay minerals [15,42] and even pure silica [24,43] have been tested in the oxidation of organic pollutants in most wastewaters. The latter usually become acidic once oxidized by free air, and the resulting acidity fluctuations may influence their interactions with the catalyst, more particularly aluminosilicates (AS). In optimal pH and catalyst amount, AS showed improved catalytic activity in the total mineralization of fairly refractory organic compounds such as oxalic acid [11,15,18], due to enhanced clay exfoliation, cations release and reactant concentration in the vicinity of the solid surface.

Montmorillonite (Mt) is a low cost and widely available aluminosilicate that can acquire optimal acid-base and hydrophobic interactions with organic species in water through mere and convenient purification and modification. These properties strongly influence the adsorption-desorption equilibrium of ozonation intermediates and products, whose presence usually induces pH fluctuations that determines the charge and dispersion of Mt lamellae. Less oxidized and bulkier intermediates must behave differently as compared to short chain acids with respect to the clay surface. Deeper insights in the catalyst basicity and hydrophilic character can allow elucidating the catalyst interactions with the organic substrate, water and ozone in correlation with the structures of both the catalyst and dye molecule. This is the main objective of this work that was achieved through thermal programmed desorption (TPD) of carbon dioxide (CO_2) and water, which also provided the strength distribution of the adsorption sites. Comparative ozonation tests of different organic dyes were performed in the presence of ion-exchanged (NaMt and Fe(II)Mt), crude bentonite and acid-activated counterparts (HMt). The investigated interactions are herein discussed in terms of electrostatic and hydrophobic interaction and contribution of the adsorption step to the

process kinetics. To the best of our knowledge, such an approach has never been tackled so far.

1.2 Experimental

1.2.1 Materials and methods

Two cationic dyes (Methylene Blue, MB and Methyl Green, MG) and two anionic counterparts (Methyl Orange, MO and Methylthymol Blue, MTB) provided by MERCK (USA) were used as probe molecules (Table S1.1). The clay catalysts were prepared starting from a crude bentonite (1.24 μm particle size) supplied by Sigma-Aldrich (USA). For simulating dye-rich wastewaters after primary treatments, aqueous 10^{-4} M dye solutions were prepared by dissolving accurately weighted amount of dyestuff in deionized and nanopure water.

1.2.2 Catalyst preparation

Dye ozonation was investigated in the presence of ion-exchanged montmorillonite (NaMt and Fe(II)Mt), crude bentonite and acid-activated counterparts (HMt). The starting bentonite was previously purified into a fully ion-exchanged Na^+-montmorillonite-rich material (NaMt) through repeated impregnation with 2–5 M aqueous NaCl solutions at 80 °C for 4–5 h under vigorous stirring and periodical ash removal after settling [15]. Fe(II)Mt was obtained through NaMt impregnation with aqueous Fe^{2+} solution ($FeCL_2.4H_2O$). The choice of these two catalysts was based on previous works [15,18,44]. NaMt and Fe(II)Mt were further washed with distilled water and then repeatedly dialyzed in cellophane bags immersed in fresh distilled water

until no chloride was detected by $AgNO_3$ test in the dialysate. Both catalysts were recovered by centrifugation and then air-dried at 40 °C overnight.

For deeper insights in the effect of silicon content, additional catalysts (HMt-1, HMt-4, HMt-8, HMt-15 and HMt-24) were prepared through acid activation of bentonite. For this purpose, 200 g clay samples were impregnated by 1000 mL of aqueous 5 M sulphuric acid solution at 80 °C for various contact times (1, 4, 8, 15 and 24 h, respectively) under mild stirring as fully described elsewhere [45–47]. The powders were recovered by filtration, repeatedly washed with distilled water until neutral pH and dried at 100 °C for 12 h. The as activated bentonite samples were softly ground and sieved into a 75 μm particle size (200 mesh ASTM).

1.2.3 Catalyst characterization

All catalysts including crude bentonite were characterized by X-ray diffraction (Siemens D5000, CuKα, λ = 1.54051 Å), while their chemical compositions were assessed through X-ray fluorescence (S-4 Pioneer equipment; Brüker Rh tube; Powder press 34 mm with 10% boric acid; standardless method with 0.5% error) as already reported [47]. The marked sharpening of the broad 001 XRD reflection after bentonite purification and full ion-exchange into NaMt and Fe(II)Mt accounts for a perfectly parallel arrangement of the clay lamellae. No crystallinity loss was noticed for bentonite samples acid-treated for 1–15 hours, and only slight depletion of the XRD line was observed for the sample treated for 24 h. The particle size was determined using a Malvern-Zetasizer Nanoseries in water and in aqueous dye solutions, while the Zeta potential was assessed with a Brookhaven instrument. The surface basicity and hydrophilic character were evaluated through Thermal Programmed Desorption measurements of carbon dioxide (CO_2-TPD) and moisture (H_2O-TPD) under a 15 mL min^{-1} nitrogen stream with a 5 °C min^{-1} heating rate from 22 to 450 °C. Thus, non

dehydrated catalysts (45–50 mg) with 0.1–0.2 mm particle size were introduced in the glass tubular oven (2 mm internal diameter) coupled to a Li-840 A dual CO_2/H_2O Gas Analyzer (Li−COR Bioscience Inc., USA) and further contacted with dry and pure N60 grade CO_2 till saturation for 20–30 minutes. The excess CO_2 was purged at room temperature under dry N_2 flow prior to TPD runs. H_2O-TPD measurements were achieved through the same procedure. The basicity and hydrophilic character were estimated from the area described by the TPD pattern and expressed in terms of CO_2 and water retention capacities (CRC and WRC, respectively) [48–51].

1.2.4 Ozonation tests

Ozonation tests were performed in different samples exposed to various ozonation times at room temperature (RT) in cylindrical PVC vessels (28 × 115 mm) containing 20 mL samples of 10^{-4} M aqueous solutions of organic substrates at intrinsic initial pH. The dye solutions were previously prepared using deionized and nanopure water. Ozone was produced from air using a portable A_2Z-AQUA-6 ozone generator (A_2Z Ozone Inc., USA), and bubbled in each 20 mL sample at a constant 600 mg h^{-1} throughput. After 10 s of bubbling the ozone concentration reaches a constant concentration of ca. 0.40-0.45 mol L^{-1}, as assessed by conventional iodometry using aqueous solutions of KI (O.2 M) HCl (2 M) and $Na_2S_2O_3$ (0.05 M). For the kinetical study additional ozonation attempts were run for reaction times below 1 min.

1.2.5 Ozonation products analysis

After ozonation and catalyst removal by centrifugation, the supernatant each ozonated sample was analyzed by UV–Vis spectrophotometry using a 1 cm quartz cell and a Varian-Cary 5000 instrument (Agilent Technologies, USA). Highly linear calibration plots (Fig. S1.1-S1.2) and accurate assessment of the molar absorptivity (Table S1.2) were achieved between 190 nm and 800 nm only within the $0\text{-}10^{-5}$ M dye concentration range. This range turned out to be suitable for detecting slight fluctuations of all UV–Vis bands during ozonation and for accurate estimation of the dye removal yield (Equation S1).

The evolution in time of the ozonation process for all UV–Vis bands was assessed through determination of the residual concentration using calibration curves with 1–2% accuracy (Fig. S1.1-S1.2). The dye conversion yield was calculated using the UV–Vis bands appearing at the highest wavelength, with a standard deviation of 2%. For the sake of accuracy, the reaction mixture was also analyzed by liquid chromatography (HPLC, Waters 2487 Dual λ absorbance detector coupled to a Waters- Alliance 2695 equipment, 100 mm x 4.6 mm C18 column with a 3.5 µm particle size and a 0.5 mL min^{-1} throughput of a 95:5 water-acetonitrile mobile phase, UV–Vis detector) and its time of Flight - mass spectrometry variant (HPLC-ToF-MS, Agilent 1200 Series HPLC instrument, Agilent Eclipse plus C18 column (3 × 50 mm, particle size1.8 µm) at RT. The dye conversion yield was mainly estimated by HPLC using calibration curves. Full details are providing as supporting information. After optimized ozonation, only carbonic acid was detected, but traces of formic, acetic and oxalic acids were also identified in other conditions.

1.3 Results and discussion

1.3.1 Effect of initial dye concentration on non-catalytic ozonation

Quick tests of 5 min ozonation of the studied dyes induced marked changes of the UV–Vis spectra, characterized by a total discoloration of the respective aqueous solutions of MB, MTB and MO (Fig. 1.1). MB displayed initially seven absorption bands, which significantly depleted after five min ozonation, except the 234 nm band (Fig. 1.1a). The total disappearance of the 660 nm band and its splitting derivative at 614 nm as a result of partial dimerization in water indicates a complete degradation of the phenyl ring and C–S^{+}=C bond [52–56]. This is confirmed by the marked decay in intensity of the 498 and 403 nm bands attributed to the resonance of this conjugated system [57]. Traces of MG still persist under similar ozonation conditions. Color persistence indicates incomplete phenyl ring cleavage after 5 min ozonation (Fig. 1.1b).

Similarly, marked depletion of the 465, 277 and 200 nm bands for MO (Fig. 1.1c) and the 612, 444, 293 and 204 nm bands for MTB (Fig. 1.1d) were noticed. For MO, an attenuation of the π-π* transition (277 nm) due to the –N= N– azo group located on the aromatic rings under the strong influence of the electron-donating dimethylamino group is expected [58,59]. Among the five UV–Vis bands of MG, those persisting at 253 and 320 nm and attributed to π-π* transitions of the aromatic rings and n-π* transitions, respectively [60] indicate a slightly higher chemical stability as compared to the other counterparts.

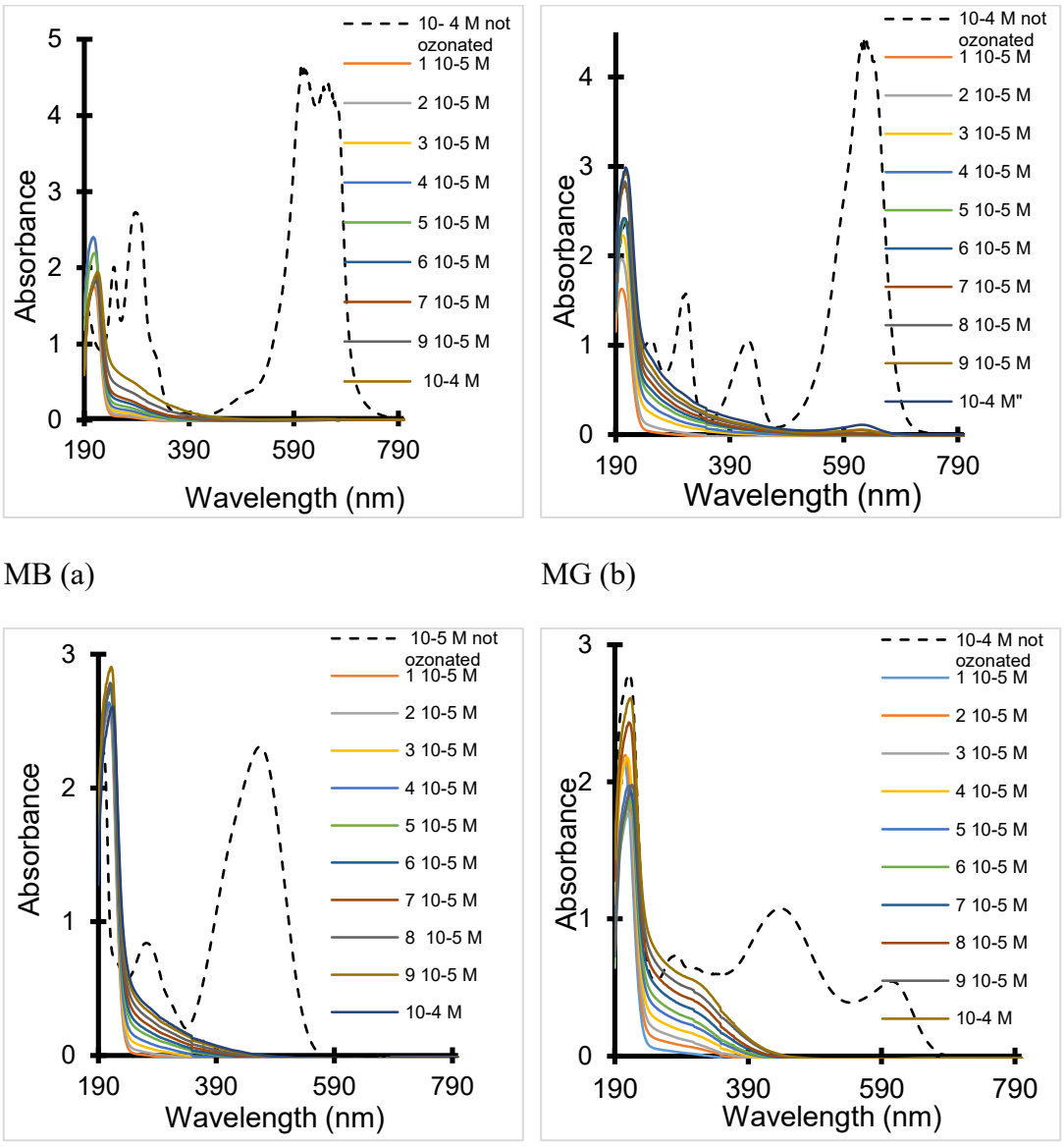

Fig. 1.1. Effect of the concentration on the UV–Vis spectra of MB, MG, MO and MTB after 5 min ozonation in distilled water. T = 22 °C. pH = intrinsic value. Quartz cell = 1 cm. O_3 throughput: 600 mg h^{-1}. Sample volume = 20 mL. Initial dye concentration: 10^{-4} M.

As a general tendency, all band absorbances decreased with decreasing dye concentration, i.e. when ozone is bubbled in excess with respect to the dye amount. Increasing dye concentration resulted in lower ozonation efficiency, as supported by the increase in intensity of the residual UV–Vis bands remaining after discoloration (Fig. 1.2).

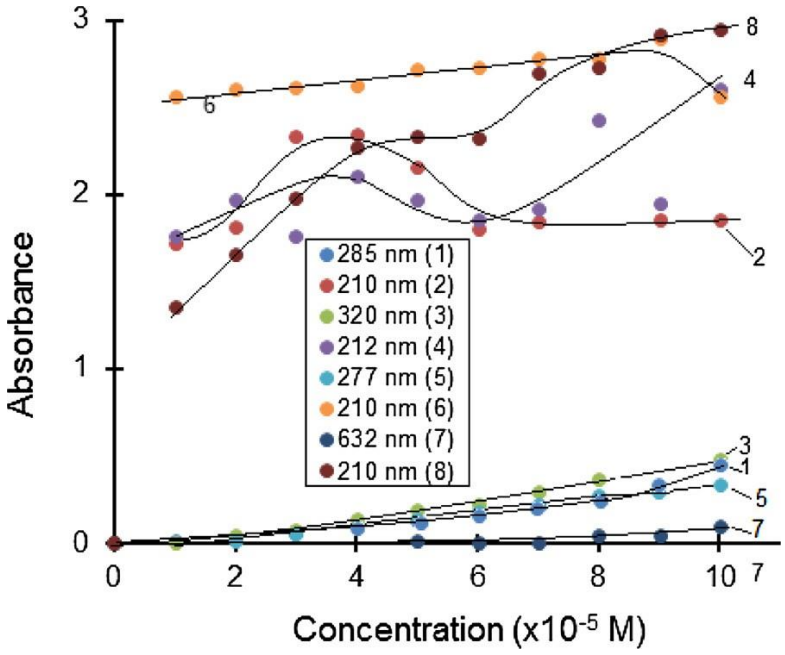

Fig. 1.2. Evolution of the absorbance of the residual UV–Vis bands after 5 min ozonation of MB (1–2), MTB (3–4), MO (5–6) and MG (7–8) in distilled water. T = 22 °C. pH = intrinsic value. Quartz cell = 1 cm. O_3 throughput: 600 mg h^{-1}. Sample volume = 20 mL. Initial dye concentration: 10^{-4} M.

This intensity increase appears to be much more pronounced for the 210–212 nm UV bands (2, 4, 6 and 8), most probably due to the formation of oxidized derivatives and H-bridge interaction with water. The other bands (1, 5 and 7) totally disappeared after 5 min for dye concentration below 2×10^{-4} M. Thus, ozonation is suitable for diluted solutions [61], as justified by the choice of the concentration range.

1.3.2 Evolution in time of non-catalytic ozonation

Deeper insight in the effect of the ozonation time revealed marked intensity depletion for most bands (Fig. S1.3). Paradoxically, the intensity of those appearing at 214–220 nm increased in time (Fig. 1.3), due to the formation of oxidized species, possibly including short chain acids.

The total disappearance of the 498 and 403 nm bands of MB after only 1 min ozonation was accompanied by a total discoloration of the solution after 2 min. This is supported by the marked depletion of the 660 nm, which indicates a fast degradation of the chromophore [24].

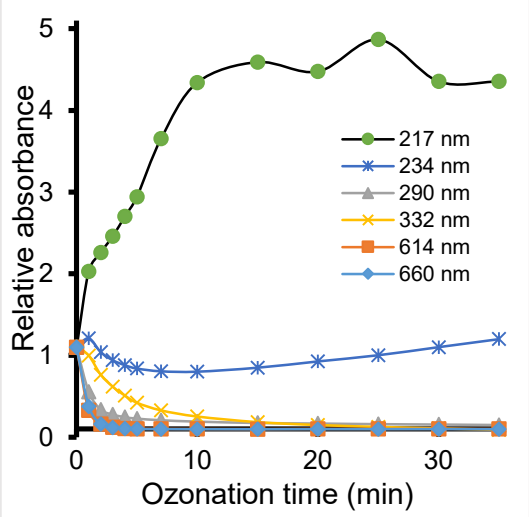

MB

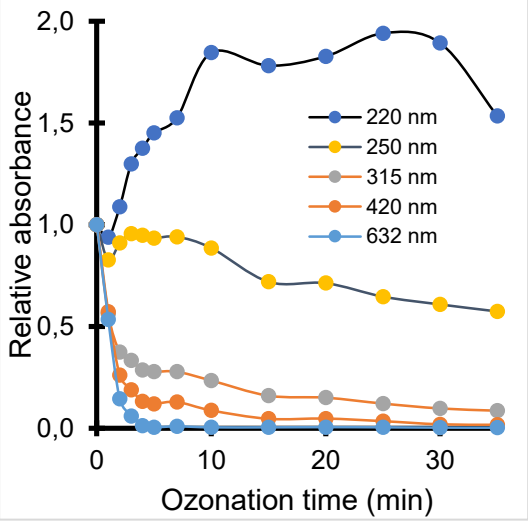

MG

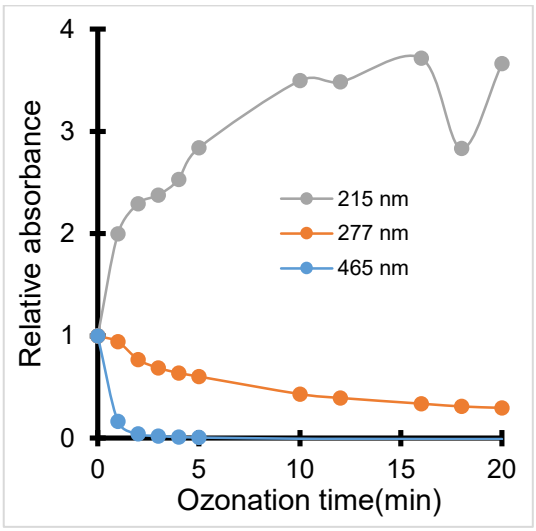

MO

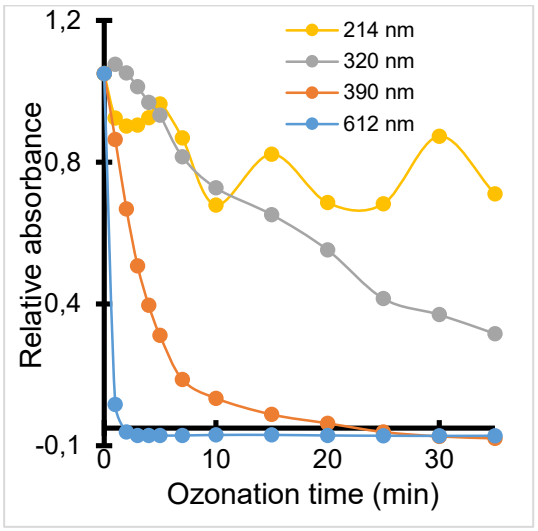

MTB

Fig. 1.3. Evolution in time of the relative absorbance of cationic (MB, MG) and anionic (MTB, MO) dyes during ozonation in distilled water. T = 22 °C. pH = intrinsic value. Quartz cell = 1 cm. O_3 throughput: 600 mg h^{-1}. Sample volume = 20 mL. Initial dye concentration: 10^{-4} M.

A progressive disappearance in time of the 332 nm band and the rise of a band at 217 nm were also observed, suggesting the formation of oxidized derivatives as confirmed further by HPLC-ToF-MS analysis. This is a common behavior of MO and MG, which slight differs for MTB. Here, the molecular structure of the dye should play a key role [62,63], since unlike for MG, the 465 nm band of MO totally disappeared after 2 min ozonation due to a direct and fast ozone attack on the azo group (-N=N-) [64]. It is worth mentioning that after 5 min ozonation MTB displayed the lowest relative absorbances and presumably highest reactivity to ozone. This must be due to its high molecular weight, given that the chemical stability against ozone decreases with increasing molecular size [11,24,65].

Analysis of the effect of the ozone-to-dye ratio revealed that ca. 10000–60000 ozone molecules per dye molecule are needed for the total disappearance of the visible bands in the absence of catalyst. This accounts for large amounts of unused ozone, whose solubility in water is the main constraint. For comparable ozone dosages, non catalytic ozonation gave higher conversions yields as those reported for more oxidized chemical species, but in the same magnitude as other organic molecules [10,11,15,18,24,65].

1.3.3 Effect of clay catalyst addition

Catalyst addition resulted in more pronounced changes in time of the relative absorbances of most UV–Vis bands below 350 nm, due to the formation of oxidized derivatives [24,43,65]. Simultaneously, fast discoloration of the dye solution was noticed, as supported by the total disappearance of the visible bands of MB beyond 400 nm in less than 5–10 min ozonation (Fig. 1.4).

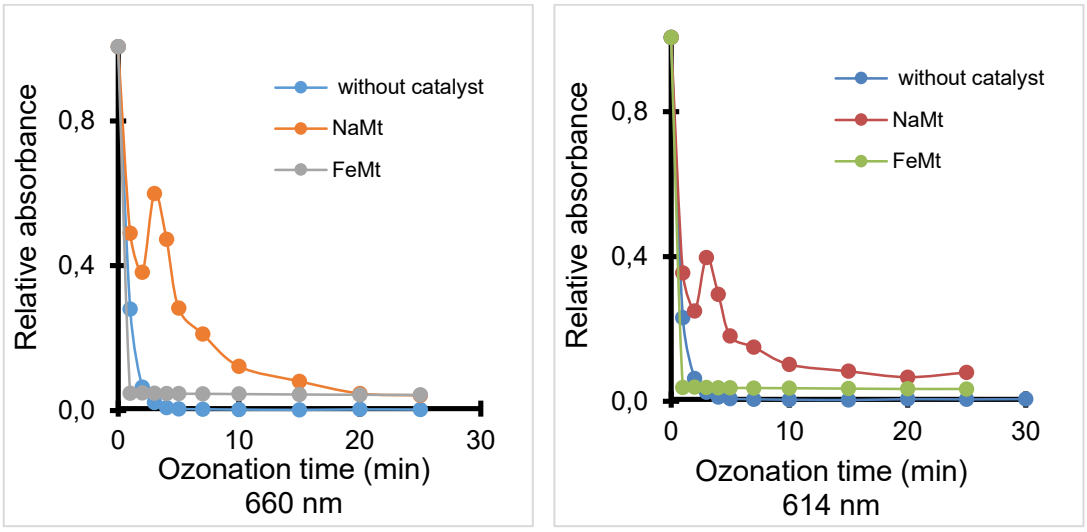

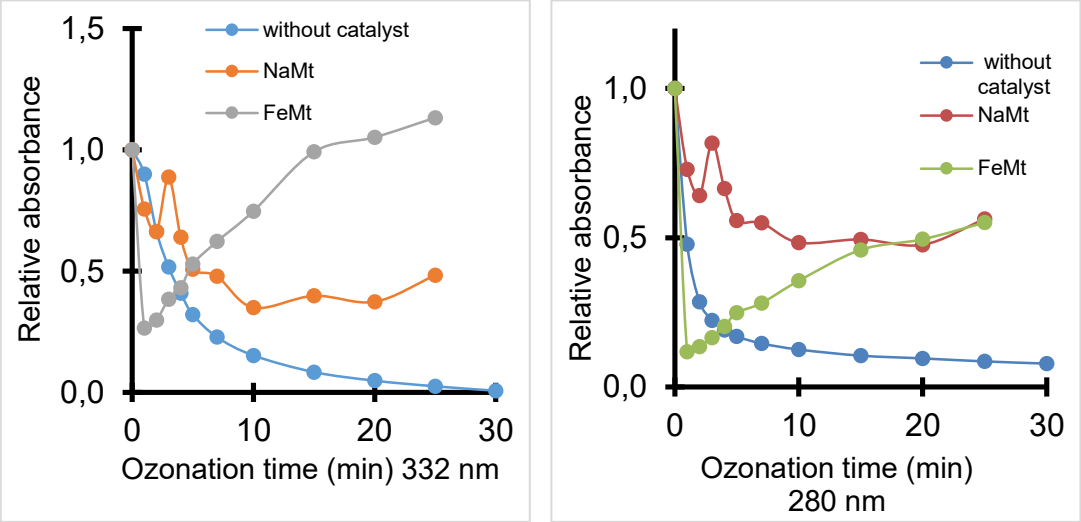

Fig. 1.4. Evolution in time of the relative absorbance of MB during ozonation in distilled water. T = 22 ° C. pH = intrinsic value. Quartz cell = 1 cm. O_3 throughput: 600 mg h^{-1}. Sample volume = 20 mL. Initial dye concentration: 10^{-4} M. Catalyst amount = 40 mg of dry catalyst.

Addition of NaMt produced noticeable changes in the UV–Vis spectra of all dye molecules (Fig. S1.5). This agrees with the specific ozone consumption by each structural group of a given dye molecule (Fig. S1.6-S1.7). The effect of catalyst addition appears to differ depending on the UV–Vis band and exchangeable cation (Fig. S1.11-S1.13).

Fe(II)Mt showed higher activity in the discoloration of cationic molecules (MB and MG), as supported by a faster decay of the 660 nm band as compared to NaMt. Deeper insights in process kinetics and catalyst surface properties could be useful in this regard.

1.3.4 Ozonation kinetics

Model validation for all UV–Vis bands based on R^2 values close to unity (0.9965-0.9995) (Tables S1.3-S1.5) showed that ozonation fits better 1st order kinetics during the three first minutes of ozonation without and with catalyst, when a first and fast step triggers in the aqueous dye solution with a constant ozone concentration due its low solubility, generating most intermediates [15,24,65].

$$Ln\left(\frac{C_0}{C_t}\right) = k_1.t \qquad (1)$$

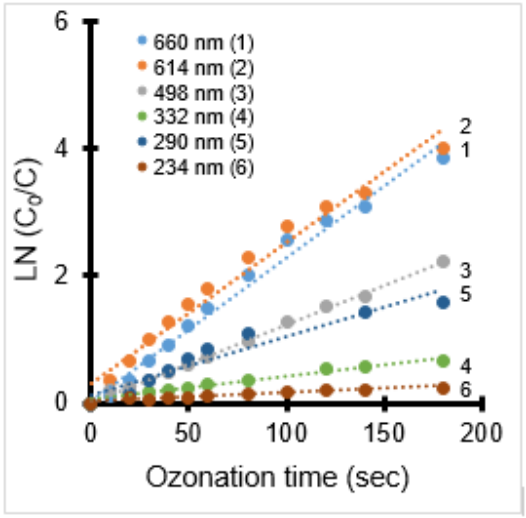

MB

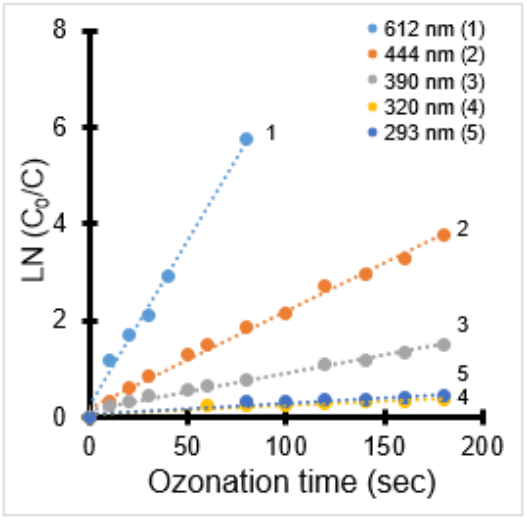

MTB

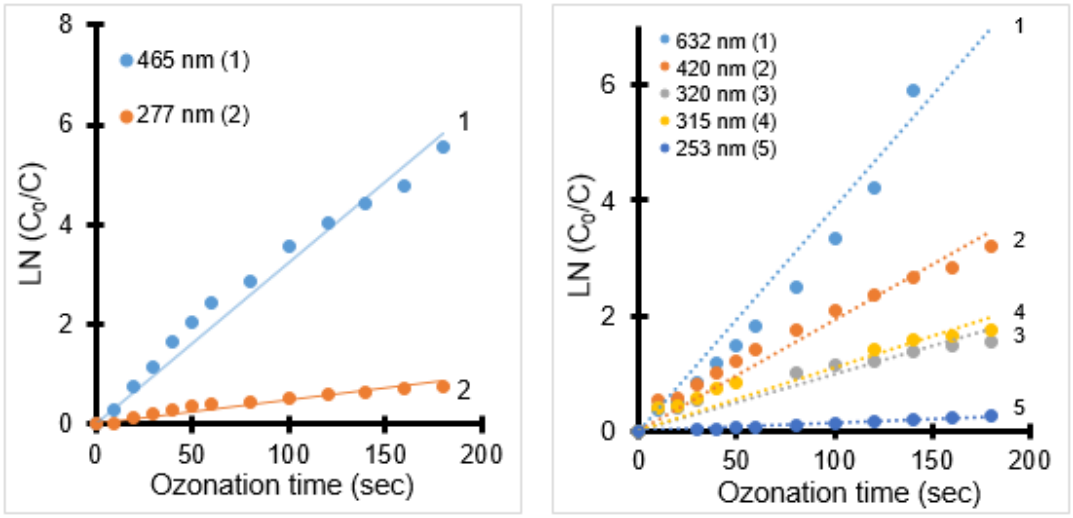

MO MG

Fig. 1.5. First-order plot for non-catalytic dye ozonation kinetics.

High linearity of Eq. (1), where C_0 is the initial concentration value of the dye, C_t - the instant concentration and k_1 - the first order rate constant, and t is the time was obtained for most UV–Vis bands (Fig. 1.5). For almost all dye UV–Vis bands, the 1st order model was validated when excluding the first 10–100 seconds of ozonation, presumably due to the slow ozone dissolution. This variable delay from an UV–Vis band to another for a given dye molecule must be due to different reactivity of the structural groups, as supported by different rate constants. The fact that few R^2 values close to unity were also registered when applying both models for some UV–Vis bands suggests a mixture of 1st and 2nd order kinetics, presumably due to interactions between dye molecules and oxidized derivatives.

Catalyst addition should induce fluctuations in the ozone concentration in the bulk solution through adsorption. The predominance of the 2nd order kinetics for almost all UV–Vis band and higher rate constants for catalytic ozonation provide evidence of this contributions of the catalyst surface and exchangeable cation.

1.3.5 Effect of exchangeable cation on dye adsorption

Crude bentonite gave lower dye conversion yield not exceeding 25–35%. This lower catalytic activity was already by the presence of carbonates and higher amounts of non smectitic impurities (quartz, cristoballite, carbonates,…). This is supposed to reduce the density of exchangeable cations and of surface charge [15,18,65]. The role of the exchangeable cation was reflected by higher dye degradation yield for Fe(II)Mt, than for NaMt, more particularly for cationic MG and MG molecules (Table S1.6). After 2 min ozonation, degradation yields of 60–92% as estimated by (1-C/Co) values for decreasing UV–Vis bands beyond 400 nm were registered in the presence of NaMt versus 78–99% for Fe(II)Mt (Table 1.1). More precise but almost similar values were obtained by HPLC with only slight discrepancy not exceeding 3–5% as compared to UV–Vis measurements.

Longer ozonation times of 20 min were required for achieving degradation yields of 69–100% for cationic dye and to 84–98% for anionic molecules with NaMt. These performances are much higher than those reported for many catalysts such as simple or metal-doped metal oxides, carbon nanotubes, zeolites and others for ozone dosages in the same magnitude order [11].

The higher effectiveness of Fe(II)Mt was already explained in terms of partial Fe^{2+} cations release in the vicinity of the catalyst in acidic media [10,11,15,65]. However, dye adsorption on Fe(II)Mt should also contribute to the catalytic process, as reflected by the almost total disappearance of the 660 nm band of MB after ca. 50 min (Fig. S1.14-a, S1.15-a). In the absence of ozone, mere dye adsorption produces similar depletion in time for all UV–Vis bands, but in the presence of ozone, increase in time of UV-bands below 400 nm is a precise index of the simultaneous occurrence of the

catalytic oxidation reaction and appearance of oxidized derivatives, as supported by HPLC-ToF-MS analyses.

Unlike with NaMt, much more pronounced Fe^{2+} release was observed with anionic dyes, which seem to act as ‘‘iron pump’’, as supported darker green-blue coloration of MTB solution and the significant increase in the relative intensity of the 612 nm band (Fig. S1.14-b, S1.15-b). This was found to reduce MTB degradation yield from 92% (612 nm) and 84% (446 nm) down to 49% (Table 1.1). However, excessive Fe^{2+} loss is expected to reduce the surface positive charge, thereby affecting adsorption of anionic dyes. Indeed, weaker adsorption was noticed for MTB as compared to MB in the absence of ozone. This was reflected by the fact that the 446 nm band of MTB did not disappear even after 50 min, compared to the total adsorption of MB illustrated by the total disappearance of the 660 nm band after only 25 min. Thus, it clearly appears that dye adsorption is an essential requirement for high catalytic effectiveness, and that electrostatic interaction prevails for certain dyes on certain catalysts. Here, ozonation should occur on the surface or nearby, where ozone concentration must also be influenced by adsorption phenomena, in agreement with the 2nd order kinetics.

Table 1.1. UV-Vis band removal yield (%) after ozonation with different clay catalysts

Dye molecule	UV-Vis bands (nm)	UV-Vis band evolution yield (%)[a]			
		After 02 min ozonation with		After 20 min ozonation with	
		NaMt	Fe(II)Mt	NaMt	Fe(II)Mt
MB	660	62	96	96	96
	614	77	97	100	97
	498	70	78	100	84
MG	632	77	96	91	97
	420	60	99	69	100
MO	465	92	96	98	98
MTB	612	73	-	92	49
	444	56	89	84	49

[a] Decreasing C/C_o for UV–Vis bands beyond 400 nm accounts for the actual decomposition yield of a dye molecule. The dye conversion yield was calculated with a standard deviation of 2%. HPLC measurements gave almost similar values of the conversion with 3–5% discrepancy with respect to the spectrophotometric measurements.

The bathochromic effect of the 660, 280 and 234 nm red shifted to 670, 296 and 250 nm can arise from diverse interactions between the non-binding electron pairs of dye N and S atoms, oxidized species and free water molecules. The magnitude of this effect is expected to strongly depend on the acid-base properties and hydrophilic character of the clay surface. Interesting, fast and almost thorough decomposition of MTB and MO was noticed after only 2 min with both NaMt and Fe(II)Mt. This result clearly demonstrates that the exchangeable cation plays a key role in the ozonation of cationic dye, and showed no influence in that of anionic molecules. Here, Fe^{2+} cation is expected to induce change in the initial pH of the reaction mixture, which, in turn, should involve electrostatic interactions in adsorption.

1.3.6 Role of silanols on dye adsorption

NaMt addition was found to raise the initial pH of MB, MG, MTB and MO solutions from 5.47, 5.12, 7.61 and 5.40, respectively to 6.77, 6.73, 7.96 and 7.76. This is supposed to confer neutral charges to cationic dyes (MB and MG) but negative charges to anionic ones (Table 1.2).

This should induce changes in water:dye interaction, as reflected by a bathochromic shift of the visible band beyond 600 nm of these molecules, explained in terms of molecule conformation [67]. For planar conformation, the π-π* transitions of aromatic

molecules produce red shift. Larger bathochromic shifts were ascribed to H-bridges with proton donors.

Table 1.2. Effect of exchangeable cation on the charge of dye molecules and silanol groups.

Without catalyst			With NaMt				With Fe(II)Mt			
Dye	pKa	pH[b]	pH[c]	Dye charge	Out-of-plane pKa=5.6[e]	In-plane pKa 8.5[e]	pH[d]	Dye charge	Out-of-plane pKa=5.6[e]	In-plane pKa=8.5[e]
MB	3.8	5.47	6.77	Neutral	SiO^-	$SiOH_2^+$ to neutral	2.52	R_3N^+	$SiOH_2^+$	$SiOH_2^+$
MG	0.2-1.8	5.12	6.73	Neutral	Neutral	$SiOH_2^+$ to neutral	2.57	Neutral	$SiOH_2^+$	$SiOH_2^+$
MTB	3.0 3.3 3.8 7.2-7.4 11.5 13.4	7.61	7.96	SO_3^- CO_2^-	Neutral	$SiOH_2^+$ to neutral	2.59	R_3N^+	$SiOH_2^+$	$SiOH_2^+$
MO	3.4-3.5	5.40	7.76	SO_3^-	Neutral	$SiOH_2^+$ to neutral	2.62	R_3N^+	$SiOH_2^+$	$SiOH_2^+$

[a] The charge of the exchangeable cation when hydrated, if any, is expected to bear less positive charge, due to water dissociation: $[Fe(H_2O)_x]^{2+} \rightarrow [Fe(H_2O)_{x-1}.OH]^{+} + H^+$.
[b] Intrinsic pH of the aqueous solution of the respective dye at room temperature.
[c] pH of the aqueous solution of the respective dye at room temperature after addition of NaMt without triggering the ozonation.
[d] pH of the aqueous solution of the respective dye at room temperature after addition of Fe(II)Mt without triggering the ozonation.
[e] These pKa values of the silanol groups are supposed to be similar to those of pure silica [63].

On one hand, by analogy with pure silica, deprotonation should prevail on NaMt at pH level higher than 2 [68], conferring negative to NaMt in the presence of all dye molecules. This agrees with the negative Zeta potential of NaMt and its increase after dye addition from -42.19 mV (Table 1.3) up to -52.59 mV (for MB), -50.2 mV (for MO) and -54.44 mV (on MTB) (Table S1.7). On the other hand, all pH values

(6.73–7.96) were comprised between the pKa values of out-of-plane (pKa = 5.6) and in-plane silanols (pKa = 8.5) of pure silica, which are assumed to also occur in aluminosilicates [66]. Under these conditions, silanol protonation, if any, should be very weak, and all silanols of NaMt are supposed to mostly exhibit slightly positive to neutral charge, except with MB (Table 1.2). This is supposed to slightly favor adsorption of anionic dyes (MTB and MO) which bear negative charges. The decrease in particle size is due to the low pHs (2.33–4.18) of the clay suspension, which induces higher clay dispersion as compared to NaMt.

Table 1.3. CRC, WRC, particle size of the investigated catalysts and induced Zeta potential and initial.

Catalyst	Activation time (h)	Si/Al mole ratio	Particle size (µm)	pH[a]	Zeta potential (±3.50 mv)[b]	Retention capacity [mmol.g^{-1}][c]		Initial pH after catalyst addition			
						CRC	WRC	MB	MG	MO	MTB
Bentonite	0	2.50	1.24	9.69	- 31.25	2.39	0.141	8.61	7.15	9.33	7.86
NaMt	0	2.50	6.49	8.77	- 42.19	3.82	0.112	6.77	6.73	7.76	7.96
Fe(II)Mt	0	2.50	2.45	2.33	+ 16.20	1.110	0.117	2.52	2.57	2.62	2.59
HMt-1	1	2.69	1.99	4.18	- 43.02	1.28	0760	3.97	3.65	4.79	4.68
HMt-4	4	3.00	2.04	4.15	- 38.36	1.04	0.682	3.90	3.58	4.74	4.37
HMt-8	8	3.47	2.14	4.04	- 43.12	1.18	0.623	3.76	3.41	4.28	4.01
HMt-15	15	4.03	2.26	3.92	- 42.18	1.06	0.501	3.72	3.43	4.25	4.13
HMt-24	24	4.36	2.35	3.96	- 37.62	1.38	0.528	3.83	3.61	4.54	4.53

[a]Average pH of the aqueous suspension of clay minerals at room temperature (Triplicate).

[b]These Zeta potential values were measured in the absence of dye molecules.

[c]The CO_2 and water retention capacity (CRC and WRC, respectively) were assessed with 3% accuracy through TPD measurements in the temperature range.20–450 °C.

Unlike anionic dyes, cationic dyes (MB and MG) should bear no charges, and should not adsorb via electrostatic interactions. No electrostatic adsorption is expected to occur on out-of-plane silanols which have predominantly neutral charges. The slight

contribution of electrostatic adsorption of anionic dyes to the catalytic process was reflected by relatively higher UV–Vis band removal yields (56–92%) as compared to their cationic counterparts (60–77%) after 2 min ozonation (Table 1.1). This tendency was somehow maintained even after 20 min.

With Fe (II)Mt, the initial pH decrease confers positive charges to all silanols groups and ammonium groups of most dye molecules but neutral charges on MG (Table 1.2). This is expected to impede electrostatic adsorption. The decrease in Zeta potential from 16.20 mV (Table 1.3) down to +13.00 mV (for MB), 3.90 mV (for MG), 7.32 mV (for MO) and 3.36 mV (on MTB) (Table S1.7) suggests a depletion of positively charged species on Fe(II)Mt, presumably due to Fe^{2+} cation release in the solution. This is consistent with the higher catalytic activity of Fe(II)Mt, inasmuch as Fe^{2+} mobility in the vicinity of the catalyst surface was already observed even at pH 2.8 [15]. This is supposed to produce a beneficial and non-selective effect for effective ozonation of all organic substrates [10,24,65] as reflected by removal yields in the same magnitude order for most UV–Vis band after 2 min ozonation (Table 1.1). This tendency was not maintained for MTB after 20 min ozonation, presumably due to specific Fe(II)Mt-intermediates interaction. The higher catalytic activity of Fe(II)Mt must rather involve Fe^{2+} cation mobility and adsorption via hydrophobic interaction. The latter should however be less pronounced than on NaMt, which displayed weaker hydrophilic character reflected by lower WRC (112 mmol g^{-1}) as compared to Fe(II)Mt (117 mmol g^{-1}) (Table 1.3).

The most significant factor in such a process is undoubtedly pH, which determines the catalytic activity and selectivity of aluminosilicates in ozonation processes in water. In neutral to acidic pH, ozone is stable, and barely starts decomposing beyond pH 9. Under these conditions, the oxidation reduction potential of ozone (ORP) almost remains at its highest level of 2.07 V, and should not vary significantly upon slight pH fluctuations, more particularly for relatively high ozone concentration in the range 0.4-0.45 mmol L^{-1}, as determined by conventional iodometry. This allows concluding that

the different performances of the investigated clay catalysts arise from their very structure and chemical composition that determine dye adsorption according to dye-catalyst interactions.

1.3.7 Acid-base properties and hydrophilic character

The key role of the silanol groups was herein demonstrated by deeper insights using iron-free bentonite samples obtained through acid activation at different contact times. Increasing Si/Al ratio was found to reduce markedly the initial pH in all dye solutions, but which still remains higher than those induced by addition of Fe(II)Mt. (Table 1.3). The negative values of the zeta potential of HMt samples must be due to silanol deprotonation beyond pH 2 similar to that reported for silica [68]. The low fluctuations of the zeta potential after dye addition can be included within the standard deviation range (+ 3.50 mV), suggesting only weak electrostatic dye-HMt interactions through silanol groups.

Higher Si contents are known to enhance the Lewis acidity at the expense of Bronsted acidity as a result of a depletion of the cation- exchange capacity of the clay catalyst [69–72]. This was confirmed by a significant decay of the surface basicity, expressed in terms of decrease in CO_2 retention capacity (CRC) from 2.39 mmol g^{-1} for bentonite and 3.82 mmol g^{-1} for NaMt down to 1.28 mmol g^{-1} for HMt. NaMt and Fe(II)Mt exhibited different acid-base properties, which also differ from those of proton in HMt samples, as supported by specific TPD profiles (Fig. 1.6).

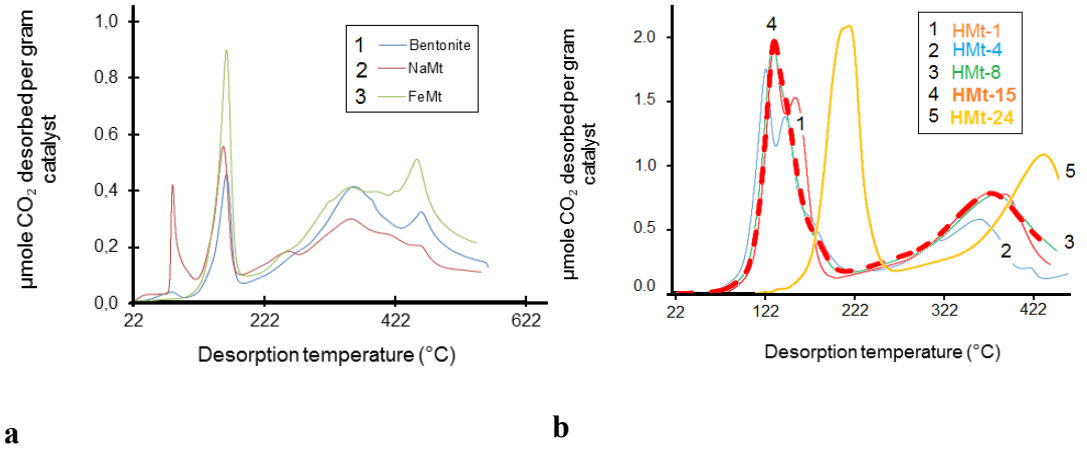

Fig. 1.6. CO_2-TPD profiles of clay catalysts (a) and their acid-activated counterparts (b).

Unlike Fe(II)Mt, NaMt displayed an additional desorption peak around 70–110 °C corresponding to weakly basic sites. In contrast, Fe(II)Mt is expected to display higher acidity and hydrophilic character, assuming that cation basicity decreases with increasing charge and decreasing size [72]. This was confirmed by a lower CRC of 1.11 mmol g^{-1} for Fe(II)Mt as compared to 3.82 mmol g^{-1} for NaMt, but higher water retention capacity (WRC) of 116.5 µmol g^{-1} as compared to NaMt (111.5 µmol g-1). Besides, Fe(II)Mt displays additional Bronsted acidity from the dissociation of water molecules surrounding hydrated Fe^{2+} cation ($[Fe(H_2O)_x]^{2+}$ $[Fe(H_2O)_{x-1}.OH]^{+-} + H^+$).

The resulting decreases of surface positive charge and proton release are expected to produce pH decrease leading to changes in dye:water, water:catalyst and dye:catalyst interactions. This can be accentuated by unavoidable protonation of both types of silanols, which will attract negatively charged SO_3^- and CO_2^- groups, favoring thereby adsorption of anionic MTB and MO dyes. Such interactions explain the red and blue shifts observed for the main UV–Vis bands of the dye molecules (Fig. S1.8-S1.10). For NaMt, this effect should have minor or no contribution because of its low hydration grade of Na^+ cation. The total disappearance of the 660, 614, 498, 403 and 332 nm

bands of cationic dye molecules after five minutes ozonation (Table 1.4) accounts for a faster decomposition of the phenyl and heteroaromatic rings and cleavage of the C-S^+=C bonds [73,74], in agreement with other works [15,75].

Table 1.4. UV-Vis band removal yield (%) after 05 min ozonation for acid-activated clay catalysts.

Dye	UV-Vis band (nm)	UV-Vis band removal yield (%) after 05 min ozonation[a]							
		Bentonite	NaMt	Fe(II) Mt	HMt-1	HMt-4	HMt-8	HMt-15	HMt-24
MB	660	94	72	96	100	100	100	100	100
	614	97	86	97	100	100	100	100	100
	498	89	105	80	100	100	100	100	100
	403	16	55	100	100	100	100	100	100
	332	75	49	47	98	99	100	100	100
	280	82	44	75	98	98	99	99	99
	234	24	-	-	85	84	84	84	84
MG	632	100	80	96	100	100	100	100	100
	420	99	60	99	100	100	100	100	100
	320	95	37	66	98	100	100	100	100
	253	72	-	14	93	95	97	95	95
MO	465	96	96	95	99	100	100	100	100
	277	2	-	-	86	90	90	89	90
	200	21	7	-	27	27	27	28	30
MTB	612	96	87	-	100	100	100	100	100
	444	89	70	92	92	94	95	94	93
	393	68	-	-	72	75	78	76	75
	204	-5	-	22	-	-	30	28	24

[a]The dye conversion yield was calculated using the UV-Vis bands appearing at the highest wavelength, with a standard deviation of 2%. HPLC measurements gave almost similar values of the conversion with 3-5% discrepancy.

The globally higher catalytic activity of HMt samples (Table 1.4) must arise from increased density of silanol and -Si-O-Si- and Si-OH groups that promote the hydrophobic character. This indicates the rise of more pronounced organophilic

interactions on HMts as compared to NaMt and Fe(II)Mt. These interactions should take place non-selectively with all dye molecules.

Weaker dye degradation was noticed for anionic dyes after 05 min ozonation, as supported by lower UV–Vis removal yields for the bands below 400 nm. Here, due to the absence of charges in MTB and MO at pH 3.92–4.18 induced by HMts (Table 1.3), adsorption of anionic dyes, if any, should involve mainly hydrophobic interactions, given the lowest hydrophilic character of HMts catalysts, which showed much lower WRC (50.1–75.5 μmol g^{-1}) than their non-activated counterparts (111.5–140.5 μmol g^{-1}). Obviously, the extent of the specific surface area (SSA) increased upon acid attack [47], and should play a key role in this regard. However, no correlation with the catalytic activity is possible due SSA variations in aqueous suspension of clay minerals due to the swelling and coagulation-flocculation capacities pH fluctuations.

1.3.8 Ozonation intermediates and products

As a common feature, ozonation of all dyes gave similar inter- mediates and products but in specific distributions according to the molecular structure. This is well argued by HPLC-ToF-MS analysis which revealed similar low-molecular weight organic products after ozonation of MB and MO without and with catalyst (Fig. S1.16). For MB, C-S^{+}=C group cleavage should be the first step of its oxidation into C-S(=O)-C [76,77]. Non-catalytic ozonation (a) produced various peaks at 270, 252, 241, 225, 137.95, 131.91,121 and 109.94 amu. The 270 amu peak accounts for 3-(dimethylamino)-7-(methylamino) phenothiazin-5-ium (Azur B $C_{15}H_{16}N_3S$), which results from CH_2 loss from the MB molecule.

The same products were also identified after Fe(II)Mt-catalyzed ozonation, but with lower intensity. The marked decrease in time of the peak intensity for the positive ion

of MB (m/z = 284) ($C_{16}H_{18}N_3S^+$) is a precise indicator of the beneficial role of Fe(II)Mt. The increase in time of the 109 amu peak in the presence of Fe(II)Mt catalyst corresponds to the formation of C_6H_7ON. The predominant peak at 121 amu ($C_8H_{11}N$) and those appearing at 137 amu and at 109.94 amu were attributed to N,N dimethyl benzenamine, $C_8H_{13}N_2$ (p-dimethylaminoaniline) and $C_3H_6O_2$, (propionic acid), respectively.

MO ozonation for 1 min produced the same peaks at 201,185 and 172.5 amu before and after addition of Fe(II)Mt (Fig. S1.17). Here, also, the predominant peaks at 121 amu, 137 ($C_8H_{13}N_2$) and 109.94 amu correspond to N,N dimethylbenzenamine, p-dimethylaminoaniline and propionic acid ($C_3H_6O_2$), respectively. Addition of Fe(II)Mt and NaMt led to significant improvements in dye removal, in agreement with other data [24,43,78]. Fe(II)Mt produced faster decay in time of the main UV–Vis bands as compared to NaMt, but resulted in similar short chain products.

1.4 Conclusion

The results obtained herein allow concluding that clay catalysts improve dye ozonation. CO_2 and water TPD measurements turned out to be a judicious approach to correlate the acid-base properties and hydrophilic character of the clay catalysts with the dye behavior in water. Electrostatic interactions appear to be essential for triggering adsorption and further ozonation of anionic dyes on NaMt, but adsorption of all dye molecules involves mainly hydrophobic interaction. On Fe(II)Mt, anionic dyes seem to act as " iron pump'', inducing massive iron release that reduce the surface positive charge and catalyst effectiveness. Thus, dye adsorption turns out to be an essential requirement for high catalytic effectiveness, and that electrostatic interaction prevails for certain dyes on certain catalysts. On Fe(II)Mt, the contributions of hydrophobic

interaction, cation-exchange and Fe^{2+} mobility to the catalytic activity should prevail. Acid activation produced a beneficial effect on the catalytic activity due increased density of silanols and -Si-O-Si- groups. Acid-activated clay catalysts produced complete dye degradation in shorter ozonation times, mainly via hydrophobic interaction that favors adsorption on the catalyst surface, given the lowest hydrophilic character of HMts catalysts as assessed by TPD. Slight silanol protonation in acidic media induced by HMt dispersion favors only weak adsorption of anionic dyes molecules through electrostatic interaction. Organophilic interaction should take place with all dye molecules. Regardless to the catalyst, short ozonation of all dye molecules produced similar short chain derivatives, which totally disappeared after prolonged reaction times. These findings provide fundamental knowledge for designing efficient technologies that target total mineralization of organic pollutants with neither water contamination by neither metals nor traces of persistent derivatives using low cost and natural aluminosilicate-based catalysts.

REFERENCES

[1] T. Robinson, G. McMullan, R. Marchant, P. Nigam, Remediation of dyes in textile effluent: a critical review on current treatment technologies with a proposed al- ternative, Bioresour. Technol. 77 (2001) 247–255.

[2] J.S. Do, M.L. Chen, Decolourization of dye-containing solutions by electro-coagulation, J. Appl. Electrochem. 24 (1994) 785–790.

[3] Y. Bulut, H. Aydın, A kinetics and thermodynamics study of methylene blue adsorption on wheat shells, Desalination 194 (2006) 259–267.

[4] P. Mokhtari, M. Ghaedi, K. Dashtian, M.R. Rahimi, M.K. Purkait, Removal of methyl orange by copper sulfide nanoparticles loaded activated carbon: kinetic and iso- therm investigation, J. Mol. Liq. 219 (2016) 299–305.

[5] B. Iurascu, I. Siminiceanu, D. Vione, M.A. Vicente, A. Gil, Phenol degradation in water through a heterogeneous photo-Fenton process catalyzed by Fe-treated la- ponite, Water Res. 43 (2009) 1313–1322.

[6] E. Hu, X. Wu, S. Shang, X.-m. Tao, S.-x. Jiang, L. Gan, Catalytic ozonation of simulated textile dyeing wastewater using mesoporous carbon aerogel supported copper oxide catalyst, J. Cleaner Prod. 112 (Part 5) (2016) 4710–4718.

[7] Y. Bulut, H. Aydın, A Kinetics and Thermodynamics Study of Methylene Blue Adsorption on Wheat Shells, (2006).

[8] M. Numata, T. Yarita, Y. Aoyagi, M. Yamazaki, A. Takatsu, Investigation of saponification for determination of polychlorinated biphenyls in marine sediments, J. Chemosphere. 58 (2005) 865–875.

[9] G.L. Northcott, K.C. Jones, Validation of procedures to quantify nonextractable polycyclic aromatic hydrocarbon residues in soil, J. Environ. Qual. 32 (2003) 571–582.

[10] A. Azzouz, Advances in oxidative decomposition of oxalic acid in aqueous media, in: J.C. Taylor (Ed.), Advances in Chemistry Research, Nova-Publishers, New-York, USA, 2012, pp. 1–31 2nd quarter.

[11] D. Shahidi, R. Roy, A. Azzouz, Advances in catalytic oxidation of organic pollutants– prospects for thorough mineralization by natural clay catalysts, Appl. Catal., B 174-175 (2015) 277–292.

[12] H. Ma, B. Wang, X. Luo, Studies on degradation of Methyl Orange wastewater by combined electrochemical process, J. Hazard. Mater. 149 (2007) 492–498.

[13] I.M. Sasidharan Pillai, A.K. Gupta, Effect of inorganic anions and oxidizing agents on electrochemical oxidation of methyl orange, malachite green and 2,4-dini- trophenol, J. Electroanal. Chem. 762 (2016) 66–72.

[14] L. Xu, J. Wang, Fenton-like degradation of 2,4-dichlorophenol using Fe3O4 mag- netic nanoparticles, Appl. Catal. B: Environ. 123–124 (2012) 117–126.

[15] D. Shahidi, R. Roy, A. Azzouz, Total removal of oxalic acid via synergistic para- meter interaction in montmorillonite catalyzed ozonation, J. Environ. Chem. Eng. 2 (2014) 20–30.

[16] S. Karthikeyan, A. Titus, A. Gnanamani, A.B. Mandal, G. Sekaran, Treatment of textile wastewater by homogeneous and heterogeneous Fenton oxidation processes, J. Desalination 281 (2011) 438–445.

[17] A. Azzouz, Advances in oxidative oxidation of oxalic acid in aqueous media, in: J.C. Taylor (Ed.), Advances in Reserach Chemistry, Nova-Science Publishers, New- York, 2012.

[18] A. Azzouz, A. Kotbi, P. Niquette, T. Sajin, A.V. Ursu, A. Rami, F. Monette, R. Hausler, Ozonation of oxalic acid catalyzed by ion-exchanged montmorillonite in moderately acidic media, Reaction Kinetics, Mechanisms and Catalysis 99 (2010) 289–302.

[19] S.J. George, R. Gandhimathi, P.V. Nidheesh, S.T. Ramesh, Electro-Fenton oxidation of salicylic acid from aqueous solution: batch studies and degradation pathway, clean-Soil, Air, Water 42 (2014) 1701–1711.

[20] G. Moussavi, A.A. Aghapour, K. Yaghmaeian, The degradation and mineralization of catechol using ozonation catalyzed with MgO/GAC composite in a fluidized bed reactor, Chem. Eng. J. 249 (2014) 302–310.

[21] X. Li, Q. Zhang, L. Tang, P. Lu, F. Sun, L. Li, Catalytic ozonation of p-chlorobenzoic acid by activated carbon and nickel supported activated carbon prepared from petroleum coke, J. Hazard. Mater. 163 (2009) 115–120.

[22] J. Hoigné, H. Bader, Rate constants of reactions of ozone with organic and inorganic compounds in water-II: dissociating organic compounds, Water Res. 17 (1983) 185–194.

[23] R. Andreozzi, V. Caprio, A. Insola, R. Marotta, Advanced oxidation processes (AOP) for water purification and recovery, Catal. Today 53 (1999) 51–59.

[24] S. Larouk, R. Ouargli, D. Shahidi, L. Olhund, T.C. Shiao, N. Chergui, T. Sehili, R. Roy, A. Azzouz, Catalytic ozonation of Orange-G through highly interactive contributions of hematite and SBA-16 – to better understand azo-dye oxidation in nature, Chemosphere 168 (2017) 1648–1657.

[25] İ. Arslan, I. Akmehmet Balcioğlu, T. Tuhkanen, Oxidative treatment of simulated dyehouse effluent by uv and near-UV light assisted Fenton's reagent, Chemosphere 39 (1999) 2767–2783.

[26] H.S. Lade, T.R. Waghmode, A.A. Kadam, S.P. Govindwar, Enhanced biodegradation and detoxification of disperse azo dye Rubine GFL and textile industry effluent by defined fungal-bacterial consortium, International Biodeterioration & Biodegradation 72 (2012) 94–107.

[27] P.C.C. Faria, J.J.M. Órfão, M.F.R. Pereira, Mineralisation of coloured aqueous solutions by ozonation in the presence of activated carbon, Water Res. 39 (2005) 1461–1470.

[28] P.C.C. Faria, J.J.M. Órfão, M.F.R. Pereira, Ozone decomposition in Water catalyzed by activated carbon: influence of chemical and textural properties, Ind. Eng. Chem. Res. 45 (2006) 2715–2721.

[29] S. Pirgalıoğlu, T.A. Özbelge, Comparison of non-catalytic and catalytic ozonation processes of three different aqueous single dye solutions with respect to powder copper sulfide catalyst, Appl. Catal. A: Gen. 363 (2009) 157–163.

[30] S. Tang, D. Yuan, Q. Zhang, Y. Liu, Q. Zhang, Z. Liu, H. Huang, Fe-Mn bi-metallic oxides loaded on granular activated carbon to enhance dye removal by catalytic ozonation, Environ. Sci. Pollut. Res. 23 (2016) 18800–18808.

[31] X.F. Zhu, X.H. Xu, The mechanism of Fe (III)-catalyzed ozonation of phenol, J. Zhejiang Univ. Sci. 5 (2004) 1543–1547.

[32] D.S. Pines, D.A. Reckhow, Effect of dissolved cobalt(II) on the ozonation of oxalic acid, Environ. Sci. Technol. 36 (2002) 4046-4051.

[33] D. Chatterjee, S. Dasgupta, R.S. Dhodapkar, N.N. Rao, Simultaneous degradation of non-emissive and emissive dyes on visible light illuminated TiO_2 surface, J. Mol. Catal. A: Chem. 260 (2006) 264-268.

[34] F.J. Beltrán, F.J. Rivas, R. Montero-de-Espinosa, Catalytic ozonation of oxalic acid in an aqueous TiO_2 slurry reactor, Appl. Catal., B 39 (2002) 221-231.

[35] S. Chaliha, K.G. Bhattacharyya, Using Mn(II)-MCM41 as an environment-friendly catalyst to oxidize phenol, 2-chlorophenol, and 2-nitrophenol in aqueous solution, Ind. Eng. Chem. Res. 47 (2008) 1370-1379.

[36] J. Wu, L. Ma, Y. Chen, Y. Cheng, Y. Liu, X. Zha, Catalytic ozonation of organic pollutants from bio-treated dyeing and finishing wastewater using recycled waste iron shavings as a catalyst: removal and pathways, Water Res. 92 (2016) 140-148.

[37] K. Yong, J. Wu, S. Andrews, Heterogeneous catalytic ozonation of aqueous reactive dye, Ozone: Sci. Eng. 27 (2005) 257-263.

[38] H. Jung, H. Choi, Catalytic decomposition of ozone and para-chlorobenzoic acid (pCBA) in the presence of nanosized ZnO, Appl. Catal. B: Environ. 66 (2006) 288–294.

[39] F.J. Beltrán, F.J. Rivas, L.A. Fernández, P.M. Álvarez, R. Montero-de-Espinosa, Kinetics of catalytic ozonation of oxalic acid in water with activated carbon, Ind. Eng. Chem. Res. 41 (2002) 6510-6517.

[40] J.P. Kaptijn, The Ecoclear® Process. Results from full-scale installations, Ozone: Sci. Eng. 19 (1997) 297-305.

[41] U. Jans, J. Hoigné, Activated carbon and carbon black catalyzed transformation of aqueous ozone into OH-radicals, Ozone: Sci. Eng. 20 (1998) 67-90.

[42] J.-N. Park, J. Wang, K.Y. Choi, W.-Y. Dong, S.-I. Hong, C.W. Lee, Hydroxylation of phenol with H_2O_2 over Fe^{2+} and/or Co^{2+} ion-exchanged NaY catalyst in the fixed-bed flow reactor, J. Mol. Catal. A: Chem. 247 (2006) 73-79.

[43] R. Ouargli, S. Larouk, I. Terrab, R. Hamacha, N. Benharrats, A. Bengheddach, A.Azzouz, Intrinsic activity of SBA-like silica in the catalytic ozonation of organic pollutants, Ozone: Sci. Eng. 38 (2016) 48-61.

[44] D. Shahidi, A. Moheb, R. Abbas, S. Larouk, R. Roy, A. Azzouz, Total mineralization of sulfamethoxazole and aromatic pollutants through Fe^{2+}-montmorillonite catalyzed ozonation, J. Hazard. Mater. 298 (2015) 338-350.

[45] M.A. Didi, B. Makhoukhi, A. Azzouz, D. Villemin, Colza oil bleaching through optimized acid activation of bentonite. A comparative study, Appl. Clay Sci. 42 (2009) 336-344.

[46] B. Makhoukhi, M.A. Didi, D. Villemin, A. Azzouz, Acid activation of bentonite for use as a vegetable oil bleaching agent, Grasas Aceites 60 (2009) 343-349.

[47] V.A. Arus, S. Nousir, R. Sennour, T.C. Shiao, I.D. Nistor, R. Roy, A. Azzouz, Intrinsic affinity of acid-activated bentonite towards hydrogen and carbon dioxide, Int. J. Hydrogen Energy 43 (2018) 7964-7972.

[48] A. Azzouz, A.-V. Ursu, D. Nistor, T. Sajin, E. Assaad, R. Roy, TPD study of the reversible retention of carbon dioxide over montmorillonite intercalated with polyol dendrimers, Thermochim. Acta 496 (2009) 45-49.

[49] A. Azzouz, D. Nistor, D. Miron, A.V. Ursu, T. Sajin, F. Monette, P. Niquette, R. Hausler, Assessment of acid–base strength distribution of ion-exchanged mon- tmorillonites through NH_3 and CO_2-TPD measurements, Thermochim. Acta 449 (2006) 27-34.

[50] A. Azzouz, D. Messad, D. Nistor, C. Catrinescu, A. Zvolinschi, S. Asaftei, Vapor phase aldol condensation over fully ion-exchanged montmorillonite-rich catalysts, Appl. Catal., A 241 (2003) 1-13.

[51] S. Nousir, N. Platon, K. Ghomari, A.-S. Sergentu, T.C. Shiao, G. Hersant, J.-Y. Bergeron, R. Roy, A. Azzouz, Correlation between the hydrophilic character and affinity towards carbon dioxide of montmorillonite-supported polyalcohols, J. Colloid Interface Sci. 402 (2013) 215-222.

[52] A. Mills, J. Wang, Photobleaching of methylene blue sensitised by TiO_2: an ambiguous system? J. Photochem. Photobiol., A 127 (1999) 123-134.

[53] C. Yogi, K. Kojima, N. Wada, H. Tokumoto, T. Takai, T. Mizoguchi, H. Tamiaki, Photocatalytic degradation of methylene blue by TiO_2 film and Au particles-TiO_2 composite film, Thin Solid Films 516 (2008) 5881–5884.

[54] P.A.R. Tafulo, R.B. Queirós, G. González-Aguilar, On the "concentration-driven" methylene blue dimerization, Spectrochim. Acta Part A: Mol. Biomol. Spectrosc. 73 (2009) 295-300.

[55] K. Patil, R. Pawar, P. Talap, Self-aggregation of Methylene Blue in aqueous medium and aqueous solutions of Bu4NBr and urea, Phys. Chem. Chem. Phys. 2 (2000) 4313-4317.

[56] A. Ghanadzadeh, A. Zeini, A. Kashef, M. Moghadam, Concentration effect on the absorption spectra of oxazine1 and methylene blue in aqueous and alcoholic solutions, J. Mol. Liq. 138 (2008) 100-106.

[57] H. Hichem, A. Djamila, A. Hania, Optical, electrical and photoelectrochemical characterization of electropolymerized poly methylene blue on fluorine doped tin oxide conducting glass, Electrochim. Acta 106 (2013) 69-74.

[58] C. Galindo, P. Jacques, A. Kalt, Photodegradation of the aminoazobenzene acid orange 52 by three advanced oxidation processes: UV/H_2O_2, UV/TiO_2 and VIS/TiO_2: comparative mechanistic and kinetic investigations, J. Photochem. Photobiol. A: Chem. 130 (2000) 35-47.

[59] T. Shen, C. Jiang, C. Wang, J. Sun, X. Wang, X. Li, A TiO2 modified abiotic-biotic process for the degradation of the azo dye methyl orange, RSC Adv. 5 (2015) 58704-58712.

[60] X. Ren, Z. Hu, H. Hu, R. Qiang, L. Li, Z. Li, Y. Yang, Z. Zhang, H. Wu, Noncovalently- functionalized reduced graphene oxide sheets by water-soluble methyl green for supercapacitor application, Mater. Res. Bull. 70 (2015) 215-221.

[61] A. Khataee, M. Sheydaei, A. Hassani, M. Taseidifar, S. Karaca, Sonocatalytic removal of an organic dye using TiO_2/Montmorillonite nanocomposite, Ultrason. Sonochem. 22 (2015) 404-411.

[62] J. Qu, H. Li, H. Liu, H. He, Ozonation of alachlor catalyzed by Cu/Al_2O_3 in water, Catal. Today 90 (2004) 291–296.

[63] L. Zhao, J. Ma, Z.-z. Sun, Oxidation products and pathway of ceramic honeycomb-catalyzed ozonation for the degradation of nitrobenzene in aqueous solution, Appl. Catal. B: Environ. 79 (2008) 244-253.

[64] J.M. Joseph, H. Destaillats, H.-M. Hung, M.R. Hoffmann, The sonochemical degradation of azobenzene and related azo dyes: rate enhancements via Fenton's reactions, J. Phys. Chem. A 104 (2000) 301-307.

[65] D. Shahidi, A. Moheb, R. Abbas, S. Larouk, R. Roy, A. Azzouz, Total mineralization of sulfamethoxazole and aromatic pollutants through Fe^{2+}-montmorillonite catalyzed ozonation, J. Hazard. Mater. 298 (2015) 338-350.

[66] M. Sulpizi, M.-P. Gaigeot, M. Sprik, The silica–water interface: how the silanols determine the surface acidity and modulate the water properties, J. Chem. Theory Comput. 8 (2012) 1037-1047.

[67] G. Rytwo, S. Nir, M. Crespin, L. Margulies, Adsorption and interactions of methyl green with montmorillonite and sepiolite, J. Colloid Interface Sci. 222 (2000) 12-19.

[68] B.M. Lowe, C.K. Skylaris, N.G. Green, Acid-base dissociation mechanisms and energetics at the silica-water interface: an activationless process, J. Colloid Interface Sci. 451 (2015) 231-244.

[69] J.A. Lercher, A. Jentys, Application of microporous solids as catalysts, Handbook of Porous Solids, Wiley-VCH Verlag GmbH, 2008, pp. 1097–1156.

[70] R.J. Gorte, Surface acidity, Handbook of Porous Solids, Wiley-VCH Verlag GmbH, 2008, pp. 432-464.

[71] M. Elanany, M. Koyama, M. Kubo, E. Broclawik, A. Miyamoto, Periodic density functional investigation of Lewis acid sites in zeolites: relative strength order as revealed from NH3 adsorption, Appl. Surf. Sci. 246 (2005) 96-101.

[72] J. Weitkamp, M. Hunger, Chapter 22 - acid and Base catalysis on zeolites, in: J. Čejka, H. van Bekkum, A. Corma, F. Schüth (Eds.), Studies in Surface Science and Catalysis, Elsevier, 2007, pp. 787-835.

[73] M.A. Rauf, M.A. Meetani, A. Khaleel, A. Ahmed, Photocatalytic degradation of Methylene Blue using a mixed catalyst and product analysis by LC/MS, Chem. Eng. J. 157 (2010) 373-378.

[74] R. Zuo, G. Du, W. Zhang, L. Liu, Y. Liu, L. Mei, Z. Li, Photocatalytic degradation of methylene blue using TiO_2 impregnated diatomite, Adv. Mater. Sci. Eng. 2014 (2014) 7.

[75] M. Vinuth, H.S.B. Naik, B.M. Vinoda, H. Gururaj, N. Thomas, G. Arunkumar, Enhanced removal of methylene blue dye in aqueous solution using eco-friendly Fe (III)-montmorillonite, Mater. Today: Proc. 4 (2017) 424-433.

[76] A. Houas, H. Lachheb, M. Ksibi, E. Elaloui, C. Guillard, J.-M. Herrmann, Photocatalytic degradation pathway of methylene blue in water, Appl. Catal. B: Environ. 31 (2001) 145-157.

[77] L.V. Trandafilović, D.J. Jovanović, X. Zhang, S. Ptasińska, M.D. Dramićanin, Enhanced photocatalytic degradation of methylene blue and methyl orange by ZnO:Eu nanoparticles, Appl. Catal. B: Environ. 203 (2017) 740-752.

[78] N. Al-Hayek, B. Legube, M. Doré, Ozonation catalytique (FeIII/$A1_2O_3$) Du phénol et de ses produits d'ozonation, Environ. Technol. Lett. 10 (1989) 415-426.

CHAPITRE II

ARTICLE II: THOROUGH BISPHENOL-A REMOVAL THROUGH OZONATION WITH SILICA-BASED CATALYSTS. ROLE OF THE SI CONTENT ON CATALYST-CONTAMINANT INTERACTIONS

Farida Boudissa[a], Alisa-Vasilica Arus[b], Rachida Ouargli[c], Ileana-Denisa Nistor[b]
René Roy[a], Abdelkrim Azzouz[a,*]

[a] *Nanoqam, Department of Chemistry, University of Quebec at Montreal, QC, Canada H3C 3P8.*

[b] *Catalysis and Microporous Materials Laboratory, Vasile-Alecsandri University of Bacau, Romania.*

[c] *Department of Materials Engineering, University of Science and Technology, Oran, Algeria.*

**Correspondence: azzouz.a@uqam.ca; Tel: 1 514-987-3000, ext. 4119*

Contribution des co-auteurs

Ma contribution personnelle à cet article: Réalisation des expériences, obtention des résultats et traitement des données, conception des figures et des tableaux, essais d'interprétation des résultats. Rédaction préliminaire de l'article et prise en charge des soumissions au nom de l'auteur correspondant.

Vasilica-Alisa Arus : Synthèse et caractérisation complète des bentonites activées à l'acide.

Rachida Ouargli: Ozonation du bisphénol a en présence de silice mésoporeuse de type SBA-15 et caractérisation.

Ileana-Denisa Nistor: Échanges de résultats de tests expérimentaux sur l'ozonation du bisphenol-A.

Roy René : Correction de l'article.

Azzouz Abdelkrim : Conception et direction de la recherche sur l'ozonation des polluants organiques, vérification et corrections des interprétations des résultats, finalisation de l'article.

CHAPITRE II

ARTICLE II: THOROUGH BISPHENOL-A REMOVAL THROUGH OZONATION WITH SILICA-BASED CATALYSTS. ROLE OF THE SI CONTENT ON CATALYST-CONTAMINANT INTERACTIONS.

Abstract

Catalytic ozonation for total mineralization of bisphenol-A (BPA) from aqueous solution was investigated in the presence of mesoporous silica, acid activated bentonite (HMt) and montmorillonite-rich materials (Mt) ion-exchanged by Na^{+} and Fe^{2+} cations (NaMt and Fe(II)Mt). The effects of the catalyst activity and BPA interactions with the catalyst surface were studied by correlating the acid-base properties and hydrophilic character through CO_2 and water TPD measurements, zeta potential measurements and particle sizes assessment. To the best of our knowledge, this approach has barely been tackled so far. Acid-activated and iron-free clay catalysts produced complete BPA degradation in short ozonation times. The catalytic activity was found to strongly depend on the surface basicity and hydrophilic character, which, in turn, depend on the Si content and exchangeable cation. Catalyst interactions with water and BPA appear to determine the catalyst particle dispersion in aqueous media, promoting hydrophobic adsorption in high Si catalysts, at the expense of electrostatic interactions which were mainly involved in low silica materials. These findings are of a great importance,

because they allow tailoring specific catalyst properties for specific features of the waters to be treated.

2.1 Introduction

Water pollution has become a growing concern as more and more wastewaters are released in aquatic media. Waters can be polluted by industrial, agricultural and household wastewaters containing chemicals, heavy metals, diverse organic pollutants, pesticides, drugs, pharmaceuticals and others. Among these, Endocrine-Disrupting Compounds (EDCs) are a major family of emerging pollutants of waters, and were found to have a negative impact on human health and biodiversity, involving harmful effects on human and animal fertility, nervous system function, and inducing cancers, immune function, obesity, and diverse diseases. Human digestive tract is usually the most affected when exposed to these pollutants via food ingestion, dust, water and from pregnant women to foetus and/or child transfer via breast feeding.

2,2-bis-(4-hydroxyphenyl) propane so-called bisphenol-A (BPA) is a major EDC, being widely used in the composition of adhesives, plastics (baby bottles), food and beverage containers, paints, paper derivatives, textiles, dental sealants and others [1, 2]. Exposition to BPA is often associated to endocrine disorder, inducing harmful effect on reproduction and malformations [3, 4], aquatic species feminization [5-7], breast and prostate cancers, obesity, diabetes…etc [8] .

BPA is frequently detected in surface and groundwater along with in water treatment sewage. For instance, BPA concentration reached 21.5 μg L^{-1} in urban wastewaters [9], 1.92-11.1 μg L^{-1} in industrial wastewaters [10], 0.14-0.98 μg L^{-1} in treated effluents [11] and even 0.5-2 ng L^{-1} in drinking water [12]. BPA is also still detected in fruits,

vegetables, meat, serum of pregnant women, breast milk, placental tissues and saliva [13-15].

Thus, Thorough BPA elimination from waters without residual traces has become a major challenge to be addressed. So far, BPA removal issue has been tackled through different approaches, involving more or less conventional methods. The latter often turned out to be quite unsatisfactory [16, 17], being mostly characterized by a low removal yield, high energy consumption and use of chemicals.

Advanced Oxidation Processes (AOPs) including, Fenton's process, electrochemical irradiation, oxidation via ozone or hydrogen peroxide [18, 19] and catalytic ozonation have been used more or less successfully in many attempts to convert EDCs and BPA into supposedly less toxic and more biodegradable products [20-26]. Most of these attempts failed because of the knowledge lack regarding the role of the catalyst surface properties in correlation with the organic pollutant behavior in aqueous media.

Ozonation is an interesting route, but ozone alone is generally unable to produce complete mineralization of the organic molecules, often resulting in the accumulation of residual organic by-products. The latter consist mainly of aldehydes, ketones and short chain organic acids [27-31], some of these being sometimes more harmful than the parent pollutant. This is mainly due to the low solubility of ozone in water, which usually imposes high ozone and energy consumption that limit the interest devoted to conventional ozonation techniques for water treatment [32].

Ozonation can be enhanced by effective silica-based catalyst such as clay minerals, zeolites and pseudozeolites [23, 25, 31, 33]. The main role of the catalyst resides in reducing ozone consumption, inasmuch as ozonation in the presence of solid catalysts was found to require almost 4 times less ozone than without catalyst [34]. Unlike dissolved catalysts, solid counterparts can be recovered and reused [35]. Catalytic ozonation combines the effect dissolved, adsorbed ozone and gas bubbles with both the

adsorptive and oxidative properties of the solid catalyst. Such a complex process can even produce total mineralization of refractory organic compounds into to carbon dioxide, water and mineral acids [23, 31, 36]. The effectiveness of the solid catalyst strongly depends on its textural features, inasmuch as high surface areas provide more active sites, while large pore size allow easy reactant diffusion towards these active sites [37].

So far, several types of catalysts such as activated carbon, zeolites, organized mesoporous silica SBA-15 and clay minerals [38-40] have been used in the degradation of organic pollutants, and a wide variety of catalysts have been tested in BPA removal [41-52]. Given the high performances of silica-based catalysts in organic pollutant ozonation, acid-activated bentonites turned out to be particularly interesting owing to the key-role of their increased number of silanols groups [53]. The catalytic activity of bentonite was already explained by the role of montmorillonite, the main component of bentonites, its silica content [53] and exchangeable cations [23, 53, 54] .

The growing interest devoted to montmorillonite arises from its availability and ability of be modified through convenient and very different procedures, leading to wide variety of technological and environmental purposes. Investigations on the effect of the silica content will be extended to BPA ozonation attempts in the presence of mesoporous SBA-like silica [55-59]. This is a judicious approach, given the high amount of silanols and expanded structures of SBA-15, which displays parallel channels.

It would be worth investigating the role iron-containing compounds and well-known catalytic activity of Fe^{2+} cations. Natural iron oxides are common raw materials, and their wide occurrence in nature could explain the role of soils in the oxidation of organic molecules and both vegetal and animal biomasses into humic acids and CO_2. Major iron oxides include goethite (α-FeOOH), hematite (α-Fe_2O_3), maghemite (γ-

Fe_2O_3), lepidocrocite (γ-FeOOH) and magnetite (Fe_3O_4). Some of them already exhibited catalytic activity in oxidation processes [56, 60]. Here, the role of pH was found to be essential, assuming that iron acts mainly as partially dissolved Fe^{2+} cations in the vicinity of the catalysts surface [23, 56].

The main objective of this work consists in achieving advanced BPA degradation in water in the presence of silica based catalysts ranging from pure silica (SBA-15) to diverse montmorillonite samples with different silica contents and exchangeable cations. Correlation of the catalytic activity with the surface basicity, hydrophilic character as determined through thermal programmed desorption of CO_2 and water, and with the zeta potential and particle size are expected to allow explaining the role of the silanols groups in terms of Lewis-Acid-Base interactions between the involved reactants, catalyst surface and water.

2.2 Experimental

2.2.1 Catalyst preparation

The activated bentonite (HMt) were prepared through acid activation of clay. For this reason, 200 g crud bentonite were impregnated by 1000 mL of aqueous 5 M sulfuric acid solution under mild stirring for various times (1, 4, 8, 15 and 24 hours, respectively). The samples, denoted as HMt-1, HMt-4, HMt-8, HMt-15 and HMt-24, were repeatedly washed with distilled water until neutral pH and then dried at 100 °C for 12 h. Acid-activated clays were crushed and then sifted [61, 62]. The powders were recovered by filtration, repeatedly washed with distilled water until neutral pH and

dried at 100 °C for 12 h. Acid-activated clays were crushed and then sifted into 75 μm particle size (200 mesh ASTM).

Bentonite was previously purified into a montmorillonite-rich material (Mt) through repeated impregnations with 2–5 M aqueous NaCl solutions at 80 °C for 4-5 h, under vigorous stirring were necessary to reach full ion exchange into NaMt form. The latter was washed with distilled water and then dialyzed in cellophane bags repeatedly immersed in fresh water until no chloride was detected by $AgNO_3$ test in the dialysate. Fe(II)Mt was further obtained through NaMt impregnation with aqueous solutions containing nitrate salts of Fe^{2+} ($FeCl_2$ $4H_2O$). The choice of these two catalysts was based on their different catalytic activity according to previous works [23, 31, 53]. NaMt and Fe(II)Mt were air-dried at 40 ^oC overnight.

SBA-16-like silica was synthesized according to a procedure reported in the literature [57, 59, 63]. Shortly, a 0.47 g amount of Pluronic P123 copolymer, (MW = 5800, Sigma–Aldrich) and 2.33 g quantity of Pluronic F127 block-copolymer (Aldrich) were dissolved in a mixture of 24 g of water, and 113 g of HCl (2 M) under vigorous stirring at 300 K for 1 hour. After complete dissolution, 10.4 g of TEOS were added and the water-copolymer mixture was stirred 20 h at 310 K. The resulting suspension was then heated at 383 K without stirring for 48 h. The white solid powder obtained was filtered, repeatedly washed with deionized water, air dried and calcined at 773 K for 6 h at a 1 K min^{-1} heating rate. The resulting and uncalcined material was denoted as SBA-15-NC. This material was tested in BPA ozonation as such or mixed to hematite previously crushed, repeatedly washed in distilled water and then dried at 45 °C.

2.2.2 Catalyst characterization

The acid-activated bentonites [57], montmorillonite and its ion-exchanged counterparts [23, 33] and SBA-15 mesoporous silica [56, 57, 64] were fully characterized through diverse techniques. The latter include powder X-ray diffraction (XRD) (Siemens D5000 X-ray diffractometer and a Co-Kα radiation at λ=1.7890Å), transmission electron microscopy (TEM) (JEOL electron microscope JEM-2100F,with an accelerating 200 kV voltage coupled to energy-dispersion X-ray fluorescence (ED-XRF) analysis, scanning electron microscopy (SEM) (HITACHI S-4300SE/N-VP Emission Scanning Electron Microscope), Fourier transform IR spectroscopy (Magma Nicolet IR-550 spectrometer), nitrogen adsorption-desorption isotherms at -195.7 ºC, using a Quantachrome device with an Autosorb automated gas system control, thermal gravimetric analysis (TG and DTG) by means of a TG/TDA-6200 thermal analyzer (Seiko instrument Inc.), under a 100 mL min^{-1} nitrogen stream and 5 ^{o}C min^{-1} heating rate, Fourier transform Infrared spectroscopy by means of a Model Nicolet 6700 FTIR instrument, in attenuated total reflectance (ATR) mode (Diamond ATR crystal).

2.2.3 Ozonation tests and product analysis

Aqueous 10^{-4} M solution was prepared by dissolving pure bisphenol-A (BPA) (≥ 98 %) as supplied by Sigma–Aldrich in distilled water under vigorous stirring for 1 day due to its low solubility. The concentration of the BPA solution was analysed by UV-Visible spectrophotometry using a Varian-Cary 5000 instrument (Agilent Technologies. USA) between 190 nm and 800 nm and a 1cm quartz cell.

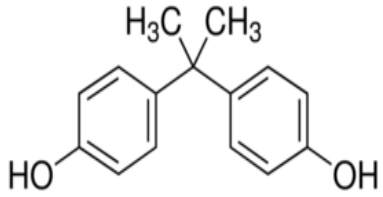

Scheme 2.1. Structural representation of BPA molecule.

Diverse materials such as bentonite (Sigma-Aldrich, USA) acid-activated with different Si/Al ratios [65], montmorillonite exchanged with Na^{+} and Fe^{2+} cations [25, 31, 33], SBA-15 silica [57] and raw natural iron oxide (Hematite) in its native form originating from Chaabet-El-Ballout (Algeria) [18] were used as catalysts or co-catalysts in the ozonation of bisphenol-A in deionized water at room temperature.

Samples of 20 mL of 10^{-4} BPA solution, were ozonated at different time in 50 mL cylindrical tubes. Ozonation attempts were performed without and with 40 mg of catalyst (bentonite, NaMt, FeMt and HMt). Ozone was generated in a laboratory ozone generator (A_2Z Ozone Inc., USA), from pure oxygen. The gas flow rate is 600 mg h^{-1}. After ozonation and catalyst removal by centrifugation, the supernatant was analyzed by UV-visible spectrophotometry. The ozonation mixture was periodically analyzed by UV-visible spectrophotometry also were examined by high-performance liquid chromatography (HPLC) by means of a Waters Alliance 2695 HPLC system equipped with a Agilent C18 column (4.6 mm x 100mm, 3.5 μm particle size.) and a UV detector (Waters 2487 HPLC Absorbance UV-Vis Detector). The mobile phase was an acetonitrile/water mixture (60:40, v/v) at a 1 mL min^{-1} flow rate with automatic injections. The injection volume was of 20 μL. The wavelength was fixed at 278 nm.

2.3 Results and discussion

2.3.1 Non-catalytic ozonation

Calibration curves based on the variation of the absorbance of the different UV-Vis bands of BPA versus BPA concentration (Fig. S2.1) allowed assessing the molar extinction coefficients (Table S2.2). In water, BPA displayed a UV-Vis spectrum typical of phenol derivatives with three absorption bands at 278, 225 and 200 nm. The 225 nm band corresponds to the transition π-π*,while that appearing at 278 nm accounts for n-π* transitions involving electrons n of the oxygen atoms of the OH groups on the aromatic ring [66]. As expected [24], Ozone showed effectiveness in BPA degradation in water, since a first overview of the variation of BPA UV-Vis spectra during ozonation showed a progressive disappearance of the 278 nm band (Fig. 2.1).

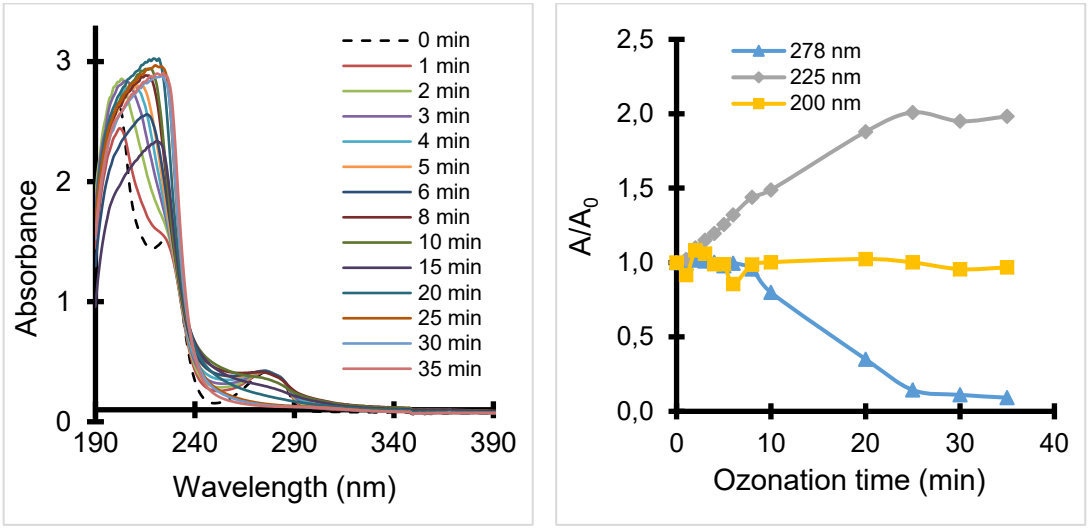

a **b**

Fig. 2.1. Evolution in time of BPA UV-Vis spectrum (a) and relative absorbance of the three UV-Vis bands (b) during non-catalytic ozonation in distilled water. T = 22 °C. pH = intrinsic value. Quartz cell = 1 cm. O_3 throughput: 600 mg h^{-1}. Sample volume = 20 mL. Initial BPA concentration: 10^{-4} M.

The intensity decay in time for this band can be regarded as a precise indicator of BPA degradation. The latter took place slowly during the first 8 minutes, presumably due to the low ozone solubility in water. BPA removal yield significantly increased from 2 % after 5 min of ozonation up to 91% after 35 min. Such an effectiveness of short ozonation times suggests advanced degradation level that may include severe attack on the aromatic ring [67]. Non-catalytic ozonation was already found to lead to complete BPA degradation in less than 4 min, but without total mineralization of the intermediates since only 35% conversion of the total organic carbon (TOC) was registered after 60 min, but this value raised up to 90% in the presence of 1 g L^{-1} alumina [30]. The relative absorbance of the 225 nm band increased in time with slight shift towards lower wavelengths. This indicates the formation of oxidized derivatives such as catechol, acetone, hydroquinone, formaldehyde, acetic, formic, maleic and

oxalic acids and appearance of H-bridge interactions. The persistence of the latter can be explained by their increased resistance to ozonation once oxidized [51, 68].

2.3.2 Effect of montmorillonite addition

Addition of montmorillonite induced significant changes in the evolution in time of the UV-Vis spectrum of the ozonation mixture. These changes appear to differ according to the exchangeable cation (Fig. 2.2). Addition of NaMt resulted in an extension of the UV-Vis absorbance region up to 600 nm and even beyond (Fig. 2.2-a). This is presumably due to the formation of slightly tinted polycondensation products. Such a phenomenon was already reported for ethinylestradiol (EE2), and attributed to hypothetical protected EE2 forms (hydroperoxides) generated via quick reaction of phenoxyl radicals with superoxide anion [69]. Such hydroperoxides are supposed to be weakly reactive toward ozone, and decompose reversibly into the parent molecule through slow dioxygen release.

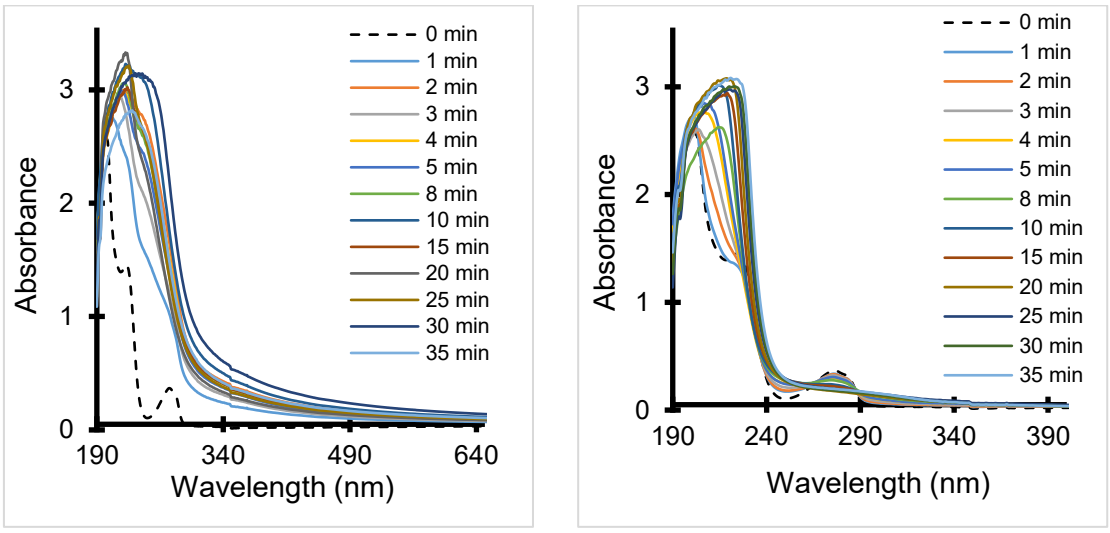

Fig. 2.2. Evolution in time of the UV-Vis spectra of BPA during ozonation in presence of NaMt (a) and Fe(II)Mt (b).

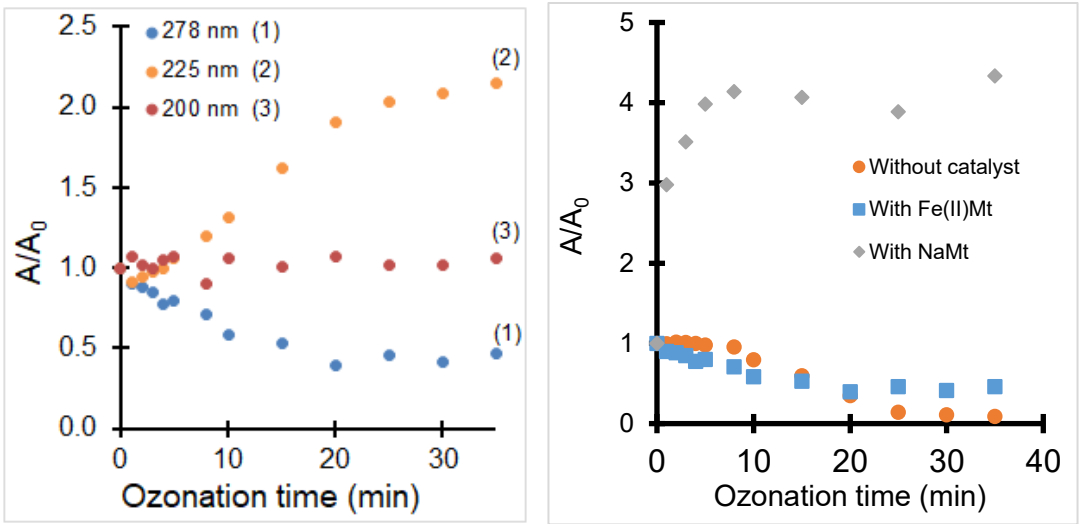

Fig. 2.3. Evolution in time of the relative absorbance of BPA of all three UV-Vis bands during Fe(II)Mt-catalyzed ozonation (a) and of the 278 nm band with and without Fe(II)Mt (b) in distilled water.

The general tendency is that all BPA bands increased in intensity during ozonation in the presence of NaMt. This is due to the formation of intermediates absorbing in the same UV-Vis region. In contrast, only the 200 nm and 225 nm bands showed intensity increase in the presence of Fe(II)Mt (Fig. 2.3-a). The relative absorbance of the 278 nm band progressively decreased from 1 down to ca. 0.4 after 20 min ozonation in the presence of Fe(II)Mt. This accounts for an increase in the BPA removal yield of approximately 60%. Seemingly, the latter was lower than that of 90% registered after 35 min ozonation in the absence of catalyst (Fig. 2.3-b). This was already explained in terms of formation of protected BPA hydroperoxides, as already assumed for ethinylestradiol [69]. The apparently high reactivity of BPA towards ozone. The paradoxically pronounced BPA degradation in the absence of catalyst contrasts with the persistence of the 200 and 225 nm even after 60 min ozonation, suggesting an accumulation of hydroxylated BPA derivate due to weak further oxidation.

2.3.3 Effect of acid activated bentonite

After addition of HMt catalysts, a much pronounced depletion of the A/Ao for the 278 nm band occurred from 1.0 down to less than 0.2 for HMt-4 and ca. 0.3 for HMt-15 after 20 min ozonation (Fig. 2.4). This indicates an enhanced BPA degradation as supported by HPLC measurements (Fig. 2.5-a). The barely detectable increase of the 200 nm band must be due simultaneous formation and consecutive consumption of hydroxylated derivatives, indicating a higher catalytic activity of HMts as compared to Fe(II)Mt.

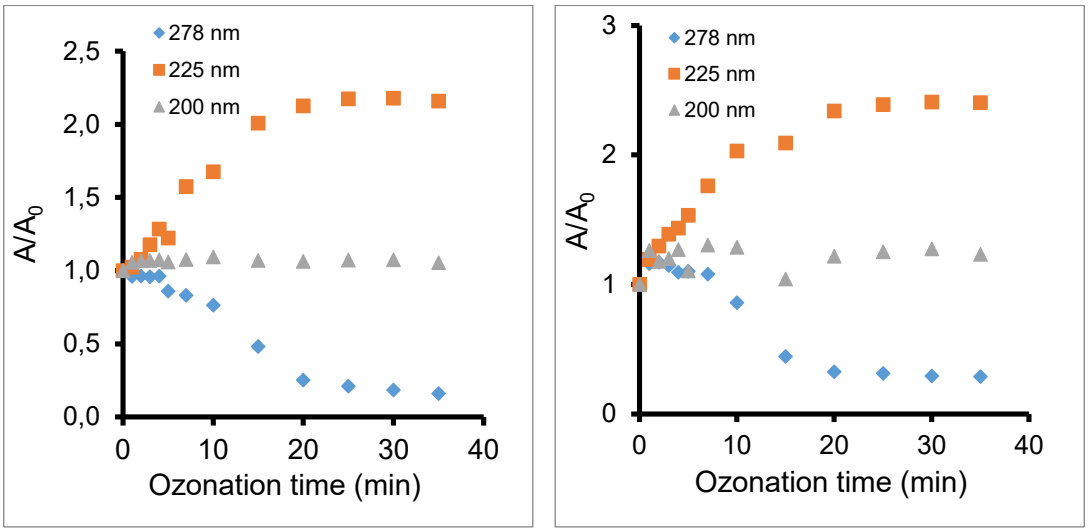

a. HMt-4 **b. HMt-15**

Fig. 2.4. BPA relative absorbance of the 278 nm band during ozonation in distilled water. T = 22 °C. pH = intrinsic. Concentration: 10^{-4} M. Catalyst concentration: $2gL^{-1}$.

Here also, the possible formation of hydroperoxides is expected to shade the actual BPA degradation, mitigating the decay of the 278 nm band. Additional BPA titration through HPLC-UV allowed overcoming this shortcoming. This provided much more accurate assessment of the decomposition yield, as illustrated by the marked BPA depletion during the first 5 min of ozonation in the presence of HMt catalysts (Fig. 2.5). A first overview of the HPLC patterns revealed a fast depletion of BPA peak and rapid rise of new peaks that progressively disappear at shorter retention times in the presence of HMt-1. This indicates the formation of BPA derivatives with higher polarity [70].

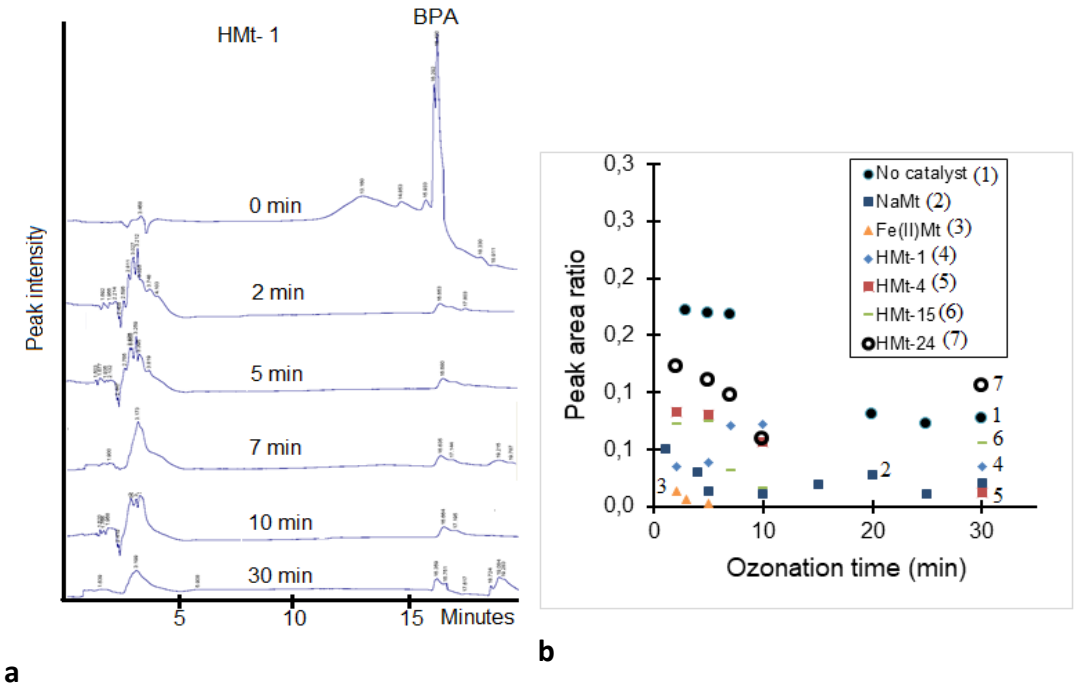

Fig. 2.5. Evolution of the reaction mixture during HMt-1-catalyzed ozonation (a) and of BPA peak as detected by UV-Vis at 278 nm (b). T = 22 °C. pH = intrinsic. BPA concentration: 10^{-4} M. Catalyst concentration: 2 g L^{-1}. O_3 throughput: 600 mg h^{-1}. Sample volume = 20 mL.

Total mineralization of BPA, monitored by total degradation of these intermediates, was achieved with HMt-1, HMt-4 and HMt-8 after 40-60 min ozonation. Here, the degradation time appears to vary according to the catalyst. Moderately activated bentonites showed highest performances, affording degradation yield of 83% (HMt-4) and 86% (HMt-8) after only 10 min ozonation (Fig. 2.6).

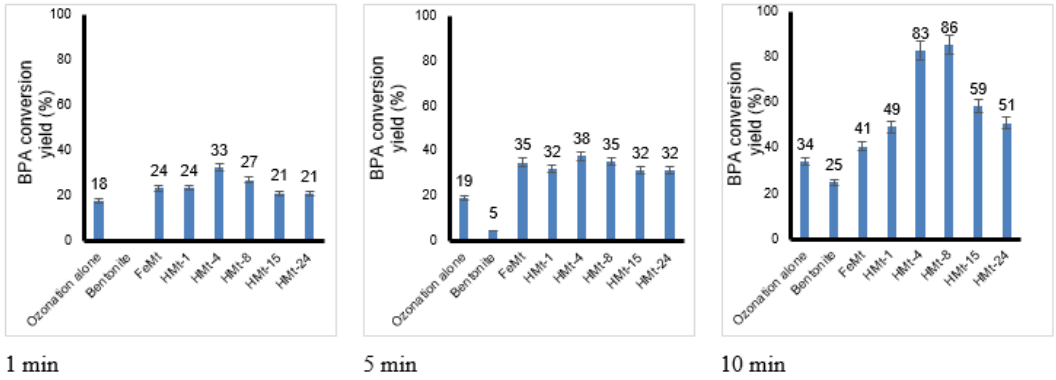

Fig. 2.6. BPA removal yield as assessed by HPLC after short ozonation times for different catalysts (2 g L^{-1}). T = 22 °C. O_3 throughput: 600 mg h^{-1}. Sample volume = 20 mL. Initial concentration: 10^{-4} M.

This provides evidence of the key-role of the Si/Al ratio and of subsequently of the silanols groups. Fe(II)Mt produced lower BPA degradation yield than HMt samples, suggesting that Fe^{2+} cation is not an essential requirement for advanced BPA degradation. The fact that highly acid-activated bentonites (HMt-15 and HMt-24) showed lower effectiveness must be due to a pronounced hydrophobic character that reduces the contribution of BPA adsorption through electrostatic interaction. An additional explanation should consist in the relatively high pKa value of BPA, which is supposed to attenuate or even hinder acid-base interactions with amphoteric to slightly basic surface. Here, partial protonation or deprotonation of the silanols groups should control the contributions of electrostatic, organophobic and Lewis-Acid-Base (LAB) interactions.

2.3.4 BPA adsorption and hydrophobicity inversion

Additional BPA adsorption tests performed by impregnating 40 mg of catalyst by 20 ml of a BPA solution (10^{-4} M) in the absence of ozone for 24 hours revealed highest BPA removal yield through adsorption for Fe(II)Mt (14%), HMt-4 (17%), HMt-8 (15%) and HMt-15 (13%) (Fig. 2.7). A possible explanation for HMt behavior should consist in optimum BPA:catalyst interactions due to a combination of optimum catalyst dispersion and hydrophobicity.

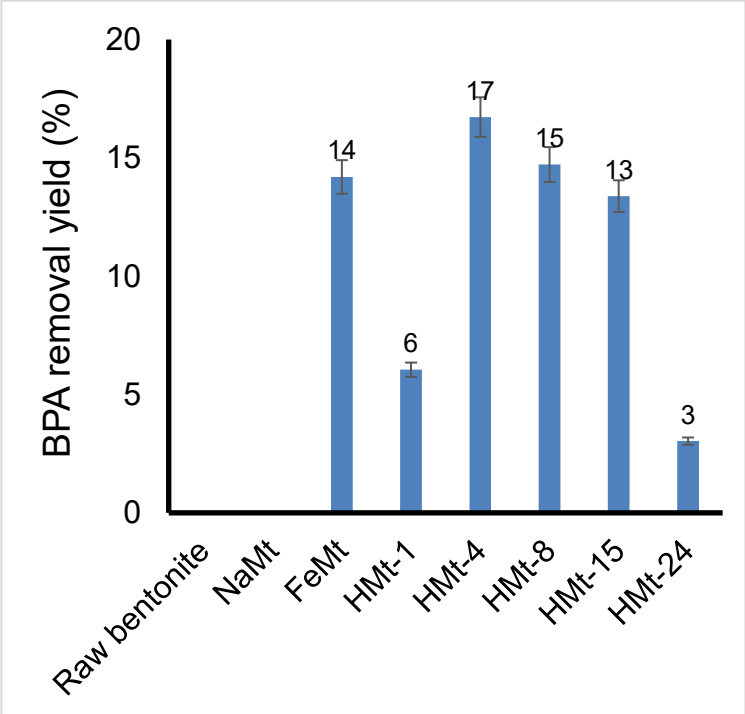

Fig. 2.7. BPA removal yield by adsorption on different catalysts after 24 h contact time as assessed by UV-Vis measurements at 278 nm. T = 22 °C. Quartz cell = 1 cm. Sample volume = 20 mL. Initial concentration: 10^{-4} M. Adsorbent amount = 40 mg.

In the absence of BPA, there exists a reverse proportionality between the particle size and WRC of HMt catalysts (Fig. 2.8). This result was somehow expected, inasmuch as enhanced dealumination and decationization should result in higher hydrophobicity but lower catalyst dispersion in water. This phenomenon was reversed in the presence of BPA, because of BPA adsorption via organophilic methyl groups. The marked decrease in particle size when contacted with BPA solution provides clear evidence of BPA molecule adsorption through their hydrophobic side. The resulting orientation of the hydroxyl groups of adsorbed BPA molecules towards the bulk solution is expected to confer a hydrophilic character to the BPA-clay composite, favoring clay aggregates dispersion and particle size decrease.

Therefore, optimum acid attack should result in optimum particle size and amount of BPA-clay composite than can undergo oxidation in the presence of ozone. The fact that HMt-4, HMt-8 and HMt-15 exhibited simultaneously the highest catalytic activity (Fig. 2.6) and amounts of adsorbed BPA (Fig. 2.7) allowed demonstrating the key contribution of the adsorption step within the global catalytic process.

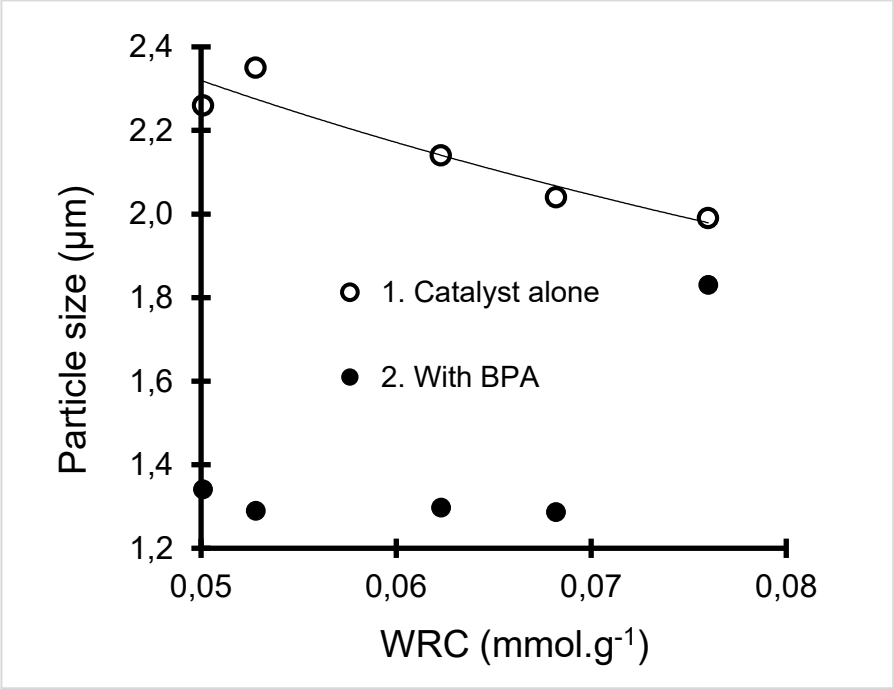

Fig. 2.8. HMt particle size before (1) and after BPA adsorption after 24 h contact time (2) versus water retention capacity (WRC) as assessed by thermal programmed desorption.

Adsorption on HMt samples should involve mainly hydrophobic interaction as supported by their weak affinity towards water expressed in terms of low water retention capacity [53]. On HMt catalysts, BPA adsorption via electrostatic interaction and ion-exchange is expected to play minor roles, given the low density of positive and negative charges as a result of dealumination.

Hydrophobicity inversion and catalyst dispersion enhancement appear to also occur on pure SBA-15 silica as supported by the decrease in particle size from 1.92 down to 1.58 µm and to a much lesser extent on NaMt (from 0.649 nm to 0.534 µm) (Table 2.1). In contrast, Fe(II)Mt and bentonite showed rather particle size increase from 1.24 to 1.404 µm and from 2.45 to 3.897 µm, respectively. Their relatively high hydrophilic character reflected by their higher WRC (0.195 and 0.126 mmol g^{-1}) suggests that BPA

adsorption takes place via other interactions, presumably through cation exchange in agreement with our previous statements.

All these investigations allow concluding that the structure of the Si-containing material and modification procedure play key-roles in BPA ozonation in aqueous media. SBA-15 appears to act through its silanols groups that can protonate/deprotonate according to the pH of the reaction mixture, without achieving high BPA conversion yield. Attempts to achieve high silanols materials through acid attack resulted in much higher degradation yield as compared to SBA-15. The most plausible explanation resides in that unlike SBA-15, clay mineral dispersion and even exfoliation and delamination in water allow avoiding possible pore obturation by BPA molecule adsorption at the pore entry and inclusion of ozone bubbles within the channels. The pH of the reaction mixture is expected to display a significant effect on the zeta potential of the catalyst surface and clay dispersion, which can modulate the magnitude of the available active surface accessible for BPA and ozone molecules.

2.3.5 Role of silanols on BPA adsorption

The intrinsic pH of BPA solution increased from 5.64 up to 7.92 and 6.55 in the presence of bentonite or NaMt. This is supposed to induce slight deprotonation of the out-of-plane silanols (pKa 5.6) and protonation of the in-plane counterparts (pKa 8.5), while BPA molecule (9.56-10.2) should display neutral to weakly positive charge. In contrast, in the presence of Fe(II)Mt, the initial pH dropped down to 2.38, conferring positive charges to all silanols and BPA that hinder electrostatic attraction. Acidic pHs were also registered in BPA solution after addition of HMts (4.27 to 3.86 with increasing Si/Al ratio) and SBA-15 (5.27). These acidity levels should induces neutral

to positive charges on BPA molecules and all silanols impeading thereby adsorption via electrostatic interactions.

Table 2.1. Some feature of BPA solution, clay catalysts suspension and their mixture

	WRC [a] nmol.g^{-1}	Si/Al mole ratio	Clay suspension				BPA Charge [f]	Catalyst particle size (μm)	
			pH		Zeta potential (± 3.50 mv)			Alone	With BPA
			Alone[b]	With BPA[c]	Alone[d]	With BPA[e]			
Bentonite	126	2.50	9.69	7.92	- 31.25	- 27.44	Neutral to +	1.24	1.404
NaMt	96	2.50	8.77	6.55	- 42.19	- 38.79	Neutral to +	0.649	0.534
Fe(II)Mt	195	2.50	2.33	2.38	+ 16.20	- 48.71	+	2.45	3.897
HMt-1	76	2.69	4.18	4.27	- 43.02	- 35.24	+	1.99	1.830
HMt-4	68.2	3.00	4.15	4.10	- 38.36	- 41.20	+	2.04	1.287
HMt-8	62.3	3.47	4.04	3.96	- 43.12	- 34.88	+	2.14	1.297
HMt-15	50.1	4.03	3.92	3.86	- 42.18	- 39.60	Neutral to +	2.26	1.341
HMt-24	52.8	4.36	3.96	3.86	- 37.62	- 36.72	Neutral to +	2.35	1.290
SBA-15	-	-	5.81	5.27	-31.49	-22.22	Neutral	1.92	1.58

[a]Water retention capacity (WRC) of the catalysts was assessed with 3% accuracy through TPD measurements in the temperature range 20-450 °C. The WRC is proportional to the hydrophilic character of the catalyst surface.
[b]Average pH of the aqueous suspension of catalyst particles at room temperature (Triplicate).
[c]Average pH of the aqueous suspension of catalyst particles in the presence of BPA at room temperature (Triplicate).
[d]These Zeta potential values were measured in the absence of BPA molecules.
[e]These Zeta potential values were measured in the presence of BPA molecules.
[f]BPA pKa: 9.56-10.2; Intrinsic pH of 10^{-4} BPA solution : 5.64.
[g]Catalyst particle size as measured in distilled water.
[h]Catalyst particle size as measured in the 10^{-4} BPA solution.

The acidic character of Fe(II)Mt reflected by its low CO_2 retention capacity (CRC) [53] promotes rather beneficial LAB interaction for BPA adsorption [71]. The much higher catalytic activity of Fe(II)Mt must also involve hydrophobic interaction and/or cation-exchange on the catalyst surface. Hydrophobic interaction, if any, should have only a minor contribution, given the relatively low hydrophobicity of BPA [67]. In contrast, cation exchange must prevail, and is expected to enhance ozonation through Fe^{2+} cation release in the vicinity of the catalyst surface, as already reported for other organic substrates [33, 72].

2.3.6 Silanols-pH correlation

Deeper insights in the role of silanols and its dependence on pH were achieved using pure SBA-15-like silica in ozonation at previously optimized pH [23, 33]. In the presence of 1 g L^{-1} catalyst, increasing pH from 1.80 up to 3.80 induced a slight enhancement of BPA decomposition reflected by a decrease of the relative intensity of the 278 nm (Fig. 2.9-a).

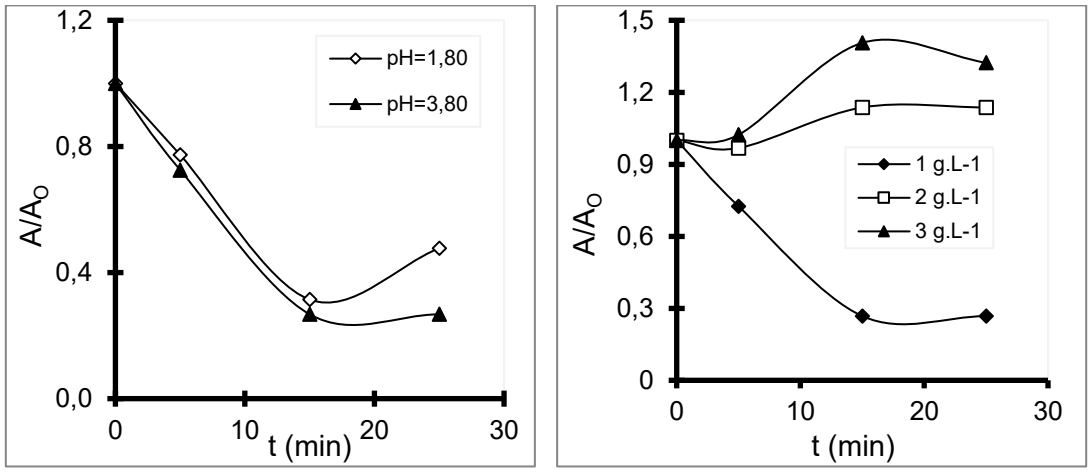

a **b**

Fig. 2.9. Influence of pH in the presence of 1 g L^{-1} of SBA-15 (b) and of catalyst amount at pH 2.80 (b) on BPA degradation (10^{-4} M). T = 22 °C, O_3 = 600 mg h and λ = 278 nm.

However, increasing SBA-15 concentration from 1 to 3 g L^{-1} SBA-15 at optimum pH of 2.80 appears to mitigate ozonation, as supported by the marked increase in A/Ao (Fig. 2.9-b). This reverse effects of pH and SBA-15 amounts provides evidence of the role of pH in silica-catalyzed ozonation. Interestingly, the total absence of aluminum in SBA-15 gave almost similar BPA conversion yield of 90% and beyond but with lower catalyst amount (1 g L^{-1} at pH 2.80) as compared to HMt samples ((1 g L^{-1}) at intrinsic pH of PBA solution. The weak acidity of the out-of-plane silanols of SBA-15 [73] should not produce their protonation, and BPA adsorption must involve more hydrophobic interaction than on HMt samples.

2.3.7 Role of iron

Fe^{2+} cation already showed appreciable catalytic activity in montmorillonite-catalyzed ozonation processes [23, 25, 31, 33, 74]. The catalytic activity of Fe^{2+} cation was supported by HPLC measurements, which revealed higher BPA degradation yield of 41% with less intermediate in the retention time range 2.5-7.0 min after 10 min ozonation for Fe(II)Mt as compared to non-catalyzed ozonation (Fig. 2.10).

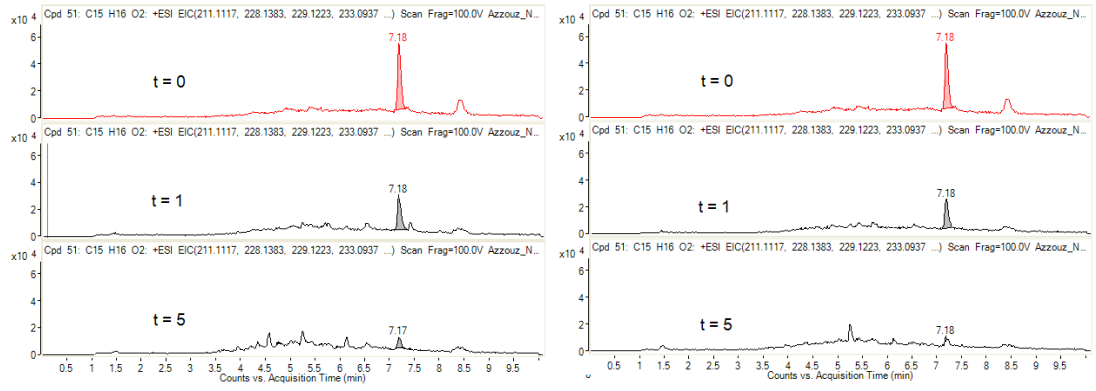

Fig. 2.10. LC-ToF-MS diagram of BPA ozonation mixture in the absence (a) and presence of Fe(II)Mt (b). Initial BPA concentration = 100 µM.

Fe(II)Mt still displayed higher catalytic activity affording higher BPA degradation yield of 24-41% than bentonite (0-25%) after 1-10 min ozonation time (Fig. 2.6). This performance was however lower than those produced by all HMt-samples after 10 min ozonation (49-86%). In the meantime, in the absence of ozone, Fe(II)Mt also showed lower BPA removal yield through adsorption after 24 hours contact time (14%) than HMt-4 (17%) and HMt-8 (15%) but still higher than bentonite (0%), NaMt (0%) and some HMt samples such as HMt-1 (6%), HMt-15 (13%) and HMt-24 (3%) (Fig. 2.7). The fact that moderately acid-treated HMt catalysts display highest BPA removal yield

through both adsorption and ozonation indicates that adsorption is a key-step in clay-catalyzed ozonation, and that the surface basicity and hydrophobicity have more significant influence than Fe^{2+} cation.

Deeper insights in the role of iron were achieved through BPA adsorption tests with different amounts of hematite (1-3 g L^{-1}). The latter already showed catalytic activity in dye oxidation [18, 75]. A quick overview of the data obtained in the absence of ozone revealed a slight decrease in time of the relative absorbance of the 278 nm band after 5 min contact time (Fig. 2.11-a). This indicates the occurrence of BPA interactions with hematite that remain to be elucidated. No significant changes in the evolution in time of the relative absorbance of the 278 nm band were noticed upon increasing amount of hematite, suggesting a weak influence of hematite concentration.

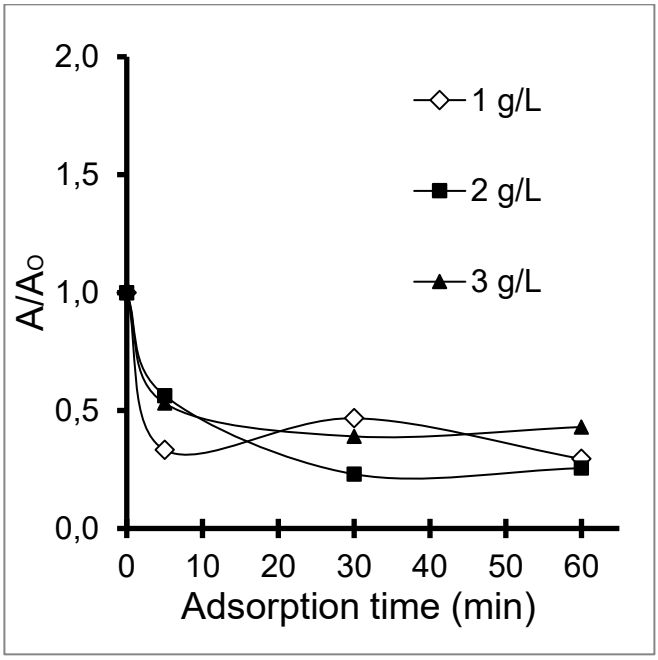

Fig. 2.11. Evolution in time of A/Ao of the 278 nm band during BPA adsorption on different amounts of hematite at intrinsic pH (a) and ozonation at different pH in the presence of 1 g L^{-1} of hematite (b). O_3 throughput: 600 mg h^{-1}. Sample volume = 20 mL. Initial concentration: 10^{-4} M.

This apparently weak influence of hematite amount on BPA adsorption must arise from complex processes and compensatory effects that include partial hematite dissolution at intrinsic pH of the reaction mixture and changes in particle size and others.

Hematite combination with ozone produced much marked decrease in the relative absorbance of the 278 nm band that indicates advanced BPA decomposition (Table 2.2). Hematite-catalyzed ozonation of BPA allowed affording degradation yield of up 94% after only 25 min ozonation in the presence of 1 g L^{-1} hematite and 89% after only 15 min ozonation in the presence of 3 g L^{-1} hematite at pH 3.8. It results that less acidic pH promote BPA degradation with lesser hematite amount.

Table 2.2. BPA degradation yield by ozonation as assessed by the relative absorbance of the 278 nm band.

Hematite concentration (g L^{-1})	t (min)	Removal yield (%)[a]	Initial pH of the reaction mixture	Removal yield (%)[b]
1	15	54	1.8	40
	25	94		33
2	15	23	2.8	31
	25	25		31
3	15	89	3.8	54
	25	87		94

[a] These values were obtained for a pH value of 3.8.
[b] these values were obtained with hematite amount of 1 g L^{-1}.

The fact that possible hematite dissolution at intrinsic pH of BPA solution (5.64) is supposed to release Fe^{3+} cation. The latter is well known to display much lower catalytic activity than its bivalent counterpart. This result is of great importance, because its allow demonstrating that the presence of Fe^{2+} cation is not an essential requirement for advanced BPA degradation, thereby confirming our previous statement.

In combination with SBA-16, the catalytic activity was explained in terms of hematite dissolution and Fe^{3+} cation release in acidic pH [56]. Unlike this mesoporous silica material, SBA-15 was found to exhibit lower acidity, i.e slightly higher Lewis basicity, due its parallel and unintersected channels that offer much more amphoteric in-plane silanols groups [57]. Increasing SBA-15 concentration was found to enhance ozonation, most likely due to a partial contribution of BPA adsorption via hydrophobic interaction, as already stated above. Ozone concentration around adsorbed BPA molecules and/or adsorption on the solid surface are also expected to contribute to the global BPA degradation process [76, 77].

2.4 Conclusion

The results obtained herein allow concluding that the Si/Al ratio and of subsequently of the silanols groups play key-roles in silicate-catalyzed ozonation of bisphenol-A. Fe(II)Mt produced lower BPA degradation yield than moderately acid-activated bentonite, suggesting that Fe^{2+} cation is not an essential requirement for advanced BPA degradation. BPA adsorption on HMt samples appears to be a key-step with the global ozonation process, because hydrophobic BPA interaction with acid-activated surface produces beneficial hydrophobicity inversion. The latter is responsible for clay dispersion, and particle size decrease that promote interaction of adsorbed BPA

molecules through their hydroxyl groups with the aqueous media. These findings of great usefulness for designing low cost clay catalyzed oxidative treatments for thorough organic contaminant removal.

REFERENCES

[1] A. Schecter, N. Malik, D. Haffner, S. Smith, T.R. Harris, O. Paepke, L. Birnbaum, Bisphenol A (BPA) in U.S. Food, Environmental Science & Technology, 44 (2010) 9425-9430.

[2] C.G. Campbell, S.E. Borglin, F.B. Green, A. Grayson, E. Wozei, W.T. Stringfellow, Biologically directed environmental monitoring, fate, and transport of estrogenic endocrine disrupting compounds in water: A review, Chemosphere, 65 (2006) 1265-1280.

[3] J.D. Meeker, S. Ehrlich, T.L. Toth, D.L. Wright, A.M. Calafat, A.T. Trisini, X. Ye, R. Hauser, Semen quality and sperm DNA damage in relation to urinary bisphenol A among men from an infertility clinic, Reproductive Toxicology, 30 (2010) 532-539.

[4] T.H. Lassen, H. Frederiksen, T.K. Jensen, J.H. Petersen, U.N. Joensen, K.M. Main, N.E. Skakkebaek, A. Juul, N. Jørgensen, A.-M. Andersson, Urinary Bisphenol A Levels in Young Men: Association with Reproductive Hormones and Semen Quality, Environmental Health Perspectives, 122 (2014) 478-484.

[5] C.D. Metcalfe, T.L. Metcalfe, Y. Kiparissis, B.G. Koenig, C. Khan, R.J. Hughes, T.R. Croley, R.E. March, T. Potter, Estrogenic potency of chemicals detected in sewage treatment plant effluents as determined by in vivo assays with Japanese medaka (Oryzias latipes), Environmental Toxicology and Chemistry, 20 (2001) 297-308.

[6] U. Schulte-Oehlmann, M. Tillmann, D. Casey, M. Duft, B. Markert, J. Oehlmann, Östrogenartige wirkungen von bisphenol a auf vorderkiemenschnecken (Mollusca: Gastropoda: Prosobranchia), Umweltwissenschaften und Schadstoff-Forschung, 13 (2001) 319.

[7] J. Chen, K.S. Saili, Y. Liu, L. Li, Y. Zhao, Y. Jia, C. Bai, R.L. Tanguay, Q. Dong, C. Huang, Developmental bisphenol A exposure impairs sperm function and reproduction in zebrafish, Chemosphere, 169 (2017) 262-270.

[8] I.A. Lang, T.S. Galloway, A. Scarlett, W.E. Henley, M. Depledge, R.B. Wallace, D. Melzer, Association of Urinary Bisphenol A concentration with medical disorders and laboratory abnormalities in adults, JAMA - J. American Medical Association, 300 (2008) 1303-1310.

[9] J. Jackson, R. Sutton, Sources of endocrine-disrupting chemicals in urban wastewater, Oakland, CA, Science of The Total Environment, 405 (2008) 153-160.

[10] J. Sánchez-Avila, J. Bonet, G. Velasco, S. Lacorte, Determination and occurrence of phthalates, alkylphenols, bisphenol A, PBDEs, PCBs and PAHs in an industrial sewage grid discharging to a Municipal Wastewater Treatment Plant, Science of The Total Environment, 407 (2009) 4157-4167.

[11] M.J. Gómez, M.J. Martínez Bueno, S. Lacorte, A.R. Fernández-Alba, A. Agüera, Pilot survey monitoring pharmaceuticals and related compounds in a sewage treatment plant located on the Mediterranean coast, J. Chemosphere, 66 (2007) 993-1002.

[12] H.M. Kuch, K. Ballschmiter, Determination of Endocrine-Disrupting Phenolic Compounds and Estrogens in Surface and Drinking Water by HRGC−(NCI)−MS in the Picogram per Liter Range, Environmental Science & Technology, 35 (2001) 3201-3206.

[13] R. Braunrath, D. Podlipna, S. Padlesak, M. Cichna-Markl, Determination of bisphenol A in canned foods by immunoaffinity chromatography, HPLC, and fluorescence detection, Journal of Agricultural and Food Chemistry, 53 (2005) 8911-8917.

[14] S.J. Oppeneer, K. Robien, Bisphenol A exposure and associations with obesity among adults: a critical review, Public Health Nutrition, 18 (2014) 1847-1863.

[15] J. Xue, P. Kannan, T.A. Kumosani, A.L. Al-Malki, K. Kannan, Resin-based dental sealants as a source of human exposure to bisphenol analogues, bisphenol A diglycidyl ether, and its derivatives, J. Environmental Research, 162 (2018) 35-40.

[16] M. Numata, T. Yarita, Y. Aoyagi, M. Yamazaki, A. Takatsu, Investigation of saponification for determination of polychlorinated biphenyls in marine sediments, J. Chemosphere, 58 (2005) 865-875.

[17] G.L. Northcott, K.C. Jones, Validation of procedures to quantify nonextractable polycyclic aromatic hydrocarbon residues in soil, J. environmental quality, 32 (2003) 571-582.

[18] S. Larouk, R. Ouargli, D. Shahidi, L. Olhund, T.C. Shiao, N. Chergui, T. Sehili, R. Roy, A. Azzouz, Catalytic ozonation of Orange-G through highly interactive contributions of hematite and SBA-16 – To better understand azo-dye oxidation in nature, J. Chemosphere, 168 (2017) 1648-1657.

[19] İ. Arslan, I. Akmehmet Balcioğlu, T. Tuhkanen, Oxidative treatment of simulated dyehouse effluent by uv and near-UV light assisted Fenton's reagent, J. Chemosphere, 39 (1999) 2767-2783.

[20] H. Ma, B. Wang, X. Luo, Studies on degradation of Methyl Orange wastewater by combined electrochemical process, J. Hazardous Materials, 149 (2007) 492-498.

[21] I.M. Sasidharan Pillai, A.K. Gupta, Effect of inorganic anions and oxidizing agents on electrochemical oxidation of methyl orange, malachite green and 2,4-dinitrophenol, J. Electroanalytical Chemistry, 762 (2016) 66-72.

[22] L. Xu, J. Wang, Fenton-like degradation of 2,4-dichlorophenol using Fe3O4 magnetic nanoparticles, Applied Catalysis B: Environmental, 123–124 (2012) 117-126.

[23] D. Shahidi, R. Roy, A. Azzouz, Total removal of oxalic acid via synergistic parameter interaction in montmorillonite catalyzed ozonation, J. Environmental Chemical Engineering, 2 (2014) 20-30.

[24] S. Karthikeyan, A. Titus, A. Gnanamani, A.B. Mandal, G. Sekaran, Treatment of textile wastewater by homogeneous and heterogeneous Fenton oxidation processes, Desalination, 281 (2011) 438-445.

[25] D. Shahidi, R. Roy, A. Azzouz, Advances in catalytic oxidation of organic pollutants-Prospects for thorough mineralization by natural clay catalysts, Applied Catalysis B: Environmental, 174-175 (2015) 277-292.

[26] A. Azzouz, Advances in Oxidative Oxidation of Oxalic Acid in Aqueous media, in: J.C. Taylor (Ed.) Advances in Reserach Chemistry, Nova-Science Publishers, New-York, 2012.

[27] P.C.C. Faria, J.J.M. Orfão, M.F.R. Pereira, Mineralisation of coloured aqueous solutions by ozonation in the presence of activated carbon, Water research, 39 (2005) 1461-1470.

[28] P.C.C. Faria, J.J.M. Órfão, M.F.R. Pereira, Ozone Decomposition in Water Catalyzed by Activated Carbon: Influence of Chemical and Textural Properties, Industrial & Engineering Chemistry Research, 45 (2006) 2715-2721.

[29] S. Pirgalıoğlu, T.A. Özbelge, Comparison of non-catalytic and catalytic ozonation processes of three different aqueous single dye solutions with respect to powder copper sulfide catalyst, Applied Catalysis A: General, 363 (2009) 157-163.

[30] R. Keykavoos, R. Mankidy, H. Ma, P. Jones, J. Soltan, Mineralization of bisphenol A by catalytic ozonation over alumina, Separation and Purification Technology, 107 (2013) 310-317.

[31] A. Azzouz, A. Kotbi, P. Niquette, T. Sajin, A.V. Ursu, A. Rami, F. Monette, R. Hausler, Ozonation of oxalic acid catalyzed by ion-exchanged montmorillonite in moderately acidic media, Reaction Kinetics, Mechanisms and Catalysis, 99 (2010) 289-302.

[32] S. Tang, D. Yuan, Q. Zhang, Y. Liu, Q. Zhang, Z. Liu, H. Huang, Fe-Mn bi-metallic oxides loaded on granular activated carbon to enhance dye removal by catalytic ozonation, Environmental Science and Pollution Research, 23 (2016) 18800-18808.

[33] D. Shahidi, A. Moheb, R. Abbas, S. Larouk, R. Roy, A. Azzouz, Total mineralization of sulfamethoxazole and aromatic pollutants through Fe^{2+}-montmorillonite catalyzed ozonation, J. Hazardous Materials, 298 (2015) 338-350.

[34] K. Yong, J. Wu, S. Andrews, Heterogeneous Catalytic Ozonation of Aqueous Reactive Dye, Ozone: Science & Engineering, 27 (2005) 257-263.

[35] L. Zhao, J. Ma, Z. Sun, H. Liu, Mechanism of heterogeneous catalytic ozonation of nitrobenzene in aqueous solution with modified ceramic honeycomb, Applied Catalysis B: Environmental, 89 (2009) 326-334.

[36] B. Kasprzyk-Hordern, M. Ziółek, J. Nawrocki, Catalytic ozonation and methods of enhancing molecular ozone reactions in water treatment, Applied Catalysis B: Environmental, 46 (2003) 639-669.

[37] S. Chaliha, K.G. Bhattacharyya, Using Mn(II)−MCM41 as an Environment-Friendly Catalyst to Oxidize Phenol, 2-Chlorophenol, and 2-Nitrophenol in Aqueous Solution, Industrial & Engineering Chemistry Research, 47 (2008) 1370-1379.

[38] F.J. Beltrán, F.J. Rivas, L.A. Fernández, P.M. Álvarez, R. Montero-de-Espinosa, Kinetics of Catalytic Ozonation of Oxalic Acid in Water with Activated Carbon, Industrial & Engineering Chemistry Research, 41 (2002) 6510-6517.

[39] J.P. Kaptijn, The Ecoclear® Process. Results from Full-Scale Installations, Ozone: Science & Engineering, 19 (1997) 297-305.

[40] U. Jans, J. Hoigné, Activated Carbon and Carbon Black Catalyzed Transformation of Aqueous Ozone into OH-Radicals, Ozone: Science & Engineering, 20 (1998) 67-90.

[41] J. Lee, H. Park, J. Yoon, Ozonation characteristics of bisphenol a in water, J. Environmental Technology, 24 (2003) 241-248.

[42] S. Irmak, O. Erbatur, A. Akgerman, Degradation of 17β-estradiol and bisphenol A in aqueous medium by using ozone and ozone/UV techniques, J. Hazardous Materials, 126 (2005) 54-62.

[43] M. Deborde, S. Rabouan, J.P. Duguet, B. Legube, Kinetics of aqueous ozone-induced oxidation of some endocrine disrupters, J. Environmental Science and Technology, 39 (2005) 6086-6092.

[44] K.J. Choi, S.G. Kim, C.W. Kim, J.K. Park, Removal efficiencies of endocrine disrupting chemicals by coagulation/flocculation, ozonation, powdered/granular activated carbon adsorption, and chlorination, Korean J. Chemical Engineering, 23 (2006) 399-408.

[45] B. Xu, N. Gao, M. Rui, H. Wang, H. Wu, Degradation of endocrine disruptor bisphenol A in drinking water by ozone oxidation, Frontiers of Environmental Science & Engineering in China, 1 (2007) 350-356.

[46] S.E. Kim, N.S. Park, H. Yamada, H. Tsuno, modeling of decomposition characterisitics of estrogenic chemicals during ozonation, J. Environmental Technology, 29 (2008) 287-296.

[47] S. Baig, G. Hansmann, B. Paolini, Ozone oxidation of oestrogenic active substances in wastewater and drinking water, Water Sci Technol, 58 (2008) 451-458.

[48] M. Deborde, S. Rabouan, P. Mazellier, J.-P. Duguet, B. Legube, Oxidation of bisphenol A by ozone in aqueous solution, Water Research, 42 (2008) 4299-4308.

[49] F.J. Rivas, Á. Encinas, B. Acedo, F.J. Beltrán, Mineralization of bisphenol A by advanced oxidation processes, J. Chemical Technology & Biotechnology, 84 (2009) 589-594.

[50] T. Garoma, S. Matsumoto, Ozonation of aqueous solution containing bisphenol A: Effect of operational parameters, J. Hazardous Materials, 167 (2009) 1185-1191.

[51] I. Gultekin, V. Mavrov, N.H. Ince, Degradation of Bisphenol-A by ozonation, J. Advanced Oxidation Technologies, 12 (2009) 242-248.

[52] L. Leal, H. Temmink, G. Zeeman, C. Buisman, Removal of micropollutants from aerobically treated grey water via ozone and activated carbon, 2011.

[53] F. Boudissa, D. Mirilà, V.-A. Arus, T. Terkmani, S. Semaan, M. Proulx, I.-D. Nistor, R. Roy, A. Azzouz, Acid-treated clay catalysts for organic dye ozonation – Thorough mineralization through optimum catalyst basicity and hydrophilic character, J. Hazardous Materials, 364 (2019) 356-366.

[54] J.-N. Park, J. Wang, K.Y. Choi, W.-Y. Dong, S.-I. Hong, C.W. Lee, Hydroxylation of phenol with H2O2 over Fe^{2+} and/or Co^{2+} ion-exchanged NaY catalyst in the fixed-bed flow reactor, J. Molecular Catalysis A: Chemical, 247 (2006) 73-79.

[55] D. Zhao, J. Feng, Q. Huo, N. Melosh, G.H. Fredrickson, B.F. Chmelka, G.D. Stucky, Triblock Copolymer Syntheses of Mesoporous Silica with Periodic 50 to 300 Angstrom Pores, Science, 279 (1998) 548.

[56] S. Larouk, R. Ouargli, D. Shahidi, L. Olhund, T.C. Shiao, N. Chergui, T. Sehili, R. Roy, A. Azzouz, Catalytic ozonation of Orange-G through highly interactive contributions of hematite and SBA-16 - To better understand azo-dye oxidation in nature, J. Chemosphere, 168 (2017) 1648-1657.

[57] R. Ouargli, S. Larouk, I. Terrab, R. Hamacha, N. Benharrats, A. Bengheddach, A. Azzouz, Intrinsic Activity of SBA-like Silica in the Catalytic Ozonation of Organic Pollutants, Ozone: Science & Engineering, 38 (2016) 48-61.

[58] M. Kruk, M. Jaroniec, C.H. Ko, R. Ryoo, Characterization of the Porous Structure of SBA-15, J. Chemistry of Materials, 12 (2000) 1961-1968.

[59] D. Zhao, Q. Huo, J. Feng, B.F. Chmelka, G.D. Stucky, Nonionic Triblock and Star Diblock Copolymer and Oligomeric Surfactant Syntheses of Highly Ordered, Hydrothermally Stable, Mesoporous Silica Structures, J. American Chemical Society, 120 (1998) 6024-6036.

[60] J.K. Leland, A.J. Bard, Photochemistry of colloidal semiconducting iron oxide polymorphs, The. Physical Chemistry, 91 (1987) 5076-5083.

[61] M.A. Didi, B. Makhoukhi, A. Azzouz, D. Villemin, Colza oil bleaching through optimized acid activation of bentonite. A comparative study, Applied Clay Science, 42 (2009) 336-344.

[62] B. Makhoukhi, M.A. Didi, D. Villemin, A. Azzouz, Acid activation of Bentonite for use as a vegetable oil bleaching agent, Grasas y Aceites, 60 (2009) 343-349.

[63] R. Ouargli, N. Bouazizi, M. Khelil, S. Nousir, R. Benslama, S. Ammar, A. Azzouz, SBA-15-supported iron nanoparticles with improved optical properties, conductance and capacitance, Chemical Physics Letters, 673 (2017) 30-37.

[64] N. Bouazizi, R. Ouargli, S. Nousir, R.B. Slama, A. Azzouz, Properties of SBA-15 modified by iron nanoparticles as potential hydrogen adsorbents and sensors, J. Physics and Chemistry of Solids, 77 (2015) 172-177.

[65] V.A. Arus, S. Nousir, R. Sennour, T.C. Shiao, I.D. Nistor, R. Roy, A. Azzouz, Intrinsic affinity of acid-activated bentonite towards hydrogen and carbon dioxide, International Journal of Hydrogen Energy, 43 (2018) 7964-7972.

[66] P. Mazellier, J. Leverd, Transformation of 4-tert-octylphenol by UV irradiation and by an H_2O_2/UV process in aqueous solution, Photochemical & Photobiological Sciences, 2 (2003) 946-953.

[67] Y. Liu, J. Zhao, Z. Li, G. Li, W. Li, X. Gao, Catalytic ozonation of bisphenol A in aqueous solution using Mn-Ce/HZSM-5 as catalyst, Water Science and Technology, 72 (2015) 696.

[68] T. Garoma, S.A. Matsumoto, Y. Wu, R. Klinger, Removal of Bisphenol A and its Reaction-Intermediates from Aqueous Solution by Ozonation, Ozone: Science & Engineering, 32 (2010) 338-343.

[69] M.M. Huber, T.A. Ternes, U. von Gunten, Removal of estrogenic activity and formation of oxidation products during ozonation of 17alpha-ethinylestradiol, Environmental science & technology, 38 (2004) 5177-5186.

[70] J. Ma, N.J.D. Graham, Degradation of atrazine by manganese-catalysed ozonation-influence of radical scavengers, Water Research, 34 (2000) 3822-3828.

[71] R. Sturza, M. Melenciuc, D. Nistor, F. Boudissa, T. Terkani, N.-H.H. Abdelkader, A. Abdelkrim, recyclable porous materials for the uptake of bisphenol A, 2017, 16 (2017).

[72] A. Azzouz, Advances in oxidative decomposition of oxalic acid in aqueous media,J. Advances in Chemistry Research, 14 (2012) 1-31.

[73] M. Sulpizi, M.-P. Gaigeot, M. Sprik, The Silica–Water Interface: How the Silanols Determine the Surface Acidity and Modulate the Water Properties, J. Chemical Theory and Computation, 8 (2012) 1037-1047.

[74] A. Azzouz, Advances in Oxidative Decomposition of Oxalic Acid in Aqueous Media, Nova-Publishers, New-York, USA, New York, 2012 2nd quarter.

[75] T. Sreethawong, S. Chavadej, Color removal of distillery wastewater by ozonation in the absence and presence of immobilized iron oxide catalyst, J. Hazardous Materials, 155 (2008) 486-493.

[76] Y.D. Shahamat, M. Farzadkia, S. Nasseri, A.H. Mahvi, M. Gholami, A. Esrafili, Magnetic heterogeneous catalytic ozonation: a new removal method for phenol in industrial wastewater, J. Environmental Health Science and Engineering, 12 (2014) 50.

[77] R. Rosal, M. S. Gonzalo, A. Rodríguez, J. Perdigón-Melón, E. García-Calvo, Catalytic ozonation of atrazine and linuron on $MnOx/Al_2O_3$ and MnOx/SBA-15 in a fixed bed reactor, 2010.

CHAPITRE III

ARTICLE III: CLAY-CATALYZED OZONATION FOR EFFECTIVE REMOVAL OF ENDOCRINE-DISRUPTING COMPOUNDS IN SOLVENT-FREE MEDIA

Farida Boudissa[a], Meriem Zekkari[b], Rachel Levesque-Bélanger[a], Rachida Ouargli-Saker[b], René Roy[a], Abdelkrim Azzouz[a,*]

[a] *Nanoqam, Department of Chemistry, University of Quebec at Montreal, QC, Canada H3C 3P8.*

[b] *Department of Materials Engineering, University of Science and Technology, Oran, Algeria.*

**Correspondence: azzouz.a@uqam.ca; Tel: 1 514-987-3000, ext. 4119*

Contribution des co-auteurs

Ma contribution personnelle à cet article: Réalisation des expériences, obtention des résultats et traitement des données, conception des figures et des tableaux, essais d'interprétation des résultats. Rédaction préliminaire de l'article et prise en charge des soumissions au nom de l'auteur correspondant.

Zekkari Meriem: Réalisation d'une recherche bibliographique, synthèse et caractérisation de SBA-15 et participation aux tests expérimentaux.

Levesque-Bélanger Rachel: Étude de l'effet de co-solvant sur l'ozonation de l'éthinylestradiol en présence de Fe(II)Mt.

Ouargli-Saker Rachida: Échange de résultats expérimentaux complémentaires.

Roy René : Correction de l'article.

Azzouz Abdelkrim : Conception et direction de la recherche sur l'ozonation des polluants organiques, vérification et corrections des interprétations des résultats, finalisation de l'article.

CHAPITRE III

ARTICLE III: CLAY-CATALYZED OZONATION FOR EFFECTIVE REMOVAL OF ENDOCRINE-DISRUPTING COMPOUNDS IN SOLVENT-FREE MEDIA

Abstract

An original approach never tackled so far allowed correlating the basicity and hydrophilic character of clay catalysts to surface interaction with EE2 and water. The clay catalysts were found to behave specifically according to their chemical composition like soils in natural oxidative processes. Acid-activated bentonites (HMt) and ion-exchanged montmorillonite (NaMt and Fe(II)Mt) showed catalytic activity in the ozonation of 17α-ethinylestradiol (EE2) in aqueous media. In the absence of catalyst, the degradation of (EE2) reached 72 % after one minute of ozonation and 99.5% after 60 minutes. In the presence of Fe(II)Mt, EE2 degradation (96 %) was achieved after only one minute ozonation. Under similar conditions, almost total degradation to 99.99 % was registered in 15 minutes of ozonation but without total mineralization of the intermediates. Moderately acid-activated bentonites exhibited higher activity affording total mineralization within short ozonation. The catalytic activity of clay catalysts was found to correlate with their surface basicity and hydrophilic character. The results obtained herein allow envisaging effective clay catalysts with surface properties judiciously tailored according to the organic pollutants.

3.1 Introduction

Oxidative processes naturally occur in soils, and organic pollutants carried by waters decompose more or less rapidly in nature according to the chemical compositions of the organic molecules and type of soils. The use of soils as catalysts still remains a major challenge given the high number of parameters that can influence the oxidative process. However, investigation of the catalytic properties of isolated key-components of soils such smectite-type materials in oxidative processes would be an interesting route to be explored. That is why the present work was undertaken.

Soils are first contaminated when wastewaters containing endocrine disrupting compounds (EDCs) are released in nature. This has direct negative impact on human health and biodiversity, and has become a global concern that has focused scientist interest in recent years. EDCs may arise from agriculture (herbicides and pesticides), industrial and household wastewaters. 17α-Ethinylestradiol (EE2) is an EDC used as oral contraceptive and postmenopausal hormonal supplement [1, 2]. EE2 is usually found in household wastewaters [3-5], reaching concentrations ranging from 0.2 to 7.0 ng L^{-1} in rivers and streams [6]. Compared to natural estrogens, EE2 displays low biodegradation capacity [7, 8] and can accumulate into algae and fish [9]. EE2 has a strong feminization effect on male fish and affects fertility in aquatic populations [10-16]. Exposure to EE2 has also been linked to the development of prostate cancer [17].

EE2 detection in aquatic environments is due to its incomplete removal by conventional treatment procedures [18-20]. The latter are not specifically designed for steroid removal. For EE2 removal during wastewaters treatments, most methods such as electrochemical techniques [21,22], biological processes [23,24], and

photodegradation under sunlight exposure [25] turned out to be unsatisfactory, given the low biodegradability [7,8] and high bioaccumulation of the compound. Chlorination is an effective technique that allow affording complete EE2 degradationchlorination [26-28], but the unavoidable formation of carcinogenic chlorinated by-products is a major drawback.

Ozone could be a promising alternative to chlorine in oxidation processes, being a clean and powerful oxidizing agent that generates only CO_2, water and at most small amounts of NOx and Sox in optimal conditions. However, in spite of the high reactivity of ozone, conventional ozonation of emerging contaminants usually leads to incomplete mineralization, producing harmful intermediates that exhibit sometimes even higher toxicity than the parent molecule [29, 30].

Very few studies and incomplete data are available on the degradation of EE2 in pure water, probably because of its very low solubility in water and highly hydrophobic character [32]. In contrasts, there exists an ample literature on EE2 removal attempts involving solubility enhancement using water-miscible organic solvent such as acetonitrile, ethanol and others [31-33]. In these works, the co-solvent is supposed to display low reactivity toward ozone. The latter is often subtracted through blank tests without taking into account the solvent contribution to the interactions occurring between the different components of the reaction mixture. Such approaches cannot allow accurate assessment of the intrinsic reactivity of EE2 towards ozone and neglect the intrinsic interactions of EE2. These interactions are often involved with the oxidizing agent, water and solid particles in suspension when contacting wastewaters with soils. Furthermore, the use of co-solvent induces additional ozone consumption and production of more derivatives, raising both the operating costs and pollution risks. This is doomed to failure, and cannot be regarded as a viable and eco-friendly alternative in water treatment.

The low solubility in water should not be regarded as an obstacle for investigating EE2 degradation processes, but rather beneficial for energy considerations when using ozone in tertiary treatments of waters with low EE2 contents, if any. In this regard, to address this issue the main objective of the present work was focused on the ozonation of very diluted EE2 aqueous solution. This allows achieving an oxidative process in solvent-free aqueous media.

Catalytic ozonation turned out to be a more effective method for removing organic micro pollutants as a potential tertiary treatment step in wastewater treatment plants [34-36], but high operating costs still limit its implementation as a viable water treatment route [37] . In order to overcome these drawbacks, the use of solid catalysts was already found to be beneficial due to the contribution of adsorption in the catalytic process, as this unavoidably occurs in soils. Natural microporous materials such as clay minerals were recently used for improving the catalytic ozonation thanks to their lamellar structure with large specific surface area, high cation exchange capacities, high sorption capacity, lack of toxicity, harmlessness and low cost production [38, 39]. Catalysts based on montmorillonite (Mt) ion exchanged with different cations in the forms Fe(II)Mt and NaMt allowed affording fast and almost total removal of the organic pollutants [34-36].

For reasons related to cost and process profitability, EE2 decomposition was achieved in the presence of eco-friendly montmorillonite-based catalysts and acid-activated bentonites. The latter are expected to exhibit different silica-to alumina ratio and account for various types of soil-inspired catalysts. The catalytic activity was correlated with the acid-base properties and moisture content as assessed through thermal programmed desorption technique (TPD). The catalyst dispersion in aqueous media is a key-factor that determines the extent of the specific surface area and porosity, and was examined through Zeta potential and particle size measurements and hydrophilic-hydrophobic character assessment. The improvements brought by the clay catalyst the

ozonation process is herein discussed in terms of adsorption and contributions of Lewis-acid-base and hydrophilic-hydrophobic interactions of the involved chemical species and solid surface.

3.2 Experimental

3.2.1 Materials and reagents

17α-Ethinylestradiol (EE2) (> 98%) was supplied by Sigma–Aldrich (St. Louis, MO, USA). The physicochemical properties of 17α-ethinylestradiol (EE2) (Scheme 3.1) are given in Table S3.1. Ethanol and acetonitrile HPLC-grade were also purchased from Sigma-Aldrich (St. Louis, MO, USA). Nanopure water was used throughout this work. All chemicals and reagents used in this work were not previously purified.

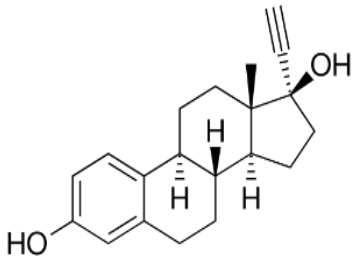

Scheme 3.1. Structural representation of EE2 molecule.

EE2 solution (10^{-5} M) was prepared by dissolving appropriate amount of EE2 in water under vigorous stirring for 5 days due to its low solubility in water. The prepared solution preserved in a sealed air-free vessel protected from light with an aluminum foil. The dilutions were made from Standard Stock solution for the preparation of different EE2 concentration.

To investigate the effect of the co-solvent, a second EE2 solution (11.06 x 10^{-6} M) was prepared in a 500 mL volumetric flask by dissolving 1.65 mg of EE2 in distilled water. Given that EE2 is very sparingly soluble in water, 7 µL of ethanol was added (H_2O/C_2H_5OH = 99.998/0.001). The mixture of EE2 in water and ethanol (0.239 x10^{-9} M) was slightly warmed in an oil bath (T = 37.0 ± 0.5 °C) under vigorous and continuous stirring for 5 days.

3.2.2 Catalyst preparation

The clay catalysts were prepared starting from a crude bentonite supplied by Sigma-Aldrich (USA). Montmorillonite-rich material (Mt) was obtained through bentonite purification and full ion-exchange into NaMt form, according to a procedure already described elsewhere [35, 40] and then into Fe(II)Mt by further NaMt impregnation with saturated aqueous solutions containing nitrate salts of Fe^{2+} ($FeCl_2$ $4H_2O$). Rely on the previous researches, we chose these exchangeable cations [35, 41]. After cation exchange, the Fe(II)Mt was washed with distilled water by centrifugation and then followed by filtration, until no chloride was detected while washing by $AgNO_3$ test. The resulting powder (Fe(II)Mt) dried at 80 °C for 24 hours and softly crushed into a powder form. The acid-activated catalysts (HMt) were prepared through acid activation of crude bentonite. For this purpose, 200 g of clay were impregnated by 1000 mL of aqueous 5 M sulfuric acid solution (98%) at 80 °C for different contact times (1, 4, 8, 15 and 24 hours, respectively) under mild stirring [42-44]. HMt samples, denoted as HMt-1, HMt-4, HMt-8, HMt-15 and HMt-24, were further washed with distilled water until neutral pH and dried at 100 °C for 12 h.

3.2.3 Catalyst characterization

The crude bentonite, ion-exchanged montmorillonite and acid-activated bentonite were characterized through X-ray diffraction (XRD) using a Siemens D5000 instrument (CuKα, λ = 1.54051 A°). Bentonite purification and full ion-exchange into a homo-ionic clay mineral was found to produce a marked sharpening of the broad 001 XRD line. This indicates a perfectly parallel arrangement of the clay lamellae. No crystallinity loss was noticed after 1-15 hours of acid activation. Slight depletion of the main XRD line was observed for the raw bentonite treated for 24 h. Powder X-ray diffraction (XRD)measurements of the SBA samples were carried out using a Siemens D5000 X-ray diffractometer and a Co-Kα radiation (λ = 1.7890 A°). The chemical compositions of the mineral clay was assessed through X-ray fluorescence (S-4 Pioneer equipment; Brüker Rh tube; Powder press 34 mm with 10% boric acid; standardless method with 0.5% error) as already reported.

The adsorptive properties were evaluated through measurements of CO_2 and water retention capacity (CRC and WRC, resp.) for all the investigated catalysts. This was achieved by thermal programmed desorption of carbon dioxide (CO_2-TPD), under a and 5 mL min^{-1} nitrogen stream at 5 °C min^{-1} heating rate (in tubular glass reactor coupled to a Li-840A CO_2/H_2O Gas detector (Systech Instruments Ltd., USA). The montmorillonite based catalyst was analysed between 20 and 450 °C and for SBA analysed was analysed between 20 and 80 °C [45-47]. The particle size was determined using a Malvern-Zetasizer Nanoseries device in water and in aqueous EE2 solutions, while the Zeta potential was assessed with a Brookhaven instrument.

3.2.4 Ozonation tests

An amount of 20 mL of solutions (10^{-5} M), without or with 40 mg of dry catalyst was ozonated at different times at room temperature. Ozone was supplied at a 600 mg h^{-1} flow rate by a portable ozone generator (A_2Z Ozone Inc, USA) from air. Catalytic ozonation attempts were performed at room temperature in the presence of 2 mg of solid catalyst (SBA-16 or Fe-SBA-16). More specifically, 20 ml samples of EE2 (6.76 μmol L^{-1}, 33.73 μmol L^{-1} and 100 μmol L^{-1}) aqueous solutions were introduced in a 2 cm x 6 cm cylindrical PVC reactor, and then exposed to ozone bubbling.

3.2.5 Products analysis

After ozonation and catalyst removal by centrifugation, the concentration of EE2 in the supernatant of the reaction mixture was periodically analyzed by UV-Visible spectrophotometry (Varian-Cary 5000 instrument, Agilent Technologies. USA). The pH level was simultaneously measured with a Fisher Scientific Accumet XL 600 pH metre and Accumet® model 15 pH-meter. Complementary measurements of the evolution in time of EE2 concentration during ozonation was achieved through high-performance liquid chromatography (Waters Alliance 2695 HPLC system) equipped with a C18 column (4.6 mm x 100 mm x 3.5 μm particle size. Agilent USA) and coupled to a UV detector (Waters 2487 HPLC Absorbance UV-Vis Detector). An acetonitrile/water mixture (50:50, v/v) was injected as a 0.65 mL min^{-1} mobile phase. The injection volume was of 20 μL. The wavelength was fixed at 280 nm.

Early ozonation intermediates were identified by additional analysis of short time ozonation mixtures (1-10 min, 20 μL of injected sample) using high performance liquid

chromatography time-of-flight mass spectrometry (HPLC-ToF-MS) [27]. For this purpose, an Agilent Eclipse Plus C18 column was employed (1.8 μm; 3 x 50 mm), with water-formic acid (A) and acetonitrile (ACN)-formic acid (B) mixtures used as the mobile phases. In such analyses, only the mixture B was prone to a gradient variation (Table S2). The flow rate of the HPLC pump was 0.4 mL min^{-1}.

3.3 Results and Discussion

3.3.1 Non-catalytic ozonation in water

Preliminary experiments providing different UV-Vis spectra achieved at various EE2 concentrations (Fig. S3.1) allowed plotting calibration curves (Fig. S3.2). As a common feature of phenolic derivatives, three main absorption bands were noticed for EE2 at 278-280, 220 and 198 nm. A weak intensity band observed at 280 nm corresponds to the n-π* transition which is related to an intramolecular charge transfer band of the hydroxyl free electron pair of phenol conjugated with the π unsaturated system [48]. This band is expected to progressively disappear during EE2 oxidation, indicating the ozonation advancement in time and providing a fairly accurate assessment of the degradation yield of EE2. The 220 nm band accounts for π-π* transitions. The most intense is rather a shoulder observed at 198 nm band, being a common feature of OH-compounds. The intensity of these three bands increased linearly with increasing EE2 concentration within specific concentration ranges. This allowed and assessing the molar extinction coefficient for each of these bands according to Beer-Lambert's law with correlation coefficient (R^2) exceeding 0.97 (Table. S3.1). The spectral feature of the reaction mixture were found to significantly

vary in time (Fig. 3.1), indicating the occurrence of a reaction between ozone and EE2. The marked intensity increase in the region 190-250 nm is a clear confirmation of the enhanced formation of oxidized species bearing hydroxyl groups [33].

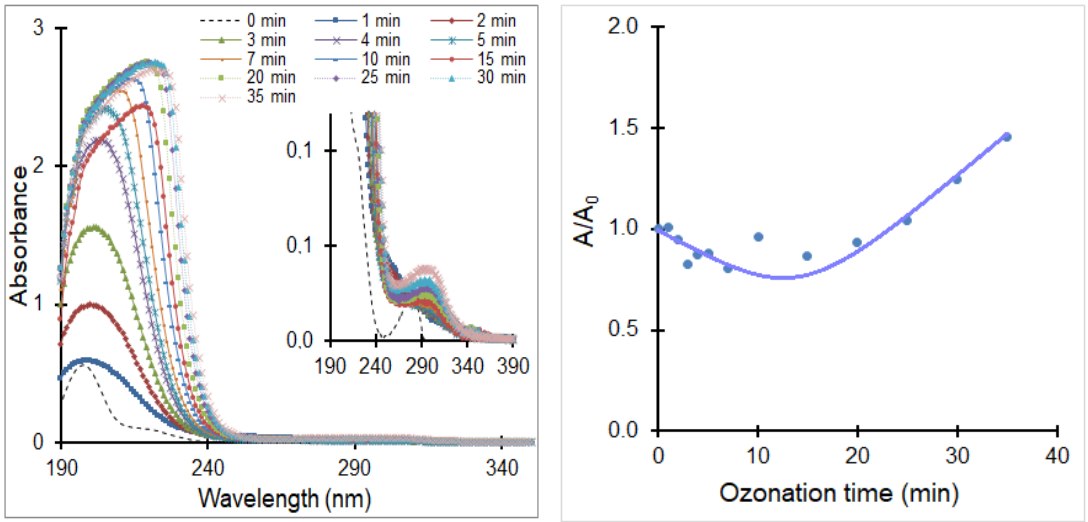

Fig. 3.1. Evolution of the UV-Vis spectrum of EE2 in aqueous solution during ozonation (a) and relative absorbance at 280 nm (b) of EE2. T = 22 °C. pH = 5.28. Quartz cell = 1 cm. O_3 throughput: 600 mg h^{-1}. Sample volume = 20 mL. Initial EE2 concentration: 10^{-5} M.

As previously stated, this broad region is not specific but rather common feature to OH-compounds including acids, aldehydes, alcohols and water, as already reported for many organic substrates [35, 40,59-54]. All oxygenated EE2 derivatives should absorb in the same UV-Vis region, and their progressive appearance in this region is reflected by a paradoxical intensity increase in time as EE2 is decomposed. Subsequently, notwithstanding that these bands cannot be used in the calculation of the conversion yield, they provide valuable information about the ozonation advancement in time.

Deeper insights in the evolution of EE2 UV-Vis spectra in time (Fig. 3.1-a) showed the progressive and slightly delayed rise in time of a new band at 280-310 nm. Such a band is supposed to arise from the production of hypothetical protected EE2 forms

(hydroperoxides) via fast reaction of phenoxyl radicals with superoxide anion as already reported [55]. Such hydroperoxides are supposed to be weakly reactive toward ozone, and decompose reversibly into the parent EE2 molecule through slow dioxygen release. This induced a shading effect after 10-15 min ozonation on the visible intensity decay for the 268 nm band (Fig. 3.1-b), which is supposed to account for EE2 depletion in time. Consequently, attempts to achieve at most approximate assessment of EE2 degradation by UV-Vis, if any, should be restricted to ozonation time not exceeding 10 min.

3.3.2 EE2 identification and quantification during ozonation

HPLC measurements allowed overcoming this shortcoming through clear discrimination of EE2 with its characteristic peak at a 16.8 min retention time for EE2 UV detection at 280 nm (Fig. 3.2-a). This allowed plotting a calibration curve with two linearities for two different concentration ranges (2-b). This linearity loss with increasing concentrations must be due the appearance of interaction between EE2, derivatives molecules and water that produced shift of the analyzed UV-Vis band. A significant depletion of the EE2 peak was noticed during non-catalytic ozonation (Fig. 3.3-a). Fast reaction occurred during the first 2-3 min, as supported by the marked decrease in EE2 peak area ratio followed by a marked attenuation for longer ozonation times (Fig. 3.3-b). In the meantime, a wide variety of new three peaks appeared at shorter retention time between 2 and 4 min (Table S3.4), indicating the formation of by-product compounds with lower molecular weight and higher polarity [56].

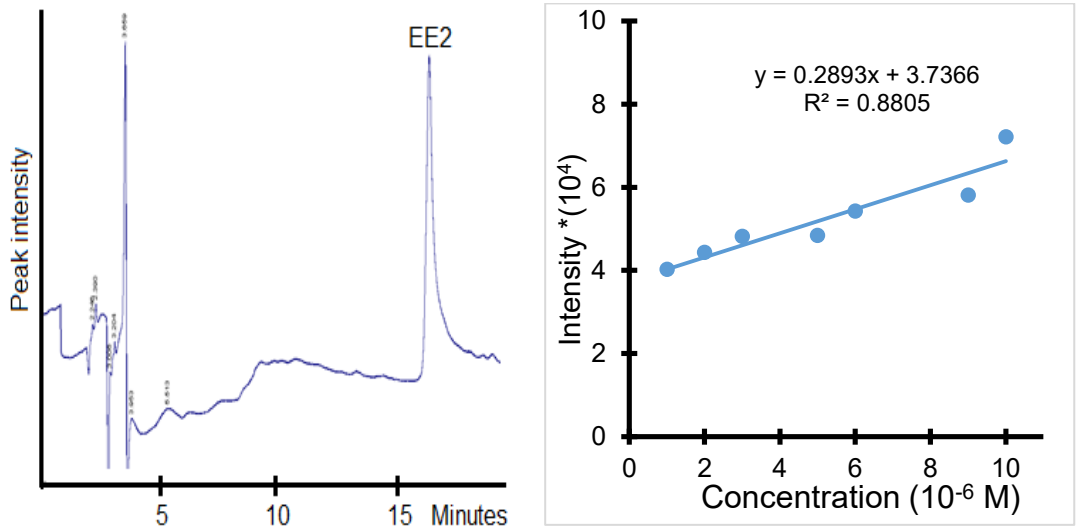

a **b**

Fig. 3.2. HPLC chromatogram (a) and calibration curve (b) of EE2 in aqueous solution detected by UV detector at wavelength of 280 nm. T = 22 °C. pH = 5.28. EE2 concentration: 10^{-5} M.

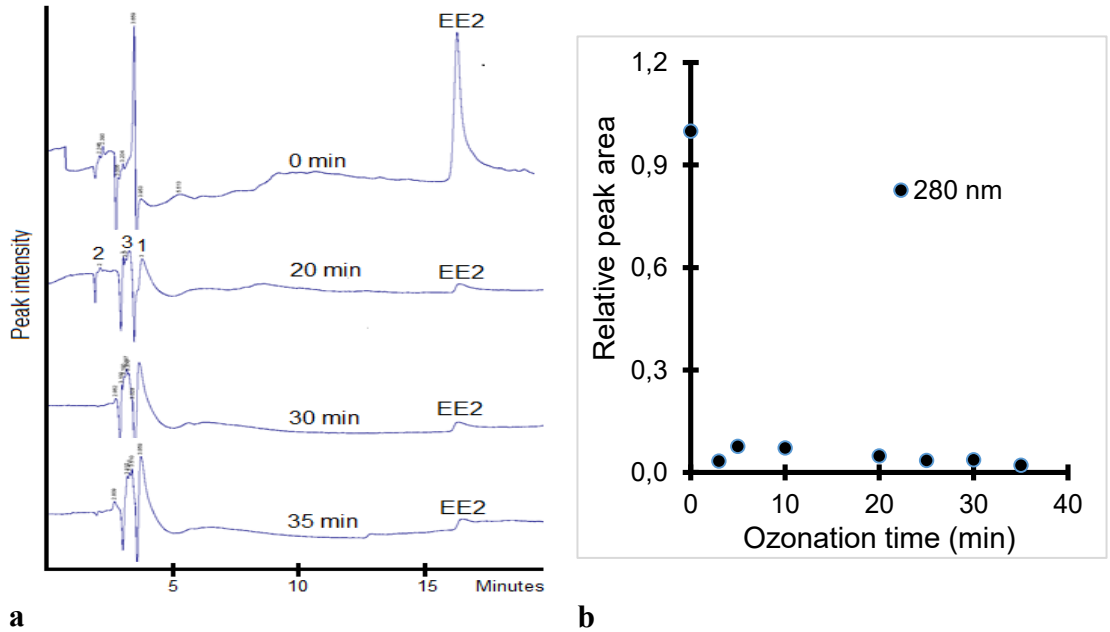

a **b**

Fig. 3.3. Evolution in time of the HPLC-UV diagram (a) and of the relative EE2 peak area (b) during non-catalysed EE2 ozonation in distilled water. Analyzed by HPLC-UV at wavelength of 280 nm. T = 22 °C. pH = intrinsic. Initial concentration: 10^{-5} M.

This provides evidence of EE2 oxidation by ozonation, affording ca. 93% degradation yield after only 10 min of reaction. This can be regarded as promising result that demonstrates that in spite of incomplete mineralization, estrogenic activity is significantly reduced [57]. The intensity of one of these three peaks (Intermediate 1) continuously increased in time, being presumably quite refractory to oxidation, unlike the two other peaks (Intermediates 2 and 3) (Fig. 3.4). The latter showed two bumps each, indicating two formation and two decomposition processes. This suggests that both intermediates originate from at least two different reactants in two successive ozonation steps.

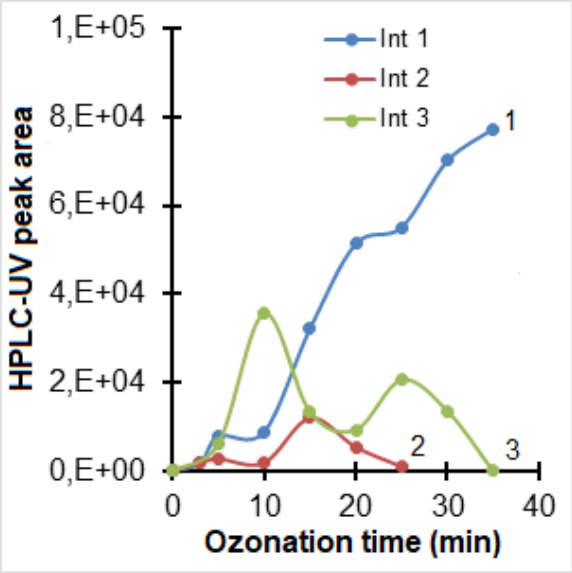

Fig. 3.4. Evolution in time of non-catalysed ozonation of EE2 ozonation in distilled water. Analysed by HPLC- UV at wavelength of 280 nm. T = 22 °C. pH = intrinsic. Concentration: 10^{-5} M.

3.3.3 Effect of catalyst addition in the presence of a solvent

The effect of catalyst addition was investigated by using Fe^{2+}-exchanged montmorillonite (Fe(II)Mt), which turned out to be the most effective catalyst in the ozonation of organic substrates [34-36]. Due to the low solubility of EE2, preliminary tests of ozonation were performed in the presence of ethanol as the solvent. As expected, the relative absorbance for all UV-Vis-bands disappeared within less than 2 min of ozonation (Fig. 3.5-a). Almost total degradation of EE2 was achieved after only 1 min ozonation in the presence of Fe(II)Mt but more than 12 min when no catalyst was used.

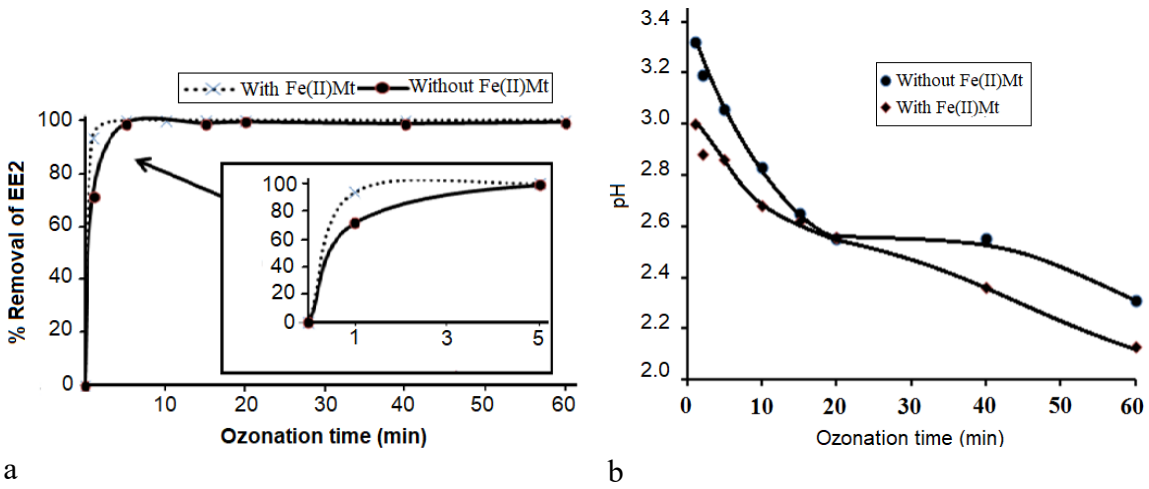

Fig. 3.5. Evolution in ozonation time of EE2 removal yield (a) and pH (b) in aqueous-ethanol solution. pH initial 3.32 without catalyst and 3.0 in the presence of Fe(II)Mt. EE2 initial concentration 11.06 μmol L^{-1}, λ = 280 nm, Catalyst concentration = 2 gL^{-1}.

During ozonation, the pH decreased in time due to the formation of acidic species by non-catalytic ozonation (Fig. 3.5-b). This pH decrease was more accentuated in the presence of catalyst (Fe(II)Mt), and appears to take place in two successive steps. This was confirmed by HPLC-ToF-MS analysis (negative ion mode), which revealed low retention time for such compounds (0.8 min), which should have lower molecular weight but greater polarity (Fig. 3.6).

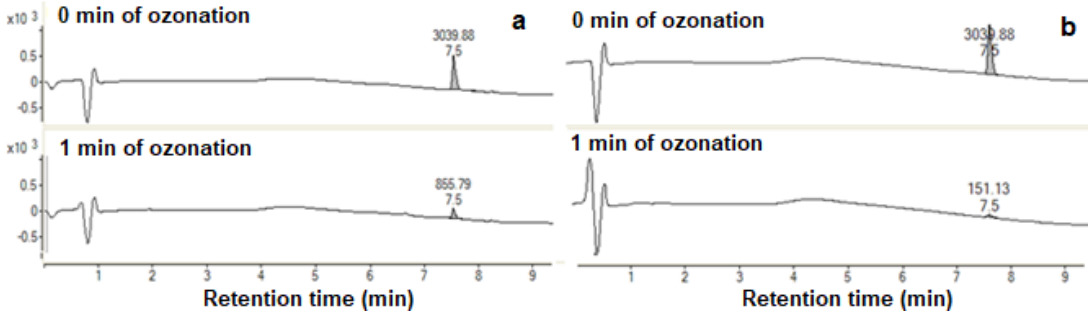

Fig. 3.6. HPLC-ToF-MS chromatogram of EE2 ozonation mixture after 1 min ozonation in the absence (A) and presence of Fe(II)Mt (B) in aqueous-ethanol solution. Initial EE2 concentration = 11.06 µM.

Their higher peak intensity in the presence of Fe(II)Mt and almost total disappearance of EE2 peak after 1 min ozonation (Fig. 3.6-b) are due to the beneficial effect of catalyst addition. The intermediates identified by HPLC-ToF-MS in negative ion mode (Table 3.1) are the most preponderant, with molecular weight of 144 g mol^{-1} ($C_7H_{12}O_3$), 296 g mol^{-1} ($C_{20}H_{24}O_2$) and 314 g mol^{-1} ($C_{15}H_{22}O_7$). The latter was also detected in other works [58]. The compound corresponding to the 346 g mol^{-1} molecular weight and detected at a retention time of 7.2 min could not be identified. Investigations are still in progress in this direction.

Among these, the only acid appearing at the beginning of the reaction was identified as being 1-hydroxy-cyclohexane carboxylic acid ($C_7H_{12}O_3$). The continuous production of this intermediate during ozonation should involve further non-selective oxidation of most EE2 derivatives (Fig. 3.7-a). The early presence of such a small species is supported by its maximum concentration in the ozonation mixture after ca. 2 min reaction, and is a precise indicator of the effectiveness of EE2 degradation. The latter was confirmed by the almost total disappearance of this intermediate after less than 60 min ozonation.

Table 3.1. Identification of major intermediates degradation of EE2 ozonation by HPLC-ToF-MS [58].

Products	Retention time (min)	Chemical formula	Molar mass (g mol)	m/*z*
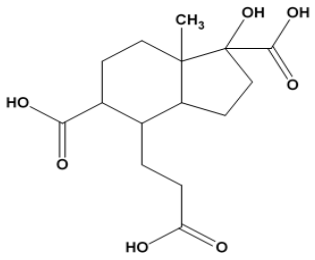	6.8	$C_{15}H_{22}O_7$	314	313.2
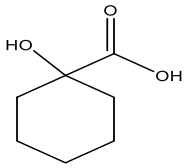	0.8	$C_7H_{12}O_3$	144	142.9

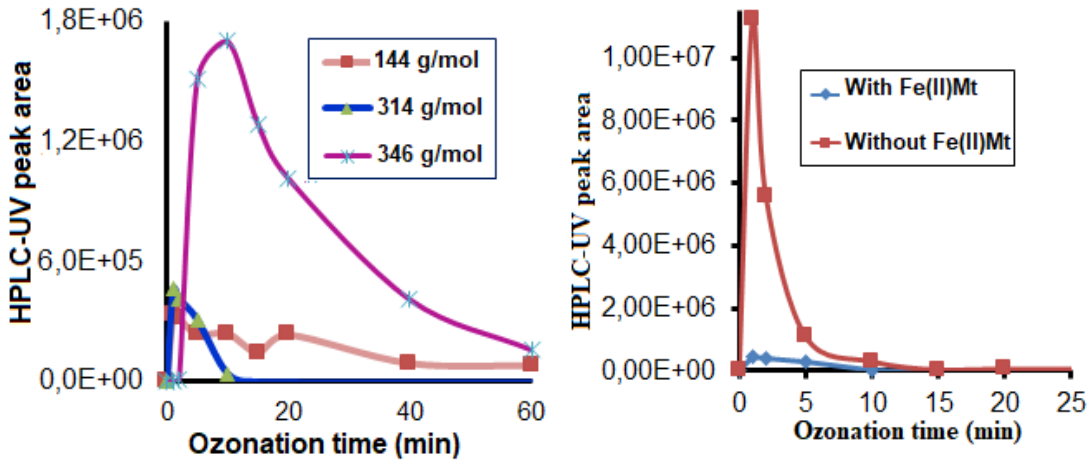

Fig. 3.7. Evolution of the HPLC-ToF-MS peak intensity of EE2 intermediates during catalytic ozonation (a) and 314 g mol^{-1} intermediate (b) in aqueous-ethanol solution**.** Initial EE2 concentration = 11.06 µmol L^{-1}, Fe(II)Mt concentration: 2 g L^{-1}, Ozone dose: 600 mg h^{-1} at 22 °C.

The peak succession in time indicates that this acidic species appears earlier as compared to the 346 g mol^{-1} intermediate, and thereby does not result only from the oxidation of its bulkier counterparts. The detection of $C_{15}H_{22}O_7$ (molecular weight 314 g mol^{-1}) after the first minutes of ozonation and its fast disappearance after only 10 min provide clear confirmation that EE2 hydroxylation is the first step of ozonation, followed by phenyl ring cleavage, in agreement with our previous works [35, 36, 40, 52]. The formation of the 314 g mol^{-1} intermediate was significantly enhanced in the presence of Fe(II)Mt (Fig. 3.7-b), suggesting that clay-catalysts promote pronounced hydroxylation process.

3.3.4 Effect of catalyst addition in solvent-free media

Additional attempts for EE2 degradation in solvent-free media revealed thorough conversion of EE2 within short ozonation time as supported by the total disappearance of the corresponding HPLC-ToF-MS peak (retention time 7.63 min) after only 1 min clay-catalyzed ozonation (Fig. S3.3), i.e. after shorter reaction time as compared to ozonation in the presence of solvent (Fig. 3.5 and 3.6). Here, ethanol addition appears to mitigate the ozonation effectiveness, most likely due to its simultaneous ozonation that involves competitive ozone consumption.

In the meantime, a variety of EE2 derivatives were detected at shorter retention times of 6.06, 6.53, 6.84 and 7.27 min. The latter were identified through their m/z values (Fig. S3.3 and S3.4). Two EE2 by-products were identified , as corresponding to a 344 g mol^{-1} intermediate ($C_{20}H_{24}O_5$) [59] with an open phenolic ring structure and a 302 g mol^{-1} derivative ($C_{18}H_{22}O_4$) with also an open phenolic ring but with loss of the acetylenic and hydroxyl groups (Table 3.2), in agreement with other works [57,59].

The identification of compounds with suggested molecular weights of 302 and 344 was already reported by Larcher et al. [59], which confirmed that the aromatic ring opens even before the attack on the alkyne group. The catalytic step on an aluminosilicate surface inevitably involves adsorption of EE2 and its intermediates. This step can displace the electronic densities of the adsorbed species thereby modifying the reactivities of the different chemical groups. This could explain, at least partially, the unexpectedly weaker reactivity of the alkyne group towards ozone. In addition, the appearance of alkene groups is unavoidable arising from phenyl ring clivage, as reported by an ample literature. Given that ozone is usually supposed to readily react with isolated alkenes, it appears that the catalytic ozonation involves operating conditions that differ greatly from those of conventional organic chemical reactions.

Research should be pursued in order to assess the activation energy of the main reactions that may be involved in the first stage of EE2 ozonation.

The high resolution HPLC-ToF-MS data show another peak at 330 g mol^{-1}. O'Grady et al. provides a clear molecular structure ($C_{20}H_{26}O_4$) of this intermediate with a molecular weight of rather 330 g mol^{-1} [60]. This compound was obtained in biological conditions that may involve specific enzymatic processes, but its formation cannot explain the migration of: ***i.*** the ethinyl moiety from C-17 beta to C-16 position; ***ii***. and that of the hydroxyl group from C-17 alpha to C-17 beta. Unless clay minerals act as chiral catalysts inducing asymmetry, such a structure, probably an isomer, still remains hypothetical, because comparison with the NIST data base is not a rigorous identification approach, which usually requires additional IR, NMR and XRD analyses. Besides, the question of why ozonation does not produce acetyl group in position C-17 beta remains to be answered, as well.

The peak intensity of the 344 g mol^{-1} intermediate decreased after 5 min of ozonation, while that corresponding to the 302 g mol^{-1} derivative disappeared after 5 min of reaction time. This result demonstrates the occurrence of phenol ring cleavage and that ozone is fairly selective towards EDCs degradation [55, 60-62]. Compounds with similar molecular weight of 302 and 344 amu have already been identified by complementary analysis techniques of ozonation reaction mixtures [59] but structure comparison was still based on the NIST data base. This confirms that the aromatic nucleus opens even before the alkyne group attacks. The appearance of alkene is inevitable and arises from the opening of the aromatic cycle. The high number of published work reporting the formation of –ene-type substances indicates that no ozone attack takes place instantly on isolated alkenes, presumably due to the fact that the operating conditions in our research differ greatly from those of conventional organic chemical reactions.

Table 3.2. EE2 molecule (a) and the three by-products of EE2 ozonation with mass of 344 g mol^{-1} (a) 330 g mol^{-1} (b) and 302 g mol^{-1} (c) as identified by HPLC-ToF-MC analysis at wavelength 280 nm.

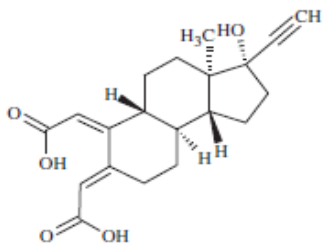	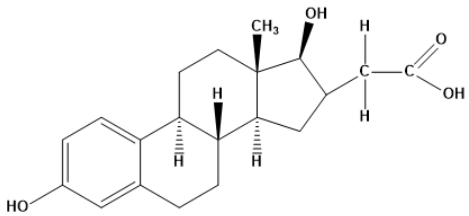	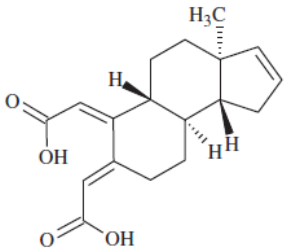
344 g mol^{-1} **(a)**	330 g mol^{-1} **(b)**	302 g mol^{-1} **(c)**

3.3.5 Effect of the exchangeable cation

NaMt and Fe(II)Mt were found to exhibit different catalytic behavior as reflected by specific UV-Vis spectra evolution in time (Fig. S3.5). The intensity increase in time for all EE2 absorbance bands during the first 15 min ozonation is a precise indicator of the reaction advancement (Fig. 3.8-a). Much higher intensity of the 280 nm band was noticed in the presence of NaMt (Fig. 3.8-b). This is mainly due to the key-role of the exchangeable cation, which first involve specific polarizing capacity. Unlike Na^{+}, Fe^{2+} cation is expected to display stronger polarizing effect on water molecules, generating Bronsted acidity. This intensity increase of the 280 nm band contrasts with its total disappearance in the HPLC-UV diagram after only 5 min ozonation in the presence of NaMt (Fig. S3.6). This must be due to the formation of EE2 intermediates with light absorption in the same UV region. This confirms once again that, unlike HPLC-UV, UV-Vis analysis cannot allow accurate assessment of the degradation yield, at least during the first 15 min of ozonation, i.e. before the degradation of such intermediates is triggered.

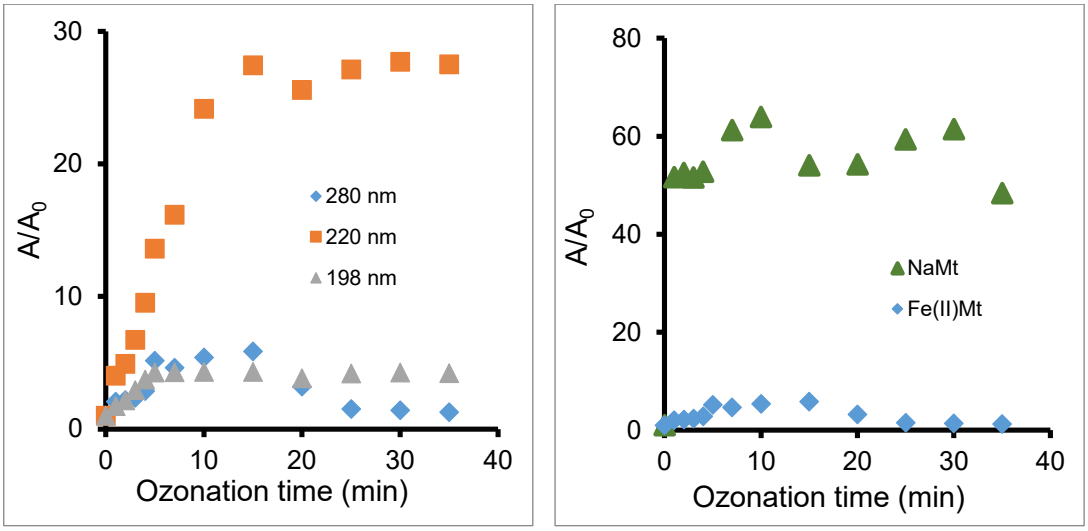

Fig. 3.8. Relative absorbance of all EE2 bands in the presence of Fe(II)Mt (a) and of the 280 nm band in the presence of NaMt and Fe(II)Mt (b) during ozonation in distilled water solutions. T = 22 °C. Quartz cell = 1 cm. O_3 throughput: 600 mg h^{-1}. Sample volume = 20 mL. EE2 initial concentration: 10^{-5} M. Catalyst amount = 40 mg.

The fact that the HPLC-UV peak of EE2 persisted even up to 35 min ozonation indicates a weaker catalytic activity of Fe(II)Mt as compared to its Na^+-exchanged counterpart (Fig. S3.6). The latter allowed affording EE2 degradation yield of ca. 98 % after 5 min and 100 % after 10 min ozonation, but only 89 % after 10 min in the presence of Fe(II)Mt under similar condition. This apparently higher catalytic activity of NaMt contrasts with its lower selectivity. Indeed, NaMt was found to produce higher number and amounts of intermediates as well argued by the higher number and intensity of the corresponding HPLC-UV peaks (Fig. 3.9-a) as compared to Fe(II)Mt (Fig. 3.9-b). As a general behavior, the latter produced faster intermediate disappearance.

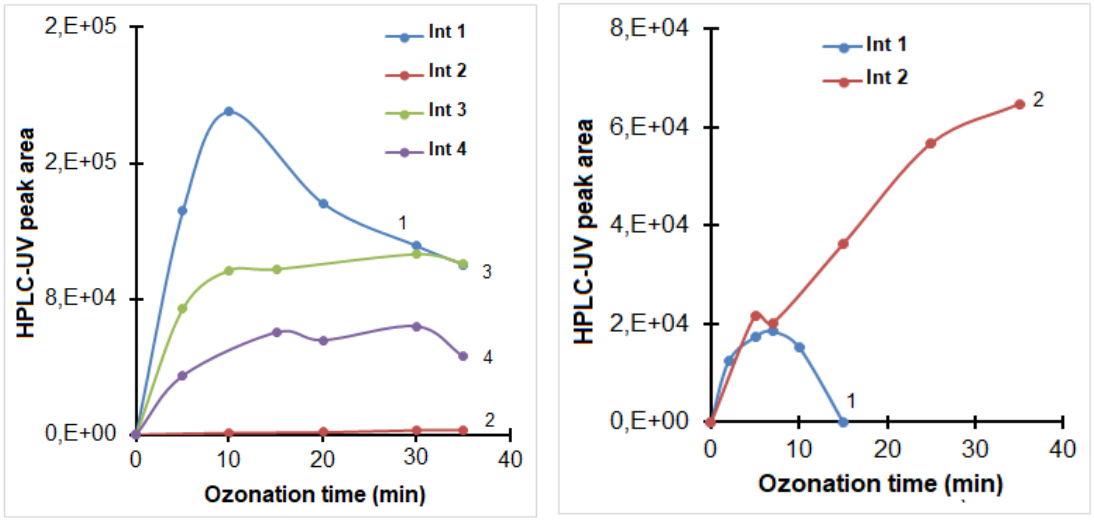

a **b**

Fig. 3.9. Evolution in ozonation time of EE2 intermediate absorbance in the presence of NaMt (a) and Fe(II)Mt (b) as analysed by HPLC-UV at wavelength 280 nm.

As a general feature, the number of intermediates in the presence of the Fe(II)Mt was lower than in non-catalytic ozonation and in the presence of NaMt (Table S3.4). This result allows concluding that NaMt is more activity in EE2 degradation into higher amounts of oxidized intermediates but not necessarily in its total mineralization as compared to Fe(II)Mt. This clearly different catalytic behavior must be due to the contribution of acid-base and hydrophilic-hydrophobic interactions between the clay mineral, EE2 and its intermediates. NaMt was already found to display higher Lewis basicity but a lower hydrophilic character compared to Fe^{2+}-exchanged montmorillonite [40]. The latter is rather known to produce Brønsted acidity in the presence of water molecule according to reaction 5 [63].

$[Fe(H_2O)_x]^{2+} \rightarrow [Fe(H_2O)_{x-1}.OH]^{+-} + H^+$ (5). In this regard, the silanol groups of the clay mineral surface are expected to play a key-role in clay-catalyzed ozonation processes in water.

3.3.6 Role of silanols on EE2 adsorption

The pH of the reaction mixture is one of the most important factors that determines both the charges of the clay catalyst surface and EE2 molecules. All pH values of the reaction mixtures at different operating conditions are lower than the pKa of EE2 (10.46 - 10.70) (Table 3.3), and should confer invariably more or less positive charges to EE2 molecules. As expected, Fe(II)Mt addition to the EE2 solution induced an initial pH decrease from 7.96 down to 3.40 that should confer similar positive charges to all silanols and EE2 molecules, given their respective pKa values (Table 3.3).

Table 3.3. EE2 removal after 10 min ozonation in correlation with the clay suspension properties.

Catalyst	Acid activation time (h)	pH[a]	pH[b]	Zeta potential (± 1.54 mV)[c]		Clay particle size (µm)		Silanol pKa		EE2 removal yield (%)
				Without EE2[c]	With EE2[d]	Without EE2[c]	With EE2[d]	Out-of-plane 5.6[e]	In-plane 8.5[e]	
NaMt	0	8.77	7.96	- 42.19	- 43.09	0.649	0.436	SiO^-	$SiOH_2^+$	100
Fe(II)Mt	0	2.33	3.40	+ 16.20	- 37.54	2.450	3.003	$SiOH_2^+$	$SiOH_2^+$	89
HMt-1	1	4.18	4.25	- 43.02	- 25.46	1.990	1.633	$SiOH_2^+$	$SiOH_2^+$	100
HMt-4	4	4.15	4.20	- 38.36	- 36.82	2.040	1.312	$SiOH_2^+$	$SiOH_2^+$	100
HMt-8	8	4.04	4.13	- 43.12	- 30.67	2.140	1.217	$SiOH_2^+$	$SiOH_2^+$	82
HMt-15	15	3.92	4.02	- 42.18	- 41.16	2.260	1.389	$SiOH_2^+$	$SiOH_2^+$	81
HMt-24	24	3.96	4.67	- 37.62	- 36.64	2.350	1.394	$SiOH_2^+$	$SiOH_2^+$	70

EE2 pKa: 10.46 - 10.70
Intrinsic pH of EE2 aqueous solution = 5.28
[a]Average intrinsic pH of the clay suspension in water at room temperature (Triplicate).
[b]Average pH of the clay suspension in water in the presence of EE2 at room temperature (Triplicate).
[c]Zeta potential of the clay suspension in water at room temperature (Triplicate) in the absence of EE2 molecules.
[d]Zeta potential of the clay suspension in water at room temperature (Triplicate) in the presence of EE2 molecules.
[e]These pKa values of the silanol groups are supposed to be similar to those of pure silica.

This appears to be a common feature of Fe(II)Mt and acid-activated-bentonites (HMt samples). Subsequently, no electrostatic adsorption of EE2 is expected to take place between EE2 molecules and the silanol groups of these samples, except for NaMt, where the out-of-plane should bear negative charges. In this case, EE2 adsorption on Fe(II)Mt and HMt catalysts, if any, should involve cation exchange and, at most, organophilic interaction, presumably on silica-rich regions on the clay surface. Cation exchange should occur on all investigated catalysts, since positively charged EE2 molecules must remove the original cations (Na^+, Fe^{2+} and H^+) from the negative charges of the clay surface as supported by the negative values of the Zeta potential.

The paradoxically lower EE2 removal yield registered with Fe(II)Mt (89%) as compared to NaMt, HMt and HMt4 (100%) can be explained by partial clay coagulation-flocculation that reduces the available catalytic surface and Fe^{2+} cation mobility. Here, the ozonation process is supposed to take place in the liquid phase in the presence of more or less mobile Fe^{2+} cation in the vicinity of the catalyst surface. Fe^{2+} cations are expected to readily interaction with traces of oxalates that act as ligands. Such a process should be very fast leading quickly to the formation of short chain products, but equilibrium should reduce the EE2 conversion yield [49,53,64].

EE2 adsorption on Fe(II)Mt must also involve acid-base interaction between the acid character of the catalyst surface and slightly basic behavior of EE2, as already reported for bisphenol-A [65]. However, here also, clay grain aggregation appears to be a limitation by mitigating such an interaction. This was supported by the higher clay particle size of Fe(II)Mt in both the absence and presence of EE2 molecules (2.450 and 3.003 μm, respectively) as compared to the other clay catalyst. This detrimental effect of clay compaction was also noticed for the other HMt samples, inasmuch as prolonging acid-activation times from 4h to 8, 15 and 24h induced a noticeable increase in particle size from 2.040 μm to 2.140, 2.260 and 2.35 μm, respectively as a results of surface charge decrease and hydrophobic character enhancement. This was

accordingly accompanied by a marked decay in the catalytic activity as well illustrated by the decrease in EE2 removal yield from 100% down to 82, 81 and 70%, respectively.

3.3.7 Catalytic activity of acid-activated bentonites

HMt-1 and HMt-4 turned to act as the most effective catalysts for EE2 ozonation, affording advanced oxidation process as supported by marked changes in the UV-Vis spectrum of the starting EE2 solution(Fig. S3.7) and total disappearance of the HPLC-UV peak of EE2 (Fig. S3.8). These catalysts even produced thorough EE2 consumption within less than 2 min ozonation, as well illustrated by the complete depletion of the relative intensity of the corresponding HPLC-UV peak (Fig. 3.10).

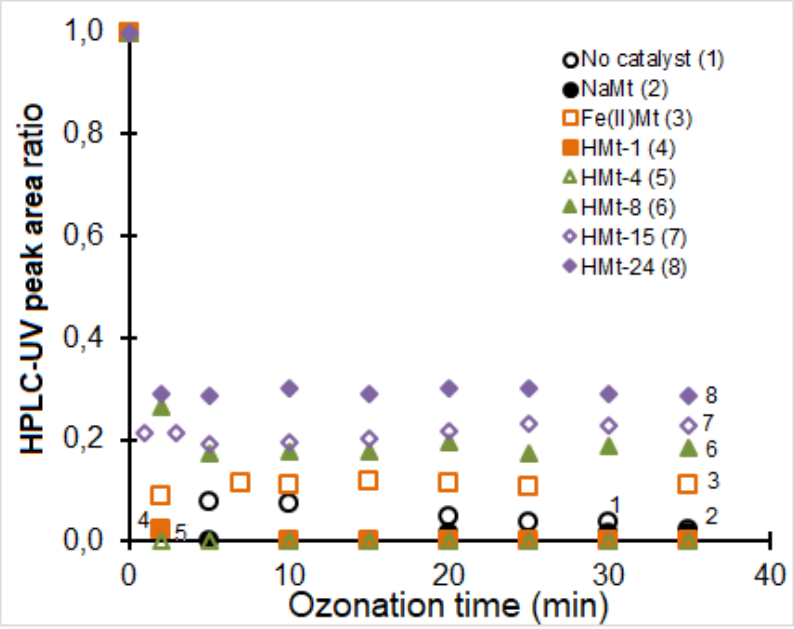

Fig. 3.10. Evolution in time of the peak area ratio of EE2 degradation in aqueous solution. Analysed by HPLC-UV at λ = 280 nm. T = 22°C. pH = intrinsic value. O_3 throughput: 600 mg h^{-1}. Sample volume = 20 mL. Initial EE2 concentration: 10^{-5} M. Catalyst amount = 40 mg.

HMt-1 and HMt-4 gather optimum features that promote adequate hydrophobic interaction and sufficient negative surface charges for effective EE2 adsorption and oxidation by ozone. This result allows concluding that moderate acid attack is an essential requirement for improving the catalytic activity in EE2 ozonation. Optimum hydrophilic character is expected to favor adsorption via both electrostatic and organophilic interactions. The latter should take place on dealuminated and hydrophobic areas of montmorillonite. Hydrophobic interactions were already reported to occur on organophilic materials such as carbon nanotubes, involving π–π* electron donor–acceptor (EDA) interactions between EE2, its oxidation intermediates and solid surface [66].

3.4 Conclusion

This study provides useful fundamental data on how clay materials exhibit similar surface properties as aluminosilicate-based soils, acting as effective catalysts in EE2 ozonation. Low cost and natural montmorillonite with judicious and convenience modification procedure such as acid-activation resulted in highly added-value catalyst for organic pollutant oxidative degradation. Achieving complete removal of EE2 in few minutes in solvent-free media without residual traces of hazardous derivatives is a novelty by itself. The judicious approach tackled provided a deeper understanding of the behavior of both the catalyst surface and organic pollutant molecules by correlating the catalytic activity with the acid-base-properties and hydrophilic character. Adsorption of the parent molecule and derivatives appears as a key-step in the global catalytic process. Ozonation of adsorbed organic substrate was found to prevail involving a clay-ozone synergy. The higher degradation yields of EE2 obtained after short ozonation times with acid-activated montmorillonite can be explained in terms of adsorption via both hydrophobic and additional acid-base interactions. Ozonation turned out to be a mixture of diverse mechanisms occurring in both the solution bulk

and on the clay catalyst surface. The clay dispersion in the aqueous media turned to be a key-factor that determines the contribution of the clay surface to the global ozonation process. These findings will certainly contribute to new knowledge advancement in designing clay catalysts for in situ total mineralization of estrogens and other harmful organic pollutants once released on soils.

REFERENCES

[1] J.R. Oesterheld, K. Cozza, N.B. Sandson, Oral Contraceptives, Psychosomatics, 49 (2008) 168-175.

[2] P. Mazellier, L. Méité, J.D. Laat, Photodegradation of the steroid hormones 17β-estradiol (E2) and 17α-ethinylestradiol (EE2) in dilute aqueous solution, J. Chemosphere, 73 (2008) 1216-1223.

[3] E.J. Routledge, D. Sheahan, C. Desbrow, G.C. Brighty, M. Waldock, J.P. Sumpter, Identification of Estrogenic Chemicals in STW Effluent. 2. In Vivo Responses in Trout and Roach, Environmental Science & Technology, 32 (1998) 1559-1565.

[4] T. Kosjek, E. Heath, A. Krbavčič, Determination of non-steroidal anti-inflammatory drug (NSAIDs) residues in water samples, Environment International, 31 (2005) 679-685.

[5] M. Adeel, X. Song, Y. Wang, D. Francis, Y. Yang, Environmental impact of estrogens on human, animal and plant life: A critical review, Environment International, 99 (2017) 107-119.

[6] C. Desbrow, E.J. Routledge, G.C. Brighty, J.P. Sumpter, M. Waldock, Identification of Estrogenic Chemicals in STW Effluent. 1. Chemical Fractionation and in Vitro Biological Screening, Environmental Science & Technology, 32 (1998) 1549-1558.

[7] S.A. Snyder, T.L. Keith, D.A. Verbrugge, E.M. Snyder, T.S. Gross, K. Kannan, J.P. Giesy, Analytical Methods for Detection of Selected Estrogenic Compounds in Aqueous Mixtures, J. Environmental Science & Technology, 33 (1999) 2814-2820.

[8] M.D. Jurgens, K.I. Holthaus, A.C. Johnson, J.L. Smith, M. Hetheridge, R.J. Williams, The potential for estradiol and ethinylestradiol degradation in English rivers, J. Environ Toxicol Chem, 21 (2002) 480-488.

[9] A.Z. Aris, A.S. Shamsuddin, S.M. Praveena, Occurrence of 17α-ethynylestradiol (EE2) in the environment and effect on exposed biota: a review, J. Environment International, 69 (2014) 104-119.

[10] K.A. Kidd, P.J. Blanchfield, K.H. Mills, V.P. Palace, R.E. Evans, J.M. Lazorchak, R.W. Flick, Collapse of a fish population after exposure to a synthetic estrogen, Proceedings of the National Academy of Sciences of the United States of America, 104 (2007) 8897-8901.

[11] R.M. Sharpe, N.E. Skakkebaek, Are oestrogens involved in falling sperm counts and disorders of the male reproductive tract?, The Lancet, 341 (1993) 1392-1396.

[12] S. Jobling, M. Nolan, C.R. Tyler, G. Brighty, J.P. Sumpter, Widespread Sexual Disruption in Wild Fish, J. Environmental Science & Technology, 32 (1998) 2498-2506.

[13] R. van Aerle, T.M. Nolan, S. Jobling, L.B. Christiansen, J.P. Sumpter, C.R. Tyler, Sexual disruption in a second species of wild cyprinid fish (the gudgeon, Gobio gobio) in United Kingdom freshwaters, J. Environ Toxicol Chem, 20 (2001) 2841-2847.

[14] S.H. Swan, E.P. Elkin, L. Fenster, The question of declining sperm density revisited: an analysis of 101 studies published 1934-1996, Environmental Health Perspectives, 108 (2000) 961-966.

[15] E. Carlsen, A. Giwercman, N. Keiding, N.E. Skakkebaek, Evidence for decreasing quality of semen during past 50 years, International Journal of Gynecology & Obstetrics, 41 (1993) 112-113.

[16] H. Segner, K. Caroll, M. Fenske, C.R. Janssen, G. Maack, D. Pascoe, C. Schäfers, G.F. Vandenbergh, M. Watts, A. Wenzel, Identification of endocrine-disrupting effects in aquatic vertebrates and invertebrates: report from the European IDEA project, Ecotoxicology and Environmental Safety, 54 (2003) 302-314.

[17] J.K. Hess-Wilson, K.E. Knudsen, Endocrine disrupting compounds and prostate cancer, Cancer letters, 241 (2006) 1-12.

[18] A. Joss, H. Andersen, T. Ternes, P.R. Richle, H. Siegrist, Removal of Estrogens in Municipal Wastewater Treatment under Aerobic and Anaerobic Conditions: Consequences for Plant Optimization, Environmental Science & Technology, 38 (2004) 3047-3055.

[19] M. Clara, N. Kreuzinger, B. Strenn, O. Gans, H. Kroiss, The solids retention time-a suitable design parameter to evaluate the capacity of wastewater treatment plants to remove micropollutants, Water Research, 39 (2005) 97-106.

[20] P.A. Segura, A. Garcia-Ac, A. Lajeunesse, D. Ghosh, C. Gagnon, S. Sauve, Determination of six anti-infectives in wastewater using tandem solid-phase extraction and liquid chromatography-tandem mass spectrometry, J. Environmental Monitoring, 9 (2007) 307-313.

[21] Z. Frontistis, C. Brebou, D. Venieri, D. Mantzavinos, A. Katsaounis, BDD anodic oxidation as tertiary wastewater treatment for the removal of emerging micro-pollutants, pathogens and organic matter, J. Chemical Technology and Biotechnology, 86 (2011) 1233-1236.

[22] K. M. Vieira, N. Nascentes, A. Motheo, R. Augusti, Electrochemical Oxidation of Ethinylestradiol on a Commercial Ti/Ru0.3 Ti0.7O_2 DSA Electrode, 2013.

[23] Y.K.K. Koh, T.Y. Chiu, A. Boobis, E. Cartmell, M.D. Scrimshaw, J.N. Lester, treatment and removal strategies for estrogens from wastewater, J. Environmental Technology, 29 (2008) 245-267.

[24] B. De Gusseme, B. Pycke, T. Hennebel, A. Marcoen, S.E. Vlaeminck, H. Noppe, N. Boon, W. Verstraete, Biological removal of 17α-ethinylestradiol by a nitrifier enrichment culture in a membrane bioreactor, Water Research, 43 (2009) 2493-2503.

[25] Y. Zuo, K. Zhang, S. Zhou, Determination of estrogenic steroids and microbial and photochemical degradation of 17alpha-ethinylestradiol (EE2) in lake surface water, a case study, Environmental science. Processes & impacts, 15 (2013) 1529-1535.

[26] G. Gervais, E. Bichon, J.-P. Antignac, F. Monteau, G. Leroy, L. Barritaud, M. Chachignon, V. Ingrand, P. Roche, B.L. Bizec, Differential global profiling as a new analytical strategy for revealing micropollutant treatment by-products: Application to ethinylestradiol and chlorination water treatment, J. Chemosphere, 83 (2011) 1553-1559.

[27] M.M. Huber, S. Canonica, G.-Y. Park, U. von Gunten, Oxidation of Pharmaceuticals during Ozonation and Advanced Oxidation Processes, J. Environmental Science & Technology, 37 (2003) 1016-1024.

[28] P. Westerhoff, Y. Yoon, S. Snyder, E. Wert, Fate of Endocrine-Disruptor, Pharmaceutical, and Personal Care Product Chemicals during Simulated Drinking Water Treatment Processes, J. Environmental Science & Technology, 39 (2005) 6649-6663.

[29] A. Pezzella, L. Lista, A. Napolitano, M. D'Ischia, Tyrosinase-catalyzed oxidation of 17β-estradiol: Structure elucidation of the products formed beyond catechol estrogen quinones, J. Chemical Research in Toxicology, 18 (2005) 1413-1419.

[30] Y. Wu, C. Wu, Y. Wang, C. Hu, Inhibition of Nano-Metal Oxides on Bromate Formation during Ozonation Process, Ozone: Science & Engineering, 36 (2014) 549-559.

[31] B.E. Segmuller, B.L. Armstrong, R. Dunphy, A.R. Oyler, Identification of autoxidation and photodegradation products of ethynylestradiol by on-line HPLC–NMR and HPLC–MS, J. Pharmaceutical and Biomedical Analysis, 23 (2000) 927-937.

[32] K.M. Vieira, C.C. Nascentes, R. Augusti, Ozonation of ethinylestradiol in aqueous-methanolic solution: direct monitoring by electrospray ionization mass spectrometry, J. Brazilian Chemical Society, 21 (2010) 787-794.

[33] X. Zhang, P. Chen, F. Wu, N. Deng, J. Liu, T. Fang, Degradation of 17α-ethinylestradiol in aqueous solution by ozonation, J. Hazardous Materials, 133 (2006) 291-298.

[34] A. Azzouz, A. Kotbi, P. Niquette, T. Sajin, A.V. Ursu, A. Rami, F. Monette, R. Hausler, Ozonation of oxalic acid catalyzed by ion-exchanged montmorillonite in moderately acidic media, Reaction Kinetics, J. Mechanisms and Catalysis, 99 (2010) 289-302.

[35] D. Shahidi, R. Roy, A. Azzouz, Total removal of oxalic acid via synergistic parameter interaction in montmorillonite catalyzed ozonation, J. Environmental Chemical Engineering, 2 (2014) 20-30.

[36] D. Shahidi, A. Moheb, R. Abbas, S. Larouk, R. Roy, A. Azzouz, Total mineralization of sulfamethoxazole and aromatic pollutants through Fe^{2+}-montmorillonite catalyzed ozonation, J. Hazardous Materials, 298 (2015) 338-350.

[37] M. Mills, K. Arias-Salazar, A. Baynes, L. Shen, J. Churchley, N. Beresford, C. Gayathri, R. R. Gil, R. Kanda, S. Jobling, T. Collins, Removal of ecotoxicity of 17α-ethinylestradiol using TAML/peroxide water treatment, 2015.

[38] J.-N. Park, J. Wang, K.Y. Choi, W.-Y. Dong, S.-I. Hong, C.W. Lee, Hydroxylation of phenol with H_2O_2 over Fe^{2+} and/or Co^{2+} ion-exchanged NaY catalyst in the fixed-bed flow reactor, J. Molecular Catalysis A: Chemical, 247 (2006) 73-79.

[39] S.-r. Tian, Y.-g. Liu, S.-b. Liu, G.-m. Zeng, L.-h. Jiang, X.-f. Tan, X.-x. Huang, Z.-h. Yin, N. Liu, J. Li, Hydrothermal synthesis of montmorillonite/hydrochar nanocomposites and application for 17β-estradiol and 17α-ethynylestradiol removal, RSC advances, 2018 v.8 no.8 (2018) pp. 4273-4283.

[40] F. Boudissa, D. Mirila, V.-A. Arus, T. Terkmani, S. Semaan, M. Proulx, I.-D. Nistor, R. Roy, A. Azzouz, Acid-treated clay catalysts for organic dye ozonation - Thorough mineralization through optimum catalyst basicity and hydrophilic character, J. Hazardous Materials, 364 (2019) 356-366.

[41] D. Shahidi, A. Moheb, R. Abbas, S. Larouk, R. Roy, A. Azzouz, Total mineralization of sulfamethoxazole and aromatic pollutants through Fe2+-montmorillonite catalyzed ozonation, J. Hazardous Materials, 298 (2015) 338-350.

[42] M.A. Didi, B. Makhoukhi, A. Azzouz, D. Villemin, Colza oil bleaching through optimized acid activation of bentonite. A comparative study, Applied Clay Science, 42 (2009) 336-344.

[43] B. Makhoukhi, M.A. Didi, D. Villemin, A. Azzouz, Acid activation of Bentonite for use as a vegetable oil bleaching agent, Grasas y Aceites, 60 (2009) 343-349.

[44] V.A. Arus, S. Nousir, R. Sennour, T.C. Shiao, I.D. Nistor, R. Roy, A. Azzouz, Intrinsic affinity of acid-activated bentonite towards hydrogen and carbon dioxide, International Journal of Hydrogen Energy, 43 (2018) 7964-7972.

[45] A. Azzouz, A.-V. Ursu, D. Nistor, T. Sajin, E. Assaad, R. Roy, TPD study of the reversible retention of carbon dioxide over montmorillonite intercalated with polyol dendrimers, J. Thermochimica Acta, 496 (2009) 45-49.

[46] A. Azzouz, S. Nousir, N. Platon, K. Ghomari, T.C. Shiao, G. Hersant, J.-Y. Bergeron, R. Roy, Truly reversible capture of CO2 by montmorillonite intercalated with soya oil-derived polyglycerols, International Journal of Greenhouse Gas Control, 17 (2013) 140-147.

[47] R. Ouargli, S. Larouk, I. Terrab, R. Hamacha, N. Benharrats, A. Bengheddach, A. Azzouz, Intrinsic Activity of SBA-like Silica in the Catalytic Ozonation of Organic Pollutants, J. Ozone Science and Engineering, 38 (2016) 48-61.

[48] P. Mazellier, J. Leverd, Transformation of 4-tert-octylphenol by UV irradiation and by an H_2O_2/UV process in aqueous solution, Photochemical & Photobiological Sciences, 2 (2003) 946-953.

[49] A. Azzouz, Advances in Oxidative Decomposition of Oxalic Acid in Aqueous Media, Nova-Publishers, New-York, USA, New York, 2012 2nd quarter.

[50] A. Azzouz, A. Kotbi, P. Niquette, T. Sajin, A. Ursu, A. Rami, F. Monette, R. Hausler, Ozonation of oxalic acid catalyzed by ion-exchanged montmorillonite in moderately acidic media, Reaction Kinetics, Mechanisms and Catalysis, 99 (2010) 289-302.

[51] Azzouz A., Mirilà D., Nistor I.D., Boudissa F., Roy R., Chapter 1: Advances in the Oxidative Degradation of Organic Pollutants: Prospects for Catalyzed Oxidation Processes Targeting Total Mineralization, in: J.C. Taylor (Ed.) Advances in Chemistry Research-General Chemistry Nova Science Publishers, New-York, USA, 2019, pp. 235.

[52] S. Larouk, R. Ouargli, D. Shahidi, L. Olhund, T.C. Shiao, N. Chergui, T. Sehili, R. Roy, A. Azzouz, Catalytic ozonation of Orange-G through highly interactive contributions of hematite and SBA-16 - To better understand azo-dye oxidation in nature, J. Chemosphere, 168 (2017) 1648-1657.

[53] D. Shahidi, A. Moheb, R. Abbas, S. Larouk, R. Roy, A. Azzouz, Total mineralization of sulfamethoxazole and aromatic pollutants through Fe^{2+}-montmorillonite catalyzed ozonation, J. Hazard Mater, 298 (2015) 338-350.

[54] D. Shahidi, R. Roy, A. Azzouz, Advances in catalytic oxidation of organic pollutants-Prospects for thorough mineralization by natural clay catalysts, J. Applied Catalysis B: Environmental, 174-175 (2015) 277-292.

[55] M.M. Huber, T.A. Ternes, U. von Gunten, Removal of Estrogenic Activity and Formation of Oxidation Products during Ozonation of 17α-Ethinylestradiol, J. Environmental Science & Technology, 38 (2004) 5177-5186.

[56] J. Ma, N.J.D. Graham, Degradation of atrazine by manganese-catalysed ozonation-influence of radical scavengers, J. Water Research, 34 (2000) 3822-3828.

[57] D. Koumeir, S. Guittonneau, C. Guillard, H. El Zakhem, Oxidation kinetics of ethinylestradiol by ozone, Int. J. Sci. Environ. Tech, 4 (2015) 667.

[58] M.M. Huber, T.A. Ternes, U. von Gunten, Removal of estrogenic activity and formation of oxidation products during ozonation of 17alpha-ethinylestradiol, J. Environmental science & technology, 38 (2004) 5177-5186.

[59] S. Larcher, G. Delbès, B. Robaire, V. Yargeau, Degradation of 17α-ethinylestradiol by ozonation-Identification of the by-products and assessment of their estrogenicity and toxicity, Environment international, 39 (2012) 66-72.

[60] D. O'Grady, S. Evangelista, V. Yargeau, Removal of Aqueous 17α-Ethinylestradiol by Rhodococcus Species, J. Environmental Engineering Science, 26 (2009) 1393-1400.

[61] D. Bila, A.F. Montalvão, D.d.A. Azevedo, M. Dezotti, Estrogenic activity removal of 17beta-estradiol by ozonation and identification of by-products, J. Chemosphere, 69 (2007) 736-746.

[62] G.M. Anstead, K.E. Carlson, J.A. Katzenellenbogen, The estradiol pharmacophore: ligand structure-estrogen receptor binding affinity relationships and a model for the receptor binding site, Steroids, 62 (1997) 268-303.

[63] J. Weitkamp, M. Hunger, Chapter 22 - Acid and Base Catalysis on Zeolites, in: J. Čejka, H. van Bekkum, A. Corma, F. Schüth (Eds.) Studies in Surface Science and Catalysis, Elsevier, 2007, pp. 787-835.

[64] S. Larouk, R. Ouargli, D. Shahidi, L. Olhund, T.C. Shiao, N. Chergui, T. Sehili, R. Roy, A. Azzouz, Catalytic ozonation of Orange-G through highly interactive contributions of hematite and SBA-16 – To better understand azo-dye oxidation in nature, J. Chemosphere, 168 (2017) 1648-1657.

[65] R. Sturza, M. Melenciuc, D. Nistor, F. Boudissa, T. Terkmani, N.-H.H. Hadj-Abdelkader, A. Abdelkrim, Recyclable porous materials for the uptake of bisphenol-A, J. Food and Environment Safety Journal (Romania), 16 (2017).

[66] L. Joseph, J. Heo, Y.-G. Park, J.R.V. Flora, Y. Yoon, Adsorption of bisphenol A and 17α-ethinyl estradiol on single walled carbon nanotubes from seawater and brackish water, Desalination, 281 (2011) 68-74.

CONCLUSION GÉNÉRALE

Cette étude s'inscrit dans le cadre de l'élaboration de catalyseurs écologiques inspirés du comportement des sols pour la dégradation oxydative de polluants organique dans les traitements des eaux. Elle a pour objectif de dégrader les polluants organiques par un procédé d'oxydation avancée, plus particulièrement l'ozonation catalytique. L'analyse profonde des résultats obtenus a permis de conclure que :

- Les catalyseurs à base d'argile améliorent l'ozonation des colorants.
- Les mesures de la TPD pour le CO_2 et pour l'eau se sont avérées être une approche judicieuse pour corréler les propriétés acido-basiques et le caractère hydrophile des catalyseurs à base d'argile avec le comportement du colorant dans l'eau.
- Les interactions électrostatiques semblent essentielles pour déclencher l'adsorption et l'ozonation ultérieure des colorants anioniques sur NaMt, mais l'adsorption de toutes les molécules de colorant implique principalement une interaction hydrophobe.
- Sur Fe(II)Mt, les colorants anioniques semblent agir comme «pompe à fer», induisant une libération massive de fer qui réduit la charge positive de surface et l'efficacité du catalyseur. Ainsi, l'adsorption de colorant s'avère être une exigence essentielle pour une efficacité catalytique élevée et cette interaction électrostatique prévaut pour certains colorants sur certains catalyseurs. Sur Fe(II)Mt, les contributions de l'interaction hydrophobe, de l'échange de cations et de la mobilité de Fe^{2+} à l'activité catalytique devraient prévaloir.
- Les catalyseurs argileux activés à l'acide produisent une dégradation complète des colorants en courts temps d'ozonation, en raison de leur faible caractère hydrophile qui favorise l'interaction hydrophobe et l'adsorption des molécules

organiques (en raison de la densité élevée des groups silanols et les groupes –Si-O-Si–. Ce résultat est d'une grande importance en raison de l'élimination totale du risque de contamination de l'eau par les métaux.

- Un court temps d'ozonation des colorants organiques génère une grande variété d'intermédiaires, dont les plus oxydés sont communs. Ces derniers disparaissent en prolongeant le temps de réaction.
- Le rapport Si/Al et les groupes silanols jouent un rôle clé dans l'ozonation du bisphénol-A catalysée par un silicate.
- Fe(II)Mt a produit un rendement de dégradation du BPA inférieur à celui de la bentonite modérément activée par un acide, ce qui suggère que le cation Fe^{2+} n'est pas une condition essentielle pour la dégradation avancée du BPA.
- L'adsorption de BPA sur les catalyseurs HMt semble être une étape clé du processus d'ozonation globale, car une interaction hydrophobe de BPA avec une surface activée par un acide produit une inversion bénéfique pour l'hydrophobie. Ce dernier est responsable de la dispersion de l'argile et de la diminution de la taille des particules, ce qui favorise l'interaction des molécules de BPA adsorbées par l'intermédiaire de leurs groupes hydroxyle avec le milieu aqueux.
- La réalisation de l'élimination complète de l'éthinyletradiol (EE2) en seulement quelques minutes dans un milieu sans solvant sans produire de traces résiduelles de dérivés dangereux est une nouveauté en soi.
- L'approche judicieuse abordée a permis de mieux comprendre le comportement de la surface du catalyseur vis-à-vis des molécules de polluants organiques. Elle met en corrélation l'activité catalytique avec les propriétés acide-base et le caractère hydrophile de la surface solide.
- Dans ce cas aussi, l'adsorption du substrat organique s'est avérée avoir une contribution prédominante dans l'ozonisation en présence de catalyseurs argileux. Elle impliquerait une synergie ternaire argile-surface-ozone.

- Les rendements de dégradation plus élevés de EE2 obtenus après des temps d'ozonation courts avec la montmorillonite activée par un acide peuvent s'expliquer en termes d'adsorption via des interactions complémentaires de types acide / base et hydrophobes.
- L'ozonation s'est avérée être un mélange de divers mécanismes d'interactions se produisant à la fois entre les espèces dispersées en solution, l'ozone sous ses formes gazeuse, dissoute et adsorbée et la surface du catalyseur argileux.
- La dispersion de l'argile dans les milieux aqueux s'est révélée être un facteur clé qui détermine la contribution de la surface de l'argile au processus d'ozonation global. Cette dispersion est très conditionnée par le caractère hydrophile du catalyseur.

Comme conclusion générale, ce présent travail a permis de mettre en exergue la possibilité d'utiliser des matériaux naturels, recyclables, non polluants et surtout très disponibles pour un traitement des eaux avancé écologique et à faible coût. De plus, Ces matériaux se prêtent fort convenablement à des modifications simples sans produire de déchets. Ils se sont avérés assez flexibles pour la dégradation de polluants organiques très différents de par leur structure. Cette flexibilité requiert des conditions opératoires spécifiques à chaque type de polluant. Fort heureusement, cette spécificité des conditions opératoires n'impose pas de modifications aux caractéristiques de l'eau à traiter, qui risquent d'ailleurs de produire des déchets. Elle n'impose pas non plus des coûts supplémentaires inhérents à ces modifications. Les fondements élaborés durant cette recherche peuvent s'appliquer également à d'autres matériaux naturels de types silicates et aluminosilicates, voire même des sols argileux et seront certainement d'un grand apport aux chercheurs, scientifiques et ingénieurs opérant dans les domaines de traitement des eaux et des problématiques environnementales.

PERSPECTIVES

Plusieurs aspects importants de l'élimination des polluants organiques n'ont pas été abordés dans ce mémoire. Dans ce qui suit, nous citons quelques propositions de travail destinés à approfondir notre investigation pour se faire une représentation plus complète des phénomènes de surface impliqués dans la dégradation des différents polluants organiques. Il est possible de suggérer de poursuivre les investigations:

- Pour identifier rigoureusement les intermédiaires-clé d'ozonation; Ceci permettra de mieux cerner les types d'interactions complexes catalyseur-eau-substrat-ozone en vue de maîtriser les critères de design des catalyseurs pour ce genre d'applications.
- Pour déterminer les conditions optimales de dégradation des polluants organiques (temps d'ozonation, quantité de catalyseur, pH optimal pour augmenter la solubilité maximale de l'ozone), et les interactions binaires, ternaires ou multiples possibles entre ces paramètres
- Évaluer le taux de la minéralisation de polluant étudié grâce à la détermination du carbone organique totale et une évaluation des traces possibles de dérivés résiduels.
- Mettre en pratique ces résultats par l'investigation de la faisabilité du traitement en continue, puis l'essai de traitement d'effluents industriels par les mêmes matériaux utilisés.
- Étudier la possibilité de tester des fractions minéralogiques de divers sols pour mieux comprendre la cinétique de décomposition oxydative des polluants organiques dans la nature.

ANNEXE A

SUPPORTING INFORMATION OF ARTICLE I: ACID-TREATED CLAY CATALYSTS FOR ORGANIC DYES OZONATION – …….

Table S1.1. Structures and some physicochemical features of the investigated dye molecules

Dye structure	Charge	pK_a	Molecular weight (g/mol)
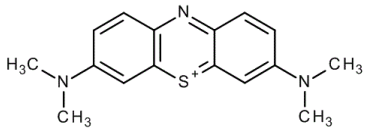 Methylene Blue (cationic)	Neutre/NaMt R_3N^+/Fe(II)Mt	3.8	388
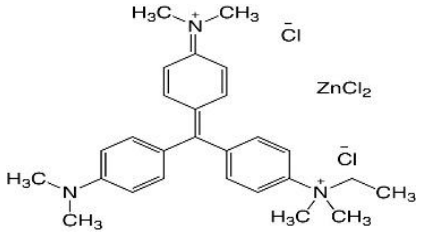 Methyl Green (cationic)	Neutre/NaMt Neutre/Fe(II)Mt	0.2-1.8	608.79

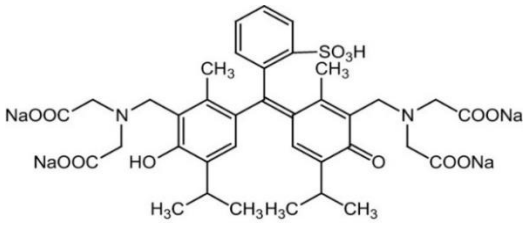 Methylthymol Blue (anionic)	SO_3^-/NaMt CO_2^-/NaMt R_3N^+/Fe(II)Mt	pK1=3.0 pK2=3.3 pK3=3.8 pK4=7,2-7.4 pK5=11.5 pH6=13,4	844.74
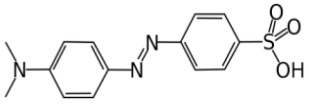 Methyl Orange (anionic)	SO_3^-/NaMt R_3N^+/Fe(II)Mt	3.39-3.46	327.34

[a] pH of the aqueous solution of the respective dye at room temperature
[b] pH of the aqueous solution of the respective dye at room temperature after addition of NaMt without triggering the ozonation.
[c] pH of the aqueous solution of the respective dye at room temperature after addition of Fe(II)Mt without triggering the ozonation.

Calculation of the removal yield.

$$\left(\frac{C_0 - C_t}{C_0}\right).100\% \qquad (1)$$

C_0; initial concentration of the dyestuff in the reaction mixture
C_t : instant concentration of the dyestuff in the reaction mixture

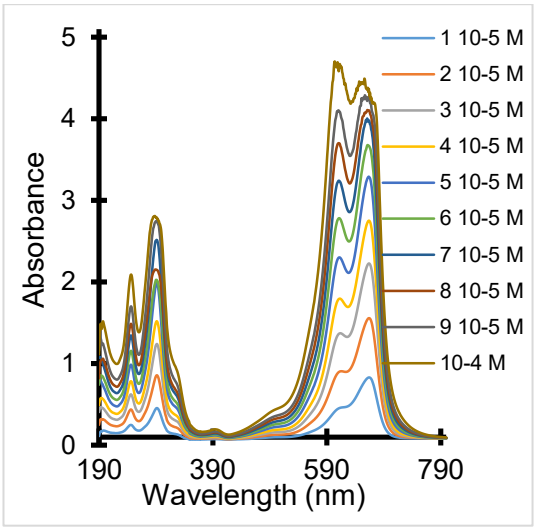

a: Methylene Blue (MB)

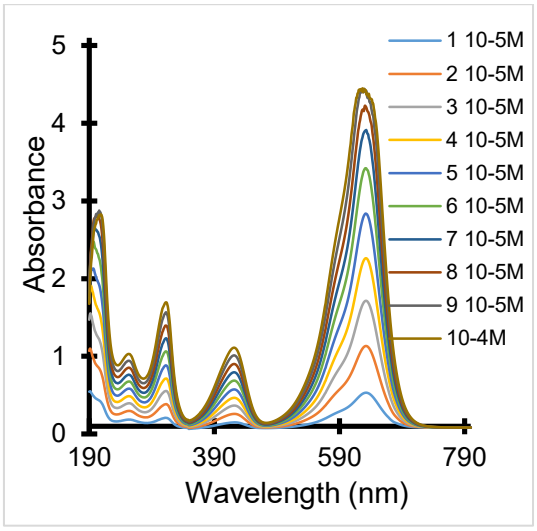

b: Methyl Green (MG)

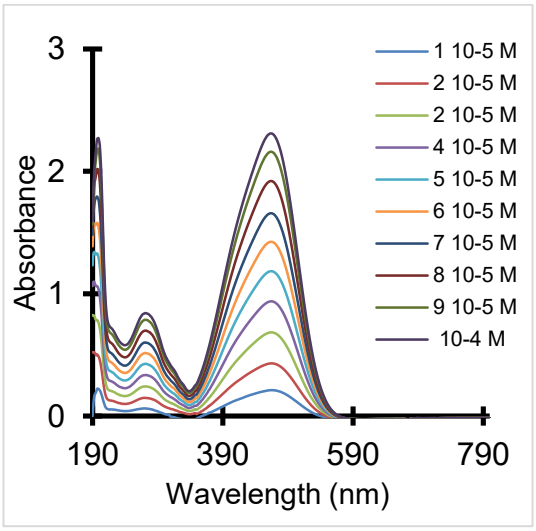

c: Methyl Orange (MO)

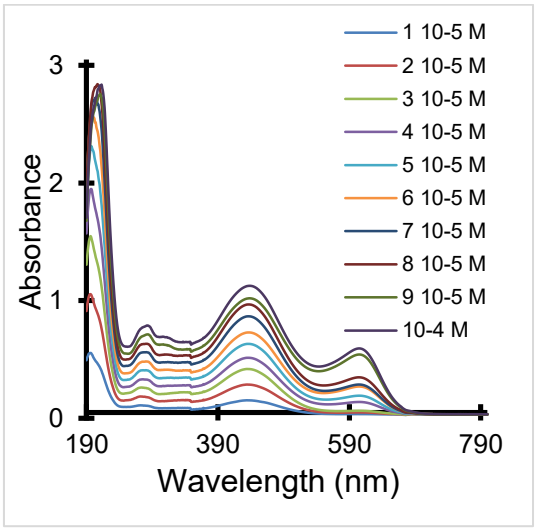

d: Methylthymol Blue (MTB)

Fig. S1.1.UV-Vis spectra of organic dyes at different concentration in distilled water. T = 22°C, pH = intrinsic value, Quartz cell = 1 cm.

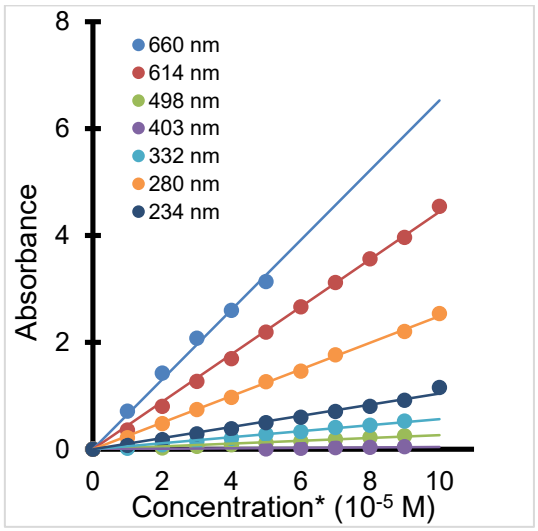

a : MB

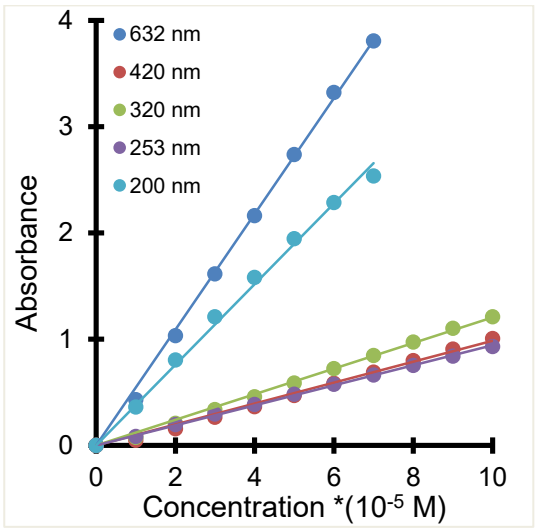

b: MG

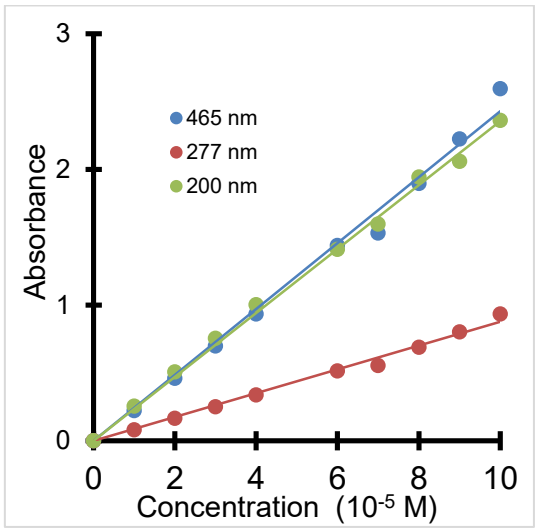

c: MO

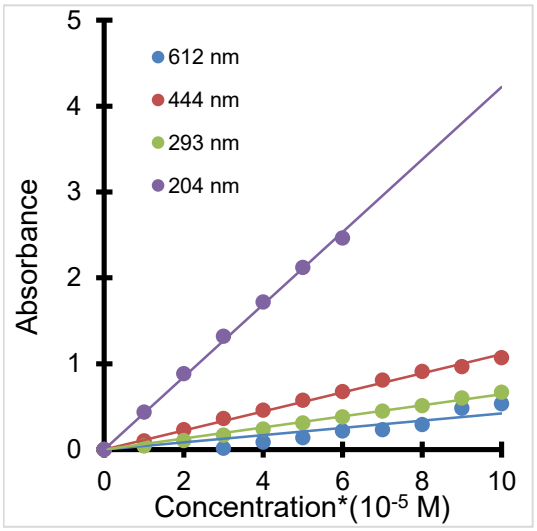

d: MTB

Fig. S1.2. Calibration curves for the investigated dye molecules in distilled water. T = 22 ° C. pH = intrinsic value. Quartz cell = 1 cm. The absorbance was calculated from triplicate runs with a standard deviation of ca. 1% for the highest UV-Vis band and 2-3% for those showing lowest absorbances.

Table S1.2. Molar extinction coefficient (ε) of the different UV-Vis bands for each each duystuff

	λ_{max}(nm)	Assignments	Molar extinction coefficient (ε): ($L.mol^{-1}.cm^{-1}$)*	Correlation coefficient R^2
	660	Heteropolyaromatic $C–S^+=C$ monomers $n– \pi^*$ [1-3]	65.280	0.9931
	614	Shoulder due to the dimer $\pi– \pi^*$ [2]	44.420	0.9984
MB	498	-	2.630	0.9698
	403	-	450	0.8143
	332	-	5.640	0.9883
	280	Benzene ring	24.940	0.9988
	234	Benzene ring	10.430	0.9852
MTB	612	-	4.200	0.8074
	444	-	11.090	0.9955
	293	Benzene ring	6.440	0.9935
	204	-	42.210	0.9979
	465	–N=N– $(\pi – \pi^*)$	24.290	0.9908
MO	277	Benzene ring	8.760	0.9912
	200	Shoulder of a very intense band located at 200 nm	23.570	0.9970
	632	-	54.460	0.9985
	420	-	9.860	0.9938
MG	320	Benzoic rings	1.2050	0.9972
	253	Benzoic rings	9.440	0.9991
	200	Benzoic rings	37.960	0.9951

* These coefficients were assessed from the slope of the linear part of the calibration curve fulfilling the Beer-Lambert's Law. The molar extinction coefficients were assessed in the concentration range [10^{-5}-10^{-4}M].

Ozonation procedure

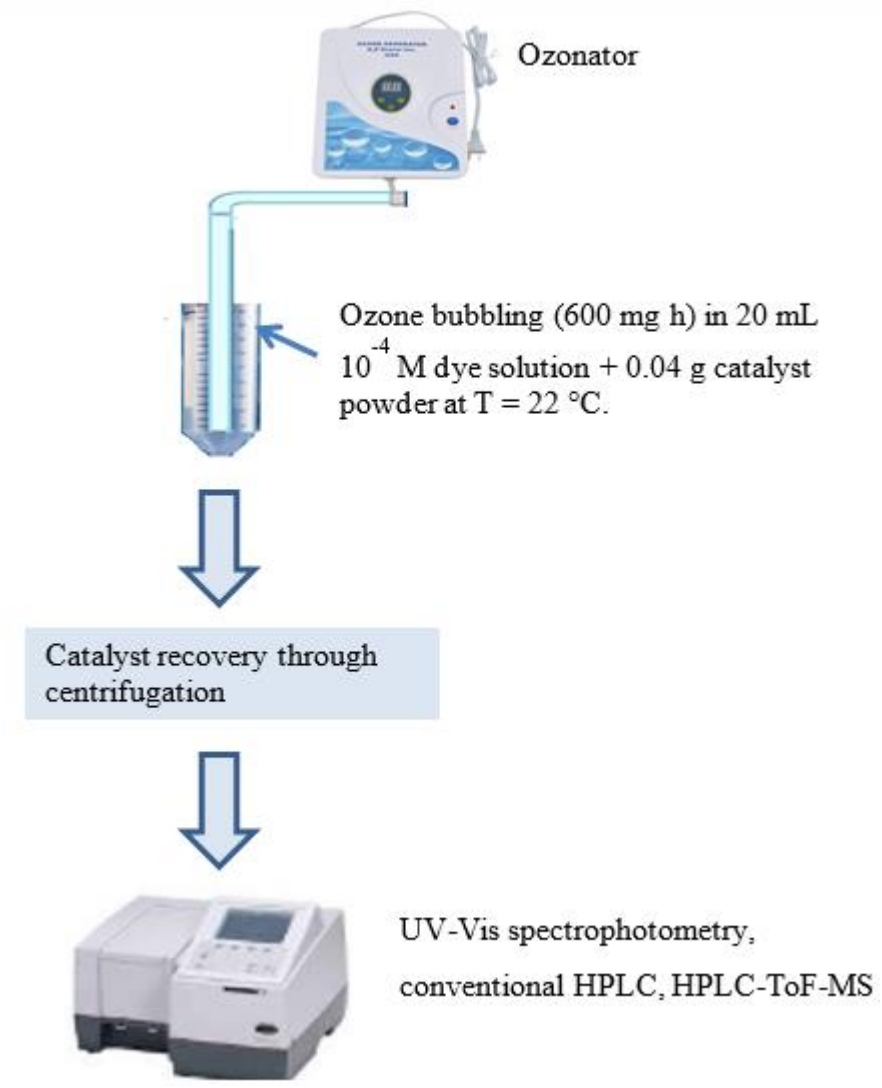

Scheme S1.1. Schematic illustration of the zonation procedure

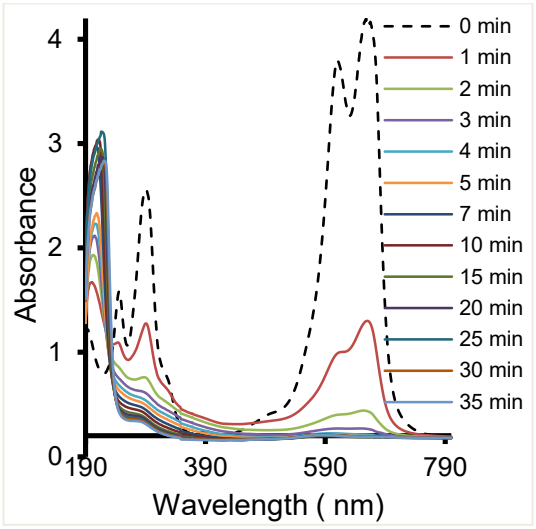

MB

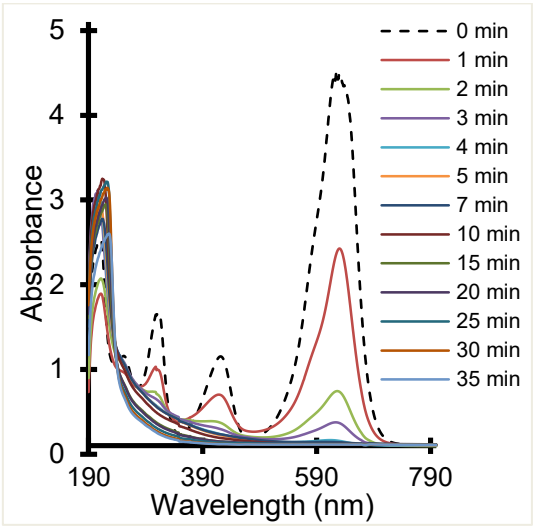

MG

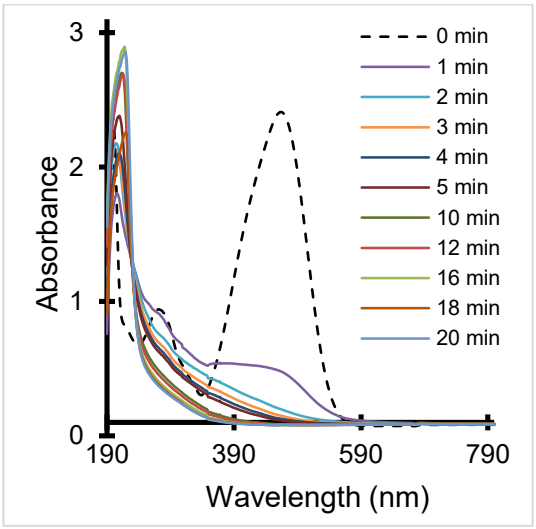

MO

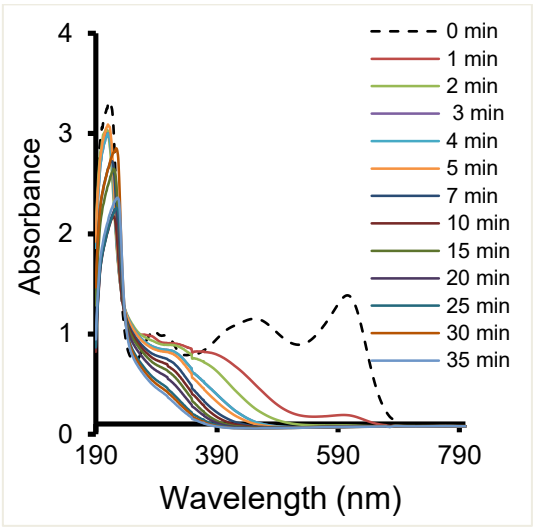

MTB

Fig. S1.3. Changes in the UV-Vis spectra of the different dyestuffs during ozonation in distilled water as compared to the non-ozonated sample (Dash line). T = 22 °C. pH = intrinsic value. Quartz cell = 1 cm. O_3 throughput: 600 mg h^{-1}. Sample volume = 20 mL. Initial dye concentration: 10^{-4} M.

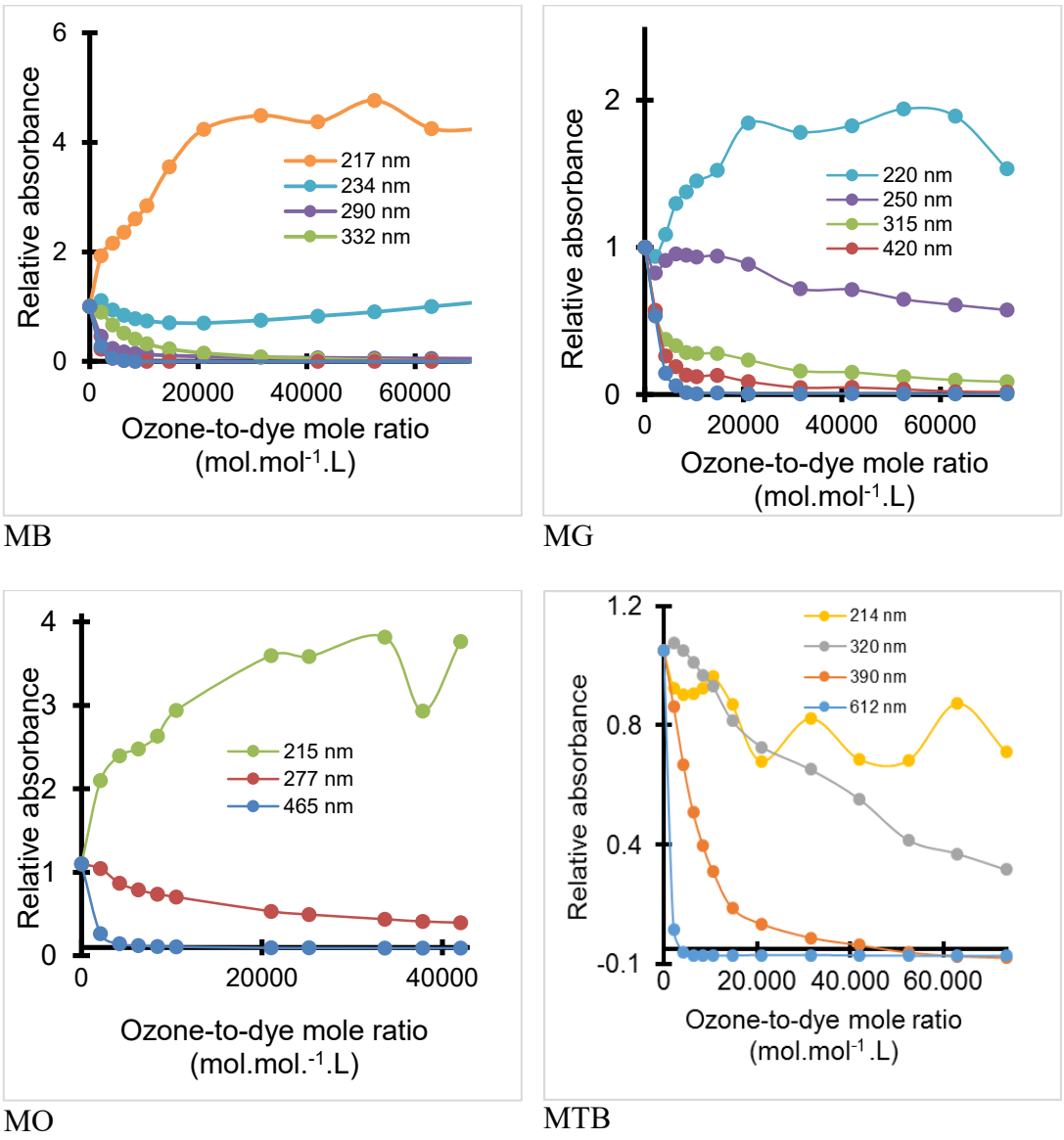

Fig. S1.4. Effect of ozone-to-dye mole ratio on the relative absorbance during ozonation in distilled water. T = 22 °C. pH = intrinsic value. Quartz cell = 1 cm. O_3 throughput: 600 mg h^{-1}. Sample volume = 20 mL. Initial dye concentration: 10^{-4} M.

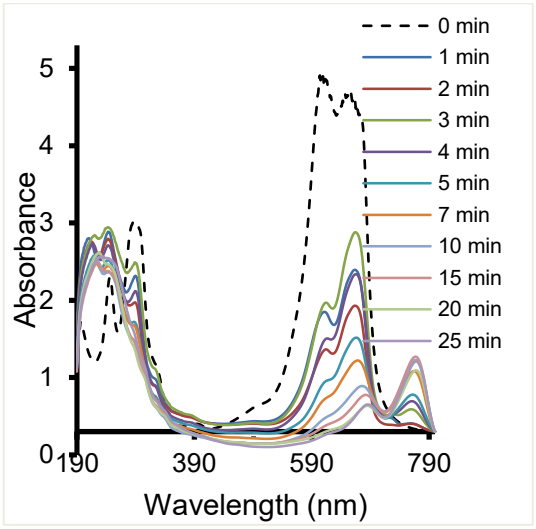

MB-NaMt

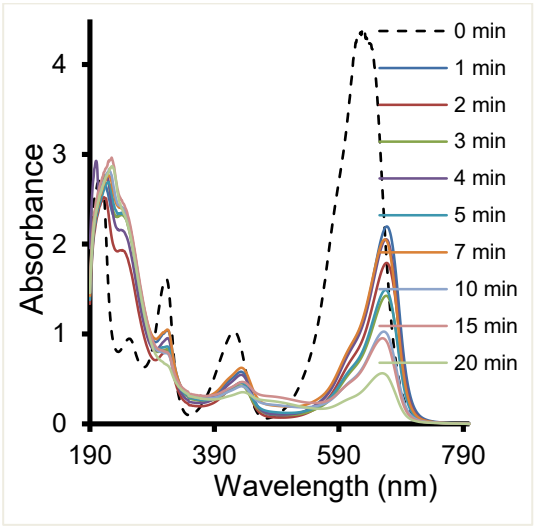

MG-NaMt

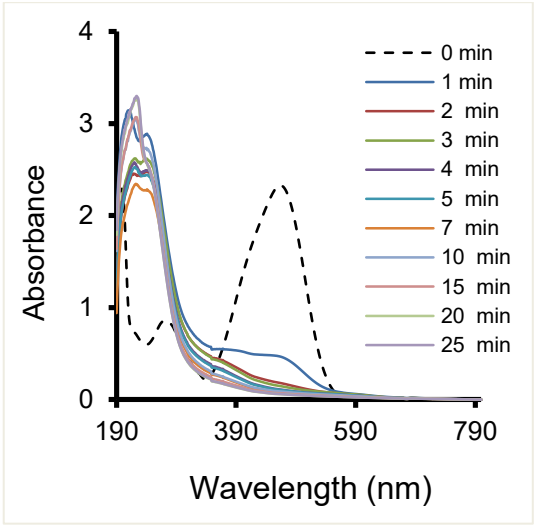

MO-NaMt

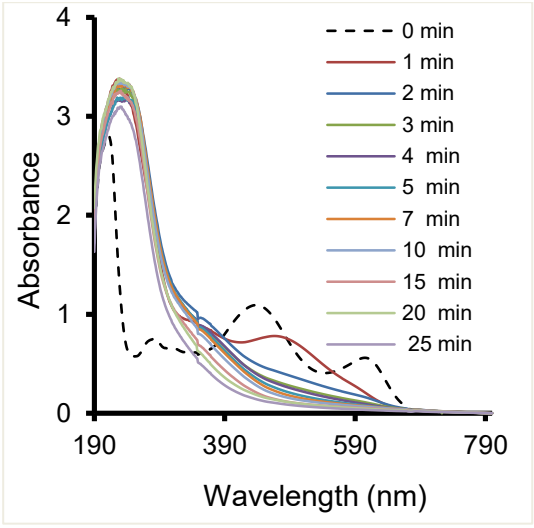

MTB-NaMt

Fig. S1.5. Changes in the UV-Vis spectra of the different dyestuffs during ozonation (NaMt) in distilled water in the presence of NaMt. T = 22 °C. pH = intrinsic value. Quartz cell = 1 cm O_3 throughput: 600 mg h^{-1}. Sample volume= 20 mL. Initial dye concentration: 10^{-4} M. Catalyst amount = 40 mg of dry NaMt.

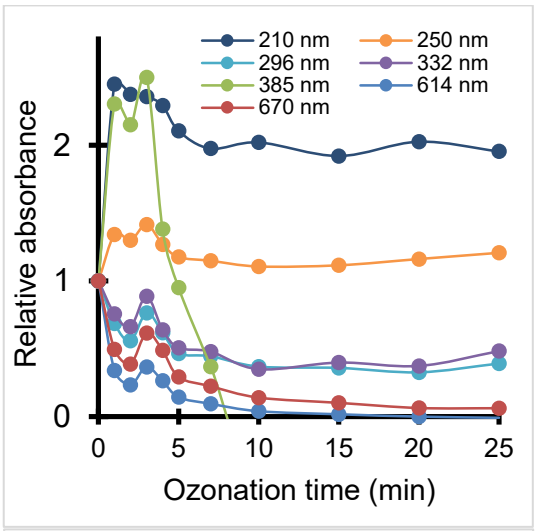

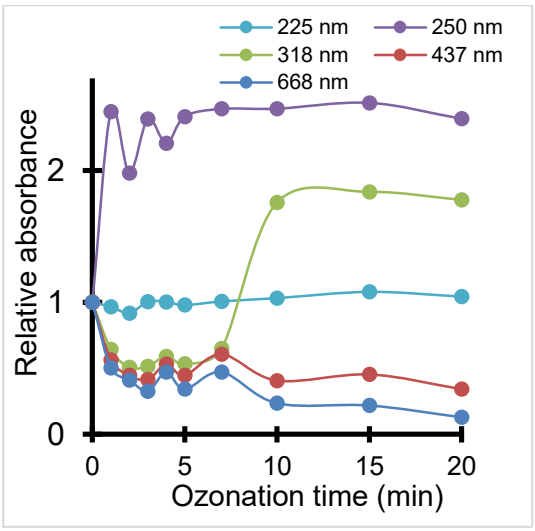

MG-NaMt

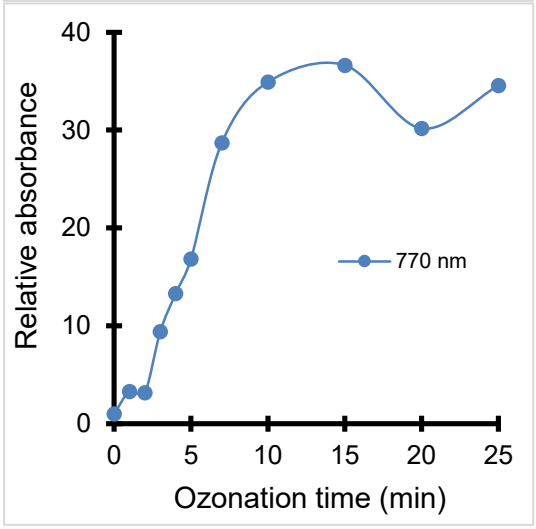

MB-NaMt

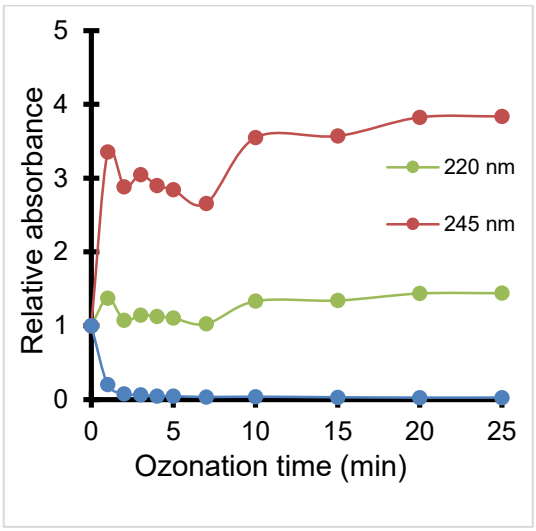

MO-NaMt

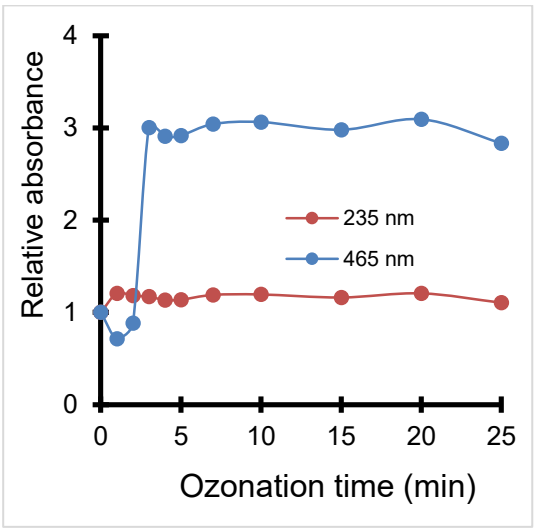

MTB-NaMt

Fig. S1.6. Evolution in time of the dye relative absorbance of during ozonation in distilled water in the presence of NaMt. T = 22 ° C. pH = intrinsic value. Quartz cell = 1 cm. O_3 throughput: 600 mg h^{-1}. Sample volume = 20 mL. Initial dye concentration: 10^{-4} M. Catalyst amount = 40 mg of dry NaMt.

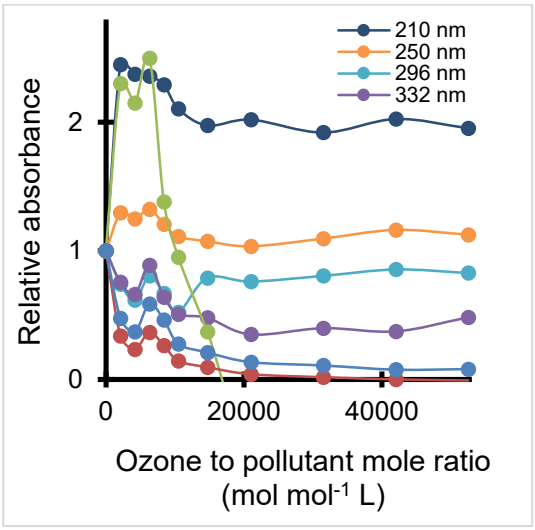

MG-NaMt

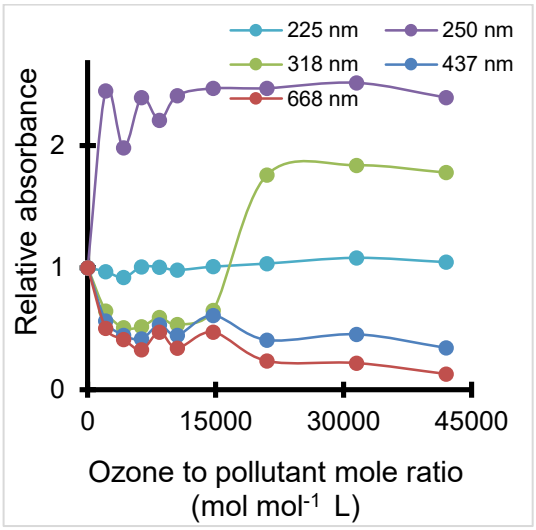

MG-NaMt

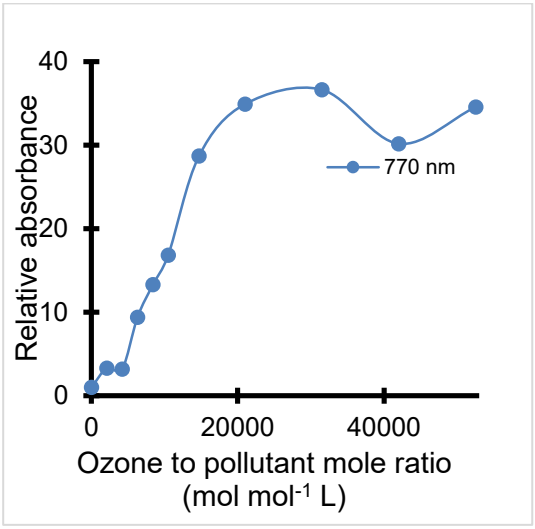

MB-NaMt

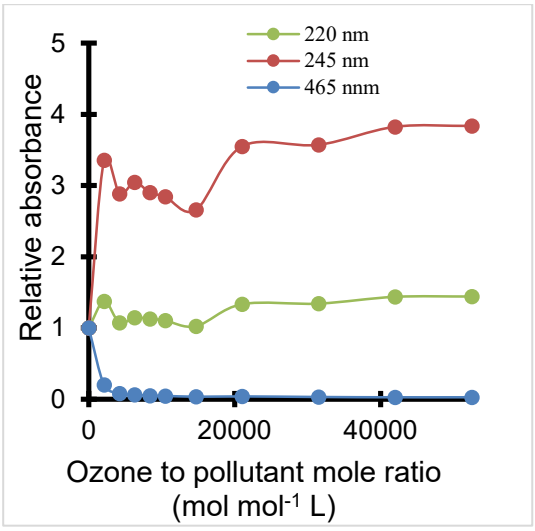

MO-NaMt

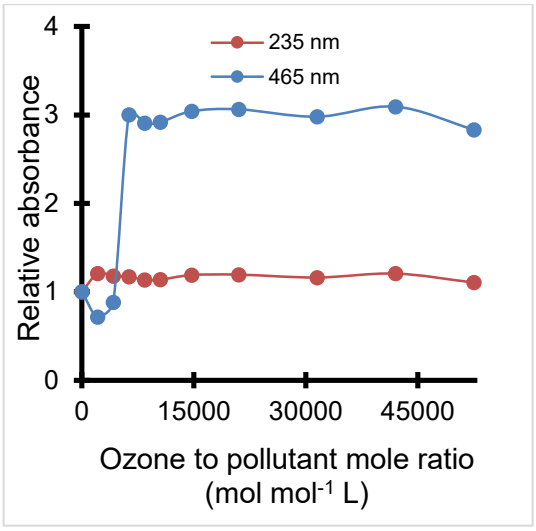

MTB-NaMt

Fig. S1.7. Effect of ozone-to-dye mole ratio on the relative absorbance during ozonation in distilled water in the presence of NaMt. T = 22 ° C. pH = intrinsic value. Quartz cell = 1 cm. O_3 throughput: 600 mg h^{-1}. Sample volume = 20 mL. Initial dye concentration: 10^{-4} M. Catalyst amount = 40 mg of dry NaMt.

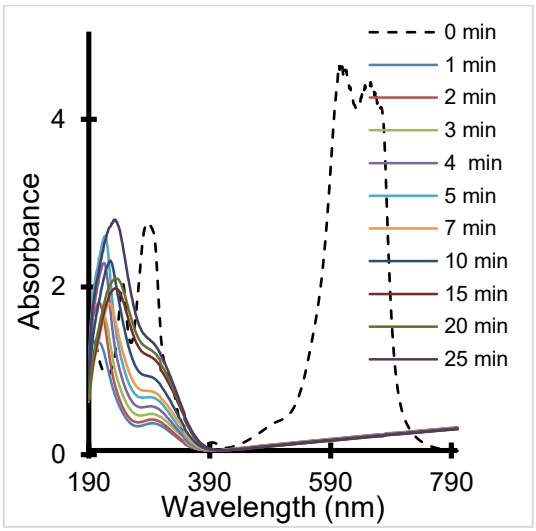

MB-Fe(II)Mt

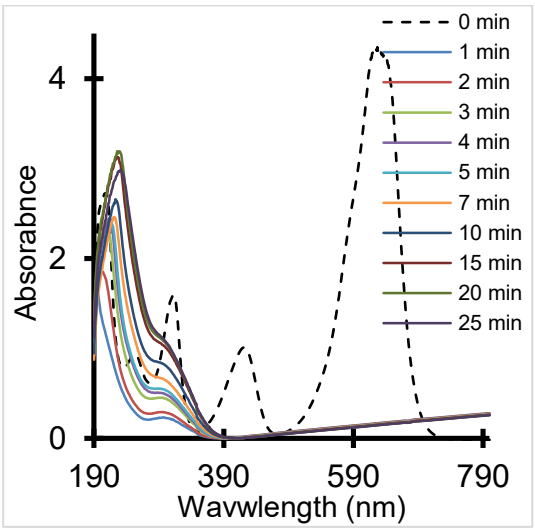

MG- Fe(II)Mt

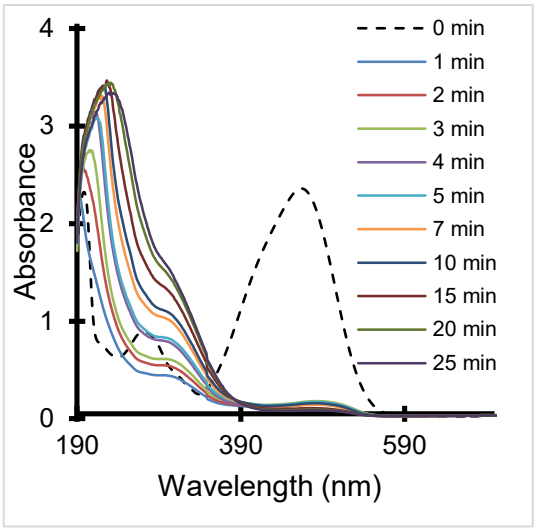

MO- Fe(II)Mt

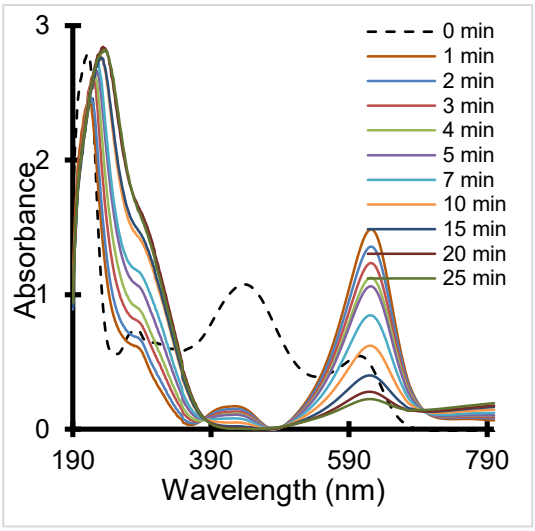

MTB- Fe(II)Mt

Fig. S1.8. Changes in the UV-Vis spectra of the different dyestuffs during catalytic ozonation with Fe(II)Mt in distilled water. T = 22 °C. pH = intrinsic value. Quartz cell = 1 cm. O_3 throughput: 600 mg h^{-1}. Sample volume = 20 mL. Initial dye concentration: 10^{-4} M. Catalyst amount = 40 mg of dry ion-exchanged montmorillonite.

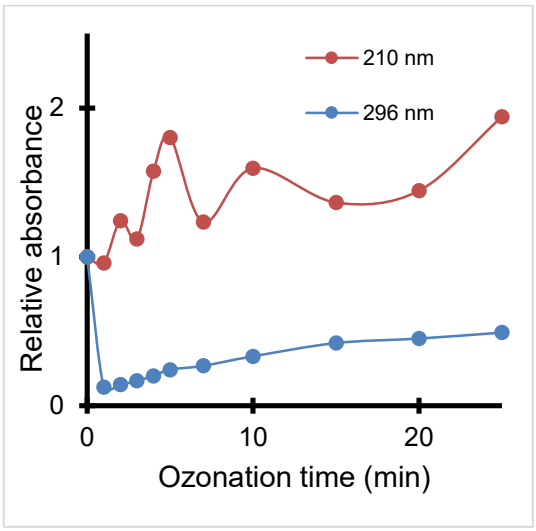

MB- Fe(II)Mt

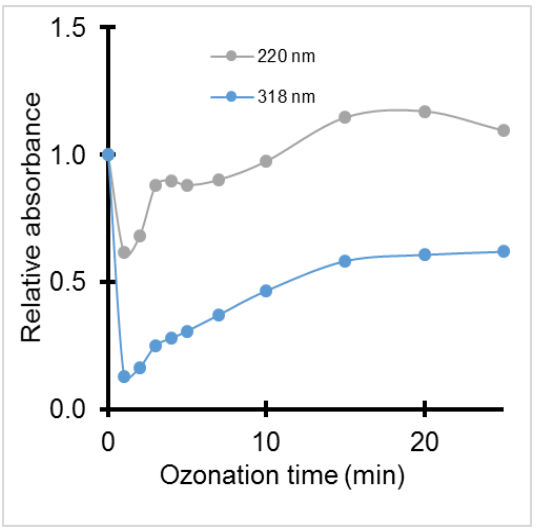

MG- Fe(II)Mt

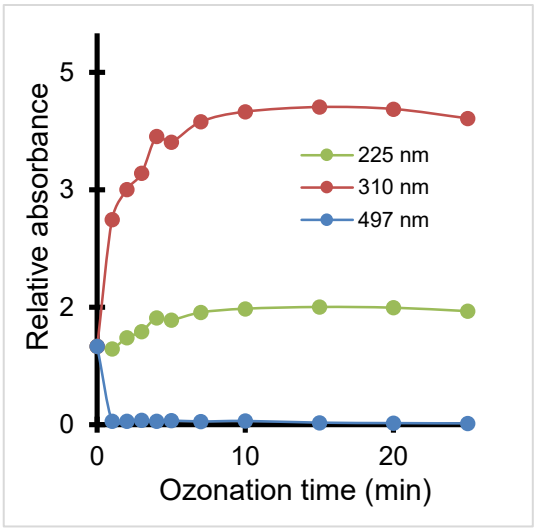

MO- Fe(II)Mt

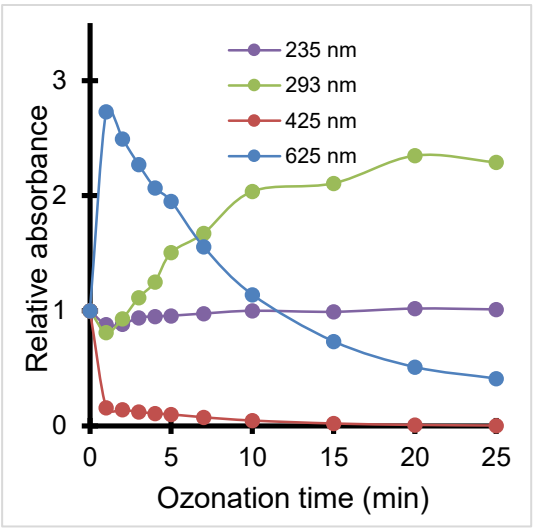

MTB- Fe(II)Mt

Fig. S1.9. Evolution in time of the relative absorbance of the different dye molecules during ozonation with Fe(II)Mt in distilled water. T = 22 ° C. pH = intrinsic value. Quartz cell = 1 cm. O_3 throughput: 600 mg h^{-1}. Sample volume = 20 mL. Initial dye concentration: 10^{-4} M. Catalyst amount = 40 mg of dry ion-exchanged montmorillonite.

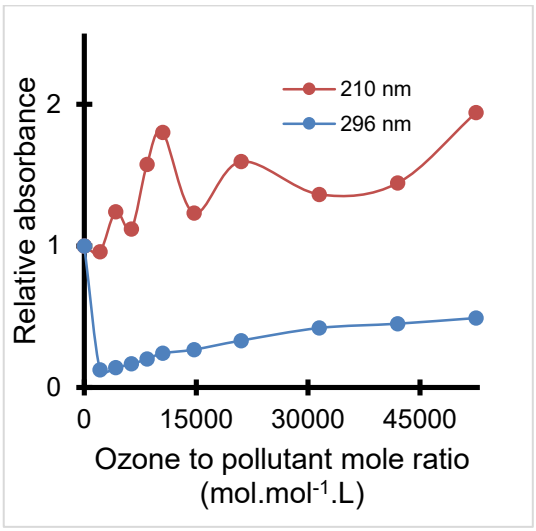

MB- Fe(II)Mt

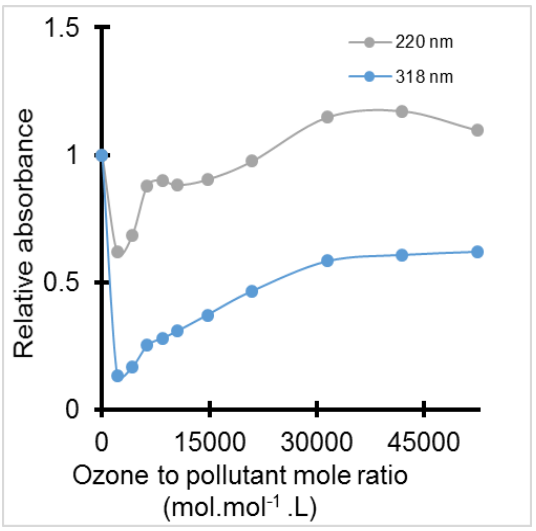

MG- Fe(II)Mt

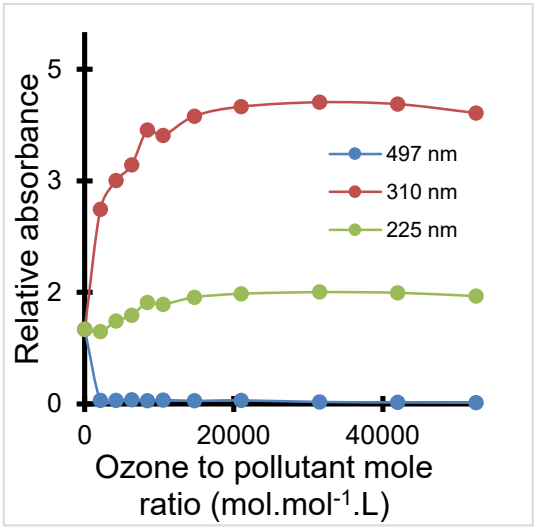

MO- Fe(II)Mt

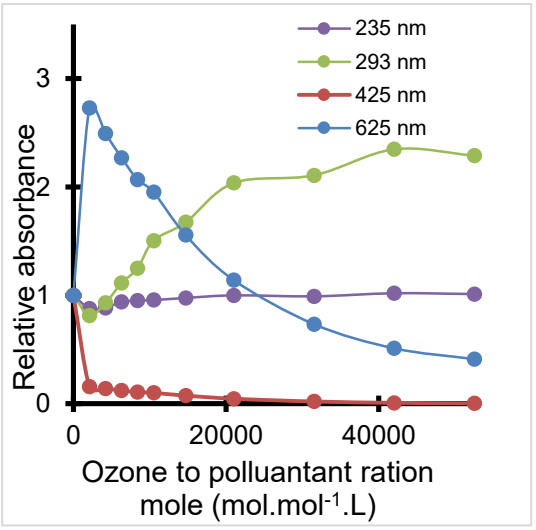

MTB- Fe(II)Mt

Fig. S1.10. Evolution in time of the ozone-to-dye mole ratio of the different dye molecules during ozonation with Fe(II)Mt in distilled water. T = 22 ° C. pH = intrinsic value. Quartz cell = 1 cm. O_3 throughput: 600 mg h^{-1}. Sample volume = 20 mL. Initial dye concentration: 10^{-4} M. Catalyst amount = 40 mg of dry ion-exchanged montmorillonite.

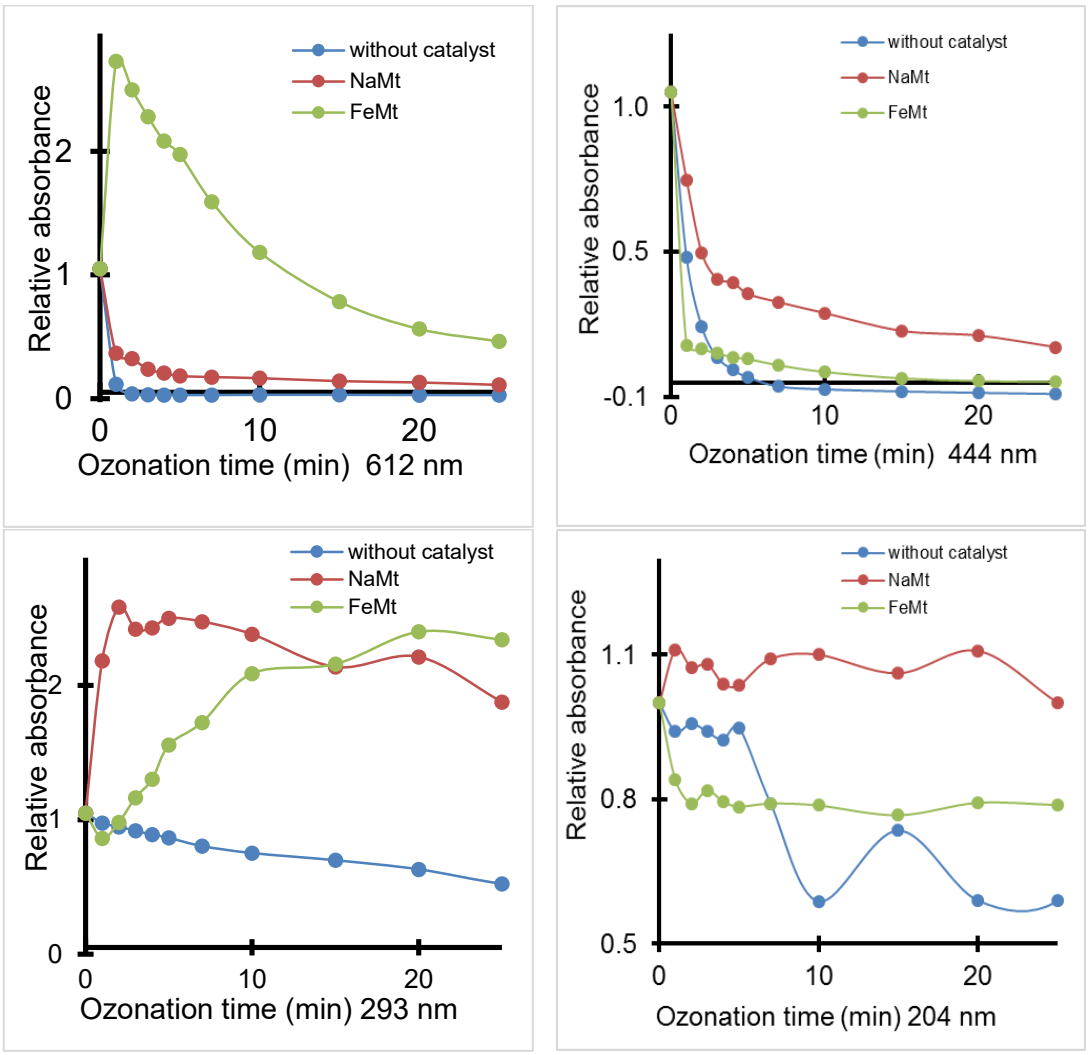

Fig. S1.11. Evolution in time of the relative absorbance of MTB during ozonation in distilled water. T = 22 ° C. pH = intrinsic value. Quartz cell = 1 cm. O_3 throughput: 600 mg h^{-1}. Sample volume = 20 mL. Initial dye concentration: 10^{-4} M. Catalyst amount = 40 mg of dry catalyst.

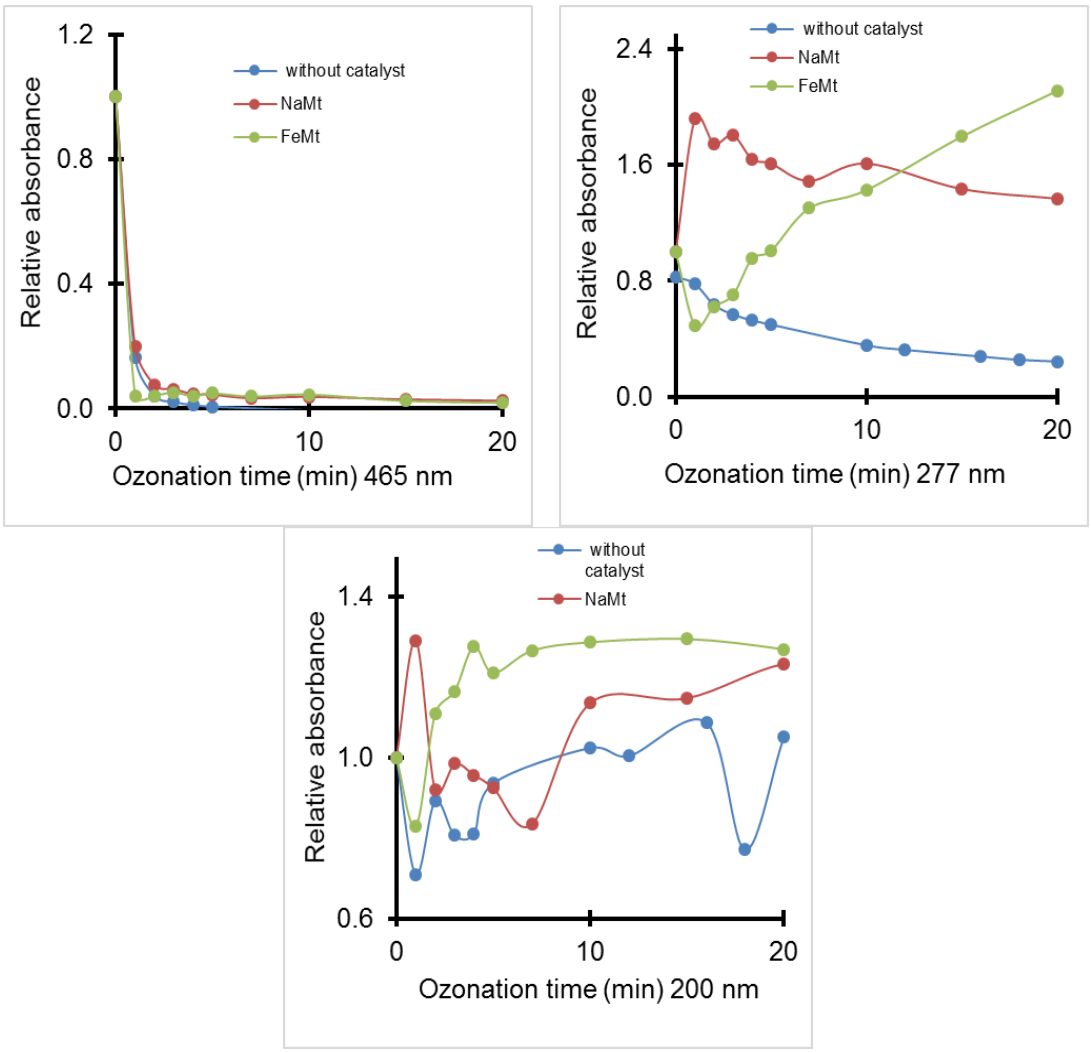

Fig. S1.12. Evolution in time of the relative absorbance of MO during ozonation in distilled water. T = 22 ° C. pH = intrinsic value. Quartz cell = 1 cm. O_3 throughput: 600 mg h^{-1}. Sample volume = 20 mL. Initial dye concentration: 10^{-4} M. Catalyst amount = 40 mg of dry catalyst.

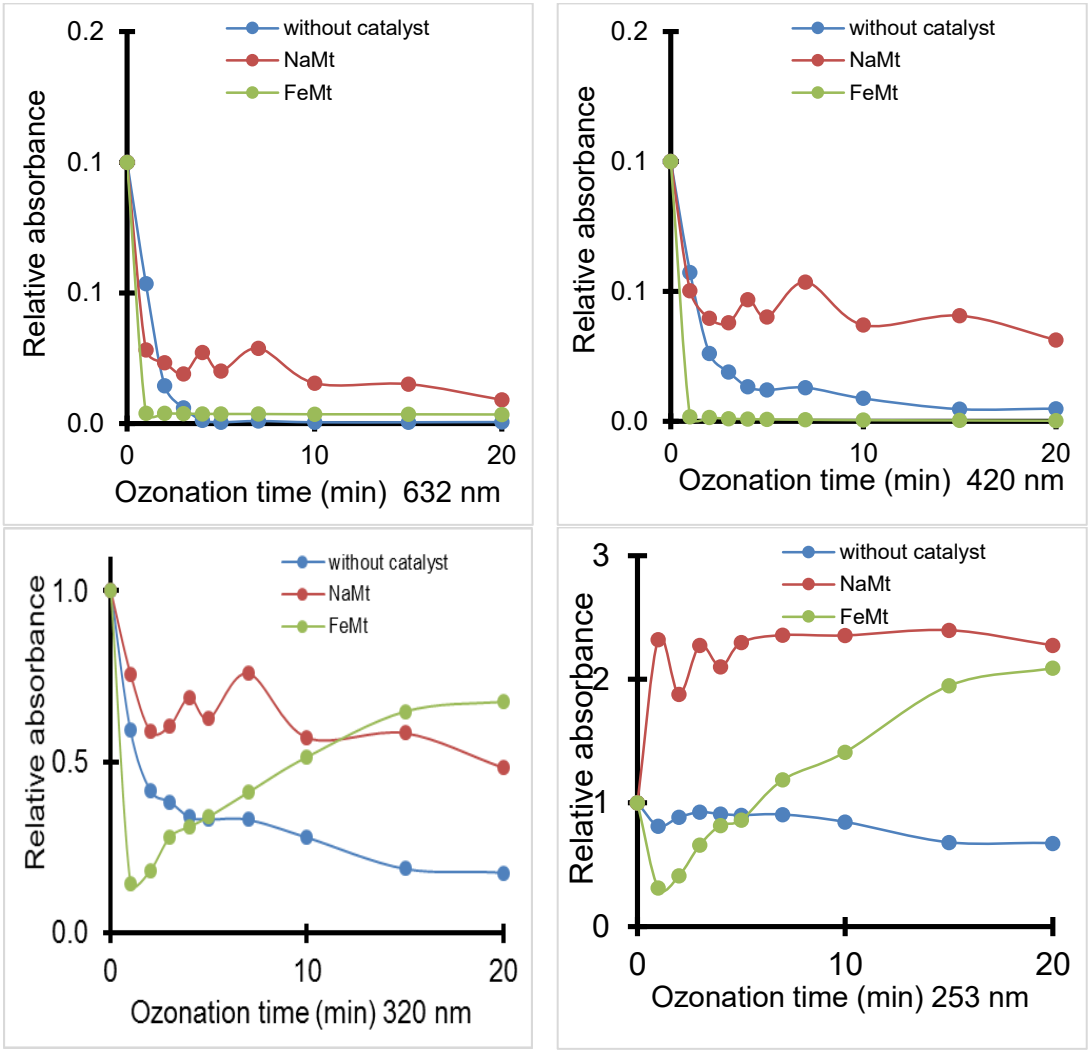

Fig. S1.13. Evolution in time of the relative absorbance of MG during ozonation in distilled water. T = 22 ° C. pH = intrinsic value. Quartz cell = 1 cm. O_3 throughput: 600 mg h^{-1}. Sample volume = 20 mL. Initial dye concentration: 10^{-4} M. Catalyst amount = 40 mg of dry ion-exchanged montmorillonite.

Table S1.3. Application of different kinetic models and validation time ranges based on R^2 for the main UV-Vis band of dye molecules in non-catalyzed ozonation.

Dye	UV-Vis band (nm)	First order kinetics[a]			Second order kinetics	
		Time range (s)	k_1 (sec^{-1})	R^2	k_2 (M^{-1} sec^{-1})	R^2
MB	660	0-100	0.0264	0.9965	0.1101	0.8668
		10-100	0.0273	0.9995	0.1234	0.8969
		40-80	0.0272	0.9989	0.2445	0.9982
		30-80	0.0274	0.9993	0.112	0.9669
		10-60	0.0278	0.9988	0.0658	0.9566
		20-50	0.0288	0.9993	0.0647	0.9821
	614	0-180	0.0222	0.9771	0.262	0.871
		0-100	0.0274	0.9945	0.1406	0.9045
		0-60	0.03	0.9973	0.084	0.9595
		20-60	0.0285	0.9982	0.1037	0.9826
		20-50	0.0293	0.9982	0.0919	0.9882
		0-50	0.0308	0.9977	0.0735	0.9679
		0-40	0.0316	0.9975	0.0634	0.9807
		0-30	0.0329	0.9984	0.0563	0.983
	498	0-180	0.0123	0.9975	0.0411	0.904
		0-120	0.0128	0.9983	0.0287	0.94
		0-100	0.0127	0.9973	0.0245	0.9378
		0-80	0.0118	0.9919	0.0199	0.9593
		20-60	0.012	0.9985	0.0195	0.9883
		20-80	0.0124	0.9984	0.0233	0.977
		30-120	0.0132	0.999	0.035	0.9736
		50-140	0.0125	0.9929	0.0396	0.987
	403	60-180	0.0039	0.9933	-	0.9833
	332	0-100	0.0045	0.9903	0.0051	0.9386
		30-120	0.004	0.9951	0.0058	0.9912
		30-100	0.0041	0.9921	0.0057	0.9833
		30-80	0.0038	0.9968	0.0049	0.9933
	290	10-60	0.0179	0.9969	0.0276	0.9925
		20-60	0.0177	0.9949	0.0296	0.9982
	234	0-80	0.0016	0.9823	0.0011	0.4719
		30-80	0.0013	0.9957	0.0014	0.9946
	217	0-50	-0.0087	0.9811	0.0075	0.9514
MTB	612	10-60	0.512	0.9901	0.7278	0.9087
	444	0-30	0.0285	0.9977	0.0452	0.9929
		0-40	0.0299	0.9968	0.0579	0.9517
		40-180	0.0183	0.9942	0.0769	0.9701
		0-180	0.0199	0.9906	0.1959	0.8287

	390	10-40	0.0114	0.9918	0.0171	0.9801
	320	100-180	0.0014	0.9699	0.0019	0.9666
	293	80-180	0.0011	0.9918	0.0016	0.9896
		100-180	0.0012	0.9957	0.0018	0.9897
	214	0-20	0.0156	0.9904	0.0183	0.9803
MO		0-20	0.0378	0.9844	0.0565	0.9514
		0-30	0.0396	0.9929	0.074	0.9528
		0-40	0.0418	0.9940	0.1031	0.9155
	465	0-50	0.0419	0.9966	0.1314	0.914
		0-60	0.0417	0.9978	0.1675	0.8978
		20-60	0.0423	0.9984	0.2299	0.9565
		100-160	0.0197	0.9946	1.3424	0.9889
	277	20-60	0.0071	0.9904	0.0093	0.9959
		60-180	0.003	0.9941	0.0055	0.9964
		50-140	0.0033	0.9927	0.0056	0.9954
		50-180	0.0031	0.9932	0.0055	0.9972
	215 -220	60-140	-0.0025	0.9988	0.0135	0.8527
		40-140	-0.0026	0.9955	0.0104	0.9908
	200-2010 *	0-20	-0.0041	0.9204	0.0039	0.9161
MG	632	0-50	0.029	0.9908	0.0658	0.9373
		0-60	0.0297	0.9935	0.0818	0.9164
		0-80	0.0309	0.9948	0.1282	0.8415
		0-100	0.0326	0.9935	0.2297	0.7672
		0-120	0.0345	0.9918	0.4437	0.700
		20-80	0.0331	0.9996	0.1718	0.9072
		20-60	0.0325	0.9997	0.1103	0.966
		20-120	0.0364	0.9958	0.5655	0.7651
	420	40-140	0.0163	0.9958	0.1108	0.9762
		30-80	0.019	0.9987	0.0712	0.9872
		80-140	0.1367	0.9889	0.1403	0.9938
	315-320 *	30-60	0.0108	0.996	0.0214	0.9997
		30-80	0.0095	0.9891	0.0206	0.9992
		50-140	0.0068	0.9925	0.0204	0.9959
	253-250 *	50-180	0.0016	0.9906	0.0017	0.9866
		80-180	0.0017	0.9936	0.0018	0.9929
	220	40-120	-0.0008	0.9916	0.0033	0.9900
		50-120	-0.0008	0.9941		0.9929

[a] This table contains only a selection R^2 values higher than 0.99, which were used to validate a kinetical model ast the expense of the other.

Table S1.4. Application of different kinetic models and validation time ranges based on R^2 for the main UV-Vis band of dye molecules in NaMt-catalyzed ozonation.

Dye	λ (nm)	First order kinetics			Second order kinetics[a]		
		Time range (s)	k_1 (sec^{-1})	R^2	Time range (s)	k_2 (M^{-1} sec^{-1})	R^2
MB	770	20-40	-0.0376	0.9966	20-40	0.0129	0.9976
	660 →670*	60-100	-0.0094	0.9996	60-100	0.0192	0.9988
	614	60-100	-0.0084	0.998	60-100	0.0237	1
	385	60-100	-0.0179	0.9968	60-100	0.0066	0.9979
	332	0-20 60-100	0.0309 -0.0139	0.9937 0.9972	0-20 60-100	0.0428 0.0174	0.9999 0.9993
	280 →296*	60-100	-0.0094	0.9995	60-100	0.0122	0.9944
	234 →250*	60-100	-0.0084	0.991	-	-	-
	210	10-30	-0.0054	0.9913	-	-	-
MG	632 →668*	20-50	0.0192	0.9874	0-50 0-20	0.1474 0.267	0.989 0.9915
	420→437*	-	-	-	0-20	0.2037	0.9996
	315→318*	-	-	-	0-20	0.1146	0.9892
MO	465	0-60 30-50 40-60 60-100	0.036 0.0473 0.0388 0.0183	0.9973 0.9986 0.9936 0.9902	30-100 40-80	0.217 0.2236	0.9978 0.9998
MTB	612	40-180	0.0062	0.979	20-180	0.0438	0.9795

* This band was prone to a significant bathochromic or hypsochromic effects.

[a] This table contains only a selection R^2 values higher than 0.99, which were used to validate a kinetical model ast the expense of the other.

Table S1.5. Application of different kinetic models and validation time ranges based on R^2 for the main UV-Vis band of dye molecules in Fe(II)Mt-catalyzed ozonation.

Dye	λ (nm)	First order kinetics			Second order kinetics[a]		
		Validation time range (s)	k_1 (sec^{-1})	R^2	Validation time range (s)	k_2 ($M^{-1}.sec^{-1}$)	R^2
MB	280→296 *	-	-	-	20-40 50-80	0.02337 0.0433	0.9888 0.9965
MG	318	10-30 120-160	-0.0278 -0.0099	0.9953 0.9976	- -	- -	- -
	220	10-50 10-30	-0.0068 -0.0062	0.997 0.998	10-50 10-30	0.0124 0.0122	0.999 0.9961
MO	497	20-40	0.0142	0.9899	20-40	0.2543	0.9963
	205	30-80 100-140	-0.0041 -0.004	0.9916 0.9993	100-140	0.0036	0.9976
MTB	625	20-40	0.0036	0.9999	-	-	-
	425	20-40	0.0047	0.9989	20-40	0.027	0.9996

* This band was prone to a significant bathochromic effect, which produced a shift from 280 nm to 296 nm during ozonation.

[a] This table contains only a selection R^2 values higher than 0.99, which were used to validate a kinetical model ast the expense of the other.

Table S1.6. UV-Vis band removal yield (%) after ozonation with different clay catalysts

Dye	UV-Vis band (nm)	UV-Vis band evolution yield (%)[a]					
		After 02 min ozonation with			After 20 min ozonation with		
		no catalyst	NaMt	Fe(II)Mt	no catalyst	NaMt	Fe(II)Mt
MB	660	94.1	62.3	95.7	100.2	95.8	96.2
	614	94.2	76.6	96.6	99.9	100.0	97.1
	498	74.3	70.2	78.0	114.5	146.7	83.5
	403	-270.7	-62.4	96.1	229.4	171.7	95.4
	332	33.6	33.7	70.1	95.2	62.6	-5.2
	280	71.5	35.9	86.4	90.4	52.4	50.5
	234	5.9	-101.8	34.1	17.3	-92.2	-76.7
MG	632	85.5	76.8	96.1	99.4	90.9	96.5
	420	73.9	60.4	98.6	95.2	68.7	99.8
	320	58.2	40.9	81.8	82.4	51.7	32.4
	253	11.6	-87.9	59.0	32.7	-127.4	-109.0
	200	22.0	14.0	28.9	-12.5	9.3	8.5
MO	465	95.8	92.3	95.8	100.8	97.5	98.1
	277	23.1	-74.5	37.7	70.4	-36.7	-110.9
	200	10.8	8.1	-10.9	-5.2	-23.3	-26.9
MTB	612	101.1	72.8	-144.5	102.1	91.9	48.8
	444	81.0	55.5	88.6	103.6	83.9	48.8
	393	41.5	-147.1	6.9	99.5	-111.0	-134.8
	204	4.3	-7.4	20.8	41.0	-10.8	20.7

[a] UV-Vis band evolution accounts for increasing C/Co for UV-Vis bands below 250 nm related to hydroxylated derivatives (negative yields) and for removal yield for the other bands (positive yields). The latter correspond to the actual decomposition yield of a dye molecule. The error on the absorbance value was estimated to be of $\pm$1%.

Table S1.7. Zeta potential in dye solution at intrinsic pH in the presence of different clay catalysts

Clay catalysts	Zeta potential (mV) in dye solution[a]			
	MB	MG	MO	MTB
Bentonite	-37.78 ± 3.30	-48.54 ± 21	-38.04 ± 4.94	-41.01 ± 2.74
NaMt	-52.59 ± 3.49	N.D	-50.2 ± 3.02	-54.44 ±3.96
FeMt	+13.00 ± 4.8	+3.90 ± 6.65	+7.32 ± 5.21	+3.36 ± 2.04
HMt-1	-30.30 ± 5.21	-40.98 ± 4.06	-89.96 ± 2.03	-35.34 ± 5.71
HMt-4	- 34.96 ± 3.41	-38.21 ±2.31	-48.22 ±3.53	-31.79 ±3.1
HMt-8	-34.67 ± 8	-41.05 ± 1.09	-43.26 ± 2.84	-29.36 ± 3
HMt-15	-37.40 ± 5.03	-45.05 ± 4.02	-46.66 ± 3.38	-31.95 ± 4.7
HMt-24	-35.03 ± 3.67	-37.54 ± 5.40	35.04 ± 4.99	-34.97 ±4.13

[a]These measurements were carried out at T = 22 °C in 20 mL of dye solution (10^{-4} M and intrinsic pH) in the presence of 40 mg of clay catalyst, which accounts for a catalyst concentration of 2 g L^{-1}.

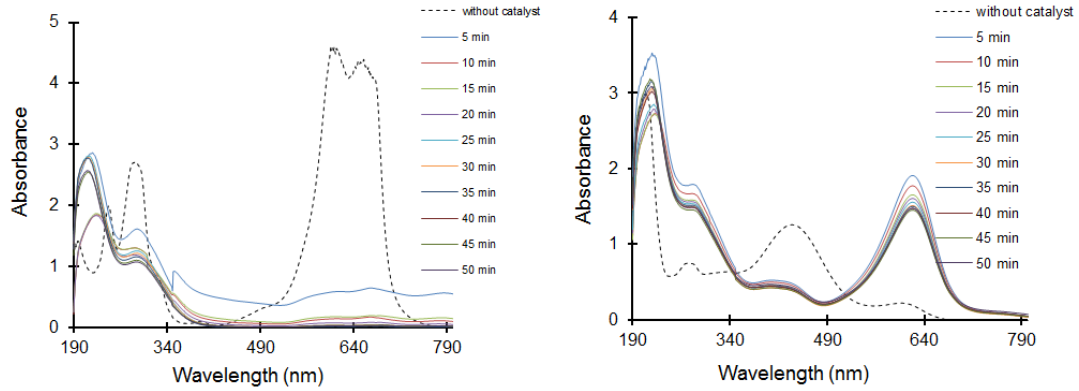

Fig. S1.14. Evolution in time of the dye UV-Vis spectra of MB (a) and MTB (b) in the presence of Fe(II)Mt without ozone. T = 22 ° C. pH = intrinsic value. Quartz cell = 1 cm. Sample volume = 20 mL. Initial dye concentration: 10^{-4} M. Catalyst amount = 40 mg of dry catalyst.

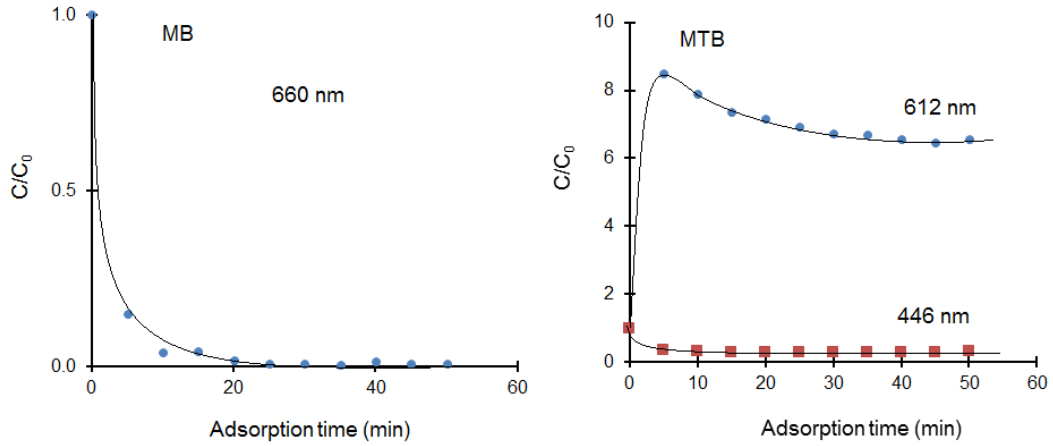

Fig. S1.15. Evolution in time of the main relative absorbance of dye molecule in the presence of Fe(II)Mt without ozone. T = 22 ° C. pH = intrinsic value. Quartz cell = 1 cm. Sample volume = 20 mL. Initial dye concentration: 10^{-4} M. Catalyst amount = 40 mg of dry catalyst.

Determination of ozone in water by iodometry

The principle involves iodide oxidation by ozone according to the reaction

$$2KI+O_3+H_2O \rightarrow I_2+2KOH+O_2 \qquad (S.1)$$

The amount of I_2 was determined by titration with sodium thiosulfate under acidic conditions:

$$I_2+2Na_2S_2O_3 \rightarrow 2I^-+Na_2S_4O_6 \qquad (S.2)$$

For the sake of sensitivity, the starch paste solution used as colored indicator was added before the end of the assay. At neutralisation, the solution color turned blue.

The experimental procedure involves to add 20 ml of KI (0.2M) and 2 ml of HCl (2M) in each of the 10 50 mL tubes. Ozone was bubbled during different times: 1, 2, 3, 4, 5, 10, 20, 30, 40 and 60 min, and then 3 drops of the starch paste was added to each tube, and each mixture was titrated with $Na_2S_2O_3$ (0.05 M) until the solution turns blue.

C-ToF-MS chrmomatographic analysis of the ozonation mixture

For the sake of brievity, only some the numerous HPLC-ToF-MS diagrams obtained are presented herein. Liquid chromatography- time of Flight-mass spectrometry (HPLC-ToF-MS) analysis of the reaction mixture was achieved by means of an Agilent 1200 Series HPLC instrument, Agilent Eclipse plus C18 column (3x50 mm, particle size1.8 µm) at (RT) and two mobiles phases, i.e. A: H_2O + 0.1% formic acid; mobile phase B: acetonitrile + 0.1% formic acid the Injection volume was of 5µL. The technical error and mass resolving power of the time-of-flight mass spectrometer in terms of mass accuracy was 5 ppm. A reserpine solution with m/z 609.2807 for $[M+H]^+$ ion was used as an internal standard for mass reference.

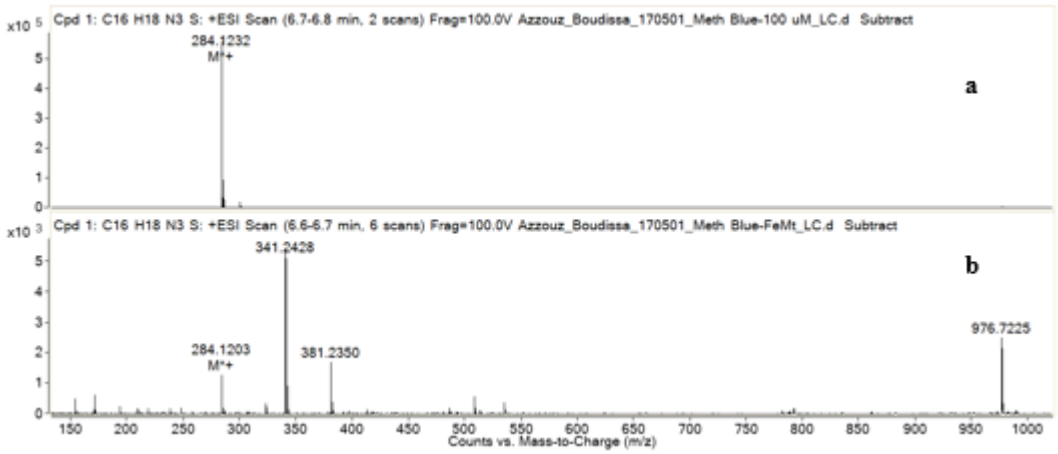

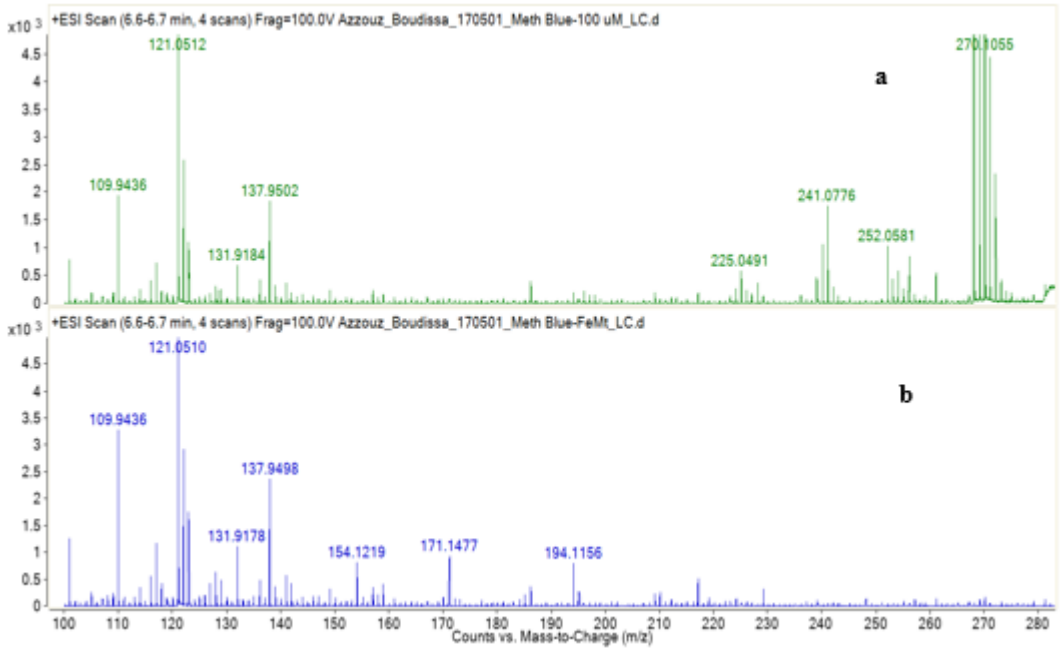

Fig. S1.16. LC-ToF-MS diagram of MO ozonation mixture after 1 min ozonation in the absence (a) and presence of Fe(II)Mt (b). Initial dye concentration = 100 µM.

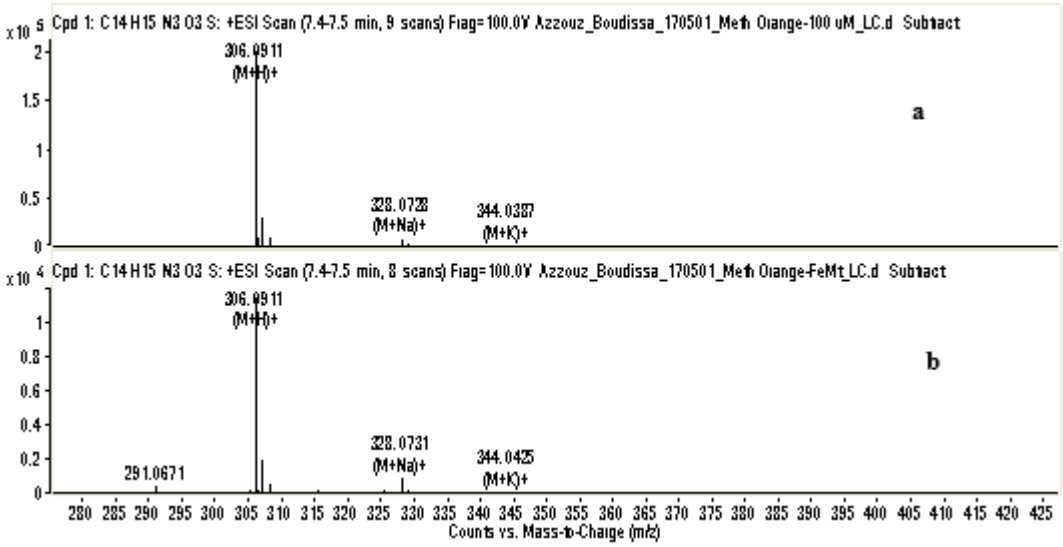

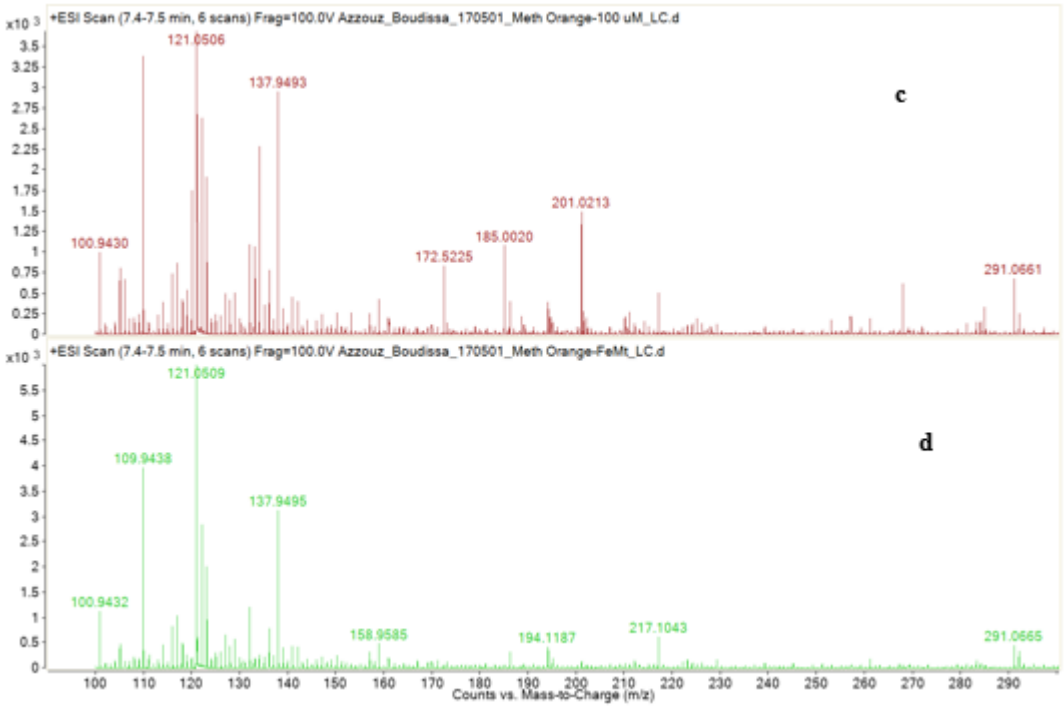

Fig. S1.17. LC-ToF-MS diagram of MO ozonation mixture after 1 min ozonation in the absence (a) and presence of Fe(II)Mt (b). Initial dye concentration = 100 µM.

REFERENCES

[1] Gao, L., et al., Degradation of cationic dye methylene blue by ozonation assisted with kaolin. J. Applied Clay Science, 46 (2009) 226-229.

[2] Tafulo, P.A.R., R.B. Queirós, and G. González-Aguilar, On the "concentration-driven" methylene blue dimerization. Spectrochimica Acta Part A: Molecular and Biomolecular Spectroscopy, 73 (2009) 295-300.

[3] Trandafilović, L.V., et al., Enhanced photocatalytic degradation of methylene blue and methyl orange by ZnO:Eu nanoparticles. J. Applied Catalysis B: Environmental, 203 (2017) 740-752.

ANNEXE B

SUPPORTING INFORMATION OF ARTICLE II: THOROUGH BISPHENOL-A REMOVAL THROUGH OZONATION WITH SILICA-BASED CATALYSTS. ROL OF……

Table S2.1. BPA oxidation in water by ozone at various operating parameters by several researchers

Medium	Ozone concentration (mgL^{-1})	Initial conc. of BPA ($mg.L^{-1}$)	Removal of BPA (%)	Ozonation time (min)	pH	Scale	Reference
Water	0.4 –2 $mg.min^{-1}$	5–50	100	7–70	2, 7, 12	Lab	[1]
Water	71.7	91	100	218	-	Lab	[2]
MilliQ Water	0.0015	0.228	100	60	7	Lab	[3]
River water	1–10	10, 5.4 - 8.4 × 10^{-4}	60–100	7	8.2–8.5	Lab/ Pilot	[4]
Drinking water	1, 1.5, 2	11	70, 82, 90	–	–	Lab	[5]
Aqueous solution	15	11.4, 22.8	99	7–34	6	Lab	[6]
Drinking water	10	0.13	>99.5	5	–	Pilot	[7]
MilliQ Water	19.2	22.8	100	60	6.5	Lab	[8]
Water	30	22.8	100	4	5	Lab	[9]
Deionized water	1.4, 2.2, 5.1	5.25 - 13	84, 92, 99	14	2, 5, 7, 10	Lab	[10]
Water	4.05 $mg.min^{-1}$	10	100	10	6	Lab	[11]
MilliQ water	8.3	0.9	>99	45	8.4	Lab	[12]

Table S2.2. physicochemical properties of BPA [13]

Property	Value
Molecular formula	$C_{15}H_{16}O_2$
structure	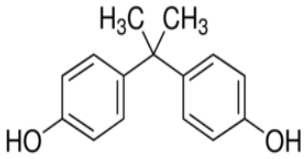
Molecular weight (g mol^{-1})	228.29
Density	1.20 g cm^{-3}
Water solubility mg L^{-1}(25 ^{0}C)	120–200
pKa	9.56 - 10.2
Melting point	153 ^{0}C
Boiling point	220 ^{0}C at 4 mmHg
Henry's law constant	1×10^{-10} at 25 ^{0}C
Vapor pressure	87 Pa at 190 ^{0}C
EcotoxicologyLog K_{ow}	3.32 at 25 ^{0}C
Appearance	White crystalline solid

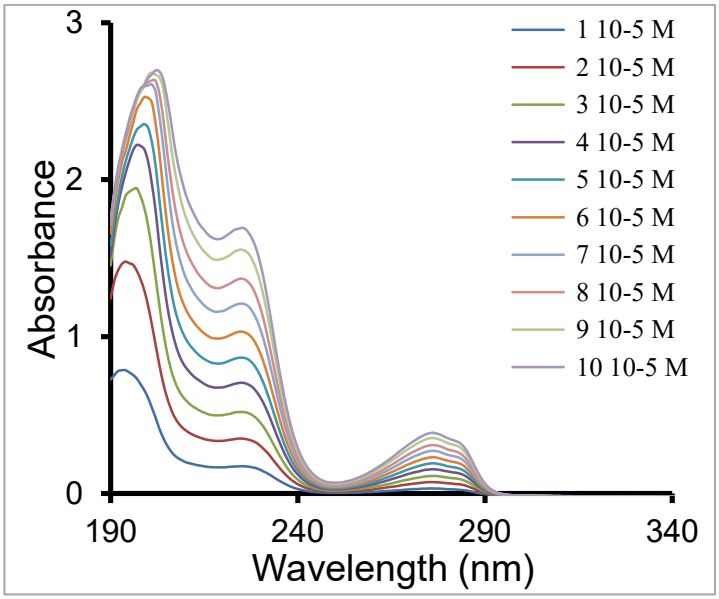

Fig. S2.1. UV-vis spectra of BPA at different concentration in distilled water. T= 22°C, pH = 5.64 value, Quartz cell = 1 cm.

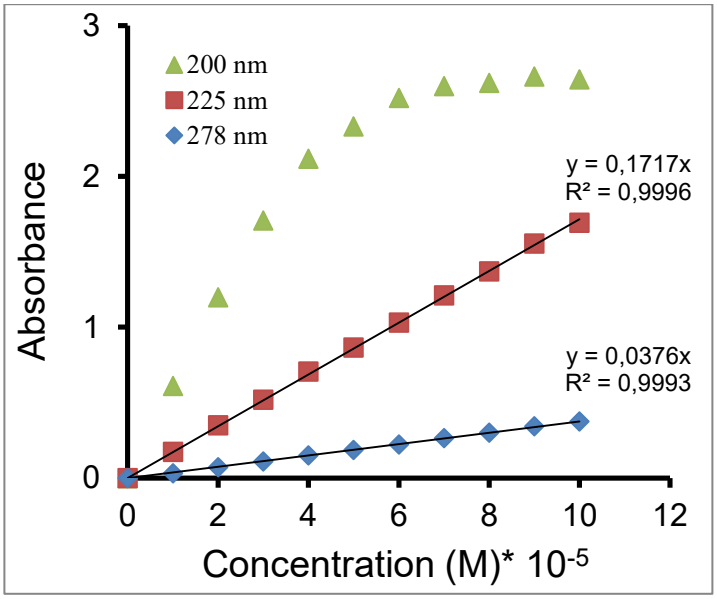

Fig. S2.2. Calibration curves for BPA in distilled water. T = 22 °C. pH = intrinsic value. Quartz cell = 1 cm.

Table S2.3. Molar extinction coefficient (ε) of the different UV-Vis bands

	Max wavelength (nm)	Molar extinction coefficient (ε) (M^{-1} cm^{-1})*	Correlation coefficient R^2
BPA	200	34530	0.6742
	225	17170	0.9996
	278	3760	0.9993

* The coefficient were assessed from the slope of the linear part of the calibration curve fulfilling the Beer's law ($A=\varepsilon bc$), where A is the absorbance of BPA solution, ε is the molar absorptivity (M^{-1} cm^{-1}), b is the path length (cm), and c is the BPA concentration (M).

REFERENCES

[1] Lee, J., H. Park, and J. Yoon, Ozonation characteristics of bisphenol a in water. J. Environmental Technology, 24 (2003) 241-248.

[2] Irmak, S., O. Erbatur, and A. Akgerman, Degradation of 17β-estradiol and bisphenol A in aqueous medium by using ozone and ozone/UV techniques. J. Hazardous Materials, 126 (2005) 54-62.

[3] Deborde, M., et al., Kinetics of aqueous ozone-induced oxidation of some endocrine disrupters. J. Environmental Science and Technology, 39 (2005) 6086-6092.

[4] Choi, K.J., et al., Removal efficiencies of endocrine disrupting chemicals by coagulation/flocculation, ozonation, powdered/granular activated carbon adsorption, and chlorination. Korean J. Chemical Engineering, 23 (2006) 399-408.

[5] Xu, B., et al., Degradation of endocrine disruptor bisphenol A in drinking water by ozone oxidation. Frontiers of Environmental Science & Engineering in China, 1 (2007) 350-356.

[6] Kim, S.E., et al., modeling of decomposition characterisitics of estrogenic chemicals during ozonation. J. Environmental Technology, 29 (2008) 287-296.

[7] Baig, S., G. Hansmann, and B. Paolini, Ozone oxidation of oestrogenic active substances in wastewater and drinking water. Water science and technology : a J. International Association on Water Pollution Research, 58 (2008) 451-458.

[8] Deborde, M., et al., Oxidation of bisphenol A by ozone in aqueous solution. Water Research, 42 (2008) 4299-4308.

[9] Rivas, F.J., et al., Mineralization of bisphenol A by advanced oxidation processes. J. Chemical Technology & Biotechnology, 84 (2009) 589-594.

[10] Garoma, T. and S. Matsumoto, Ozonation of aqueous solution containing bisphenol A: Effect of operational parameters. J. Hazardous Materials, 167 (2009) 1185-1191.

[11] Gultekin, I., V. Mavrov, and N.H. Ince, Degradation of Bisphenol-A by ozonation. J. Advanced Oxidation Technologies, 12 (2009) 242-248.

[12] Leal, L., et al., Removal of micropollutants from aerobically treated grey water via ozone and activated carbon. J.Water Res, 45 (2011) 2887-96.

[13] CRC Handbook of Chemistry and Physics, 87th ed Editor-in-Chief: David R. Lide (National Institute of Standards and Technology). CRC Press/Taylor and Francis Group: Boca Raton, FL. 2006. 2608 pp. J. American Chemical Society, 2007. **129**(3): p. 724-724.

ANNEXE C

SUPPORTING INFORMATION OF ARTICLE III: CLAY-CATALYZED OZONATION FOR EFFECTIVE REMOVAL OF ENDOCRINE-DISRUPTING…

Table S3.1. Physicochemical properties of 17α-ethinylestradiol (EE2)

Molecular formula	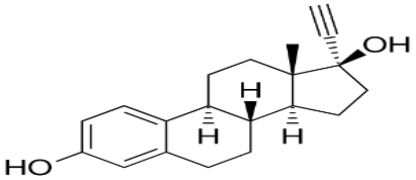
Molecular structure	$C_{20}H_{24}O_2$
Molecular weight (g mol^{-1})	296.40
Water solubility (mg L^{-1}) at 20 °C	4.8
pKa	10.46 - 10.70
Log k_{ow}	4.15
λmax (nm)	198, 220, 280 nm

Table S3.2. Gradient used in HPLC-ToF-MS chromatographic analysis

mobile-phase	Gradient	
	Time (min)	B (%)
A : H_2O + 0,1% formic acid B: ACN + 0,1% formic acid	1.0	3
	6.0	85
	10.0	95
	11.0	95
	11.1	3
	15.0	3

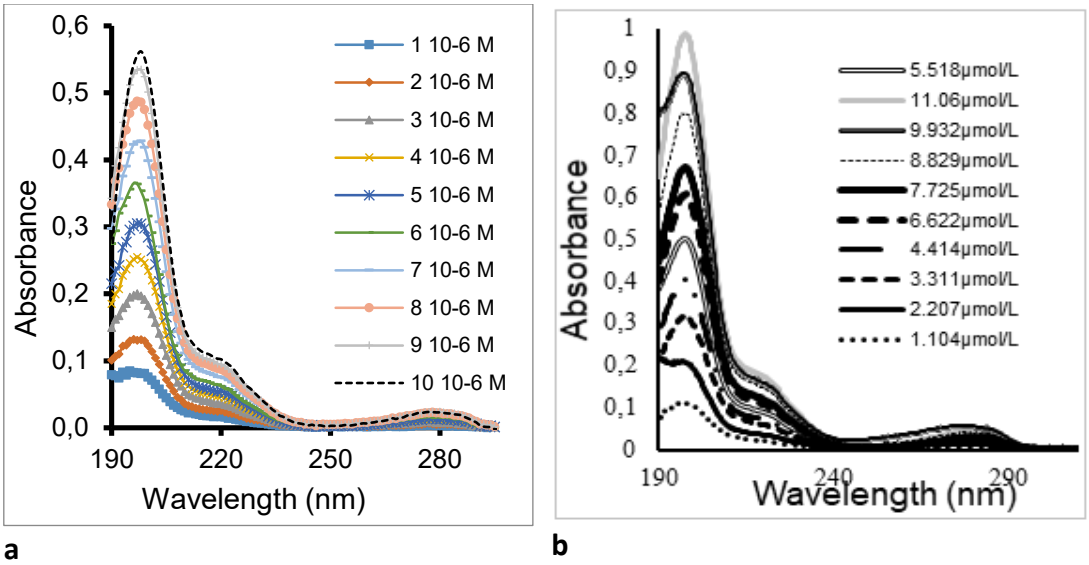

Fig. S3.1. UV-vis spectra of EE2 at different concentration in distilled water at intrinsic pH 5.28 (a) and in 99.998-0.001 water- ethanol mixture at pH 4.02 (b). Quartz cell = 1 cm. T= 22°C.

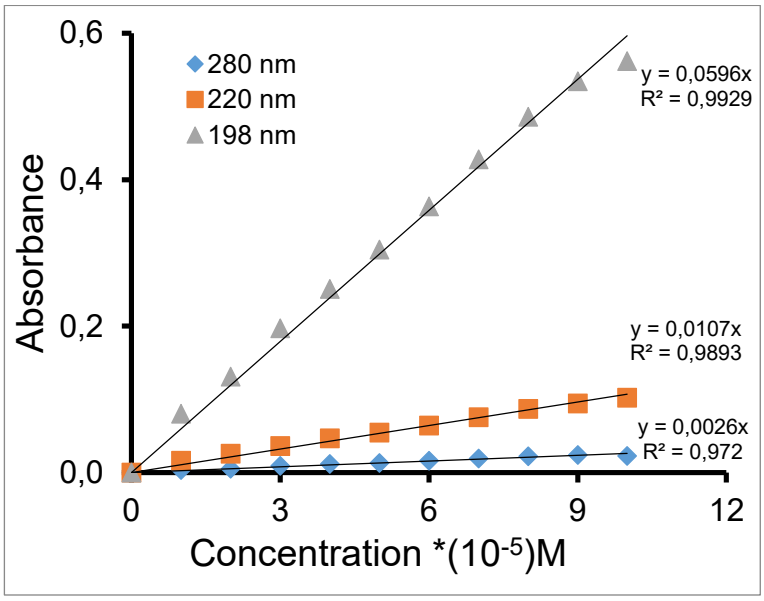

Fig. S3.2. Calibration curves for EE2 in distilled water. T = 22 °C. pH = 5.28. Quartz cell = 1 cm.

Table S3.3. Molar extinction coefficient (ε) for EE2 aqueous- ethanol (0.2398 nmol L) solution

λ_{max} (nm)	aqueous- ethanol solution			aqueous solution		
	198	220	280	198	220	280
ε (M^{-1} cm^{-1})	88100	16800	4600	5960	1070	260
R^2	0.999	0.997	0.988	0.993	0.989	0.972
[EE2] (μmolL^{-1})	0 – 11.06	0 – 11.06	0.5 – 5.5	0 – 10	0 – 10	0 – 10

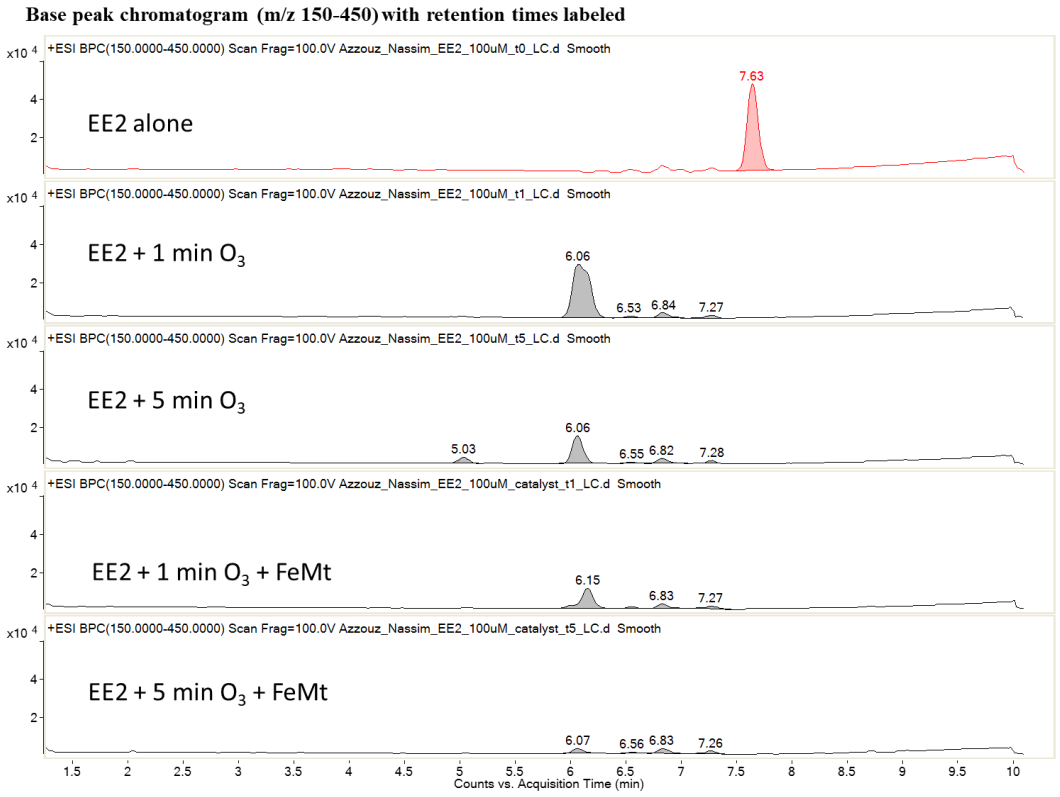

Fig. S3.3. Effect of Fe(II)Mt addition on EE2 degradation as evaluated by LC-ToF-MS analysis of the ozonation mixture in water. Initial EE2 concentration = 10^{-5} M, Fe(II)Mt concentration: 2 g L^{-1}, Ozone dose: 600 mg h^{-1} at 22 °C

T0 Base peak chromatogram (*m/z* 150-450) with retention times labeled

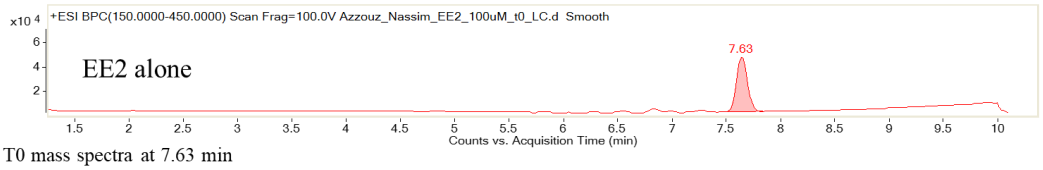

T0 mass spectra at 7.63 min

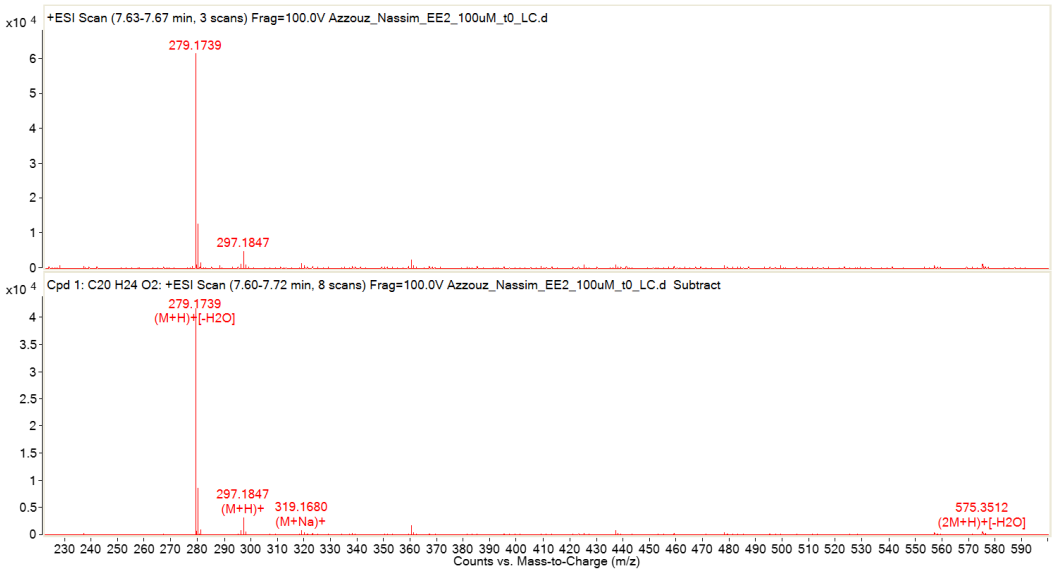

EE2 + 1 min O_3 base peak chromatogram (*m/z* 150-450) with retention times labeled

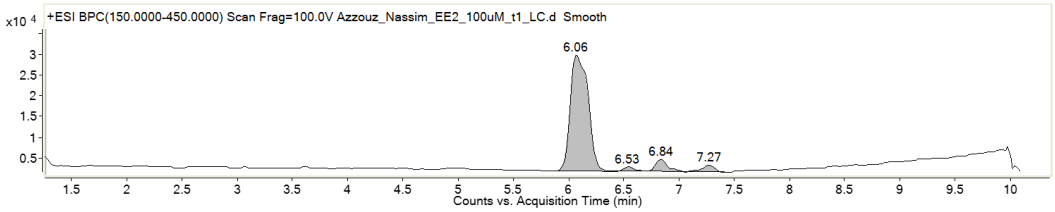

t1 mass spectra at 6.06, 6.53, 6.84, 7.27 min

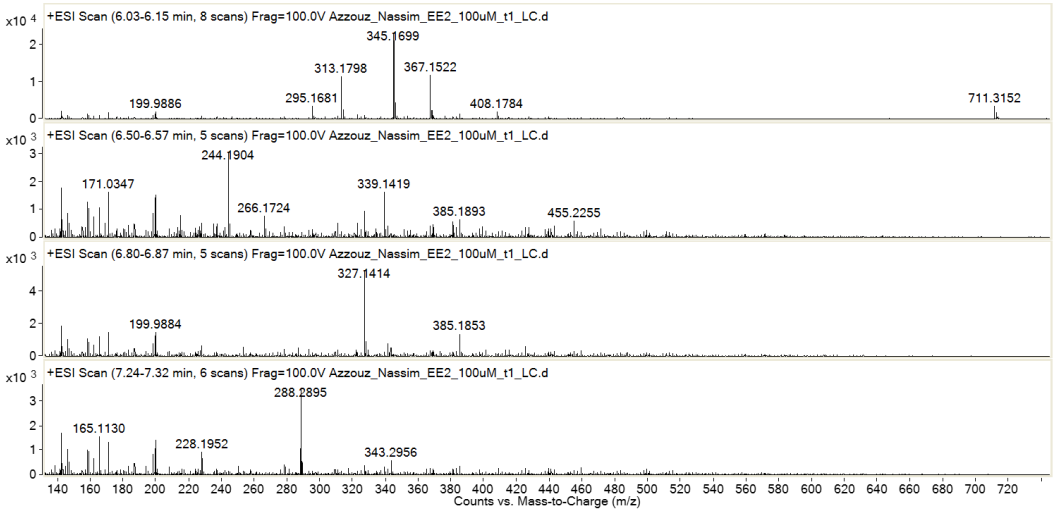

EE2 + 5 min O_3 base peak chromatogram (*m/z* 150-450) with retention times labeled

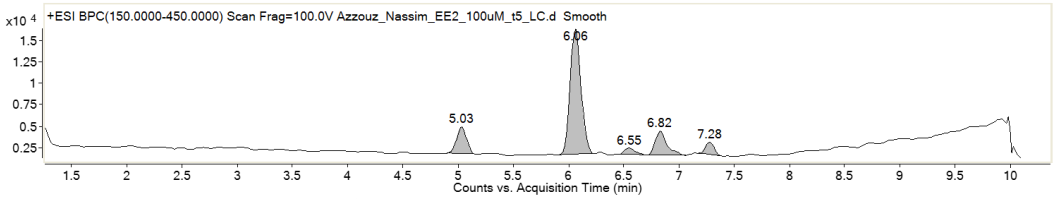

t5 mass spectra at 6.06, 6.53, 6.84, 7.27 min

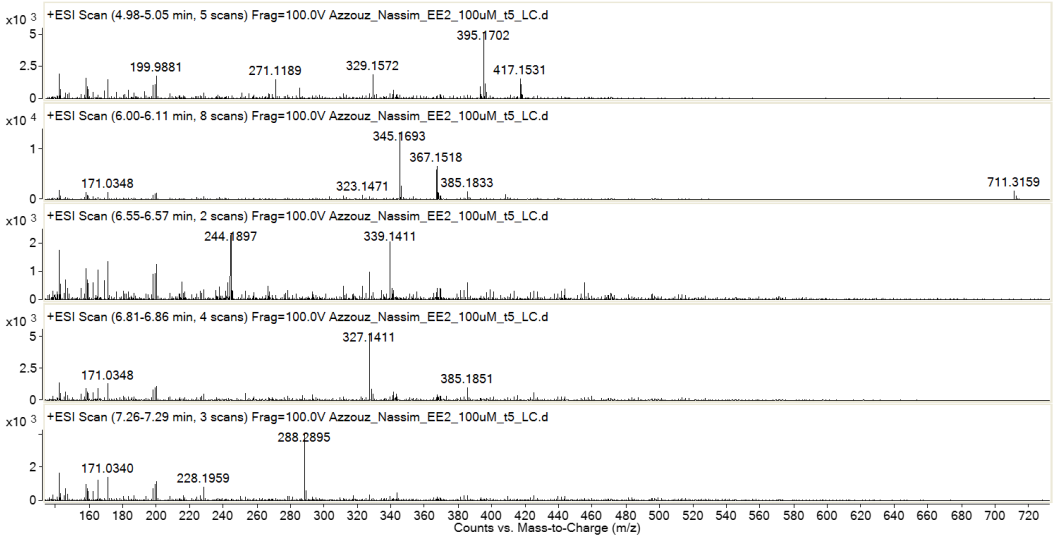

EE2 + 1 min O_3 + FeMt base peak chromatogram (*m/z* 150-450) with retention times labeled

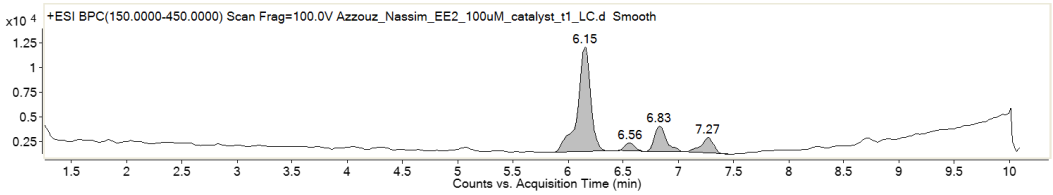

t1 + c mass spectra at 5.95, 6.15, 6.56, 6.83, 7.27 min

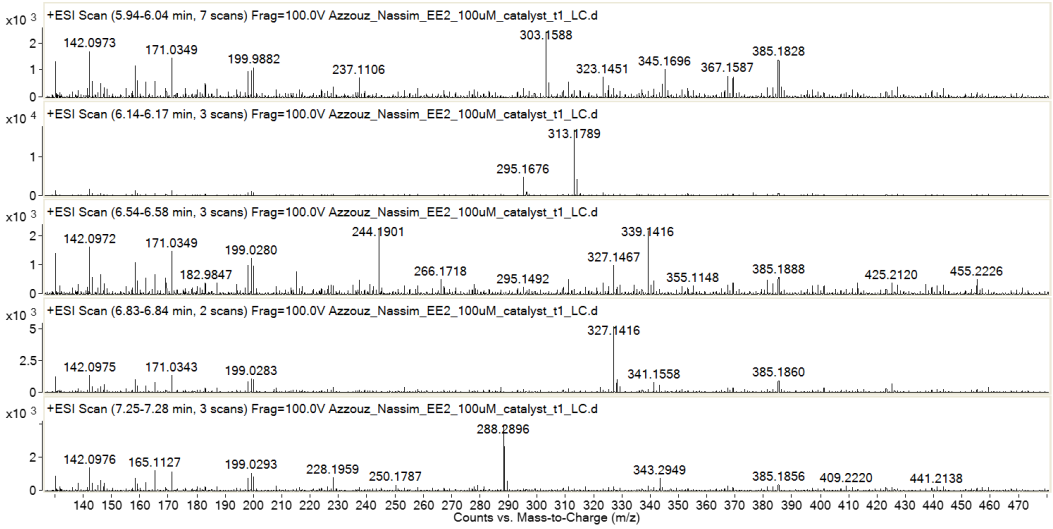

EE2 + 5 min O_3 + FeMt base peak chromatogram (*m/z* 150-450) with retention times labeled

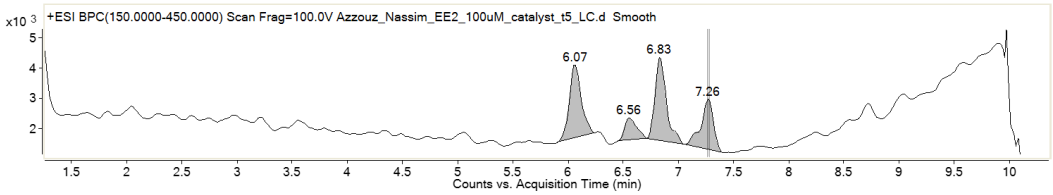

mass spectra at 6.06, 6.56, 6.83, 7.26 min

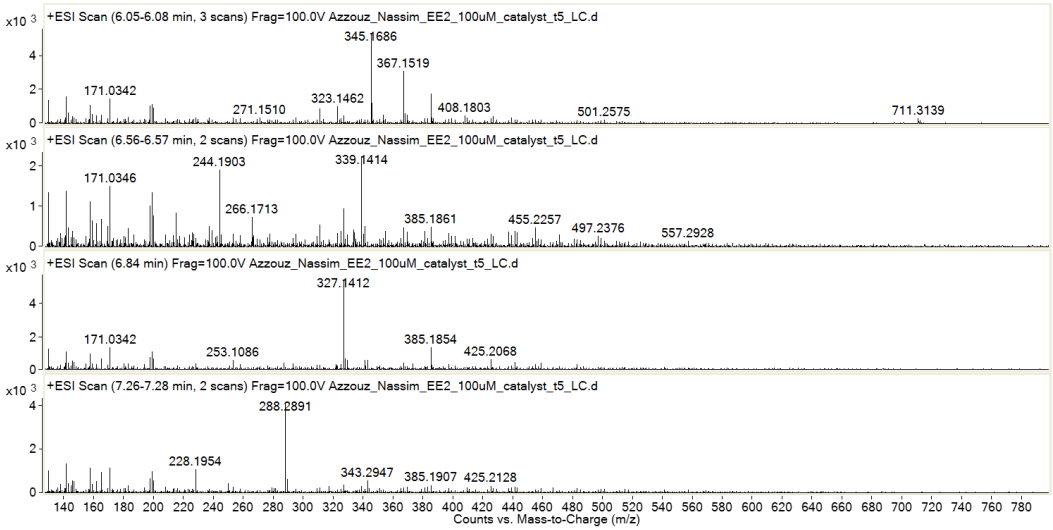

Comparison of mass spectra at 6.05 min

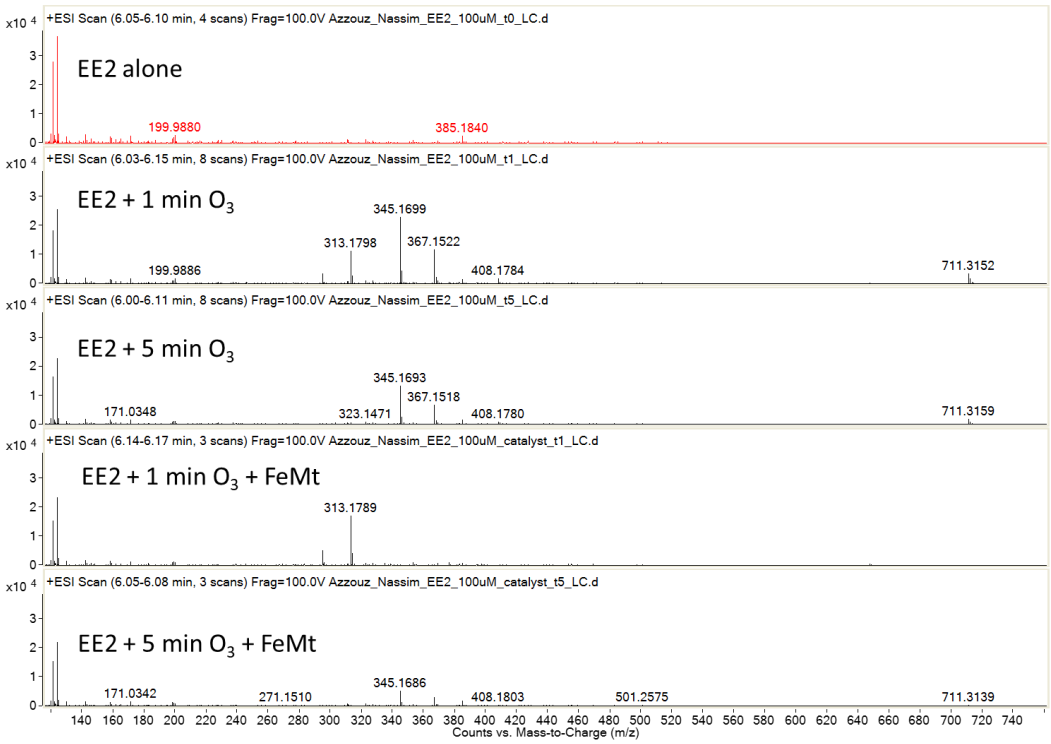

Comparison of mass spectra at 6.5 min

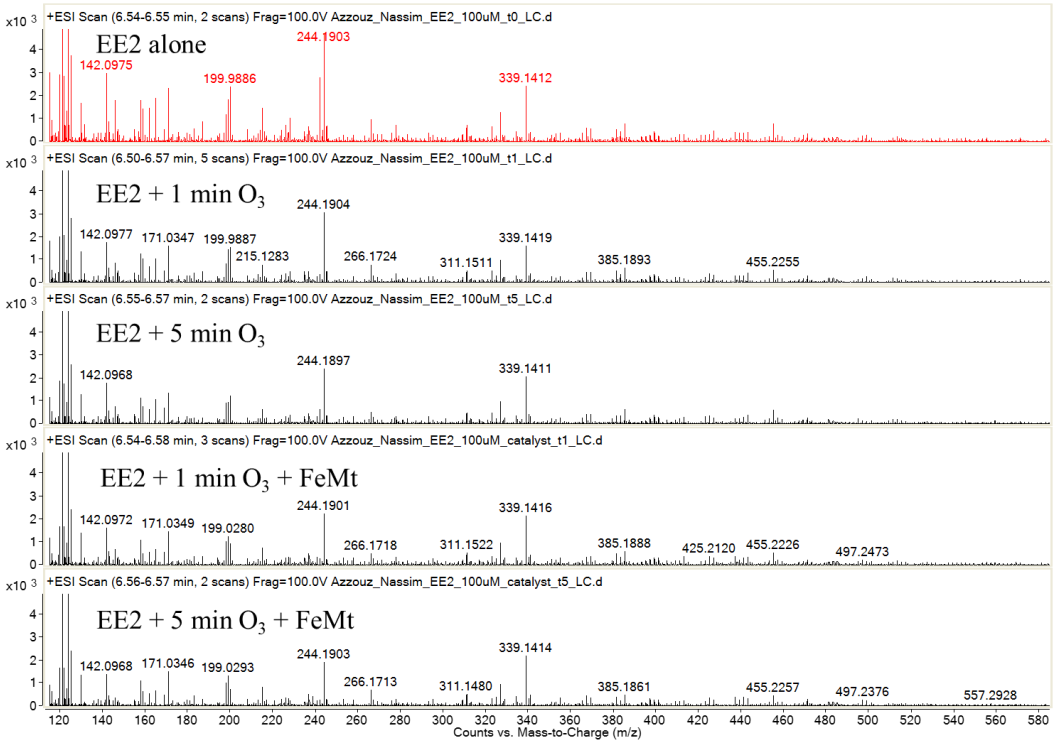

Comparison of mass spectra at 6.8 min

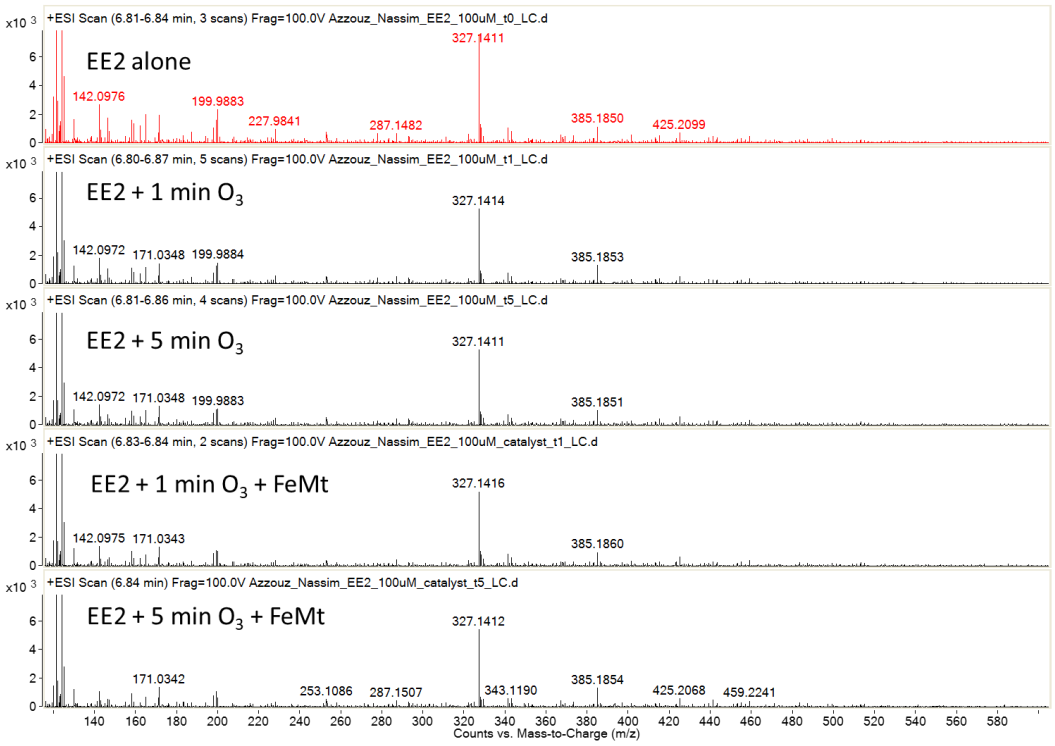

Comparison of mass spectra at 7.26 min

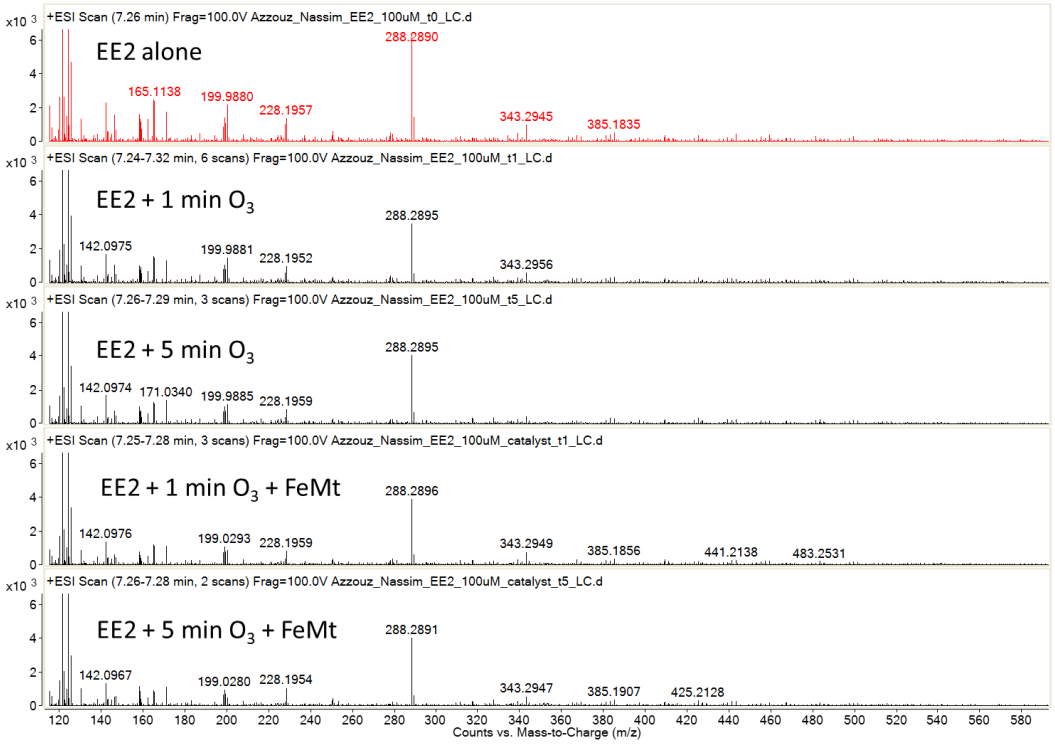

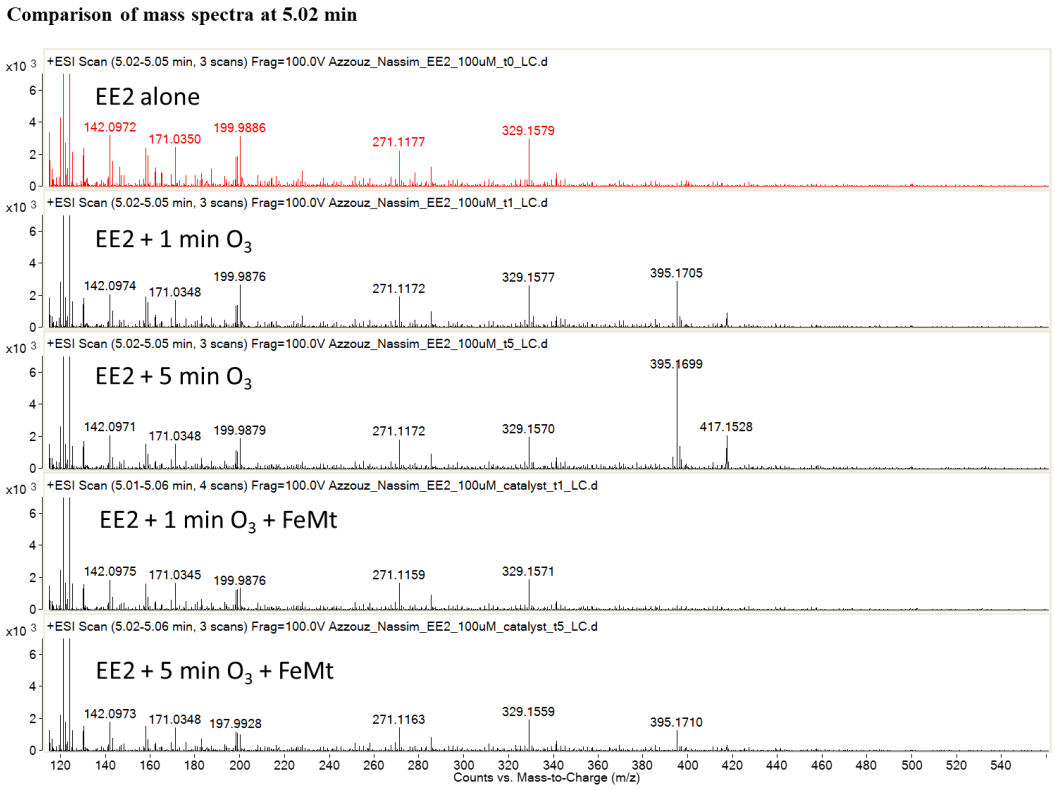

Fig. S3.4. LC-ToF-MS diagram of EE2 ozonation mixture after 1 and 5 min ozonation in the absence (a) and presence of Fe(II)Mt (b) in aqueous solution. Initial EE2 concentration = 10^{-5} M, Fe(II)Mt concentration: 2 g L^{-1}, Ozone dose: 600 mg h^{-1} at 22 °C.

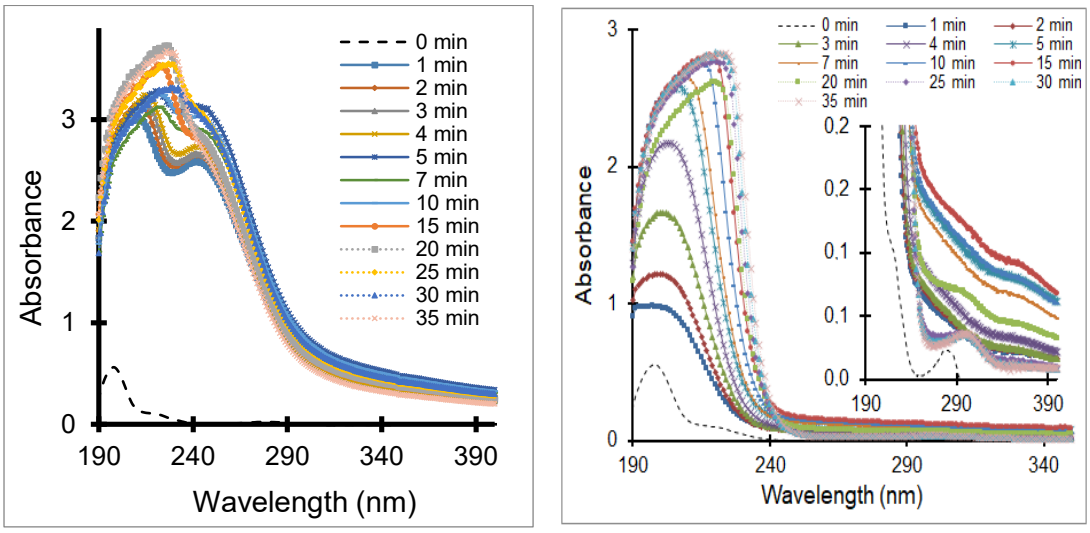

NaMt Fe(II)Mt

Fig. S3.5. UV-Vis spectra of EE2 after catalytic ozonation in aqueous solutions. T = 22 °C. pH = intrinsic. Quartz cell = 1 cm.O_3 throughput: 600 mg h^{-1}.Sample volume = 20 mL. Initial concentration: 10^{-5} M. Catalyst amount = 40 mg.

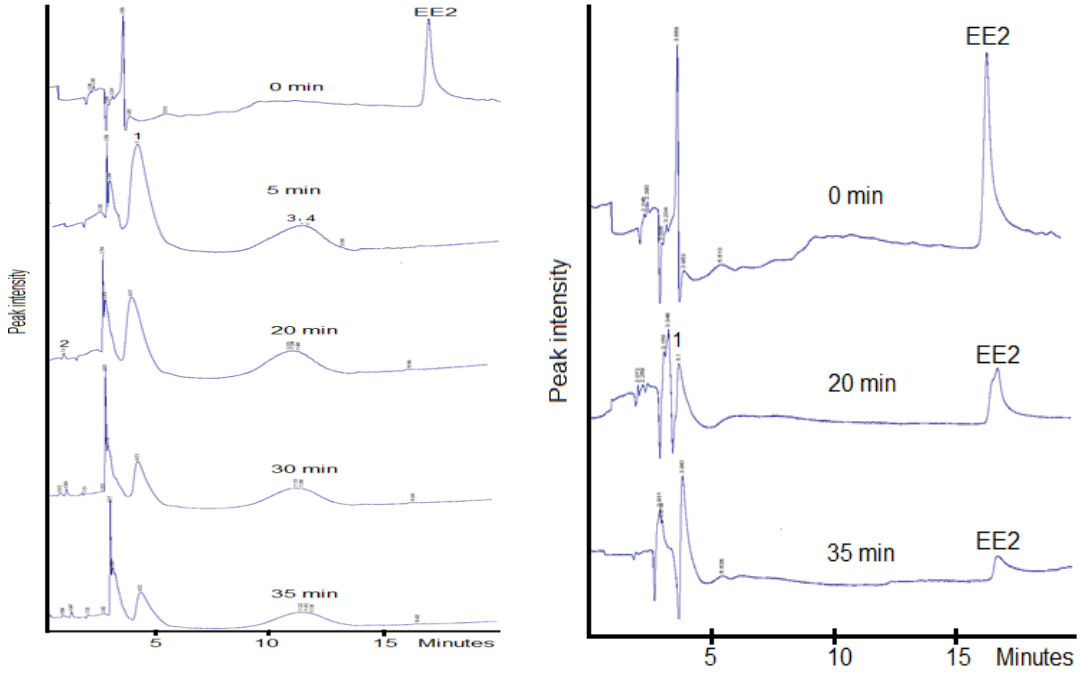

a **b**

Fig. S3.6. HPLC diagrams of the ozonation mixture in the presence of NaMt (a) and Fe(II)Mt (b) in distilled water as detected by UV detector at wavelength of 280 nm. T = 22 °C. pH = intrinsic. Concentration: 10^{-5} M.

Table S3.4. Retention time and area peak after 35 min of EE2 ozonation.

Catalyst	None		NaMt		Fe(II)Mt	
HPLC-UV peak	Retention time (min)	Peak area	Retention time (min)	Peak area	Retention time (min)	Peak area
EE2	16.69	1571	16.42	1062	16.15	7934
Intermediate 1	3.86	77373	11.74	45997	2.93	18196
Intermediate 2	3.51	25660	11.47	17592	3.02	9402
Intermediate 3	3.41	12689	11.22	102030	3.87	64836
Intermediate 4	3.32	16292	4.07	100272	5.54	2074
Intermediate 5	2.81	12043	2.83	86027	-	-
Intermediate 6	-	-	2.71	33-92	-	-
Intermediate 7	-	-	2.43	4737	-	-
Intermediate 8	-	-	1.73	1284	-	-
Intermediate 9	-	-	-.99	2856	-	-
Intermediate 10	-	-	-.6-	1129	-	-

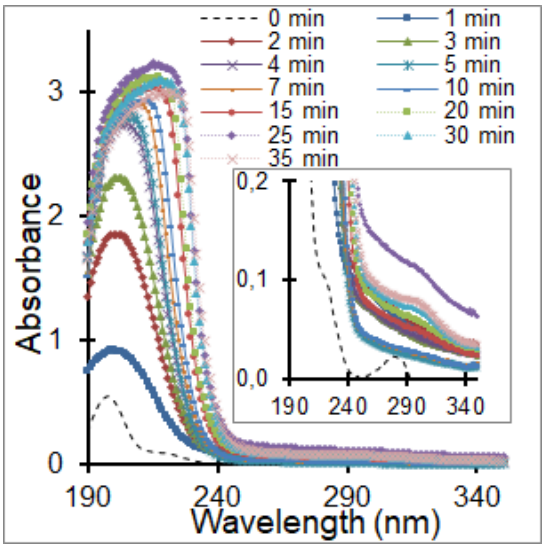

HMt-1

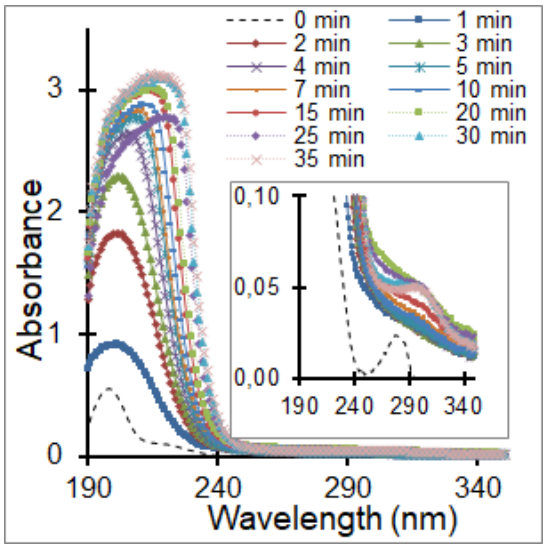

HMt-4

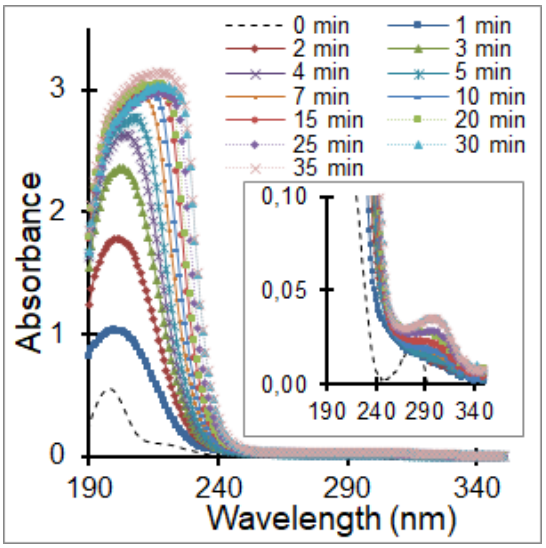

HMt-8

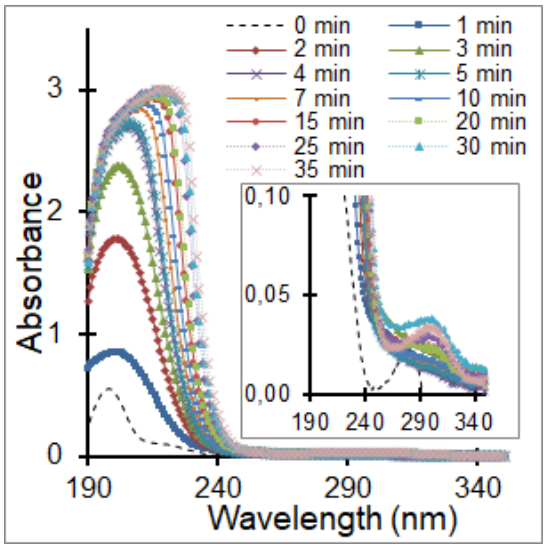

HMt-15

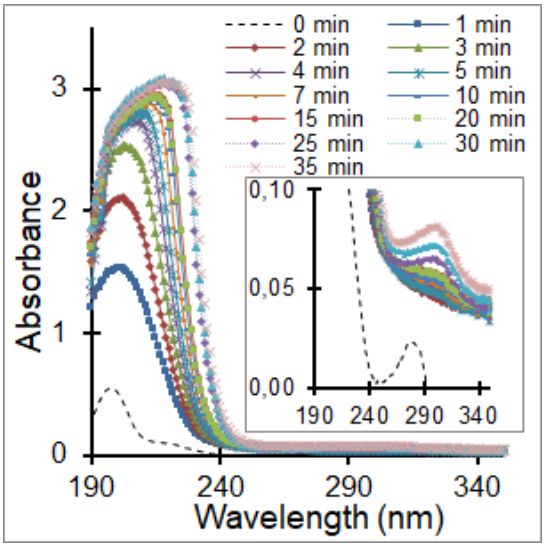

HMt-24

Fig. S3.7. UV-Vis spectra of the ozonation mixture in the presence of acid-activated bentonites in aqueous EE2 solution. T = 22 °C. Quartz cell = 1 cm.O_3 throughput: 600 mg h^{-1}.Sample volume = 20 mL. Initial concentration: 10^{-5} M. Catalyst amount = 40 mg and intrinsic initial pH.

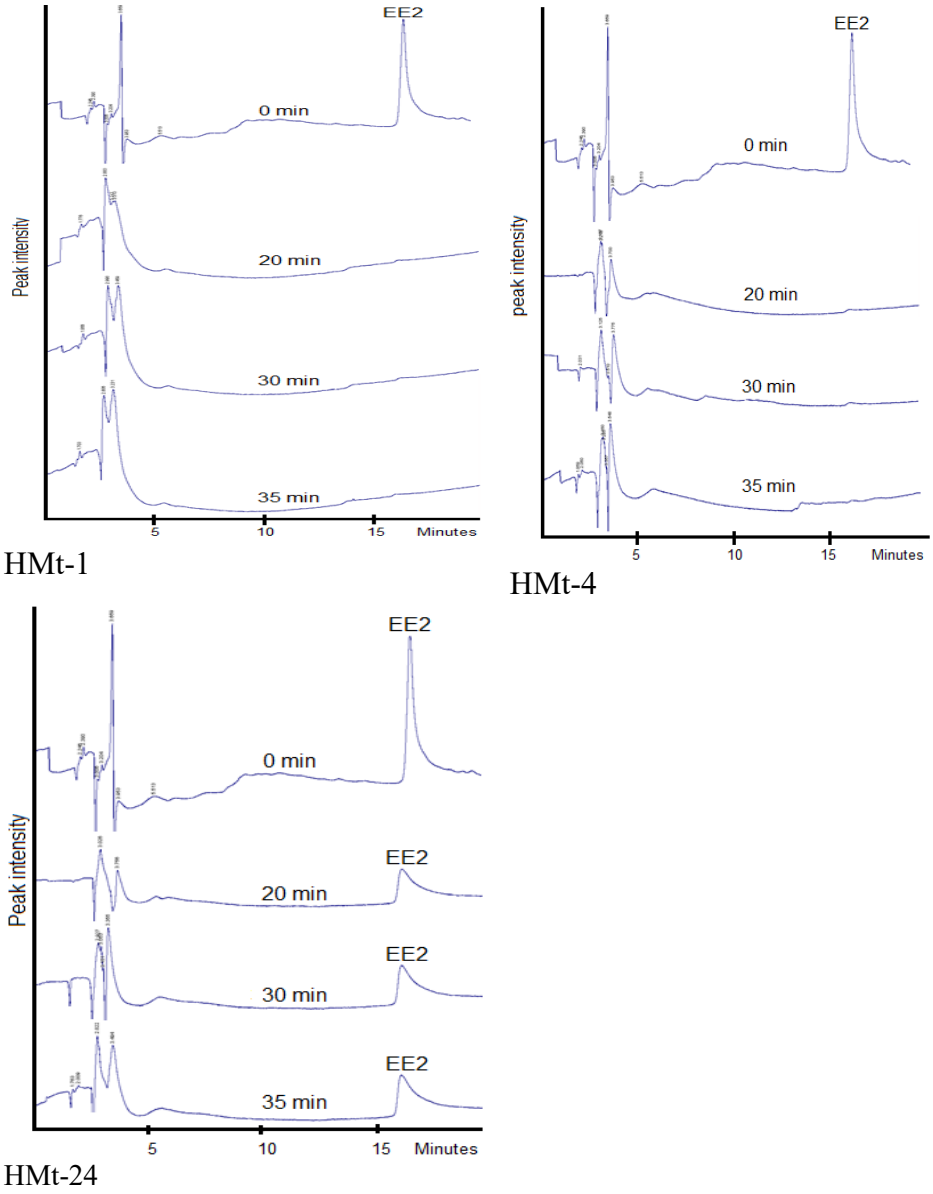

Fig. S3.8. HPLC-UV (280 nm) chromatograms of the initial solution of EE2 and of aliquots taken after different times of ozonation in the presence of HMt catalyst.

ANNEXE D: Article I publié dans Journal of Hazardous Materials 2019

Journal of Hazardous Materials 364 (2019) 356–366

Contents lists available at ScienceDirect

Journal of Hazardous Materials

journal homepage: www.elsevier.com/locate/jhazmat

Acid-treated clay catalysts for organic dye ozonation – Thorough mineralization through optimum catalyst basicity and hydrophilic character

Farida Boudissa[a], Diana Mirilà[b], Vasilica-Alisa Arus[b], Thizizi Terkmani[a], Sirène Semaan[a], Mélanie Proulx[a], Ileana-Denisa Nistor[b], René Roy[a], Abdelkrim Azzouz[a,*]

[a] Nanoqam, Department of Chemistry, University of Quebec at Montreal, QC, H3C 3P8, Canada
[b] Catalysis and Microporous Materials Laboratory, Vasile-Alecsandri University of Bacau, Romania

GRAPHICAL ABSTRACT

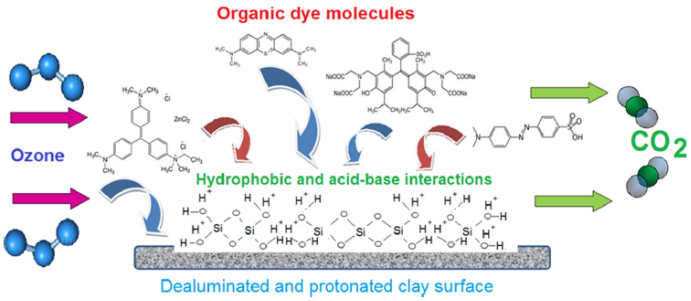

ARTICLE INFO

Keywords:
Dye removal
Ozonation
Acid-activated clays
Montmorillonite
Kinetics

ABSTRACT

Catalytic ozonation of Methylene Blue, Methyl Green, Methyl Orange and Methyl-thymol Blue was investigated in the presence of ion-exchanged montmorillonite (NaMt and Fe(II)Mt), crude bentonite and acid-activated counterparts. An original approach never tackled so far consisted in correlating the basicity and hydrophilic character to the dye-catalyst interactions occurring on the catalyst surface. This was achieved through CO_2 and water thermal programmed desorption. Kinetics study revealed that ozonation starts in the bulk solution, and dye adsorption turns out to be an essential requirement for high catalytic effectiveness. On NaMt, dye molecules appear to adsorb mainly via hydrophobic interaction. On Fe(II)Mt, the contributions of hydrophobic interaction, cation-exchange and Fe^{2+} mobility to the catalytic activity prevail. Acid activated clay catalysts exhibited lowest hydrophilic character favoring adsorption through organophilic interaction and affording thorough and fast dye mineralization. This was explained in terms of increased number of silanols and –Si-O-Si- groups. For all catalysts, short ozonation of all dye molecules resulted in similar end-chain products, which were totally eliminated after prolonged reaction times. This result is of great importance because it provides valuable theoretical findings that allow envisaging total mineralization of organic molecules by recyclable metal-free clay catalysts.

* Corresponding author.
E-mail address: azzouz.a@uqam.ca (A. Azzouz).

https://doi.org/10.1016/j.jhazmat.2018.09.070
Received 28 February 2018; Received in revised form 25 September 2018; Accepted 26 September 2018
Available online 06 October 2018
0304-3894/

1. Introduction

Textile manufacturing is undoubtedly the major source of dye-rich wastewaters [1,2], which can generate a wide variety of harmful oxidized derivatives once released in nature [3–6] with negative impacts on aquatic media and biodiversity [7] even at low concentration. Primary water treatments are well recognized to be quite unsatisfactory [8,9], and should be completed by effective techniques such as Advanced Oxidation Processes (AOPs) that lead to total mineralization of organic pollutants [10–17]. Among AOPs, ozonation is an energy-consuming method but undoubtedly the most eco-friendly and convenient route, requiring low investment and operating cost with small devices that can be implemented where needed. Unlike other oxidative treatments such as Fenton process, photooxidation, ozonation and their combined variants [10,11,18–23], catalytic ozonation can rapidly decompose a wide variety of dyes in aqueous solutions into harmless oxides [24–26] and refractory short chain acids [15,27–30].

However, total mineralization of organic substrates often requires higher ozone consumption than necessary due to the low solubility in water. Catalytic ozonation may allow overcoming this drawback, and solid catalysts appear as being much more interesting because dissolved catalysts are potential sources of water contamination [31,32]. In addition, solid catalysts should enhance reactant adsorption and/or concentration in the vicinity of the surface [33,34]. Those displaying high porosity and specific surface area should show high efficiency in this regard [35]. Catalysts may convert ozone into highly reactive radical species [36], reducing the ozonation time [37]. In some cases, they also improve the mineralization process [38].

Many types of catalysts [11] such as activated carbon [39–41], zeolites and clay minerals [15,42] and even pure silica [24,43] have been tested in the oxidation of organic pollutants in most wastewaters. The latter usually become acidic once oxidized by free air, and the resulting acidity fluctuations may influence their interactions with the catalyst, more particularly aluminosilicates (AS). In optimal pH and catalyst amount, AS showed improved catalytic activity in the total mineralization of fairly refractory organic compounds such as oxalic acid [11,15,18], due to enhanced clay exfoliation, cations release and reactant concentration in the vicinity of the solid surface.

Montmorillonite (Mt) is a low cost and widely available aluminosilicate that can acquire optimal acid-base and hydrophobic interactions with organic species in water through mere and convenient purification and modification. These properties strongly influence the adsorption-desorption equilibrium of ozonation intermediates and products, whose presence usually induces pH fluctuations that determines the charge and dispersion of Mt lamellae. Less oxidized and bulkier intermediates must behave differently as compared to short chain acids with respect to the clay surface. Deeper insights in the catalyst basicity and hydrophilic character can allow elucidating the catalyst interactions with the organic substrate, water and ozone in correlation with the structures of both the catalyst and dye molecule. This is the main objective of this work that was achieved through thermal programmed desorption (TPD) of carbon dioxide (CO_2) and water, which also provided the strength distribution of the adsorption sites. Comparative ozonation tests of different organic dyes were performed in the presence of ion-exchanged (NaMt and Fe(II)Mt), crude bentonite and acid-activated counterparts (HMt). The investigated interactions are herein discussed in terms of electrostatic and hydrophobic interaction and contribution of the adsorption step to the process kinetics. To the best of our knowledge, such an approach has never been tackled so far.

2. Experimental

2.1. Materials and methods

Two cationic dyes (Methylene Blue, MB and Methyl Green, MG) and two anionic counterparts (Methyl Orange, MO and Methylthymol Blue, MTB) provided by MERCK (USA) were used as probe molecules (Table S1). The clay catalysts were prepared starting from a crude bentonite (1.24 µm particle size) supplied by Sigma-Aldrich (USA). For simulating dye-rich wastewaters after primary treatments, aqueous 10^{-4} M dye solutions were prepared by dissolving accurately weighted amount of dyestuff in deionized and nanopure water.

2.2. Catalyst preparation

Dye ozonation was investigated in the presence of ion-exchanged montmorillonite (NaMt and Fe(II)Mt), crude bentonite and acid-activated counterparts (HMt). The starting bentonite was previously purified into a fully ion-exchanged Na^+-montmorillonite-rich material (NaMt) through repeated impregnation with 2–5 M aqueous NaCl solutions at 80 °C for 4–5 h under vigorous stirring and periodical ash removal after settling [15]. Fe(II)Mt was obtained through NaMt impregnation with aqueous Fe^{2+} solution ($FeCL_2.4H_2O$). The choice of these two catalysts was based on previous works [15,18,44]. NaMt and Fe(II)Mt were further washed with distilled water and then repeatedly dialyzed in cellophane bags immersed in fresh distilled water until no chloride was detected by $AgNO_3$ test in the dialysate. Both catalysts were recovered by centrifugation and then air-dried at 40 °C overnight.

For deeper insights in the effect of silicon content, additional catalysts (HMt-1, HMt-4, HMt-8, HMt-15 and HMt-24) were prepared through acid activation of bentonite. For this purpose, 200 g clay samples were impregnated by 1000 mL of aqueous 5 M sulphuric acid solution at 80 °C for various contact times (1, 4, 8, 15 and 24 h, respectively) under mild stirring as fully described elsewhere [45–47]. The powders were recovered by filtration, repeatedly washed with distilled water until neutral pH and dried at 100 °C for 12 h. The as-activated bentonite samples were softly ground and sieved into a 75 µm particle size (200 mesh ASTM).

2.3. Catalyst characterization

All catalysts including crude bentonite were characterized by X-ray diffraction (Siemens D5000, CuKα, $\lambda = 1.54051$ Å), while their chemical compositions were assessed through X-ray fluorescence (S-4 Pioneer equipment; Brüker Rh tube; Powder press 34 mm with 10% boric acid; standardless method with 0.5% error) as already reported [47]. The marked sharpening of the broad 001 XRD reflection after bentonite purification and full ion-exchange into NaMt and Fe(II)Mt accounts for a perfectly parallel arrangement of the clay lamellae. No crystallinity loss was noticed for bentonite samples acid-treated for 1–15 hours, and only slight depletion of the XRD line was observed for the sample treated for 24 h. The particle size was determined using a Malvern-Zetasizer Nanoseries in water and in aqueous dye solutions, while the Zeta potential was assessed with a Brookhaven instrument. The surface basicity and hydrophilic character were evaluated through Thermal Programmed Desorption measurements of carbon dioxide (CO_2-TPD) and moisture (H_2O-TPD) under a 15 mL min^{-1} nitrogen stream with a 5 °C min^{-1} heating rate from 22 to 450 °C. Thus, non dehydrated catalysts (45–50 mg) with 0.1–0.2 mm particle size were introduced in the glass tubular oven (2 mm internal diameter) coupled to a Li-840 A dual CO_2/H_2O Gas Analyzer (Li − COR Bioscience Inc., USA) and further contacted with dry and pure N60 grade CO_2 till saturation for 20–30 minutes. The excess CO_2 was purged at room temperature under dry N_2 flow prior to TPD runs. H_2O-TPD measurements were achieved through the same procedure. The basicity and hydrophilic character were estimated from the area described by the TPD pattern and expressed in terms of CO_2 and water retention capacities (CRC and WRC, respectively) [48–51].

2.4. Ozonation tests

Ozonation tests were performed in different samples exposed to various ozonation times at room temperature (RT) in cylindrical PVC vessels (28 × 115 mm) containing 20 mL samples of 10^{-4} M aqueous solutions of organic substrates at intrinsic initial pH. The dye solutions were previously prepared using deionized and nanopure water. Ozone was produced from air using a portable A_2Z-AQUA-6 ozone generator (A_2Z Ozone Inc., USA), and bubbled in each 20 mL sample at a constant 600 mg h^{-1} throughput. After 10 s of bubbling the ozone concentration reaches a constant concentration of ca. 0.40-0.45 mol L^{-1}, as assessed by conventional iodometry using aqueous solutions of KI (O.2 M) HCl (2 M) and $Na_2S_2O_3$ (0.05 M). For the kinetical study additional ozonation attempts were run for reaction times below 1 min.

2.5. Ozonation products analysis

After ozonation and catalyst removal by centrifugation, the supernatant each ozonated sample was analyzed by UV–vis spectrophotometry using a 1 cm quartz cell and a Varian-Cary 5000 instrument (Agilent Technologies, USA). Highly linear calibration plots (Fig. S1-S2) and accurate assessment of the molar absorptivity (Table S2) were achieved between 190 nm and 800 nm only within the 0-10^{-5}M dye concentration range. This range turned out to be suitable for detecting slight fluctuations of all UV–vis bands during ozonation and for accurate estimation of the dye removal yield (Equation S1).

The evolution in time of the ozonation process for all UV–vis bands was assessed through determination of the residual concentration using calibration curves with 1–2% accuracy (Fig. S1-S2). The dye conversion yield was calculated using the UV–vis bands appearing at the highest wavelength, with a standard deviation of 2%. For the sake of accuracy, the reaction mixture was also analyzed by liquid chromatography (HPLC, Waters 2487 Dual λ absorbance detector coupled to a Waters-Alliance 2695 equipment, 100 mm x 4.6 mm C_{18} column with a 3.5 µm particle size and a 0.5 mL min^{-1} throughput of a 95:5 water-acetonitrile mobile phase, UV–vis detector) and its time of Flight - mass spectrometry variant (HPLC-ToF-MS, Agilent 1200 Series HPLC instrument, Agilent Eclipse plus C18 column (3 × 50 mm, particle size1.8 µm) at RT. The dye conversion yield was mainly estimated by HPLC using calibration curves. Full details are providing as supporting information. After optimized ozonation, only carbonic acid was detected, but traces of formic, acetic and oxalic acids were also identified in other conditions.

3. Results and discussion

3.1. Effect of initial dye concentration on non-catalytic ozonation

Quick tests of 5 min ozonation of the studied dyes induced marked changes of the UV–vis spectra, characterized by a total discoloration of the respective aqueous solutions of MB, MTB and MO (Fig. 1). MB displayed initially seven absorption bands, which significantly depleted after five min ozonation, except the 234 nm band (Fig. 1a). The total disappearance of the 660 nm band and its splitting derivative at 614 nm as a result of partial dimerization in water indicates a complete degradation of the phenyl ring and C–S^+ = C bond [52–56]. This is confirmed by the marked decay in intensity of the 498 and 403 nm bands attributed to the resonance of this conjugated system [57]. Traces of MG still persist under similar ozonation conditions. Color persistence indicates incomplete phenyl ring cleavage after 5 min ozonation (Fig. 1b).

Similarly, marked depletion of the 465, 277 and 200 nm bands for MO (Fig. 1c) and the 612, 444, 293 and 204 nm bands for MTB (Fig. 1d) were noticed. For MO, an attenuation of the π-π* transition (277 nm) due to the –N = N– azo group located on the aromatic rings under the strong influence of the electron-donating dimethylamino group is expected [58,59]. Among the five UV–vis bands of MG, those persisting at 253 and 320 nm and attributed to π–π* transitions of the aromatic rings and n-π* transitions, respectively [60] indicate a slightly higher chemical stability as compared to the other counterparts.

As a general tendency, all band absorbances decreased with decreasing dye concentration, i.e. when ozone is bubbled in excess with respect to the dye amount. Increasing dye concentration resulted in lower ozonation efficiency, as supported by the increase in intensity of the residual UV–vis bands remaining after discoloration (Fig. 2).

This intensity increase appears to be much more pronounced for the 210–212 nm UV bands (2, 4, 6 and 8), most probably due to the formation of oxidized derivatives and H-bridge interaction with water. The other bands (1, 5 and 7) totally disappeared after 5 min for dye concentration below 2 × 10^{-4} M. Thus, ozonation is suitable for diluted solutions [61], as justified by the choice of the concentration range.

3.2. Evolution in time of non-catalytic ozonation

Deeper insight in the effect of the ozonation time revealed marked intensity depletion for most bands (Fig. S3). Paradoxically, the intensity of those appearing at 214–220 nm increased in time (Fig. 3), due to the formation of oxidized species, possibly including short chain acids.

The total disappearance of the 498 and 403 nm bands of MB after only 1 min ozonation was accompanied by a total discoloration of the solution after 2 min. This is supported by the marked depletion of the 660 nm, which indicates a fast degradation of the chromophore [24]. A progressive disappearance in time of the 332 nm band and the rise of a band at 217 nm were also observed, suggesting the formation of oxidized derivatives as confirmed further by HPLC-ToF-MS analysis. This is a common behavior of MO and MG, which slight differs for MTB. Here, the molecular structure of the dye should play a key role [62,63], since unlike for MG, the 465 nm band of MO totally disappeared after 2 min ozonation due to a direct and fast ozone attack on the azo group (–N=N–) [64]. It is worth mentioning that after 5 min ozonation MTB displayed the lowest relative absorbances and presumably highest reactivity to ozone. This must be due to its high molecular weight, given that the chemical stability against ozone decreases with increasing molecular size [11,24,65].

Analysis of the effect of the ozone-to-dye ratio revealed that ca. 10000–60000 ozone molecules per dye molecule are needed for the total disappearance of the visible bands in the absence of catalyst. This accounts for large amounts of unused ozone, whose solubility in water is the main constraint. For comparable ozone dosages, non catalytic ozonation gave higher conversions yields as those reported for more oxidized chemical species, but in the same magnitude as other organic molecules [10,11,15,18,24–65].

3.3. Effect of clay catalyst addition

Catalyst addition resulted in more pronounced changes in time of the relative absorbances of most UV–vis bands below 350 nm, due to the formation of oxidized derivatives [24,43,65]. Simultaneously, fast discoloration of the dye solution was noticed, as supported by the total disappearance of the visible bands of MB beyond 400 nm in less than 5–10 min ozonation (Fig. 4).

Addition of NaMt produced noticeable changes in the UV–vis spectra of all dye molecules (Fig. S5). This agrees with the specific ozone consumption by each structural group of a given dye molecule (Fig. S6-S7). The effect of catalyst addition appears to differ depending on the UV–vis band and exchangeable cation (Fig. S11-S13).

Fe(II)Mt showed higher activity in the discoloration of cationic molecules (MB and MG), as supported by a faster decay of the 660 nm band as compared to NaMt. Deeper insights in process kinetics and catalyst surface properties could be useful in this regard.

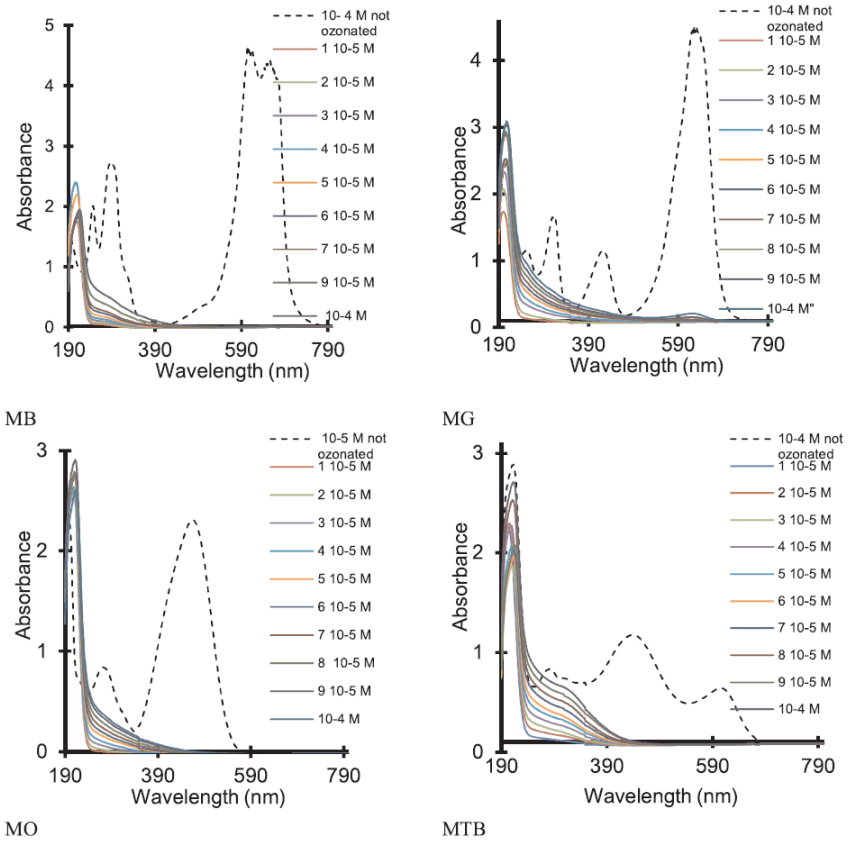

Fig. 1. Effect of the concentration on the UV–vis spectra of MB, MG, MO and MTB after 5 min ozonation in distilled water. T = 22 °C. pH = intrinsic value. Quartz cell = 1 cm. O_3 throughput: 600 mg h^{-1}. Sample volume = 20 mL. Initial dye concentration: 10^{-4} M.

3.4. Ozonation kinetics

Model validation for all UV–vis bands based on R^2 values close to unity (0.9965-0.9995) (Tables S3-S5) showed that ozonation fits better 1st order kinetics during the three first minutes of ozonation without and with catalyst, when a first and fast step triggers in the aqueous dye solution with a constant ozone concentration due its low solubility, generating most intermediates [15,24,65].

$$Ln\left(\frac{C_0}{C_t}\right) = k_1 . t \quad (1)$$

High linearity of Eq. (1), where C_0 is the initial concentration value of the dye, C_t - the instant concentration and k_1 - the first order rate constant, and t is the time was obtained for most UV–vis bands (Fig. 5). For almost all dye UV–vis bands, the 1st order model was validated when excluding the first 10–100 seconds of ozonation, presumably due to the slow ozone dissolution. This variable delay from an UV–vis band to another for a given dye molecule must be due to different reactivity of the structural groups, as supported by different rate constants. The fact that few R^2 values close to unity were also registered when applying both models for some UV–vis bands suggests a mixture of 1st and 2nd order kinetics, presumably due to interactions between dye molecules and oxidized derivatives.

Catalyst addition should induce fluctuations in the ozone concentration in the bulk solution through adsorption. The predominance of the 2nd order kinetics for almost all UV–vis band and higher rate constants for catalytic ozonation provide evidence of this contributions of the catalyst surface and exchangeable cation.

3.5. Effect of exchangeable cation on dye adsorption

Crude bentonite gave lower dye conversion yield not exceeding 25–35%. This lower catalytic activity was already by the presence of carbonates and higher amounts of non smectitic impurities (Quartz, cristoballite, carbonates,…). This is supposed to reduce the density of exchangeable cations and of surface charge [15,18,65]. The role of the exchangeable cation was reflected by higher dye degradation yield for Fe(II)Mt, than for NaMt, more particularly for cationic MG and MG molecules (Table S6). After 2 min ozonation, degradation yields of 60–92% as estimated by (1-C/C_0) values for decreasing UV–vis bands beyond 400 nm were registered in the presence of NaMt versus 78–99% for Fe(II)Mt (Table 1). More precise but almost similar values were

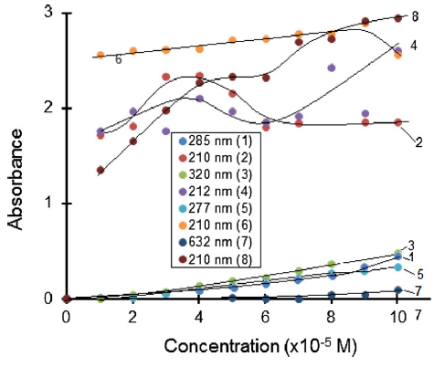

Fig. 2. Evolution of the absorbance of the residual UV–vis bands after 5 min ozonation of MB (1–2), MTB (3–4), MO (5–6) and MG (7–8) in distilled water. T = 22 °C. pH = intrinsic value. Quartz cell = 1 cm. O_3 throughput: 600 mg h^{-1}. Sample volume = 20 mL. Initial dye concentration: 10^{-4} M.

obtained by HPLC with only slight discrepancy not exceeding 3–5% as compared to UV–vis measurements.

Longer ozonation times of 20 min were required for achieving degradation yields of 69–100% for cationic dye and to 84–98 % for anionic molecules with NaMt. These performances are much higher than those reported for many catalysts such as simple or metal-doped metal oxides, carbon nanotubes, zeolites and others for ozone dosages in the same magnitude order [11].

The higher effectiveness of Fe(II)Mt was already explained in terms of partial Fe^{2+} cations release in the vicinity of the catalyst in acidic media [10,11,15,65]. However, dye adsorption on Fe(II)Mt should also contribute to the catalytic process, as reflected by the almost total disappearance of the 660 nm band of MB after ca. 50 min (Fig. S14-a, S15-a). In the absence of ozone, mere dye adsorption produces similar depletion in time for all UV–vis bands, but in the presence of ozone, increase in time of UV-bands below 400 nm is a precise index of the simultaneous occurrence of the catalytic oxidation reaction and appearance of oxidized derivatives, as supported by HPLC-ToF-MS analyses.

Unlike with NaMt, much more pronounced Fe^{2+} release was observed with anionic dyes, which seem to act as "iron pump", as supported darker green-blue coloration of MTB solution and the significant increase in the relative intensity of the 612 nm band (Fig. S14-b, S15-b). This was found to reduce MTB degradation yield from 92% (612 nm) and 84% (446 nm) down to 49% (Table 1). However, excessive Fe^{2+} loss is expected to reduce the surface positive charge, thereby affecting adsorption of anionic dyes. Indeed, weaker adsorption was noticed for MTB as compared to MB in the absence of ozone. This was reflected by the fact that the 446 nm band of MTB did not disappear even after 50 min, compared to the total adsorption of MB illustrated by the total

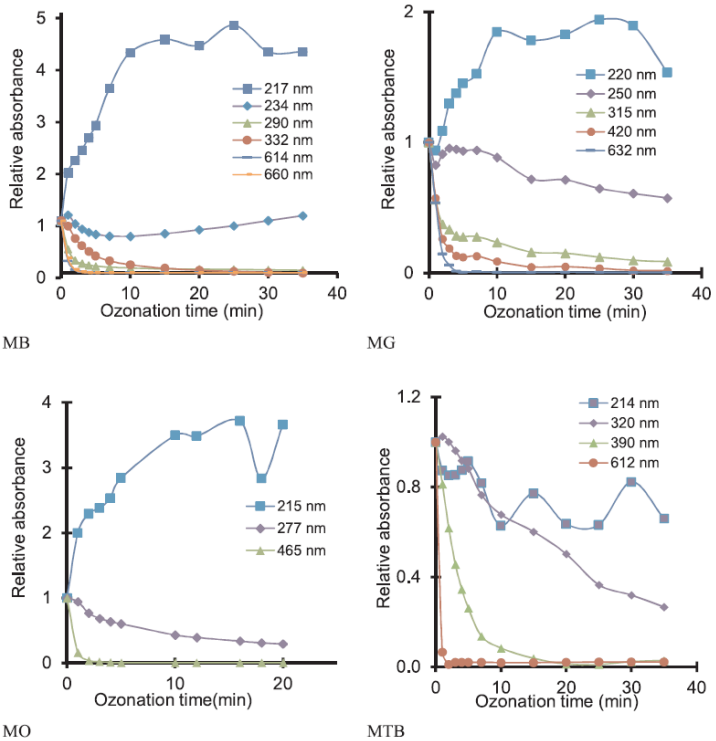

Fig. 3. Evolution in time of the relative absorbance of cationic (MB, MG) and anionic (MTB, MO) dyes during ozonation in distilled water. T = 22 °C. pH = intrinsic value. Quartz cell = 1 cm. O_3 throughput: 600 mg h^{-1}. Sample volume = 20 mL. Initial dye concentration: 10^{-4} M.

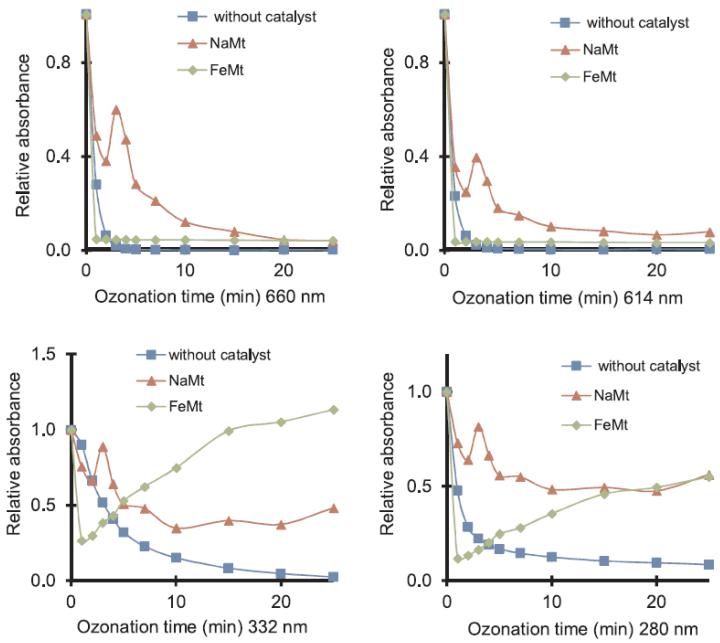

Fig. 4. Evolution in time of the relative absorbance of MB during ozonation in distilled water. T = 22 °C. pH = intrinsic value. Quartz cell = 1 cm. O_3 throughput: 600 mg h^{-1}. Sample volume = 20 mL. Initial dye concentration: 10^{-4} M. Catalyst amount = 40 mg of dry catalyst.

disappearance of the 660 nm band after only 25 min. Thus, it clearly appears that dye adsorption is an essential requirement for high catalytic effectiveness, and that electrostatic interaction prevails for certain dyes on certain catalysts. Here, ozonation should occur on the surface or nearby, where ozone concentration must also be influenced by adsorption phenomena, in agreement with the 2nd order kinetics.

The bathochromic effect of the 660, 280 and 234 nm red shifted to 670, 296 and 250 nm can arise from diverse interactions between the non-binding electron pairs of dye N and S atoms, oxidized species and free water molecules. The magnitude of this effect is expected to strongly depend on the acid-base properties and hydrophilic character of the clay surface. Interesting, fast and almost thorough decomposition of MTB and MO was noticed after only 2 min with both NaMt and Fe(II) Mt. This result clearly demonstrates that the exchangeable cation plays a key role in the ozonation of cationic dye, and showed no influence in that of anionic molecules. Here, Fe^{2+} cation is expected to induce change in the initial pH of the reaction mixture, which, in turn, should involve electrostatic interactions in adsorption.

3.6. Role of silanols on dye adsorption

NaMt addition was found to raise the initial pH of MB, MG, MTB and MO solutions from 5.47, 5.12, 7.61 and 5.40, respectively to 6.77, 6.73, 7.96 and 7.76. This is supposed to confer neutral charges to cationic dyes (MB and MG) but negative charges to anionic ones (Table 2).

This should induce changes in water:dye interaction, as reflected by a bathochromic shift of the visible band beyond 600 nm of these molecules, explained in terms of molecule conformation [67]. For planar conformation, the π→π* transitions of aromatic molecules produce red shift. Larger bathochromic shifts were ascribed to H-bridges with proton donors.

On one hand, by analogy with pure silica, deprotonation should prevail on NaMt at pH level higher than 2 [68], conferring negative to NaMt in the presence of all dye molecules. This agrees with the negative Zeta potential of NaMt and its increase after dye addition from -42.19 mV (Table 3) up to -52.59 mV (for MB), -50.2 mV (for MO) and -54.44 mV (on MTB) (Table S7). On the other hand, all pH values (6.73–7.96) were comprised between the pKa values of out-of-plane (pKa = 5.6) and in-plane silanols (pKa = 8.5) of pure silica, which are assumed to also occur in aluminosilicates [66]. Under these conditions, silanol protonation, if any, should be very weak, and all silanols of NaMt are supposed to mostly exhibit slightly positive to neutral charge, except with MB (Table 3). This is supposed to slightly favor adsorption of anionic dyes (MTB and MO) which bear negative charges. Unlike anionic dyes, cationic dyes (MB and MG) should bear no charges, and should not adsorb via electrostatic interactions. No electrostatic adsorption is expected to occur on out-of-plane silanols which have predominantly neutral charges. The slight contribution of electrostatic adsorption of anionic dyes to the catalytic process was reflected by relatively higher UV–vis band removal yields (56–92%) as compared to their cationic counterparts (60–77 %) after 2 min ozonation (Table 1). This tendency was somehow maintained even after 20 min.

With Fe(II)Mt, the initial pH decrease confers positive charges to all silanols groups and ammonium groups of most dye molecules but neutral charges on MG (Table 2). This is expected to impede electrostatic adsorption. The decrease in Zeta potential from 16.20 mV (Table 3) down to + 13.00 mV (for MB), 3.90 mV (for MG), 7.32 mV (for MO) and 3.36 mV (on MTB) (Table S7) suggests a depletion of positively charged species on Fe(II)Mt, presumably due to Fe^{2+} cation release in the solution. This is consistent with the higher catalytic activity of Fe(II)Mt, inasmuch as Fe^{2+} mobility in the vicinity of the

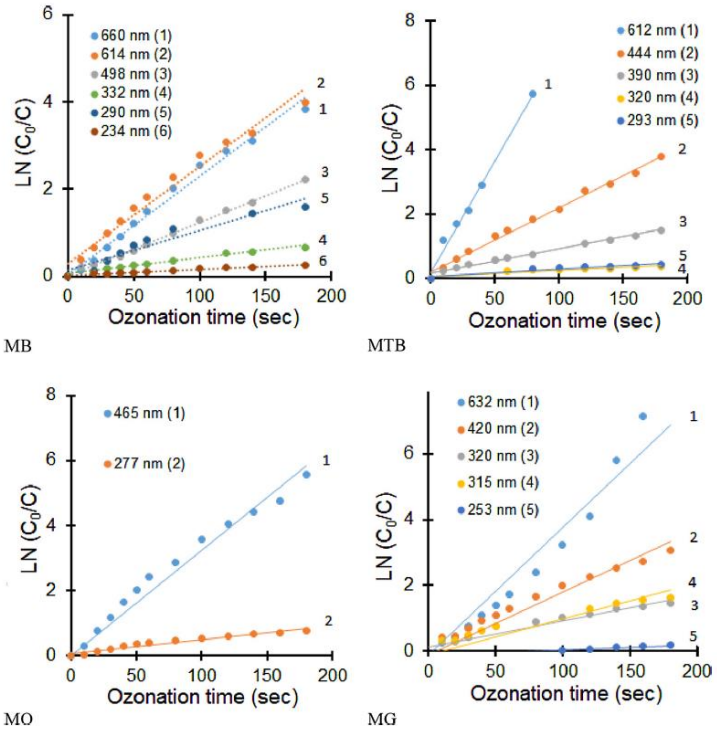

Fig. 5. First-order plot for non-catalytic dye ozonation kinetics.

Table 1
UV–vis band removal yield (%) after catalytic ozonation.

Dye molecule	UV-Vis bands (nm)	UV-Vis band removal yield (%)[a]			
		After 02 min ozonation with		After 20 min ozonation with	
		NaMt	Fe(II)Mt	NaMt	Fe(II)Mt
MB	660	62	96	96	96
	614	77	97	100	97
	498	70	78	100	84
MG	632	77	96	91	97
	420	60	99	69	100
MO	465	92	96	98	98
MTB	612	73	–	92	49
	446	56	89	84	49

[a] Decreasing C/C_0 for UV–vis bands beyond 400 nm accounts for the actual decomposition yield of a dye molecule. The dye conversion yield was calculated with a standard deviation of 2%. HPLC measurements gave almost similar values of the conversion with 3–5 % discrepancy with respect to the spectrophotometric measurements.

catalyst surface was already observed even at pH 2.8 [15]. This is supposed to produce a beneficial and non-selective effect for effective ozonation of all organic substrates [10,24,65] as reflected by removal yields in the same magnitude order for most UV–vis band after 2 min ozonation (Table 1). This tendency was not maintained for MTB after 20 min ozonation, presumably due to specific Fe(II)Mt-intermediates interaction. The higher catalytic activity of Fe(II)Mt must rather involve Fe^{2+} cation mobility and adsorption via hydrophobic interaction. The latter should however be less pronounced than on NaMt, which displayed weaker hydrophilic character reflected by lower WRC (112 mmol g^{-1}) as compared to Fe(II)Mt (117 mmol g^{-1}) (Table 3).

The most significant factor in such a process is undoubtedly pH, which determines the catalytic activity and selectivity of aluminosilicates in ozonation processes in water. In neutral to acidic pH, ozone is stable, and barely starts decomposing beyond pH 9. Under these conditions, the oxidation reduction potential of ozone (ORP) almost remains at its highest level of 2.07 V, and should not vary significantly upon slight pH fluctuations, more particularly for relatively high ozone concentration in the range 0.4-0.45 mmol L^{-1}, as determined by conventional iodometry. This allows concluding that the different performances of the investigated clay catalysts arise from their very structure and chemical composition that determine dye adsorption according to dye-catalyst interactions.

3.7. Acid-base properties and hydrophilic character

The key role of the silanol groups was herein demonstrated by deeper insights using iron-free bentonite samples obtained through acid activation at different contact times. Increasing Si/Al ratio was found to reduce markedly the initial pH in all dye solutions, but which still remains higher than those induced by addition of Fe(II)Mt. (Table 3). The negative values of the Zeta potential of HMt samples must be due to silanol deprotonation beyond pH 2 similar to that reported for silica [68]. The low fluctuations of the Zeta potential after dye addition can be included within the standard deviation range (± 3.50 mV),

Table 2
Effect of the exchangeable cation on the charge of dye molecules and silanol groups.

Without catalyst			With NaMt				With Fe(II)Mt			
Dye	pKa	pH[b]	pH[c]	Dye charge	Out-of-plane pKa = 5.6[e]	In-plane pKa 8.5[e]	pH[d]	Dye charge	Out-of-plane pKa = 5.6[e]	In-plane pKa = 8.5[e]
MB	3.8	5.47	6.77	Neutral	SiO^-	$SiOH_2^+$ to neutral	2.52	R_3N^+	$SiOH_2^+$	$SiOH_2^+$
MG	0.2-1.8	5.12	6.73	Neutral	Neutral	$SiOH_2^+$ to neutral	2.57	Neutral	$SiOH_2^+$	$SiOH_2^+$
MTB	3.0 3.3 3.8 7.2-7.4 11.5 13.4	7.61	7.96	SO_3^- CO_2^-	Neutral	$SiOH_2^+$ to neutral	2.59	R_3N^+	$SiOH_2^+$	$SiOH_2^+$
MO	3.39-3.46	5.40	7.76	SO_3^-	Neutral	$SiOH_2^+$ to neutral	2.62	R_3N^+	$SiOH_2^+$	$SiOH_2^+$

[a] The charge of the exchangeable cation when hydrated, if any, is expected to bear less positive charge, due to water dissociation: $[Fe(H_2O)_x]^{2+} \rightarrow [Fe(H_2O)_{x-1}.OH]^{+} + H^+$.
[b] Intrinsic pH of the aqueous solution of the respective dye at room temperature.
[c] pH of the aqueous solution of the respective dye at room temperature after addition of NaMt without triggering the ozonation.
[d] pH of the aqueous solution of the respective dye at room temperature after addition of Fe(II)Mt without triggering the ozonation.
[e] These pKa values of the silanol groups are supposed to be similar to those of pure silica [66].

suggesting only weak electrostatic dye-HMt interactions through silanol groups.

Higher Si contents are known to enhance the Lewis acidity at the expense of Bronsted acidity as a result of a depletion of the cation-exchange capacity of the clay catalyst [69–72]. This was confirmed by a significant decay of the surface basicity, expressed in terms of decrease in CO_2 retention capacity (CRC) from 2.39 mmol g^{-1} for bentonite and 3.82 mmol g^{-1} for NaMt down to 1.28 mmol g^{-1} for HMt. NaMt and Fe (II)Mt exhibited different acid-base properties, which also differ from those of proton in HMt samples, as supported by specific TPD profiles (Fig. 6).

Unlike Fe(II)Mt, NaMt displayed an additional desorption peak around 70–110 °C corresponding to weakly basic sites. In contrast, Fe (II)Mt is expected to display higher acidity and hydrophilic character, assuming that cation basicity decreases with increasing charge and decreasing size [72]. This was confirmed by a lower CRC of 1.11 mmol g^{-1} for Fe(II)Mt as compared to 3.82 mmol g^{-1} for NaMt, but higher water retention capacity (WRC) of 116.5 µmol g^{-1} as compared to NaMt (111.5 µmol g^{-1}). Besides, Fe(II)Mt displays additional Bronsted acidity from the dissociation of water molecules surrounding hydrated Fe^{2+} cation ($[Fe(H_2O)_x]^{2+} \rightarrow [Fe(H_2O)_{x-1}.OH]^{+} + H^+$).

The resulting decreases of surface positive charge and proton release are expected to produce pH decrease leading to changes in dye:water, water:catalyst and dye:catalyst interactions. This can be accentuated by unavoidable protonation of both types of silanols, which will attract negatively charged SO_3^- and CO_2^- groups, favoring thereby adsorption of anionic MTB and MO dyes. Such interactions explain the red and blue shifts observed for the main UV–vis bands of the dye molecules (Fig. S8-S10). For NaMt, this effect should have minor or no contribution because of its low hydration grade of Na^+ cation. The total disappearance of the 660, 614, 498, 403 and 332 nm bands of cationic dye molecules after five minutes ozonation (Table 4) accounts for a faster decomposition of the phenyl and heteroaromatic rings and cleavage of the C–S^+=C bonds [73,74], in agreement with other works [15,75].

The globally higher catalytic activity of HMt samples (Table 4) must arise from increased density of silanol and –Si–O–Si– and Si–OH groups that promote the hydrophobic character. This indicates the rise of more pronounced organophilic interactions on HMts as compared to NaMt and Fe(II)Mt. These interactions should take place non-selectively with all dye molecules.

Weaker dye degradation was noticed for anionic dyes after 05 min ozonation, as supported by lower UV–vis removal yields for the bands below 400 nm. Here, due to the absence of charges in MTB and MO at pH 3.92–4.18 induced by HMts (Table 3), adsorption of anionic dyes, if any, should involve mainly hydrophobic interactions, given the lowest hydrophilic character of HMts catalysts, which showed much lower WRC (50.1–75.5 µmol g^{-1}) than their non-activated counterparts (111.5–140.5 µmol g^{-1}). Obviously, the extent of the specific surface area (SSA) increased upon acid attack [47], and should play a key role in this regard. However, no correlation with the catalytic activity is

Table 3
CRC, WRC, particle size of the investigated catalysts and induced zeta potential and initial.

Catalyst	Activation time (h)	Si/Al mole ratio	Particle size (µm)	pH[a]	Zeta potential (± 3.50 mv)[b]	Retention capacity [mmol g^{-1}][c]		Initial pH after catalyst addition			
						CRC	WRC	MB	MG	MO	MTB
Bentonite	0	2.50	1.24	9.69	−31.25	2.39	0.141	8.61	7.15	9.33	7.86
NaMt	0	2.50	6.49	8.77	−42.19	3.82	0.112	6.77	6.73	7.76	7.96
Fe(II)Mt	0	2.50	2.45	2.33	+ 16.20	1.110	0.117	2.52	2.57	2.62	2.59
HMt-1	1	2.69	1.99	4.18	−43.02	1.28	0760	3.97	3.65	4.79	4.68
HMt-4	4	3.00	2.04	4.15	−38.36	1.04	0.682	3.90	3.58	4.74	4.37
HMt-8	8	3.47	2.14	4.04	−43.12	1.18	0.623	3.76	3.41	4.28	4.01
HMt-15	15	4.03	2.26	3.92	−42.18	1.06	0.501	3.72	3.43	4.25	4.13
HMt-24	24	4.36	2.35	3.96	−37.62	1.38	0.528	3.83	3.61	4.54	4.53

The decrease in particle size is due to the low pHs (2.33–4.18) of the clay suspension, which induces higher clay dispersion as compared to NaMt.
[a] Average pH of the aqueous suspension of clay minerals at room temperature (Triplicate).
[b] These Zeta potential values were measured in the absence of dye molecules.
[c] The CO_2 and water retention capacity (CRC and WRC, respectively) were assessed with 3% accuracy through TPD measurements in the temperature range.20–450 °C.

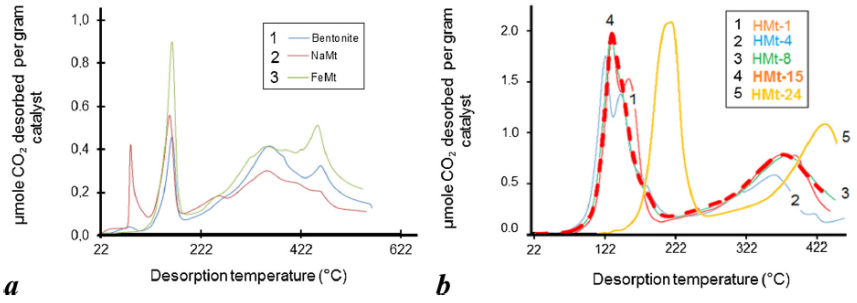

Fig. 6. CO_2-TPD profiles of clay catalysts (*a*) and their acid-activated counterparts (*b*).

possible due SSA variations in aqueous suspension of clay minerals due to the swelling and coagulation-flocculation capacities pH fluctuations.

3.8. Ozonation intermediates and products

As a common feature, ozonation of all dyes gave similar intermediates and products but in specific distributions according to the molecular structure. This is well argued by LC-ToF-MS analysis which revealed similar low-molecular weight organic products after ozonation of MB and MO without and with catalyst (Fig. S16). For MB, $C\text{-}S^+=C$ group cleavage should be the first step of its oxidation into C-S(=O)-C [76,77]. Non-catalytic ozonation (a) produced various peaks at 270, 252, 241, 225, 137.95, 131.91,121 and 109.94 amu. The 270 amu peak accounts for 3-(dimethylamino)-7-(methylamino) phenothiazin-5-ium (Azur B $C_{15}H_{16}N_3$ S), which results from CH_2 loss from the MB molecule.

The same products were also identified after Fe(II)Mt-catalyzed ozonation, but with lower intensity. The marked decrease in time of the peak intensity for the positive ion of MB (m/z = 284) ($C_{16}H_{18}N_3S^+$) is a precise indicator of the beneficial role of Fe(II)Mt. The increase in time of the 109 amu peak in the presence of Fe(II)Mt catalyst corresponds to the formation of C_6H_7ON. The predominant peak at 121 amu ($C_8H_{11}N$) and those appearing at 137 amu and at 109.94 amu were attributed to N,N dimethyl benzenamine, $C_8H_{13}N_2$ (p-dimethylaminoaniline) and $C_3H_6O_2$, (propionic acid), respectively.

MO ozonation for 1 min produced the same peaks at 201,185 and 172.5 amu before and after addition of Fe(II)Mt (Fig. S17). Here, also, the predominant peaks at 121 amu, 137 ($C_8H_{13}N_2$) and 109.94 amu correspond to N,N dimethyl benzenamine, p-dimethylaminoaniline and propionic acid ($C_3H_6O_2$), respectively. Addition of Fe(II)Mt and NaMt led to significant improvements in dye removal, in agreement with other data [24,43,78]. Fe(II)Mt produced faster decay in time of the main UV–vis bands as compared to NaMt, but resulted in similar short chain products.

4. Conclusion

The results obtained herein allow concluding that clay catalysts improve dye ozonation. CO_2 and water TPD measurements turned out to be a judicious approach to correlate the acid-base properties and hydrophilic character of the clay catalysts with the dye behavior in water. Electrostatic interactions appear to be essential for triggering adsorption and further ozonation of anionic dyes on NaMt, but adsorption of all dye molecules involves mainly hydrophobic interaction. On Fe(II)Mt, anionic dyes seem to act as "iron pump", inducing massive iron release that reduce the surface positive charge and catalyst effectiveness. Thus, dye adsorption turns out to be an essential requirement for high catalytic effectiveness, and that electrostatic interaction prevails for certain dyes on certain catalysts. On Fe(II)Mt, the contributions of hydrophobic interaction, cation-exchange and Fe^{2+} mobility to the

Table 4
UV–vis band removal yield (%) after 05 min ozonation for acid-activated clay catalysts.

Dye	UV-Vis band (nm)	UV-Vis band removal yield (%) after 05 min ozonation[a]							
		Bentonite	NaMt	Fe(II)Mt	HMt-1	HMt-4	HMt-8	HMt-15	HMt-24
MB	660	94	72	96	100	100	100	100	100
	614	97	86	97	100	100	100	100	100
	498	89	105	80	100	100	100	100	100
	403	16	55	100	100	100	100	100	100
	332	75	49	47	98	99	100	100	100
	280	82	44	75	98	98	99	99	99
	234	24	–	–	85	84	84	84	84
MG	632	100	80	96	100	100	100	100	100
	420	99	60	99	100	100	100	100	100
	320	95	37	66	98	100	100	100	100
	253	72	–	14	93	95	97	95	95
MO	465	96	96	95	99	100	100	100	100
	277	2	–	–	86	90	90	89	90
	200	21	7	–	27	27	27	28	30
MTB	612	96	87	–	100	100	100	100	100
	444	89	70	92	92	94	95	94	93
	393	68	–	–	72	75	78	76	75
	204	−5	–	22	–	–	30	28	24

[a] The dye conversion yield was calculated using the UV–vis bands appearing at the highest wavelength, with a standard deviation of 2%. HPLC measurements gave almost similar values of the conversion with 3–5% discrepancy.

catalytic activity should prevail. Acid activation produced a beneficial effect on the catalytic activity due increased density of silanols and −Si−O−Si− groups. Acid-activated clay catalysts produced complete dye degradation in shorter ozonation times, mainly via hydrophobic interaction that favors adsorption on the catalyst surface, given the lowest hydrophilic character of HMts catalysts as assessed by TPD. Slight silanol protonation in acidic media induced by HMt dispersion favors only weak adsorption of anionic dyes molecules through electrostatic interaction. Organophilic interaction should take place with all dye molecules. Regardless to the catalyst, short ozonation of all dye molecules produced similar short-chain derivatives, which totally disappeared after prolonged reaction times. These findings provide fundamental knowledge for designing efficient technologies that target total mineralization of organic pollutants with neither water contamination by neither metals nor traces of persistent derivatives using low cost and natural aluminosilicate-based catalysts.

Acknowledgements

This work was supported by grants from MDEIE-FQRNT (2011-2014) and from FODAR-UQ (2015) to A.A. and R.R. We are also grateful to Mohamad El-Akhrass for his technical assistance.

Appendix A. Supplementary data

Supplementary material related to this article can be found, in the online version, at doi:https://doi.org/10.1016/j.jhazmat.2018.09.070.

References

[1] T. Robinson, G. McMullan, R. Marchant, P. Nigam, Remediation of dyes in textile effluent: a critical review on current treatment technologies with a proposed alternative, Bioresour. Technol. 77 (2001) 247–255.
[2] J.S. Do, M.L. Chen, Decolourization of dye-containing solutions by electrocoagulation, J. Appl. Electrochem. 24 (1994) 785–790.
[3] Y. Bulut, H. Aydın, A kinetics and thermodynamics study of methylene blue adsorption on wheat shells, Desalination 194 (2006) 259–267.
[4] P. Mokhtari, M. Ghaedi, K. Dashtian, M.R. Rahimi, M.K. Purkait, Removal of methyl orange by copper sulfide nanoparticles loaded activated carbon: kinetic and isotherm investigation, J. Mol. Liq. 219 (2016) 299–305.
[5] B. Iurascu, I. Siminiceanu, D. Vione, M.A. Vicente, A. Gil, Phenol degradation in water through a heterogeneous photo-Fenton process catalyzed by Fe-treated laponite, Water Res. 43 (2009) 1313–1322.
[6] E. Hu, X. Wu, S. Shang, X.-m. Tao, S.-x. Jiang, L. Gan, Catalytic ozonation of simulated textile dyeing wastewater using mesoporous carbon aerogel supported copper oxide catalyst, J. Cleaner Prod. 112 (Part 5) (2016) 4710–4718.
[7] Y. Bulut, H. Aydın, A Kinetics and Thermodynamics Study of Methylene Blue Adsorption on Wheat Shells, (2006).
[8] M. Numata, T. Yarita, Y. Aoyagi, M. Yamazaki, A. Takatsu, Investigation of saponification for determination of polychlorinated biphenyls in marine sediments, Chemosphere 58 (2005) 865–875.
[9] G.L. Northcott, K.C. Jones, Validation of procedures to quantify nonextractable polycyclic aromatic hydrocarbon residues in soil, J. Environ. Qual. 32 (2003) 571–582.
[10] A. Azzouz, Advances in oxidative decomposition of oxalic acid in aqueous media, in: J.C. Taylor (Ed.), Advances in Chemistry Research, Nova-Publishers, New-York, USA, 2012, pp. 1–31 2nd quarter.
[11] D. Shahidi, R. Roy, A. Azzouz, Advances in catalytic oxidation of organic pollutants – prospects for thorough mineralization by natural clay catalysts, Appl. Catal., B 174-175 (2015) 277–292.
[12] H. Ma, B. Wang, X. Luo, Studies on degradation of Methyl Orange wastewater by combined electrochemical process, J. Hazard. Mater. 149 (2007) 492–498.
[13] I.M. Sasidharan Pillai, A.K. Gupta, Effect of inorganic anions and oxidizing agents on electrochemical oxidation of methyl orange, malachite green and 2,4-dinitrophenol, J. Electroanal. Chem. 762 (2016) 66–72.
[14] L. Xu, J. Wang, Fenton-like degradation of 2,4-dichlorophenol using Fe3O4 magnetic nanoparticles, Appl. Catal. B: Environ. 123–124 (2012) 117–126.
[15] D. Shahidi, R. Roy, A. Azzouz, Total removal of oxalic acid via synergistic parameter interaction in montmorillonite catalyzed ozonation, J. Environ. Chem. Eng. 2 (2014) 20–30.
[16] S. Karthikeyan, A. Titus, A. Gnanamani, A.B. Mandal, G. Sekaran, Treatment of textile wastewater by homogeneous and heterogeneous Fenton oxidation processes, Desalination 281 (2011) 438–445.
[17] A. Azzouz, Advances in oxidative oxidation of oxalic acid in aqueous media, in: J.C. Taylor (Ed.), Advances in Reserach Chemistry, Nova-Science Publishers, New-York, 2012.
[18] A. Azzouz, A. Kotbi, P. Niquette, T. Sajin, A.V. Ursu, A. Rami, F. Monette, R. Hausler, Ozonation of oxalic acid catalyzed by ion-exchanged montmorillonite in moderately acidic media, Reaction Kinetics, Mechanisms and Catalysis 99 (2010) 289–302.
[19] S.J. George, R. Gandhimathi, P.V. Nidheesh, S.T. Ramesh, Electro-Fenton oxidation of salicylic acid from aqueous solution: batch studies and degradation pathway, CLEAN – Soil, Air, Water 42 (2014) 1701–1711.
[20] G. Moussavi, A.A. Aghapour, K. Yaghmaeian, The degradation and mineralization of catechol using ozonation catalyzed with MgO/GAC composite in a fluidized bed reactor, Chem. Eng. J. 249 (2014) 302–310.
[21] X. Li, Q. Zhang, L. Tang, P. Lu, F. Sun, L. Li, Catalytic ozonation of p-chlorobenzoic acid by activated carbon and nickel supported activated carbon prepared from petroleum coke, J. Hazard. Mater. 163 (2009) 115–120.
[22] J. Hoigné, H. Bader, Rate constants of reactions of ozone with organic and inorganic compounds in water—II: dissociating organic compounds, Water Res. 17 (1983) 185–194.
[23] R. Andreozzi, V. Caprio, A. Insola, R. Marotta, Advanced oxidation processes (AOP) for water purification and recovery, Catal. Today 53 (1999) 51–59.
[24] S. Larouk, R. Ouargli, D. Shahidi, L. Olhund, T.C. Shiao, N. Chergui, T. Sehili, R. Roy, A. Azzouz, Catalytic ozonation of Orange-G through highly interactive contributions of hematite and SBA-16 – to better understand azo-dye oxidation in nature, Chemosphere 168 (2017) 1648–1657.
[25] İ. Arslan, I. Akmehmet Balcioğlu, T. Tuhkanen, Oxidative treatment of simulated dyehouse effluent by uv and near-UV light assisted Fenton's reagent, Chemosphere 39 (1999) 2767–2783.
[26] H.S. Lade, T.R. Waghmode, A.A. Kadam, S.P. Govindwar, Enhanced biodegradation and detoxification of disperse azo dye Rubine GFL and textile industry effluent by defined fungal-bacterial consortium, International Biodeterioration & Biodegradation 72 (2012) 94–107.
[27] P.C.C. Faria, J.J.M. Órfão, M.F.R. Pereira, Mineralisation of coloured aqueous solutions by ozonation in the presence of activated carbon, Water Res. 39 (2005) 1461–1470.
[28] P.C.C. Faria, J.J.M. Órfão, M.F.R. Pereira, Ozone decomposition in Water catalyzed by activated carbon: influence of chemical and textural properties, Ind. Eng. Chem. Res. 45 (2006) 2715–2721.
[29] S. Pirgalıoğlu, T.A. Özbelge, Comparison of non-catalytic and catalytic ozonation processes of three different aqueous single dye solutions with respect to powder copper sulfide catalyst, Appl. Catal. A: Gen. 363 (2009) 157–163.
[30] S. Tang, D. Yuan, Q. Zhang, Y. Liu, Q. Zhang, Z. Liu, H. Huang, Fe-Mn bi-metallic oxides loaded on granular activated carbon to enhance dye removal by catalytic ozonation, Environ. Sci. Pollut. Res. 23 (2016) 18800–18808.
[31] X.F. Zhu, X.H. Xu, The mechanism of Fe (III)-catalyzed ozonation of phenol, J. Zhejiang Univ. Sci. 5 (2004) 1543–1547.
[32] D.S. Pines, D.A. Reckhow, Effect of dissolved cobalt(II) on the ozonation of oxalic acid, Environ. Sci. Technol. 36 (2002) 4046–4051.
[33] D. Chatterjee, S. Dasgupta, R.S. Dhodapkar, N.N. Rao, Simultaneous degradation of non-emissive and emissive dyes on visible light illuminated TiO2 surface, J. Mol. Catal. A: Chem. 260 (2006) 264–268.
[34] F.J. Beltrán, F.J. Rivas, R. Montero-de-Espinosa, Catalytic ozonation of oxalic acid in an aqueous TiO2 slurry reactor, Appl. Catal., B 39 (2002) 221–231.
[35] S. Chaliha, K.G. Bhattacharyya, Using Mn(II) − MCM41 as an environment-friendly catalyst to oxidize phenol, 2-chlorophenol, and 2-nitrophenol in aqueous solution, Ind. Eng. Chem. Res. 47 (2008) 1370–1379.
[36] J. Wu, L. Ma, Y. Chen, Y. Cheng, Y. Liu, X. Zha, Catalytic ozonation of organic pollutants from bio-treated dyeing and finishing wastewater using recycled waste iron shavings as a catalyst: removal and pathways, Water Res. 92 (2016) 140–148.
[37] K. Yong, J. Wu, S. Andrews, Heterogeneous catalytic ozonation of aqueous reactive dye, Ozone: Sci. Eng. 27 (2005) 257–263.
[38] H. Jung, H. Choi, Catalytic decomposition of ozone and para-chlorobenzoic acid (pCBA) in the presence of nanosized ZnO, Appl. Catal. B: Environ. 66 (2006) 288–294.
[39] F.J. Beltrán, F.J. Rivas, L.A. Fernández, P.M. Álvarez, R. Montero-de-Espinosa, Kinetics of catalytic ozonation of oxalic acid in water with activated carbon, Ind. Eng. Chem. Res. 41 (2002) 6510–6517.
[40] J.P. Kaptijn, The Ecoclear® Process. Results from full-scale installations, Ozone: Sci. Eng. 19 (1997) 297–305.
[41] U. Jans, J. Hoigné, Activated carbon and carbon black catalyzed transformation of aqueous ozone into OH-radicals, Ozone: Sci. Eng. 20 (1998) 67–90.
[42] J.-N. Park, J. Wang, K.Y. Choi, W.-Y. Dong, S.-I. Hong, C.W. Lee, Hydroxylation of phenol with H2O2 over Fe2+ and/or Co2+ ion-exchanged NaY catalyst in the fixed-bed flow reactor, J. Mol. Catal. A: Chem. 247 (2006) 73–79.
[43] R. Ouargli, S. Larouk, I. Terrab, R. Hamacha, N. Benharrats, A. Bengheddach, A. Azzouz, Intrinsic activity of SBA-like silica in the catalytic ozonation of organic pollutants, Ozone: Sci. Eng. 38 (2016) 48–61.
[44] D. Shahidi, A. Moheb, R. Abbas, S. Larouk, R. Roy, A. Azzouz, Total mineralization of sulfamethoxazole and aromatic pollutants through Fe2+-montmorillonite catalyzed ozonation, J. Hazard. Mater. 298 (2015) 338–350.
[45] M.A. Didi, B. Makhoukhi, A. Azzouz, D. Villemin, Colza oil bleaching through optimized acid activation of bentonite. A comparative study, Appl. Clay Sci. 42 (2009) 336–344.
[46] B. Makhoukhi, M.A. Didi, D. Villemin, A. Azzouz, Acid activation of bentonite for use as a vegetable oil bleaching agent, Grasas Aceites 60 (2009) 343–349.
[47] V.A. Arus, S. Nousir, R. Sennour, T.C. Shiao, I.D. Nistor, R. Roy, A. Azzouz, Intrinsic affinity of acid-activated bentonite towards hydrogen and carbon dioxide, Int. J. Hydrogen Energy 43 (2018) 7964–7972.
[48] A. Azzouz, A.-V. Ursu, D. Nistor, T. Sajin, E. Assaad, R. Roy, TPD study of the

reversible retention of carbon dioxide over montmorillonite intercalated with polyol dendrimers, Thermochim. Acta 496 (2009) 45–49.
[49] A. Azzouz, D. Nistor, D. Miron, A.V. Ursu, T. Sajin, F. Monette, P. Niquette, R. Hausler, Assessment of acid–base strength distribution of ion-exchanged montmorillonites through NH3 and CO2-TPD measurements, Thermochim. Acta 449 (2006) 27–34.
[50] A. Azzouz, D. Messad, D. Nistor, C. Catrinescu, A. Zvolinschi, S. Asaftei, Vapor phase aldol condensation over fully ion-exchanged montmorillonite-rich catalysts, Appl. Catal., A 241 (2003) 1–13.
[51] S. Nousir, N. Platon, K. Ghomari, A.-S. Sergentu, T.C. Shiao, G. Hersant, J.-Y. Bergeron, R. Roy, A. Azzouz, Correlation between the hydrophilic character and affinity towards carbon dioxide of montmorillonite-supported polyalcohols, J. Colloid Interface Sci. 402 (2013) 215–222.
[52] A. Mills, J. Wang, Photobleaching of methylene blue sensitised by TiO2: an ambiguous system? J. Photochem. Photobiol., A 127 (1999) 123–134.
[53] C. Yogi, K. Kojima, N. Wada, H. Tokumoto, T. Takai, T. Mizoguchi, H. Tamiaki, Photocatalytic degradation of methylene blue by TiO2 film and Au particles-TiO2 composite film, Thin Solid Films 516 (2008) 5881–5884.
[54] P.A.R. Tafulo, R.B. Queirós, G. González-Aguilar, On the “concentration-driven” methylene blue dimerization, Spectrochim. Acta Part A: Mol. Biomol. Spectrosc. 73 (2009) 295–300.
[55] K. Patil, R. Pawar, P. Talap, Self-aggregation of Methylene Blue in aqueous medium and aqueous solutions of Bu4NBr and urea, Phys. Chem. Chem. Phys. 2 (2000) 4313–4317.
[56] A. Ghanadzadeh, A. Zeini, A. Kashef, M. Moghadam, Concentration effect on the absorption spectra of oxazine1 and methylene blue in aqueous and alcoholic solutions, J. Mol. Liq. 138 (2008) 100–106.
[57] H. Hichem, A. Djamila, A. Hania, Optical, electrical and photoelectrochemical characterization of electropolymerized poly methylene blue on fluorine doped tin oxide conducting glass, Electrochim. Acta 106 (2013) 69–74.
[58] C. Galindo, P. Jacques, A. Kalt, Photodegradation of the aminoazobenzene acid orange 52 by three advanced oxidation processes: UV/H2O2, UV/TiO2 and VIS/TiO2: comparative mechanistic and kinetic investigations, J. Photochem. Photobiol. A: Chem. 130 (2000) 35–47.
[59] T. Shen, C. Jiang, C. Wang, J. Sun, X. Wang, X. Li, A TiO2 modified abiotic-biotic process for the degradation of the azo dye methyl orange, RSC Adv. 5 (2015) 58704–58712.
[60] X. Ren, Z. Hu, H. Hu, R. Qiang, L. Li, Z. Li, Y. Yang, Z. Zhang, H. Wu, Noncovalently-functionalized reduced graphene oxide sheets by water-soluble methyl green for supercapacitor application, Mater. Res. Bull. 70 (2015) 215–221.
[61] A. Khataee, M. Sheydaei, A. Hassani, M. Taseidifar, S. Karaca, Sonocatalytic removal of an organic dye using TiO2/Montmorillonite nanocomposite, Ultrason. Sonochem. 22 (2015) 404–411.
[62] J. Qu, H. Li, H. Liu, H. He, Ozonation of alachlor catalyzed by Cu/Al2O3 in water, Catal. Today 90 (2004) 291–296.
[63] L. Zhao, J. Ma, Z.-z. Sun, Oxidation products and pathway of ceramic honeycomb-catalyzed ozonation for the degradation of nitrobenzene in aqueous solution, Appl. Catal. B: Environ. 79 (2008) 244–253.
[64] J.M. Joseph, H. Destaillats, H.-M. Hung, M.R. Hoffmann, The sonochemical degradation of azobenzene and related azo dyes: rate enhancements via Fenton’s reactions, J. Phys. Chem. A 104 (2000) 301–307.
[65] D. Shahidi, A. Moheb, R. Abbas, S. Larouk, R. Roy, A. Azzouz, Total mineralization of sulfamethoxazole and aromatic pollutants through Fe2+-montmorillonite catalyzed ozonation, J. Hazard. Mater. 298 (2015) 338–350.
[66] M. Sulpizi, M.-P. Gaigeot, M. Sprik, The silica–water interface: how the silanols determine the surface acidity and modulate the water properties, J. Chem. Theory Comput. 8 (2012) 1037–1047.
[67] G. Rytwo, S. Nir, M. Crespin, L. Margulies, Adsorption and interactions of methyl green with montmorillonite and sepiolite, J. Colloid Interface Sci. 222 (2000) 12–19.
[68] B.M. Lowe, C.K. Skylaris, N.G. Green, Acid-base dissociation mechanisms and energetics at the silica-water interface: an activationless process, J. Colloid Interface Sci. 451 (2015) 231–244.
[69] J.A. Lercher, A. Jentys, Application of microporous solids as catalysts, Handbook of Porous Solids, Wiley-VCH Verlag GmbH, 2008, pp. 1097–1156.
[70] R.J. Gorte, Surface acidity, Handbook of Porous Solids, Wiley-VCH Verlag GmbH, 2008, pp. 432–464.
[71] M. Elanany, M. Koyama, M. Kubo, E. Broclawik, A. Miyamoto, Periodic density functional investigation of Lewis acid sites in zeolites: relative strength order as revealed from NH3 adsorption, Appl. Surf. Sci. 246 (2005) 96–101.
[72] J. Weitkamp, M. Hunger, Chapter 22 - acid and Base catalysis on zeolites, in: J. Čejka, H. van Bekkum, A. Corma, F. Schüth (Eds.), Studies in Surface Science and Catalysis, Elsevier, 2007, pp. 787–835.
[73] M.A. Rauf, M.A. Meetani, A. Khaleel, A. Ahmed, Photocatalytic degradation of Methylene Blue using a mixed catalyst and product analysis by LC/MS, Chem. Eng. J. 157 (2010) 373–378.
[74] R. Zuo, G. Du, W. Zhang, L. Liu, Y. Liu, L. Mei, Z. Li, Photocatalytic degradation of methylene blue using TiO2 impregnated diatomite, Adv. Mater. Sci. Eng. 2014 (2014) 7.
[75] M. Vinuth, H.S.B. Naik, B.M. Vinoda, H. Gururaj, N. Thomas, G. Arunkumar, Enhanced removal of methylene blue dye in aqueous solution using eco-friendly Fe (III)–montmorillonite, Mater. Today: Proc. 4 (2017) 424–433.
[76] A. Houas, H. Lachheb, M. Ksibi, E. Elaloui, C. Guillard, J.-M. Herrmann, Photocatalytic degradation pathway of methylene blue in water, Appl. Catal. B: Environ. 31 (2001) 145–157.
[77] L.V. Trandafilović, D.J. Jovanović, X. Zhang, S. Ptasińska, M.D. Dramićanin, Enhanced photocatalytic degradation of methylene blue and methyl orange by ZnO:Eu nanoparticles, Appl. Catal. B: Environ. 203 (2017) 740–752.
[78] N. Al-Hayek, B. Legube, M. Doré, Ozonation catalytique (Fe III/A12O3) Du phénol et de ses produits d’ozonation, Environ. Technol. Lett. 10 (1989) 415–426.

ANNEXE E: Article II soumis à Journal of Hazardous Materials Juillet 2019

Elsevier Editorial System(tm) for Journal of Hazardous Materials

Manuscript Draft

Manuscript Number: HAZMAT-D-19-04731

Title: Thorough bisphenol-A removal through ozonation with Silica-based catalysts. Role of the Si content on catalyst-contaminant interactions

Article Type: Research Paper

Keywords: Bisphenol A; Ozonation; Mesoporous silica; Montmorillonite; Hematite.

Corresponding Author: Professor Abdelkrim AZZOUZ, PhD

Corresponding Author's Institution: University of Quebec at Montreal

First Author: Farida BOUDISSA, Researcher

Order of Authors: Farida BOUDISSA, Researcher; Alisa-Vasilica ARUS, PhD-Professor assistant; Meriem ZEKKARI, PhD student; Rachida OUARGLI, PhD-Professor; René ROY, PhD-Professor; Abdelkrim AZZOUZ, PhD

Abstract: Catalytic ozonation for total mineralization of bisphenol-A (BPA) from aqueous solution was investigated in the presence of mesoporous silica, acid activated bentonite (HMt) and montmorillonite-rich materials (Mt) ion-exchanged by Na+ and Fe2+ cations (NaMt and Fe(II)Mt). The effects of the catalyst activity and BPA interactions with the catalyst surface were studied by correlating the acid-base properties and hydrophilic character through CO2 and water TPD measurements, zeta potential measurements and particle sizes assessment. To the best of our knowledge, this approach has barely been tackled so far. Acid-activated and iron-free clay catalysts produced complete BPA degradation in short ozonation times. The catalytic activity was found to strongly depend on the surface basicity and hydrophilic character, which, in turn, depend on the Si content and exchangeable cation. Catalyst interactions with water and BPA appear to determine the catalyst particle dispersion in aqueous media, promoting hydrophobic adsorption in high Si catalysts, at the expense of electrostatic interactions which were mainly involved in low silica materials. These findings are of a great importance, because they allow tailoring specific catalyst properties for specific features of the waters to be treated.

Suggested Reviewers: Barbara Kasprzyk-Hordern
B.Kasprzyk-Hordern@bath.ac.uk
Expertise in the investigated topic

Garoma Temesgen
tgaroma@sdsu.edu
Expertise in the investigated topic

Sibel Irmak
sibel.irmak@unl.edu

Expertise in the investigated topic.

ANNEXE F: Article III soumis à Chemosphere Août 2019

Elsevier Editorial System(tm) for Chemosphere

Manuscript Draft

Manuscript Number:

Title: Clay-catalyzed ozonation for effective removal of Endocrine- disrupting compounds in solvent-free media

Article Type: Research paper

Section/Category: Treatment and Remediation

Keywords: Endocrine-disrupting compounds; 17α-ethinylestradiol; Ozonation; Acid-activated clays; Montmorillonite.

Corresponding Author: Professor Abdelkrim AZZOUZ, PhD

Corresponding Author's Institution: University of Quebec at Montreal

First Author: Farida Boudissa, Master

Order of Authors: Farida Boudissa, Master; Meriem Zekkari, PhD student; Vasilica-Alisa Arus, PhD; Rachida Ouargli-Saker, Professor; René Roy, Professor; Abdelkrim AZZOUZ, PhD

Abstract: The catalytic ozonation of 17α-ethinylestradiol (EE2), a harmful hormone disruptor and endocrine-disrupting compound was investigating in solvent free aqueous media. Acid-activated bentonites along with ion-exchanged montmorillonite (NaMt and Fe(II)Mt) were used as catalysts. An original approach never tackled so far consisted in correlating the basicity and hydrophilic character to the EE2-catalyst interactions occurring on the catalyst surface. In water-ethanol mixture and in the absence of catalyst, the degradation of (EE2) reached 72 % after one minute of ozonation and 99.5% after 60 minutes. In the presence of Fe(II)Mt, EE2 degradation (96 %) was achieved after only one minute ozonation, and was ca. 24 % higher than without catalyst. Under similar conditions, almost total degradation to 99.99 % was registered in 15 minutes of ozonation but without total mineralization of the intermediates. Moderately acid-activated bentonites exhibited higher activity affording total mineralization within short ozonation. The catalytic activity of clay catalysts was found to correlate with their surface basicity and hydrophilic character. The results obtained herein allow envisaging effective clay catalysts with surface properties judiciously tailored according to the organic pollutants.

Suggested Reviewers: Marcia Dezotti Dr.
Dr., Chemical Engineering Program-COPPE, Federal University of Rio de Janeiro, P.O. Box 68502, Rio de Janeiro 21941-972, Brazil
mdezotti@peq.coppe.ufrj.br
Experise in EE2 ozonation

Willy Verstraete Dr.

Dr., Laboratory of Microbial Ecology and Technology (LabMET), Faculty of Bioscience Engineering, Ghent University, Coupure Links 653, B-9000 Gent, Belgium
willy.verstraete@ugent.be
Expertise in biological removal of 17α-ethinylestradiol

Clara Manfred Dr.
Dr, Institute for Water Quality and Waste Management, Vienna University of Technology
mclara@iwag.tuwien.ac.at
Expertise in wastewater treatment plants to remove micropollutants

Alexandros Katsaounis Dr
Dr, Dept Environmental Engineering, University of Crete
alex.katsaounis@chemeng.upatras.gr
Expertise in electrochemical wastewater treatment

Yeomin Yoon Dr.
Dr., Department of Civil and Environmental Engineering, University of South Carolina, Columbia, SC 29208, USA
yoony@cec.sc.edu
Works in bisphenol A and 17α-ethinyl estradiol removal from seawater

Alan R Oyler Dr.
Dr., The R.W. Johnson Pharmaceutical Research Institute, University of Minnesota Duluth
aoyler@prius.jnj.com
Works on identification of degradation intermediates of EDCs

ANNEXE G: PARTICIPATION A LA PUBLICATION D'AUN ARTCILE SCIENTIFIQUE COMME CO-AUTEUR DURANT LE PROJET DE MAITRISE

Journal homepage: www.fia.usv.ro/fiajournal
Journal of Faculty of Food Engineering,
Ştefan cel Mare University of Suceava, Romania
Volume XVI, Issue 4 - 2017, pag. 282 - 286

FOOD AND ENVIRONMENT SAFETY

RECYCLABLE POROUS MATERIALS FOR THE UPTAKE OF BISPHENOL A

Rodica STURZA[1], Mihai MELENCIUC[1], Denisa NISTOR[2], Farida BOUDISSA[3], Thiziri TERKANI[3], Nou-Houda Hadj ABDELKADER[3], Azzouz ABDELKRIM[3]*

[1]Technical University of Moldova, Stefan cel Mare Bd. 168, Chishinau, MD-2004, Republic of Moldova
[2]University „Vasile Alecsandri" of Bacău, Calea Mărăşeşti str. 157, Bacău, 600115, Romania
[3]Université du Québec à Montréal C.P. 8888, succ. Centre-ville, Montréal (Québec), H3C 3P8, CANADA
*Corresponding author: sturzar@yandex.ru
Received 14th October 2017, accepted 29th November 2017

Abstract: *The presence of pollutants in the environment, food, drinking water and other compounds in direct or indirect contact with humans is a major environmental issue. In this regard, a privileged place reverts to the capture or decomposition of pollutants without producing traces of residual toxins. An interesting approach for depollution is the use of natural, non-toxic, recyclable materials as adsorbents and catalysts. The aim of this work was to study the ozonation of bisphenol-A in water in the presence of Bentonite and its acid-activated counterparts AAB1, AAB4, AAB8, AAB15 and AAB24 obtained after 1, 4, 15 and 24 h of acid treatment. For comparison, one also used two deriving montmorillonite-rich materials ion-exchanged with Na^+ and Fe^{2+} cation, namely, NaMT, Fe(II)MT. The kinetic and thermodynamic parameters of the process were assessed through UV-Vis spectrophotometric measurements, and were discussed in correlation with thermo-programmed desorption technique (TPD) data. Calculations of the retention capacities of CO_2 and H_2O (CRC and WRC) revealed high basic character (high CRC) for NaMT but lower hydrophilic character (low WRC) as compared to Fe(II)MT. This explains the higher catalytic activity of Fe(II)Mt by enhanced interaction with basic bisphenol (pka = 9.2 at 25°C), which favors adsorption, and higher dispersion in water, which offer higher contact surface as compared to NaMt. This provides valuable date for designing effective oxidative water treatments using clay materials and other natural's counterpart.*

Keywords: *bisphenol; ozonation; bentonite; montmorillonite; iron cation, thermal programmed desorption.*

1. Introduction

Bisphenol A is used in polycarbonates production as well as a precursor for epoxy resins [1]. In 2011, about 5.5 million tons of bisphenol A were produced, which were subsequently used for the manufacture of polycarbonate bottles and tableware, bottles for infant formula, and so on [[1], [2], [3]]. By multiple molecular mechanisms, bisphenol A has a strong disrupting effect on estrogenic activity, as well as other endocrine activities [[3], [5], [6], [7]]. Several studies and researches have shown that all age categories are affected by the action of bisphenol A because it is detected in the urine of most adults is children tested [[2], [8]]. However, small children and babies are more sensitive when exposed to the action of bisphenol A. This compound has already been detected in the serum of pregnant women, breast milk, placental tissues and fetal liver, which shows that the child is exposed to the action of bisphenol A at the stage of fetal development [[2], [7], [9], [10]].

The heat and contact with any of the components, whether basic or acidic, will accelerate the hydrolysis of the ester bonds that bind bisphenol A in the polycarbonates and resins. It is the same hydrolysis and the same thermal action that takes place during the processes of pasteurization or sterilization or by microwave heating. Preheating food or even washing food containers allows bisphenol A to enter the food [[7]].

Because of increasing environmental pollution, bisphenol A has become one of the most important pollutants and the need to eliminate it is of great importance [11]. An interesting approach for pollution abatement and prevention is the use of natural, non-toxic, recyclable materials as adsorbents and catalysts [12], [12]. This approach also involves more environmentally friendly methods of synthesizing and modifying such materials that do not use or produce potential pollutants. This will certainly open up promising prospects for a more "green" chemistry for the decontamination of water used in the food, pharmaceutical and cosmetic industries as well as for environmental sanitation in general. To achieve this objective, an experimental attempt made it possible to highlight the beneficial role of the combination of ozone with a porous aluminosilic surface such as natural bentonite and montmorillonite, its purified derivative.

2. Materials and methods

To perform the experiments we used bisphenol A (2,2-Bis(4-hydroxy-phenyl)propane) with the following parameters: assay – 97%, bp – 220°C/4 mmHg(lit.), mp – 158-159°C(lit.) [14].

Bisphenol A has been subjected to the ozonation process using a 20 mL aqueous solution (10^{-4} M) at different ozone exposure duration (1, 2, 3, 4, 5, 7, 10, 15, 20 and 25 minutes), using the respective ozonation: 10 mg / 1 min, 20 mg / 2 min, 30 mg / 3 min, 40 mg / 4 min, 50 mg / 5 min, 70 mg / 7 min, 100 mg / 10 min, 150 mg / 15 min, 200 mg / 20 min, 250 mg / 25 min.

To intensify the effect of ozone, one used two types of bentonite (BentA and BentB), ion exchange with sodium (NaMT) and iron (FeMT) montmorillonite, as well as bentonites having undergone treatment with sulfuric acid for 1, 4, 8, 15 and 24 hours (AAB1, AAB4, AAB8, AAB15 and AAB24). For the ozonation tests, 40 mg/L of each catalyst was previously inserted in 20 mL of bisphenol A solution, before triggering the bubbling of ozone at a rate of 6 mg / h.

The basic and hydrophilic characteristics were evaluated by thermo-programmed desorption analysis (DTP or TPD) of 40 mg of each catalyst, previously saturated with carbon dioxide and water vapor.

3. Results and discussion

The UV-Vis spectra made it possible to trace the evolution of the absorbance of each of the two spectral bands of Bisphenol A (Fig. 1, Fig. 2, Fig. 3, Fig. 4,Fig. 5).

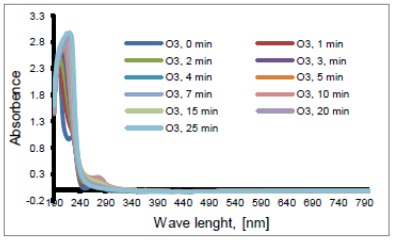

Fig. 1. Bisphenol A UV-Vis spectra at different ozonation time without catalyst: Concentration – 10^{-4} M; volume: 20 ml; ozonation regimes: 10 mg/1min, 20 mg/2 min, 30 mg/3 min, 40 mg/4 min, 50 mg/5 min, 70 mg/7 min, 100 mg/10 min, 150 mg/15 min, 200 mg/20 min, 250 mg/25 min.

Food and Environment Safety - Journal of Faculty of Food Engineering, Ştefan cel Mare University - Suceava
Volume XVI, Issue 4 – 2017

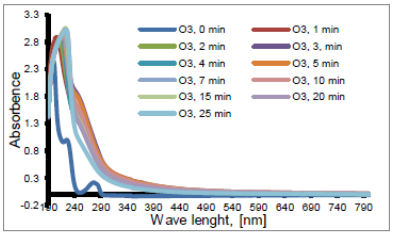

Fig. 2. Bisphenol A UV-Vis spectra at different ozonation time with Bentonite as catalyst: Concentration – 10^{-4} M; volume: 20 ml bisphenol + 40 mg BentA; ozonation regimes: 10 mg/1 min, 20 mg/2 min, 30 mg/3 min, 40 mg/4 min, 50 mg/5 min, 70 mg/7 min, 100 mg/10 min, 150 mg/15 min, 200 mg/20 min, 250 mg/25 min.

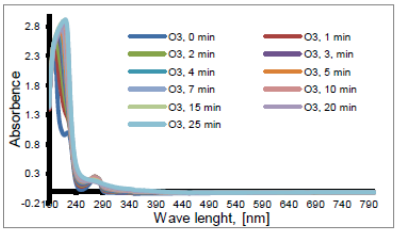

Fig. 3. Bisphenol A UV-Vis spectra at different ozonation time with FeMT as catalyst: Concentration – 10^{-4} M; volume: 20 ml bisphenol + 40 mg FeMT; ozonation regimes: 10 mg/1 min, 20 mg/2 min, 30 mg/3 min, 40 mg/4 min, 50 mg/5 min, 70 mg/7 min, 100 mg/10 min, 150 mg/15 min, 200 mg/20 min, 250 mg/25 min.

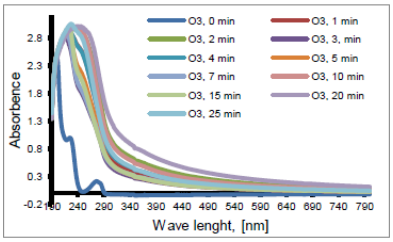

Fig. 4. Bisphenol A UV-Vis spectra at different ozonation time with NaMT as catalyst: Concentration – 10^{-4} M; volume: 20 ml bisphenol + 40 mg NaMT; ozonation regimes: 10 mg/1 min, 20 mg/2 min, 30 mg/3 min, 40 mg/4 min, 50 mg/ 5 min, 70 mg/7 min, 100 mg/10 min, 150 mg/15 min, 200 mg/20 min, 250 mg/25 min.

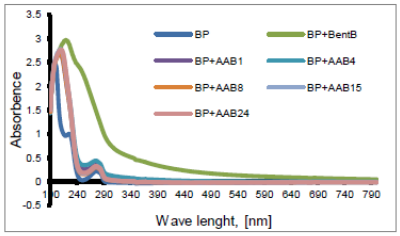

Fig. 5. Bisphenol A UV-Vis spectra at different ozonation time with Bent B, AAB1, AAB4, AAB8, AAB15 and AAB24 as catalyst: Concentration – 10^{-4} M; volume: 20 ml bisphenol + 40 mg catalyst; ozonation regimes: 50 mg/5 min.

The analysis of the UV-Vis spectra of bisphenol A subjected to the action of the ozonation process has shown that Fe (II) MT is the most effective than NaMt. This is probably due to its acidic nature, which makes it possible to retain the most basic molecule of bisphenol A (pka = 9.2 at 25°C).

This hypothesis is confirmed by the analysis of thermo-programmed desorption (TPD).

Fig. 6Fig. 7 and others relating to Fe (II) Mt have been used to calculate the values of the CO_2 and water retention capacities (CRC and WRC). These are summarized in Table 1.

Calculations of CO_2 and water retention capacities (CRC and WRC) revealed a high basic character (high CRC) for NaMT but a lower hydrophilic character (WRC low) compared to MT Fe (II). This explains the higher catalytic activity of Fe (II) Mt by a stronger interaction with basic bisphenol (pka = 9.2 at 25°C), which promotes its adsorption, and a greater dispersion in water, which offers a contact area greater than that of NaMt in water. This provides valuable data for designing effective treatments for oxidizing water using clay materials and other natural counterparts.

Food and Environment Safety - Journal of Faculty of Food Engineering, Ştefan cel Mare University - Suceava
Volume XVI, Issue 4 – 2017

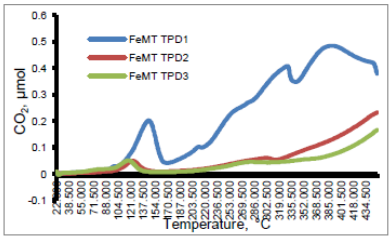

Fig. 6. TPD diagrams of CO_2 – temperature relation for the three samples of FeMT. CO_2: purge debit: 14 ml/min; TPD debit: 6 ml/min; Temperature domain: 23 ÷ 450°C.

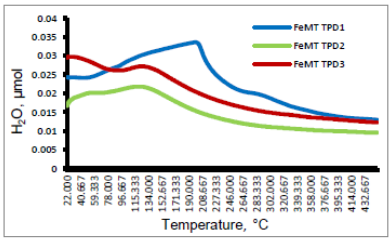

Fig. 7. TPD diagrams of H_2O – temperature relation for the three samples of FeMT. CO_2: purge debit: 14 ml/min; TPD debit: 6 ml/min; Temperature domain: 23 ÷ 450°C.

Table 1.
CRC and WRC values for the studied catalysts

Nr. of sample	CRC, [µmol/g]	WRC, [µmol/g]
NaMT TPD1	3821±5	111±5
FeMT TPD1	1109±5	116±5
BentA TPD1	2697±5	161±5
BentB TPD1	2081±5	119±5
AAB1 TPD1	2554±5	102±5
AAB4 TPD1	1976±5	97±5
AAB8 TPD1	2422±5	84±5
AAB15 TPD1	2080±5	70±5
AAB24 TPD1	2415±5	73±5

4. Conclusions

The results of this research are of great importance as they provide compelling evidence that natural materials such as clays can be used to develop inexpensive water decontamination technologies. This is all the more interesting taking into account the wide availability of such materials, their ease of handling and modification, the non-use of solvents and other polluting chemicals, and especially the high chemical stability of bisphenol A, opens promising prospects for the treatment of water, especially that related to human health such as those used or discharged by the food and pharmaceutical industries and in domestic waste.

5. Acknowledgments

The presented research was supported by Francophone University Agency as well as the subventions from MDEIE-FQRNT and FODAR-UQ (QC, Canada).

6. References

[1]. EDDO J. HOEKSTRA & CATHERINE SIMONEAU, *"Release of Bisphenol A from Polycarbonate – A Review"*, Critical Reviews in "Food Science and Nutrition" 53:4, 2013, 386-402

[2]. JOHANNA R. ROCHESTER, *"Bisphenol A and Human Health: A review of the literature"*, Reproductive Toxicology (2013), 96 p.

[3]. RUTHANN A. RUDEL, JANET M. GRAY, CONNIE L. ENGEL, TERESA W. RAWSTHORNE, ROBIN E. DODSON, JANET M. ACKERMAN et al., *"Food Packaging and Bisphenol A and Bis(2-Ethyhexyl) Phthalate Exposure: Findings from a Dietary Intervention"*, Environmental Health Perspectives, 119 : 7, 2011, 914-920

[4]. HOA H. LE, EMILY M. CARLSON, JASON P. CHUA, SCOTT M. BELCHER, *"Bisphenol A is released from polycarbonate drinking bottles and mimics the neurotoxic actions of estrogen in developing cerebellar neurons"*, Toxicol Letters, Jan 30, 208 176(2), 2008, 149-156

[5]. SARAH J OPPENEER, KIM ROBIEN, *"Bisphenol A exposure and associations with obesity among adults: a critical review"*, Public Health Nutrition: 18(10), 2014, 1847-1863

[6]. BEVERLY S. RUBIN, *"Bisphenol A: An endocrine disruptor with widespread exposure and multiple effects"*, Journal of Steroid Biochemistry & Molecular Biology 127, 2011, 27-34

[7]. CHERYL ERLER, JULIE NOVAK, *"Bisphenol A Exposure: Human Risk and Health Policy"*, Journal of Pediatric Nursing, 25, 2010, 400-407

[8]. JENNY L. CARWILE, HENRY T. LUU, LAURA S. BASSETT, DANIEL A. DRISCOLL, CATERINA YUAN, JENNIFER Y. CHANG et al., *"Polycarbonate Bottle Use and Urinary Bisphenol A Concentrations"*, Environmental Health Perspectives, 117 : 9, 2009, 1368-1372

[9]. JOE M. BRAUN, AMY E. KALKBRENNER, ANTONIA M. CALAFAT, KIMBERLY YOLTON, XIAOYUN YE, KIM N. DIETRICH, BRUCE P. LANPHEAR, *"Impact of Early-Life Bisphenol A Exposure on Behavior and Executive Function in Children"*, PEDIATRICS, 128 : 5, 2011, 873-882

[10]. THIT J. MØRCK, GIUSEPPINA SORDA, NICOLETTA BECHI, BRIAN S. RASMUSSEN, JESPER B. NIELSEN, FRANCESCA IETTA et al., *"Placental transport and in vitro effects of Bisphenol A"*, Reproductive Toxicology 30, 2010, 131-137

[11]. HENRYK METCER, GARY KLECKA, "Treatment of Wastewaters Containing Bisphenoi A: State of the Science Review", Water Environment Research, 83: 7, 2011, 650-666

[12]. ALISA V. ARUS, M. NAZIR TAHIR, RADIA SENNOUR, TZE C. SHIAO, LAMYAA M. SALLAM, ILEANA D. NISTOR, RENE ROY, ABDELKRIM AZZOUZ, *"Cu^0 and Pd^0 loaded Organo-Bentonites as Sponge–like Matrices for Hydrogen Reversible Capture at Ambient Conditions"*, Chemistry Select 2016, 1, 1452-1461

[13]. D. NISTOR, D.N. MIRON, A. AZZOUZ, *" Cinétique de rétention des éléments radioactifs sur des argiles pontées d'origine roumaine*, Studies and Scientific Research, vol. III, abstract, Issue: SCSCC6, Volume VII, No. 3 (2006), (ISSN 1582-540X).

[14]. http://www.sigmaaldrich.com/catalog/product/aldrich/133027?lang=en&region=CA

REFERENCES

[1] Routledge, E.J., et al., Identification of Estrogenic Chemicals in STW Effluent. 2. In Vivo Responses in Trout and Roach. J. Environmental Science & Technology, 32 (1998) 1559-1565.

[2] Robinson, T., et al., Remediation of dyes in textile effluent: a critical review on current treatment technologies with a proposed alternative. J. Bioresource technology, 77 (2001) 247-255.

[3] Hess-Wilson, J.K. and K.E. Knudsen, Endocrine disrupting compounds and prostate cancer. Cancer letters, 241 (2006) 1-12.

[4] Kidd, K.A., et al., Collapse of a fish population after exposure to a synthetic estrogen. Proceedings of the National Academy of Sciences, 104 (2007) 8897.

[5] Numata, M., et al., Investigation of saponification for determination of polychlorinated biphenyls in marine sediments. J. Chemosphere, 58 (2005) 865-875.

[6] Northcott, G.L. and K.C. Jones, Validation of Procedures to Quantify Nonextractable Polycyclic Aromatic Hydrocarbon Residues in Soil. J. Environmental Quality, 32 (2003) 571-582.

[7] Azzouz, A., Advances in Oxidative Decomposition of Oxalic Acid in Aqueous Media, in Advances in Chemistry Research, J. C.Taylor, Editor. 2012, 2nd quarter, Nova-Publishers: New-York, USA. p. 1-31.

[8] Shahidi, D., R. Roy, and A. Azzouz, Advances in catalytic oxidation of organic pollutants-Prospects for thorough mineralization by natural clay catalysts. J. Applied Catalysis B: Environmental, 174 (2015) 277-292.

[9] Ma, H., B. Wang, and X. Luo, Studies on degradation of Methyl Orange wastewater by combined electrochemical process. J. Hazardous Materials, 149 (2007) 492-498.

[10] Sasidharan Pillai, I.M. and A.K. Gupta, Effect of inorganic anions and oxidizing agents on electrochemical oxidation of methyl orange, malachite green and 2,4-dinitrophenol. J. Electroanalytical Chemistry, 762 (2016) 66-72.

[11] Xu, L. and J. Wang, Fenton-like degradation of 2,4-dichlorophenol using Fe_3O_4 magnetic nanoparticles. J. Applied Catalysis B: Environmental, 123 (2012) 117-126.

[12] Shahidi, D., R. Roy, and A. Azzouz, Total removal of oxalic acid via synergistic parameter interaction in montmorillonite catalyzed ozonation. J. Environmental Chemical Engineering, 2 (2014) 20-30.

[13] Karthikeyan, S., et al., Treatment of textile wastewater by homogeneous and heterogeneous Fenton oxidation processes. Desalination, 281 (2011) 438-445.

[14] Azzouz, A., et al., Ozonation of oxalic acid catalyzed by ion-exchanged montmorillonite in moderately acidic media. Reaction Kinetics, Mechanisms and Catalysis, 99 (2010) 289-302.

[15] Faria, P.C.C., J.J.M. Orfão, and M.F.R. Pereira, Mineralisation of coloured aqueous solutions by ozonation in the presence of activated carbon. J. Water research, 39 (2005) 1461-1470.

[16] Chatterjee, D., et al., Simultaneous degradation of non-emissive and emissive dyes on visible light illuminated TiO_2 surface. J. Molecular Catalysis A: Chemical, 260 (2006) 264-268.

[17] Beltrán, F.J., F.J. Rivas, and R. Montero-de-Espinosa, Catalytic ozonation of oxalic acid in an aqueous TiO2 slurry reactor. J. Applied Catalysis B: Environmental, 39 (2002) 221-231.

[18] Beltrán, F.J., et al., Kinetics of Catalytic Ozonation of Oxalic Acid in Water with Activated Carbon. J. Industrial & Engineering Chemistry Research, 41 (2002) 6510-6517.

[19] Kaptijn, J.P., The Ecoclear® Process. Results from Full-Scale Installations. Ozone: Science & Engineering, 19 (1997) 297-305.

[20] Jans, U. and J. Hoigné, Activated Carbon and Carbon Black Catalyzed Transformation of Aqueous Ozone into OH-Radicals. Ozone: Science & Engineering, 20 (1998) 67-90.

[21] Park, J.-N., et al., Hydroxylation of phenol with H_2O_2 over Fe^{2+} and/or Co^{2+} ion-exchanged NaY catalyst in the fixed-bed flow reactor. J. Molecular Catalysis A: Chemical, 247 (2006) 73-79.

[22] Shahidi, D., et al., Total mineralization of sulfamethoxazole and aromatic pollutants through Fe^{2+}-montmorillonite catalyzed ozonation. J. Hazardous Materials, 298 (2015) 338-350.